



UiT The Arctic University of Norway

Faculty of Biosciences, Fisheries and Economics

Atmospheric CO₂ drawdown, community dynamics and selection of surface microbiomes in marine cold-water ecosystems

Nerea Johanna Aalto

A dissertation for the degree of Philosophiae Doctor

August 2022



Photo credit for the front page: Katarzyna Lukaszek

A dissertation for the degree of Philosophiae Doctor

**Atmospheric CO₂ drawdown, community dynamics and selection
of surface microbiomes in marine cold-water ecosystems**

Nerea Johanna Aalto



Tromsø – August 2022

The work for this thesis was carried out from October 2017 to August 2022 in Microalgae & Microbiomes Research Group at the Norwegian School of Fishery Science at UiT – The Arctic University of Norway. This position was funded by UiT – The Arctic University of Norway and is affiliated with the Arctic Centre for Sustainable Energy – ARC.

Table of contents

TABLE OF CONTENTS	I
ACKNOWLEDGEMENTS	II
SUMMARY	III
LIST OF PAPERS AND CONTRIBUTIONS	V
ABBREVIATION	VII
1 INTRODUCTION	1
1.1 THE CHANGING ARCTIC	1
1.2 THE ROLE OF ARCTIC COASTAL AREAS IN ATMOSPHERIC CO ₂ REGULATION	2
1.3 MICROBIAL COMMUNITY STRUCTURE INFLUENCES ECOSYSTEM FUNCTION	3
1.4 BIOLOGICAL INTERACTIONS INFLUENCE CELL METABOLISM	5
1.5 ASPECTS OF ECOLOGICAL COMMUNITY PROCESSES	7
2 THESIS AIMS	9
3 METHODS	11
3.1 FIELDWORK	11
3.2 SAMPLE AND DATA COLLECTION	14
3.3 MOLECULAR ANALYSIS AND BIOINFORMATICS	14
3.4 DATA ANALYSIS	16
3.4.1 <i>Microbiome community analyses</i>	16
3.4.2 <i>Correlation and multivariate analyses</i>	18
3.4.3 <i>Null model analysis</i>	18
4 KEY FINDINGS	20
4.1 PAPER I	20
4.2 PAPER II	22
4.3 PAPER III	25
5 DISCUSSION, SYNTHESIS AND PERSPECTIVES	27
5.1 TEMPORAL AND SPATIAL VARIATION IN NORTHERN NORWEGIAN COASTAL AREA	27
5.1.1 <i>Phytoplankton blooms</i>	27
5.1.2 <i>CO₂ undersaturation and wind speed-controlled magnitude of CO₂ flux</i>	28
5.2 PHYTOPLANKTON MEDIATED MICROBIAL COMMUNITIES	30
5.3 COLD-WATER DRIVEN MICROBIOMES	32
6 CONCLUSION	34
7 REFERENCES	36

Acknowledgements

First and foremost, I would like to thank my supervisor team. You have been an invaluable support and your doors have always been open, thank you for that. Hans Christopher Bernstein, your guidance in the past years has been immeasurable. It has been a huge educational journey. Thank you for your countless comments and pushing me when it has been needed. Karley Campbell, thank you for joining my supervisor team midway. Your critical eye and knowledge on seawater chemistry have been highly valuable. Hans Christian Eilertsen, thank you for welcoming me into the lab and research group when I was still an exchange student. I could not imagine then where the journey would take me. Your enthusiasm and non-giving up mind are fascinating.

To the amazing group of people – my friends and colleagues (current and past) – at Microalgae & Microbiomes Research Group (M2RG), it has been inspiring, exciting, and so much fun working with all of you. Martina, Gunilla, Richard, Renate, Jon Brage, Lars, Linn, Ingeborg, Stina, Hannah, Dennis, Daniela, Sebastian and the newest group members, Michael, Johan and Jacob, thank you for all the help I have got from you and knowledge you have shared with me.

I would like to give special thanks to the captains and crew of RV Johan Ruud. You were the top crew to work with, always welcoming and helpful. You really made that research vessel such a memorable place.

Tiia and Daniel, my wonderful Tromsø family, with whom I have been able to experience so many great moments. I appreciate your support over the past years. Daniel, thank you for everything. To my dear family, thank you for always being there for me.

Nerea Johanna Aalto, Tromsø 25.08.2022

Summary

The European Arctic is characterized by large surface areas of coastal seas and long coastlines where important ecosystem processes are regulated by marine microbiomes that contribute to global carbon cycling via primary productivity and atmospheric CO₂ drawdown. In addition to biogeochemical cycling, these complex microbial ecosystems also support major marine food webs and lend themselves to marine bioprospecting for novel biotechnologies. However, they are not well understood and remain unpredictable. For example, northern coastal Norway is periodically affected by unwanted ecosystem functions such as sporadic harmful algae blooms that are detrimental to local aquaculture industry. These cold adapted marine microbiomes perform ecological processes that are often driven by phytoplankton and their associated heterotrophic communities which undergo strong seasonal variation within complex and variable oceanographical and biogeochemical conditions. Climate change driven temperature increases with resulting direct and indirect changes on environmental conditions have been reported to alter microbial community structures of surface microbiomes. Hence, these important microbial ecosystems are in transition, and it is difficult to predict the trajectory of how specific ecosystem functions may be changing.

This thesis is centered around cold-water communities of phytoplankton and bacterioplankton with the aim to enhance our contemporary understanding on surface microbial ecosystems and their function with respect to carbon cycling, community dynamics and community selection. Paper I and Paper II took place in northern Norwegian fjords and coastal systems where spatial variation and magnitude of atmospheric CO₂ uptake were investigated and the main physical and biological factors driving surface partial pressure of CO₂ with respect to atmospheric CO₂ were assessed in four fjords and a coastal bay through seasonal changes. The results indicate that northern Norwegian fjords free of sea-ice act as a sink for atmospheric CO₂, although the magnitude of air-to-sea CO₂ flux showed fjord-specific variation, and the biological fixation of CO₂ is a strong driver of CO₂ undersaturation. In addition, the temporal and spatial dynamics of early summer microeukaryotes with co-blooming bacteria were examined during a destructive haptophyte *Chrysochromulina leadbeateri*-associated harmful algae bloom. The coastal habitats harbor highly localized phytoplankton microbial communities which succession dynamics of blooming populations (including *C. leadbeateri*) undergo strong temporal variability. Paper III took place across a long transect from Atlantic water influenced Barents Sea to less influenced Nansen Basin in the high Arctic with the aim to understand more

about the influence of ecological community processes on the distribution of phytoplankton and microbial taxa. Inferences based on phylogenetic turnover, generated through null modeling randomization of phylogenetic relatedness, indicates that the dominant selective force is homogeneous across the studied transect despite differences regarding temperature, sea-ice conditions, and origin of a water mass. Our findings highlight that both large scale and local studies are important to form the needed comprehensive understanding of these microbial ecosystems as the regional taxonomic pool is determined by fundamental ecological processes but community structure influencing ecosystem function is instead subjected to more localized variation of abiotic and biotic factors.

List of papers and contributions

The following papers are included in this thesis:

- I Aalto NJ, Campbell K, Eilertsen HC and Bernstein HC (2021). Drivers of Atmosphere Ocean CO₂ Flux in Northern Norwegian Fjords. *Frontiers in Marine Science*, 8:692093. doi:10.3389/fmars.2021.692093.

- II Aalto NJ, Schweitzer HD, Gran-Meyer E, Krsmanovic S, Svenning JB, Dalheim L, Petters S, Ingebrigsten R, Hulatt CJ and Bernstein HC (2022). Microbial community dynamics during a harmful *Chrysochromulina leadbeateri* bloom. *bioRxiv*. doi: 10.1101/2022.06.21.496960.

- III Aalto NJ, Krsmanovic S, Schweitzer HD, Campbell K and Bernstein HC (2022). Diversity and selection of surface marine microbiomes in Atlantic-influenced Arctic. *Frontiers in Microbiology*, 2486. doi: 10.3389/fmicb.2022.892634.

Data and code repositories

Paper I: <https://osf.io/tbzse/>

Paper II: <https://osf.io/4wjhp/>

Paper III: <https://osf.io/g8wxc/>

Co-author contributions

	Paper I	Paper II	Paper III
Concept & idea	HCE & NJA	HCB & NJA	HCB & NJA
Study design & methods	HCE, NJA & HCB	HCB, NJA , HDS & SK	HCB, NJA , HDS & SK
Data gathering & interpretation	NJA	NJA , RI, EG-M, JBS, LD, SP, CJH & HCB	NJA , HCB, HS & SK
Manuscript preparation	NJA	NJA & HCB,	NJA
Manuscript revisions & editing	NJA , KC, HCE & HCB	NJA , HCB, CJH, HDS & SP	NJA , HDS, KC, SK & HCB

Authors: Chris J. Hulatt (CJH), Erlend Gran-Meyer (EG-M), Hannah D. Schweitzer (HDS), Hans C. Bernstein (HCB), Hans C. Eilertsen (HCE), Jon B. Svenning (JBS), Karley Campbell (KC), Lars Dalheim (LD), **Nerea J. Aalto (NJA)**, Richard Ingebrigsten (RI), Sebastian Petters (SP), Stina Krsmanovic (SK)

Abbreviation

$\Delta p\text{CO}_2$ – difference in partial pressure of CO_2 between air and sea surface water

1 Introduction

The Northern Hemisphere cold-water region – north of 60 °N including the Arctic Ocean and its adjacent seas – is highly variable and complex in terms of oceanographic and biological processes, and sea-ice conditions (Bluhm et al., 2015). This region has a central role in global oceanic thermohaline circulation (Rahmstorf, 2006). In addition, it is recognized for important ecosystem functions which mainly take place over the coastal seas (continental shelves). For example, these areas have a high contribution to the global carbon cycle via atmospheric carbon dioxide (CO₂) uptake and biological carbon fixation by phytoplankton and sea-ice algae (Wassmann et al., 2006; Yasunaka et al., 2016; Aalto et al., 2021). High primary productivity supports sea-ice associated, pelagic and benthic food webs linked to socio-economic welfare (Falk-Petersen et al., 1990; Søreide et al., 2010; Grebmeier et al., 2015). These ecological processes undergo strong seasonality as they are driven by extreme daylight conditions with alternation between polar night and polar day (Ardyna and Arrigo, 2020; Aalto et al., 2021).

1.1 The changing Arctic

Climate change affects the entire globe; however, its occurrence is amplified in the Arctic where increases in temperature occur at faster rate than the global average (Blunden and Arndt, 2016; Arias et al., 2021). As a result, Arctic ecosystems are in transition. For example, the Barents Sea is predicted to become more like an extension of North Atlantic due to increasing inflow of Atlantic water (a process called Atlantification) which effectively transports heat northward, to the higher Arctic resulting increase in surface temperatures and decline in sea-ice extent and volume which in turn results higher effective irradiance (Årthun et al., 2012; Polyakov et al., 2017). Arctic fjords and other nearshore ecosystems are also in transition, where Atlantification and warming is likely enhancing land-sea connectivity (Rawlins et al., 2010; Arias et al., 2021). The physiological traits and life strategies of marine life from bacteria to mammals are optimized to the cold-water environments and therefore susceptible to mostly unpredictable alterations (Kottmeier and Sullivan, 1988; Wassmann et al., 2015; Kunisch et al., 2021).

1.2 The role of Arctic coastal areas in atmospheric CO₂ regulation

The Arctic marine region can be characterized by high regional consistency on air-to-sea CO₂ exchange and disproportional contribution to the global CO₂ uptake from atmosphere (Yasunaka et al., 2016; Roobaert et al., 2019). When the Arctic is put into a global scale, its role as a carbon sink becomes even more striking as the region comprises only 1 % of world ocean volume but 25 % of global coastal sea area and 35 % of global coastline (Wassmann, 2015; Roobaert et al., 2019). Thus, a pronounced air-sea CO₂ flux occurs in the coastal seas as they are responsible for more than one-third of the global coastal ocean uptake (Roobaert et al., 2019). Although the magnitude and seasonal dynamics of air-sea CO₂ fluxes are currently relatively well established for the coastal seas in the Arctic as well as in the global scale (Yasunaka et al., 2016; Roobaert et al., 2019), nearshore environments such as coastal bays and semi-enclosed fjords still lack a quantitative understanding for their contribution to CO₂ cycling dynamics. Because these geographically narrow coastal environments are common marine features in the Arctic, they may have a substantial role in regulating regional carbon fluxes. Fjords, estuaries, and other nearshore systems are also part of land-sea coupling. They represent an interface between land and sea processes and are therefore heavily influenced by hydrographical cycles and biogeochemical properties of heterogeneous catchments (Holmes et al., 2012; Smith et al., 2015; Giesbrecht et al., 2022). Therefore, understanding the CO₂ chemistry dynamics and the underpinning biological processes in fjords can also provide an insight of impact of environmental changes in larger scales.

In principle, there is a similar interplay of processes that determine CO₂ exchange rates in fjords and coastal seas. The main driving force is a state of equilibrium between effective partial pressure of CO₂ (pCO₂) in surface water and atmosphere – stronger surface water undersaturation indicates higher CO₂ sink potential. The strength of undersaturation is determined by complex set of processes with counteracting impacts and compensating effects across these processes. For example, cooling and warming of surface water (CO₂ solubility in water), biological inorganic carbon fixation and remineralization/calcification (utilization and release of CO₂), freshening and increasing salinity (dilution and CO₂ solubility in water) are the main counteracting effects within processes (Weiss, 1974; Gattuso et al., 1995; Chierici et al., 2019). Because CO₂ has a low solubility to water, wind induced turbulence in boundary layer between atmosphere and sea surface influences gas transfer velocity (Wanninkhof, 1992). Therefore, global and local wind speed patterns can have a strong impact on the magnitude of

air-sea CO₂ flux (Chen et al., 2013; Aalto et al., 2021). The major challenge to estimate regional contribution of fjords in atmospheric CO₂ regulation is the heterogeneity of fjords making extrapolation difficult and highly uncertain. The interplay of above-described processes is often unique in each fjord and even within the same fjord because the weather, hydrology and biology of these semi-enclosed systems is determined by fjord-specific bathymetry, size, orientation, and land processes (Svendsen, 1995; Eilertsen and Skarðhamar, 2006; Aalto et al., 2021). Previous studies conducted in northern Norway and the glacier and/or sea-ice influenced fjords in Greenland and Svalbard have estimated the fjords as an annual net sink for atmospheric CO₂ (e.g., Rysgaard et al., 2012; Meire et al., 2015; Ericson et al., 2018; Jones et al., 2020; Aalto et al., 2021). This is somewhat contradictory when compared to temperate areas where coastal seas are mainly considered as net sinks but nearshore systems i.e., estuaries as net sources for atmospheric CO₂ (Chen et al., 2013). Phytoplankton primary production and remineralization of carbon including both allochthonous and autochthonous materials are major drivers controlling surface water pCO₂ seasonality in cold-water fjords (Rysgaard et al., 2012; Meire et al., 2015; Ericson et al., 2018; Jones et al., 2020). Thus, a fate of biologically fixed carbon is an important component in fjord CO₂ sink/source issues as a highly productive fjord can still be a net heterotrophic system (Smith and Hollibaugh, 1993). The processes influencing the fate of organic carbon are not easy to determine as they are complex and spread across seasons. Much depends on phytoplankton community structure and bloom phenology that are affected by seasonality and strength of summer surface stratification but also fjord-specific advection which determines availability of dissolved organic carbon (DOC) for heterotrophic bacteria utilization and vertical and lateral export of particulate and dissolved carbon (Reigstad and Wassmann, 1996; Jones et al., 2020).

1.3 Microbial community structure influences ecosystem function

Surface phytoplankton and co-occurring microbial communities are key players in several ecosystem processes in addition to carbon cycling, including: nutrient provision and regeneration, primary production, toxin biosynthesis, and elemental cycling (Falkowski et al., 1998; Azam and Malfatti, 2007). These processes are often linked to specific community structure – i.e., taxonomic composition and alpha diversity. Different kinds of phytoplankton have distinct functional traits due to size, morphology, elemental composition, life history strategy and trophic mode leading to different ecosystem signatures (Quere et al., 2005;

Litchman et al., 2015). Similarly, bacteria and archaea pose distinct ecological capabilities and roles which are mostly determined by their metabolism (Dinsdale et al., 2008). Because community members have different responses to environmental changes, are changes in these ecological processes anticipated with shifting community structures.

Climate change-related alterations in abundance and distribution of distinct yet key phytoplankton groups and species including diatoms, *Phaeocystis* sp. (haptophyte) and *Emiliania huxleyi* (haptophyte, coccolithophore), have already been reported (Assmy et al., 2017; Orkney et al., 2020; Oziel et al., 2020). This has brought up concern regarding perturbations to the marine carbon pump as these microorganisms facilitate primary production, inorganic carbon synthesis and affect transport of sinking carbon that delivers nutrients provided to benthos and planktonic food webs. Previous studies have emphasized expanding northward occurrence of summer blooming *E. huxleyi*, a major species in marine carbonate cycle, and low- and high-irradiance adapted *Phaeocystis* sp. due to advective transport of Atlantic water (Assmy et al., 2017; Oziel et al., 2020). Strong *Phaeocystis* sp. prevalence may constrain diatom blooms due to nutrient depletion (Assmy et al., 2017). Because diatoms are key players in contribution of essential high-quality fatty acids into food webs and effective deep carbon sequestration in contrast with *Phaeocystis* sp. which higher vertical flux attenuation efficiency compared to diatoms might lead to more recycling in upper water column. Thus, this can have significant ecosystem implications also including a deep ocean microbial diversity (Reigstad and Wassmann, 2007; Tréguer et al., 2018; Fadeev et al., 2021).

Bacteria are major drivers of marine nutrient cycles and remineralization of organic carbon, and they form tight mutualistic and antagonist associations with phytoplankton (Azam and Malfatti, 2007; Meyer et al., 2017; Raina et al., 2022). Therefore, it is becoming more common to study both phytoplankton and bacterioplankton as the holistic marine microbiome. Within the rapid development of molecular methods such as high-throughput sequencing of 16S and 18S ribosomal RNA (rRNA) gene amplicon DNA, Arctic microbiome research has in the last decade focused on describing the community structure variability within the full diversity of microeukaryotes (microalgae and heterotrophic protists) and prokaryotes (Bacteria and Archaea) mainly in spatial but also temporal dimensions (e.g., Fadeev et al., 2018; Rapp et al., 2018; de Sousa et al., 2019; Wietz et al., 2021). For example, this has provided an improvement on understanding contribution of diverse group of small flagellates, pico- and nanoplankton

with auto-, mixo- and heterotrophic lifestyles, to community dynamics which have often been grouped as a one component (Fadeev et al., 2018; de Sousa et al., 2019; Wietz et al., 2021). These methodologies have also helped unlock new knowledge on bacteria associations with different types of algal derived particles and taxonomy in addition to the diversity across the water column (Fadeev et al., 2018; Rapp et al., 2018; de Sousa et al., 2019).

Comparative studies along environmental gradients and between contrasting habitats including fjords, sea-ice conditions, and water masses, have previously been performed to gain understanding on environmental factors driving Arctic microbial communities (e.g., de Sousa et al., 2019; Cardozo-Mino et al., 2021; Delpech et al., 2021; Wietz et al., 2021). These findings have revealed distinct community structures across hydrological and sea-ice regimes. During the productive season, the differences in prokaryotic communities have been mainly linked to distinct phytoplankton bloom phenology as a result of nutrient and irradiance differences between sea-ice covered Polar waters and sea-ice free Atlantic waters (Cardozo-Mino et al., 2021; Wietz et al., 2021). There is also evidence that seasonal advection of Atlantic water can quickly influence the microbiome structure in otherwise Polar-dominated conditions (Wietz et al., 2021). Whereas terrestrial inputs impact prokaryotic community structure mainly via alterations in biogeochemical conditions (Delpech et al., 2021). This information has led to hypotheses on how changes from sea-ice driven habitat to light driven habitat or increasing freshwater input may change the microbiomes. An increase in chlorophyll *a* concentration and resulting contribution of organic carbon substrates may be followed by acceleration in microbial loop (Frey et al., 2021; Wietz et al., 2021). Also, alterations in wintertime community compositions are predicted including taxa related to element recycling and utilization of sea-ice derived organic material due to expected changes in water column stratification and sea-ice conditions (Wietz et al., 2021). Increases in terrestrial inputs may enhance the fraction of particle-associated and allochthonous prokaryotic taxa (Delpech et al., 2021).

1.4 Biological interactions influence cell metabolism

The metabolites of phytoplankton and prokaryotic cells are not constant but altered in response to changing environmental conditions such as temperature, irradiance, nutrient supply, and presence of interacting organisms (Bernstein et al., 2017; Khan et al., 2018; Svenning et al., 2019). Some of the changes in cell biochemistry are desired and even harnessed for

biotechnological applications e.g., pigment production and enhancement of certain fatty acids while some are unwanted such as toxin biosynthesis. Algal toxin production including allelopathic compounds is a natural cell physiology (Glibert et al., 2005). Unwanted function of toxicity is usually distinguished when it negatively affects the human activity by causing harm to environment or human health. These negative outcomes appear often due to enhanced proliferation of certain phytoplankton or cyanobacteria although consequences of toxic production can emerge in low concentrations (biomass) of causative agent (Zingone and Enevoldsen, 2000). High number of species belonging to several algal groups are reported to cause these harmful blooms (Zingone and Enevoldsen, 2000).

Temperate- and cold-water harmful algae blooms (HABs) in coastal areas, commonly tend to occur after the primary spring phytoplankton bloom in conditions of warm and stratified surface waters and often variable inorganic nutrient concentrations and ratios (e.g., Nielsen et al., 1990; Rey and Aure, 1991; Hartman et al., 2014). Thus, these factors are also linked to the formation of HABs. It is also typical that the HABs reoccur sporadically (Glibert et al., 2005; Karlson et al., 2021) although there are still major knowledge gaps around the specific combination of physical, biogeochemical, and biotic factors that induce of blooming. One of the alternative hypotheses suggested by Telesh et al. (2021) is that abiotic, stable conditions can facilitate HABs by inducing chaotic behavior where biotic interactions became a major driver of phytoplankton dynamics in the absence of external abiotic triggers.

Algae species are known to have distinct requirements for exogeneous compounds such as some vitamins that are essential for growth but cannot be synthesized by the cell (i.e., auxotrophy) instead these, and a wide range of other growth simulating compounds including trace elements and hormones, are provided in specific interactions with bacteria (Croft et al., 2005; Amin et al., 2015; Cirri and Pohnert, 2019; Raina et al., 2022). Competition for inorganic nutrients is ongoing between phytoplankton species but also between algae and bacteria (Bratbak and Thingstad, 1985; Burson et al., 2018). Species have different nutrient affinities and optimums of variable ratios of inorganic nutrients which can give them fitness advantages over others but also cause a stress in growth limiting conditions (Smayda, 1997). Nutrient limitation induced cellular stress has been linked to increasing toxicity and excretion of toxic compounds into the water of several HAB associated species in order to inhibit the growth of their competitors (Frangópulos et al., 2004; Uronen et al., 2005). However, it is still unknown why this would lead sometimes to a toxic bloom (Davidson et al., 2012).

As most “harmful” species are part of the natural phytoplankton communities it is possible that the same species can be toxic in one area with harmful effects but not toxic (or less toxic) in other areas (Glibert et al., 2005). Differences in the level of toxin production between axenic and non-axenic cultures of harmful algae has been reported supporting the connection between cell physiology and biotic interactions (Uribe and Espejo, 2003). High-frequency time series studies on phytoplankton microbial communities have enhanced the general understanding of mechanisms that lead to blooms and the findings suggest that microbial interactions may, especially after the major spring bloom, contribute to the fine-scale temporal dynamics of co-occurring prokaryotes and microeukaryotes (Needham and Fuhrman, 2016; Martin-Platero et al., 2018). Therefore, understanding the natural high-resolution spatiotemporal variation of blooming cycles of harmful algae with co-occurring microeukaryotes and prokaryotes is crucial. Since coastal areas are variable in their physical and biogeochemical properties, they offer a great environment to study natural blooming cycles of HAB-associated microbial taxa.

1.5 Aspects of ecological community processes

While studying species rich communities in the context of several environmental measurements it is challenging to determine the main selective forces responsible for structuring spatial diversity between communities (i.e., beta diversity). The spatial or temporal patterns of microbial communities in relation to environmental conditions can also be investigated using concepts of community ecology. The fundamental ecological community processes governing species occurrence can be classified as described by Vellend (2010) and Stegen et al. (2015).

- Deterministic processes:
 - o *Homogeneous and variable selection*: ecological selection is imposed by the abiotic environment and species interactions which act as a filter because different organisms have different levels of fitness in each set of environmental conditions.
- Stochastic processes:
 - o *Dispersal*: movement of organisms through space.
 - o *Ecological drift*: low rate of organism dispersion.
- Unclassified processes:

- Differences in community compositions are not primarily influenced either by selection or dispersal.

These processes are not mutually exclusive because they influence communities with relative importance, which is not necessarily spatially and/or temporally constant (Stegen et al., 2015; Wang et al., 2020). Very little is known about how these processes govern the microbiome communities in Arctic, but also globally there are not many studies relating these components to marine surface microorganisms. An advantage of inferring these processes to understand microbial selection is that the underlying observed community patterns are understood first and thereafter linked to mechanisms such as specific environmental conditions (e.g., temperature) that may or may not govern the stochastic/deterministic balance instead of directly inferring significance between community composition and environmental factors (Stegen et al., 2013). For example, if stochastic processes are dominating, the community patterns are not the outcome of environmental determined fitness (Stegen et al., 2013). In turn, the selective environment can be spatially homogeneous in which case the community members have physiologically adapted to the occurring range of spatial variability in relation to the major abiotic or biotic factor (Dini-Andreote et al., 2015).

The pattern of dominating ecological community processes can be disentangled via community phylogenetic analysis where turnover in phylogenetic community composition (phylogenetic beta diversity) is determined in relation to deviation from null expectation via randomization procedure (Stegen et al., 2012). As phylogenetic information captures the relatedness of community members, phylogenetic turnover enables to infer if the degree of relatedness is constructed by random processes (stochasticity), or selection induced by environmental conditions (deterministic processes) (Graham and Fine, 2008). Therefore, phylogenetic turnover acts in a way beyond taxonomic turnover (taxonomic beta diversity) which instead determines the overlap in species composition between communities (Graham and Fine, 2008; Stegen et al., 2012).

2 Thesis aims

The overarching aim of this thesis work was to enhance understanding on contemporary cold-water ecosystem functions related to marine phytoplankton and bacterial communities in the surface waters of northern coastal Norway and the Arctic Ocean. This was done in relation to physical oceanography in nearshore coastal and pelagic environments (Figure 1). The importance of this thesis work lies, in a large extent, on fulfilling spatial and temporal knowledge gaps on overlapping themes related to cold adapted marine microbiomes and air-sea CO₂ flux. First, the role of northern Norwegian coastal area, including interconnected but hydrographically distinct fjords and a coastal bay, as a sink or source for atmospheric CO₂ was investigated (Paper I). The aim was to quantify the magnitude and dynamics of air-sea CO₂ flux and assess the main physical and biological factors driving $\Delta p\text{CO}_2$ through an annual cycle. Second, temporal dynamics within phytoplankton microbial communities were examined during a HAB incident, partly in the same coastal area as in Paper I. As the starting point of HAB was not captured the focus was not on the initial conditions and causes of the bloom of focal taxon, *Chrysochromulina leadbeateri*. Instead, the aim was to achieve a better understanding of the focal taxon within its associated and co-blooming prokaryotes and microeukaryotes (Paper II). Third, the phytoplankton microbial community composition and diversity was studied across a large transect from open water Barents Sea to ice-covered Nansen Basin in the Arctic Ocean with the aim of disentangling the dominating community selection process and investigating spatial pattern of alpha diversity in relation to decreasing surface water temperature and influence of Atlantic water as well as presence of sea-ice (Paper III).

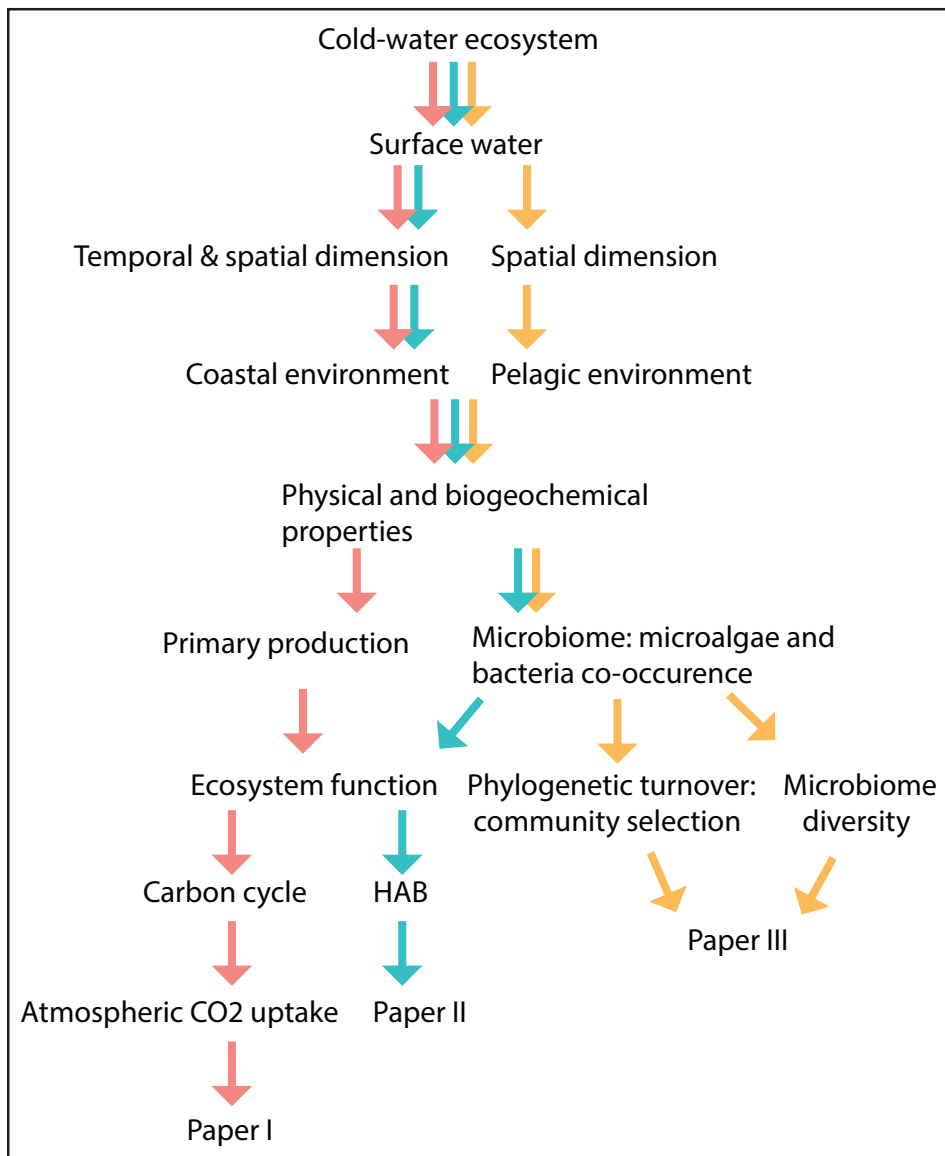


Figure 1. A conceptual presentation of the topics covered in this thesis work. Ecological processes of surface associated microbial communities in cold, marine environments is the main, connecting theme of this thesis. Both physical environment and biological components were used to answer the research questions of each study. The color denotes the thematic pathway of each study (red, Paper I; blue, Paper II; yellow, Paper III).

3 Methods

3.1 Fieldwork

There are two main study areas in this thesis work: the northern Norwegian coastal area (Paper I and Paper II), and the Arctic Ocean (Paper III; Figure 2). The studies conducted in the coast of northern Norway comprise both temporal and spatial dimensions. To answer the question on air-sea CO₂ flux magnitude and variability in time and space (Paper I), fieldwork was carried out in four fjords (Porsangerfjord, Altafjord, Balsfjord and Malangen Fjord, as listed from north to south) and a coastal bay (Finnfjord Indre) in June, October, December, January/February, March/April and May 2018-2019. A destructive HAB occurred in May-June 2019 along the coast of Nordland (southern side of Lofoten archipelago) and Troms (north form Lofoten archipelago) regions. A four-week-long sampling campaign was launched in the HAB affected area to map the presence of causative agent (focal taxon: haptophyte *Chrysochromulina leadbeateri*) including eight single-time-point stations and investigate spatial and temporal dynamics of the focal taxon with associated phytoplankton and bacterial communities at two time series stations (Paper II; Figure 2). Latitudinal sampling transect from southern Barents Sea to Nansen Basin in the Arctic was conducted in July 2019 including in total six sample stations (Figure 2) comprising four distinctly defined environmental conditions to address research questions on the spatial differences in surface water microbiome (Paper III).

As this thesis work relied on field samples, the study designs were impacted by available resources. Perhaps the biggest challenge was related to temporal and spatial resolutions as we were not always able to optimize these dimensions according to biological or physical relevance. On the other hand, the best resolution was not always fully known as we studied highly dynamic environments. The realized temporal and spatial resolutions were mainly determined by logistical, time and economic issues. For Paper I we were able to combine the sampling with a coastal environment monitoring program (discontinued after the last sampling event) operated by UiT – The Arctic University of Norway with RV Johan Ruud and scheduled to measure vertical profiles of the water column at each season in four fjords (same as listed above for Paper I) at several fixed stations. The temporal frequency was therefore dictated by a scheduled monitoring program whereas, the spatial resolution could have been higher, yet with exclusion of accompanied number of fjords due to tight time schedule assigned for the monitoring cruises. We decided to utilize the unique opportunity for between fjords comparison

instead of focusing on a within fjord changes in only one or two fjords. The main sampling campaign that served Paper II was conducted from small boats (Polarcirkel, ~5 m) that allowed more independent usage of the sampling platform. Instead, the spatial coverage was limited to the locations of available boats, and the temporal frequency achievable by our manpower due to sudden and unexpected need for intense field work. The sampling for the third study (Paper III) took a place on a large research cruise with RV Kronprins Haakon. Time delay due to unexpected heavy sea-ice conditions and other occurrences with following change in the cruise plan led to a compromised spatial resolution. Nevertheless, these three studies were successful in uncovering novel results that present new knowledge on how cold marine microbial ecosystems function with respect to carbon cycling, community selection and blooming dynamics.

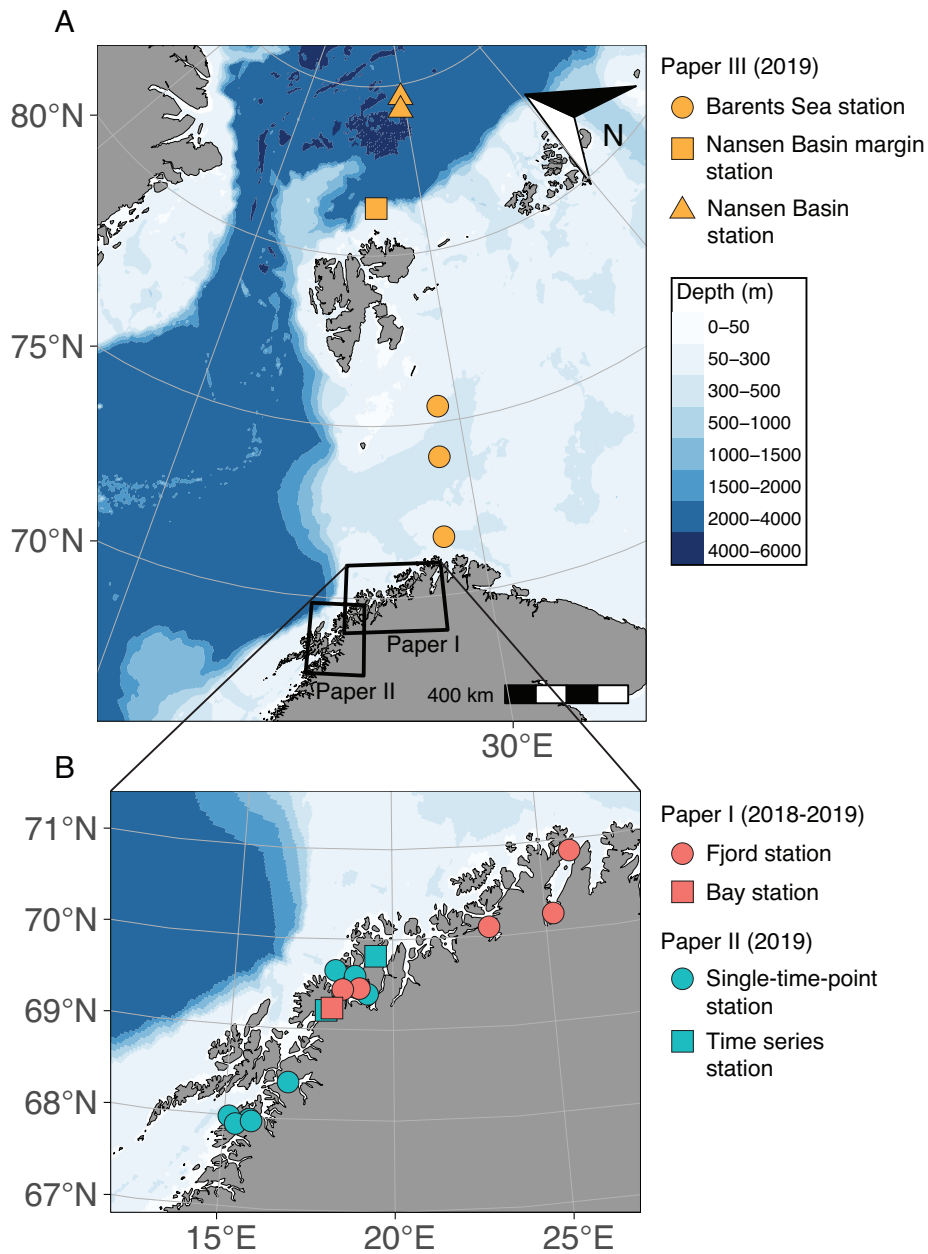


Figure 2. The geographical areas sampled to support the three studies presented in this thesis. **A)** Location of sample stations between Southern Barents Sea and Nansen Basin in the Arctic Ocean in Paper III. Black squares illustrate study areas in Paper I and Paper II along the coast of northern Norway. **B)** Stations in Paper I are marked with red and divided to fjord and coastal bay stations by shape. Paper II stations are illustrated with blue and divided by shape to single-time-point stations and two time series stations which were sampled twice a week for four weeks.

3.2 Sample and data collection

All samples were collected from surface waters at fixed depths. In Paper I the focus was at 5 m, in Paper II at 10 m depth and in Paper III at 0.5 m and 20 m depths. Biological samples for chlorophyll *a* analysis were filtered and extracted in ethanol and for phytoplankton morphology-based taxonomy and cell volume-based biomass subsamples were preserved with Lugol's iodine solution in Paper I. To investigate phytoplankton microbial communities the biomass for DNA extraction of prokaryotes and microeukaryotes was filtered and stored at -80 °C (Paper II and Paper III). The biological aspects were contextualized with abiotic conditions. Hydrographic data for vertical temperature and salinity profiles was recorded through the entire water column in Paper I and Barents Sea stations in Paper III, whereas only surface profiles down to ~50 m were measured in Paper II and in Paper III at sea-ice stations. In addition, subsamples were collected for water chemistry analysis: inorganic nutrients (Paper I–III), DOC (Paper III) and DIC (Paper III).

A portable underwater and atmospheric nondispersive CO₂-infrared detector was used to point-measure atmospheric CO₂ and pCO₂ (dissolved) in surface water at the depth of 5 m (Paper I). We also used information on daily atmospheric pressure and wind speed at time of sampling to obtain $\Delta p\text{CO}_2$ and further to calculate air-sea CO₂ flux. The values were obtained either from the nearest meteorological station or from the research vessel's automated meteorological logger. The sea-air CO₂ flux was calculated according to widely used bulk equation that relies on the difference in the partial pressure of CO₂ between the surface water and atmosphere, gas solubility (temperature and salinity) and gas transfer velocity (wind speed) (Weiss, 1974; Wanninkhof, 2014). Full details are described in Paper I.

3.3 Molecular analysis and bioinformatics

We used 16S and 18S rRNA gene based taxonomic information via amplicon sequencing to study prokaryotic and microeukaryotic communities (Paper II and Paper III). Due to rapid development of next generation sequencing techniques and availability of relatively low-cost amplicon sequencing platforms such as Illumina 16S/18S rRNA amplicon analysis has become a standard method to obtain information on microbial taxonomy to study complex microbiomes. The method has been used in global scale studies to characterize both marine and terrestrial microbiome diversities (Thompson et al., 2017; Ibarbalz et al., 2019). Since next

generation sequencing technologies produce short reads the entire 16S/18S rRNA gene is typically not amplified and sequenced. Both 16S and 18S rRNA gene contain nine variable regions (V1-V9, i.e., genetic markers) with varying conservation (Hadziavdic et al., 2014; Yang et al., 2016). Often, one or two regions are targeted with designed primer. The choice of marker gene together with chosen primer can affect the resolved taxonomy but also taxonomic resolution as differently conserved regions have distinct performance on taxonomic level identification (Bukin et al., 2019). As there is not a uniform consensus of the best performing amplicon region (marker gene) over another, the key is in consistent amplicon region and primer usage. Therefore, we followed protocols of Earth Microbiome Project (EMP, <https://earthmicrobiome.org/>) for sequencing and primer usage as these have been widely used and optimized for prokaryotes and microeukaryotes across different biomes

The downstream bioinformatics analysis has an important role regarding final output. We used the QIIME2 software application with DADA2 pipeline to process raw Illumina reads (Callahan et al., 2016). This method generates amplicon sequence variants (ASVs) which represent actual amplicon sequences with single-nucleotide resolution (Callahan et al., 2017). Several ASVs may be annotated with same taxon, thus allowing, if wanted, to study strain-level variation. Pipeline of QIIME2 combined with DADA2 has been shown to perform high sensitivity (recovery of amplicon reads) and specificity (low number of false positives) of 16S rRNA amplicon sequences (Straub et al., 2020). The final annotation of a taxonomic profile can only be as good as the reference database. For taxonomic annotation we used SILVA database which is specific for the rRNA gene. The advantage of SILVA lies on its large size, it is commonly used, regularly updated, and it improves taxonomic classification via regular curation (Pruesse et al., 2007; Robeson et al., 2021). Due to chosen biomarker gene and SILVA database properties the taxonomy is assigned in its best on genus level (Robeson et al., 2021). The usage of ready-made pipelines such as DADA2 leaves less freedom to researcher but makes the data processing faster, more transparent, and reproducible.

It is noted that the information provided by 16S/18S rRNA gene itself is somewhat limited since it does not reveal a functional role of members in the community or in the ecosystem. However, the usefulness, in addition to characterizing differences in community composition and diversity in time and space, is linked to inferences of dynamic patterns among community members which enable predictions on different type of interactions between organisms (Fuhrman et al., 2015). Thus, the ecological information obtained from 16S/18S rRNA gene

amplicon sequence analysis depends heavily on study design, contextualizing environmental data and statistical approaches.

3.4 Data analysis

A wide array of data analysis methods were used to answer the research questions in this thesis work. Most of the applied statistical methods are well established implementations of correlation and multivariate analyses. Our aim was to use statistical inferences to gain deeper understanding of the ecosystems studied in Papers II and III and not just conduct descriptive level studies. However, the spatial and temporal resolution in Paper I was considered too low to either estimate an annual atmospheric CO₂ uptake or to quantify contribution of abiotic and biotic factors on surface water pCO₂. Thus, this study stayed at a more descriptive level with respect to air-sea CO₂ flux along the coast of northern Norway.

3.4.1 Microbiome community analyses

16S/18S rRNA amplicon sequencing data reveals information on community membership (community composition) and community member abundance in relation to abundance of other members (community structure). Thus, the information on abundance is compositional and does not give evidence for absolute abundances (i.e., cell number or biomass). The type of information gathered depended on the specific research question. For example, in Papers II and III, we mainly based community analysis on community composition rather than on the abundance information. This was because the community structure can be highly time dependent, thus the results represent – especially in time limited data set (as in Paper III) – i.e., only the time of sampling campaign. Moreover, the common taxa are over emphasized and therefore inferred to play a stronger role in the results (Anderson et al., 2011). In paper III our main research questions targeted specifically taxonomic pool whereas in Paper II both types of community information were important regarding the questions we asked on spatial and temporal community dynamics, but the latter was targeted with specific analysis (described below). In addition, we used multiple measures that apply phylogenetic relatedness with the community composition information (observed taxa are placed on a phylogenetic tree) to link these measures together. These measures were: Faith's phylogenetic diversity (Paper III) as an alpha diversity metric to obtain information within a single community; Unweighted UniFrac metric (Paper II and Paper III) to measure dissimilarity between community compositions (beta

diversity); and beta-nearest-taxon-index as a community turnover inference (Paper II; described below).

The statistical inferences that incorporate information on community structure (i.e., relative abundances) were linear discriminant analysis of effect size (LEfSe; Paper III) and k-medoid clustering (Paper II). LEfSe is a differential abundance analysis that was originally developed for metagenomic biomarker discovery in clinical practice (Segata et al., 2011). However, it has been found to be a useful tool in microbial ecology to analyze communities under variable environmental conditions. The importance of LEfSe lies on its capacity to detect differentially represented rare taxa. Often the rare taxa in environmental communities are overlooked because of their low number and instead emphasis on the most abundant taxa. LEfSe analysis consists of three parts: Kruskal Wallis rank sum test, pairwise Wilcoxon test and rank of features. These steps are described in detail in Paper III. We used LEfSe to infer differentially abundant taxa in distinct environment conditions between southern Barents Sea and Nansen Basin (Paper III). As LEfSe is a relative abundance metric the results are highly time dependent because marine microbiome communities tend to undergo short-term temporal fluctuations in abundance (Martin-Platero et al., 2018). Therefore, the results cannot be generalized as they may represent only the situation at the time of sampling.

K-medoid clustering was used to determine prevalent temporal dynamics of members within prokaryotes and microeukaryotes in time series data set (Paper II). Prior to clustering the abundance data was z-transformed i.e., abundance values were converted into a z-scores, to make samples comparable by placing the taxa along a standard normal distribution. K-medoid is a distance-based (here Euclidean distance was used) clustering method that divides abundance patterns of taxa into groups i.e., clusters. The algorithm uses a randomly selected taxon as a medoid, representative for the cluster, and then partitions the other taxa to the nearest medoid in a way that the within cluster dissimilarity decreases and correspondingly between cluster dissimilarity increases (Kaufman and Rousseeuw, 1987). The difficult part is to define the number of clusters to obtain a balance between fitting and overfitting of the data. The goodness of a clustering structure can be evaluated by validation measures (Liu et al., 2010). We used a Calinski-Harabasz index in which the validation of number of clusters is based on the ratio of differences in between- and within-cluster sum of squares (Caliński and Harabasz, 1974). The final number of clusters was defined at the point where the between-cluster

difference does not anymore decrease even though the number of clusters increases (Coenen et al., 2020).

3.4.2 Correlation and multivariate analyses

Elucidation of the effect of abiotic and biotic factors on $\Delta p\text{CO}_2$ and air-sea CO_2 flux was based Spearman's nonparametric measure of rank correlation and multivariate redundancy analysis (RDA; Paper I). Whereas the relationship between the main temporal dynamics of prokaryotes and microeukaryotes and environmental factors was determined with Pearson's correlation (Paper II). The beta-diversity of microbial communities was visualized and contextualized with environmental measurements using distance-based RDA (dbRDA) that allows usage of dissimilarity metric (Unweighted UniFrac; Paper II and Paper III). The (db)RDA ordination analysis summarizes the variation in response variables ($\Delta p\text{CO}_2$, air-sea CO_2 flux and beta-diversity) that can be explained by the included set of environmental measurements (explained in detail in Paper I Figure 5).

3.4.3 Null model analysis

To disentangle dominating community selection process governing spatial phylogenetic diversity (Paper III) we quantified beta-nearest-taxon-index that provides inference on phylogenetic turnover via null model-based comparison of randomized and observed phylogeny (Stegen et al., 2012). The method is described in more detail in the conceptual presentation in Figure 3.

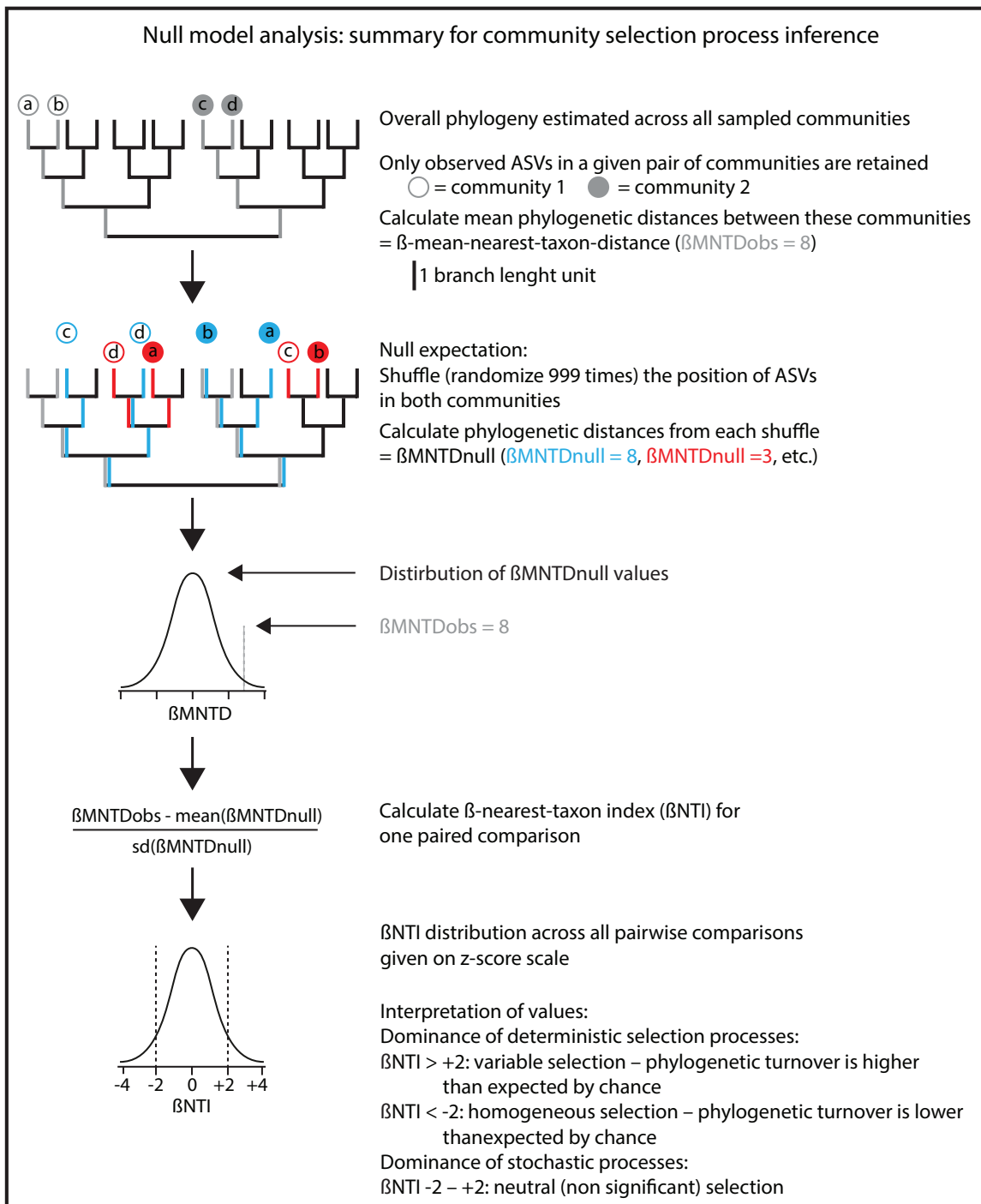


Figure 3. A graphical illustration of steps of null model analysis for determining phylogenetic turnover on community composition. The figure is modified from Figure 2 in Stegen et al., 2012 and the interpretation of results is also based on the given definitions in the same study.

4 Key findings

4.1 Paper I

Drivers of Atmosphere-Ocean CO₂ flux in Northern Norwegian Fjords.

Aalto NJ, Campbell K, Eilertsen HC and Bernstein HC

The northern Norwegian fjords and coastal region have a potential for strong atmospheric CO₂ uptake. This paper assesses the seasonal dynamics of $\Delta p\text{CO}_2$ and air-sea CO₂ flux in relation to fjord specific biological, physical and biogeochemical conditions. Thematically this study stands more on its own than the Papers II and III, yet it relates to the overarching theme of this thesis by describing spatial and temporal variability in high-latitude cold-water systems with focus on the importance and dynamics of phytoplankton primary production and localized environmental conditions.

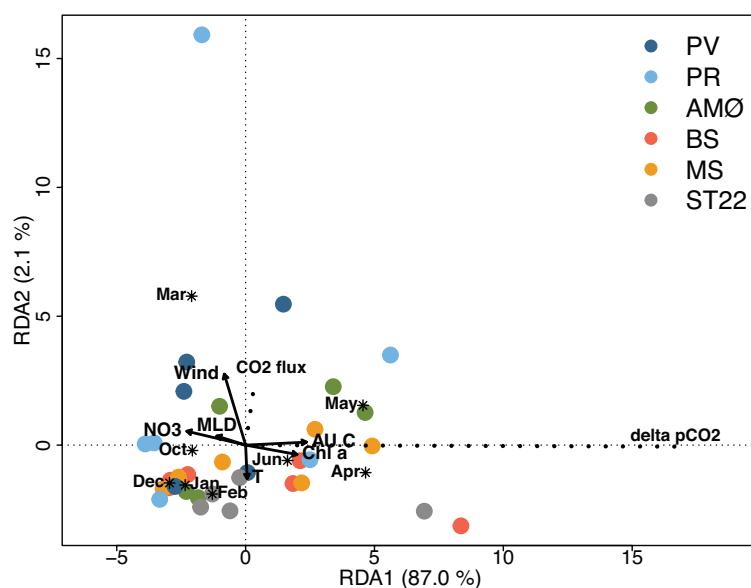


Figure 3. A triplot showing RDA ordination analysis. The eigenvalue of axis 1 (RDA1) and axis 2 (RDA2) are 0.870 and 0.021, respectively, accounting for 89.1 % of the total variance. CO₂ flux and $\Delta p\text{CO}_2$ represent species (scaled by eigenvalues) and are indicated with dashed lines. Site scores (sampling events) are weighted average of species scores (wa scores) and marked with shapes per station. Quantitative environmental factors are indicated by arrows and qualitative environmental factor (month) by asterisk (*) as centroid (weighted average) of site points belonging to the month. The scale marks along the axes apply to qualitative environmental variables and species; quantitative environmental scores were multiplied by 3 to fit in the coordinate system. Stations are marked with different colors. This figure is borrowed from Paper I (Figure 6).

Key findings:

1. Highly productive cold-water fjords and coastal areas act as sinks for atmospheric CO₂ throughout the year. This is driven by surface water undersaturation of pCO₂ with respect to atmospheric CO₂. Local wind speed had the greatest effect on temporal and spatial variability and magnitude in air-sea CO₂ flux.
2. Strong CO₂ fixation by primary producers controlled $\Delta p\text{CO}_2$ from April to June. Whereas reduction of stratification and increase in temperature had the negative effect on $\Delta p\text{CO}_2$ in autumn and early winter.
3. The factors responsible for wintertime undersaturation were not fully identified but are likely related to low temperature, the fate of biologically fixed CO₂ and fjord specific water circulation pattern.

4.2 Paper II

Microbial community dynamics during a harmful *Chrysochromulina leadbeateri* bloom.

Aalto NJ, Schweitzer HD, Gran-Meyer E, Krsmanovic S, Svenning JB, Dalheim L, Petters S, Ingebrigsten R, Hulatt CJ and Bernstein HC.

Most of the harmful algae species are natural members of complex and seasonal microbial communities. Therefore, understanding the natural variability of microbiome succession patterns is a prerequisite for predictive efforts on sporadically reoccurring HAB incidents. In this paper the temporal dynamics of early summer phytoplankton bloom and associated microbiome was investigated during a harmful *Chrysochromulina leadbeateri* bloom.

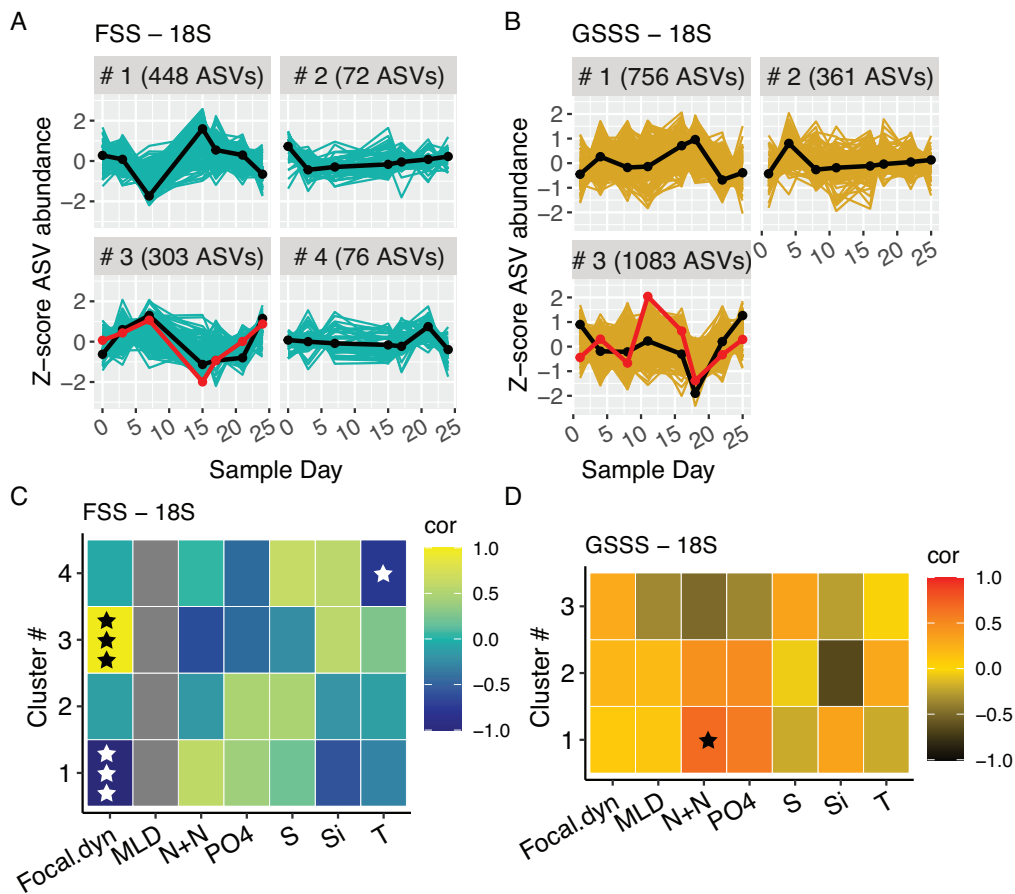


Figure 4. Characterization of major blooming patterns in microeukaryotic communities assessed by k-medoid clustering analysis with z-transformation and detrending of 18S ASVs at two time series stations, FSS and GSSS located ~60 km apart from each other, during *C. leadbeateri* bloom in the northern Norwegian coast. Temporal dynamics of microeukaryotic taxa and number of ASVs per defined cluster **A**) in FSS and **B**) in GSSS station. The blooming pattern of each cluster is specified by medoid taxon and drawn with black line. The red line specifies the blooming pattern of focal ASV. Y-axis is a z-score and a value 0 denotes the mean abundance. Heatmap of Pearson's correlation between temporal dynamics of medoid taxon (z-scores) of each cluster and focal ASV (z-scores) and environmental factors **C**) in FSS and **D**) in GSSS. Color indicates Pearson's correlation coefficient according to the color legend and level of significance is marked with ★ (★, $p \leq 0.1$; ★★, $p \leq 0.05$; ★★★, $p \leq 0.001$). The grey color for MLD in FSS denotes undefined correlation as MLD values remained the same through the study period. Focal.dyn, temporal dynamic of focal ASV; MLD, mixed layer depth; N+N, $\text{NO}_2^- + \text{NO}_3^-$; PO4, PO_4^{3-} ; S, salinity; Si, Si(OH)_4 ; T, temperature. This figure is borrowed from Paper II (Figure 4).

Key findings:

1. The early summer phytoplankton community structure was highly localized across the HAB affected area along in the northern Norway.
2. Most of the taxa including the most abundant community members and focal taxon (representing an isolate collected from the harmful *Chrysochromulina leadbeateri* bloom from 1991) revealed a strong fluctuation in their temporal succession dynamics.
3. The temporal succession dynamics were poorly connected to the measured environmental conditions suggesting that biological interactions may play an important role in late spring bloom dynamics.

4.3 Paper III

Diversity and selection of surface marine microbiomes in Atlantic-influenced Arctic.

Aalto NJ, Krsmanovic S, Schweitzer HD, Campbell K and Bernstein HC

Cold-water marine environments potentially select for similar phylogenetically related taxonomic composition. Observable differences in relative abundances of community members are likely driven by factors other than temperature. This paper investigated differences in surface microbiome diversity, community composition and structure in relation to transition from high-to-low Atlantic water influence and simultaneously changing environment conditions such as sea-ice condition, temperature, salinity and biogeochemical properties from southern Barents Sea to high-Arctic Nansen Basin.

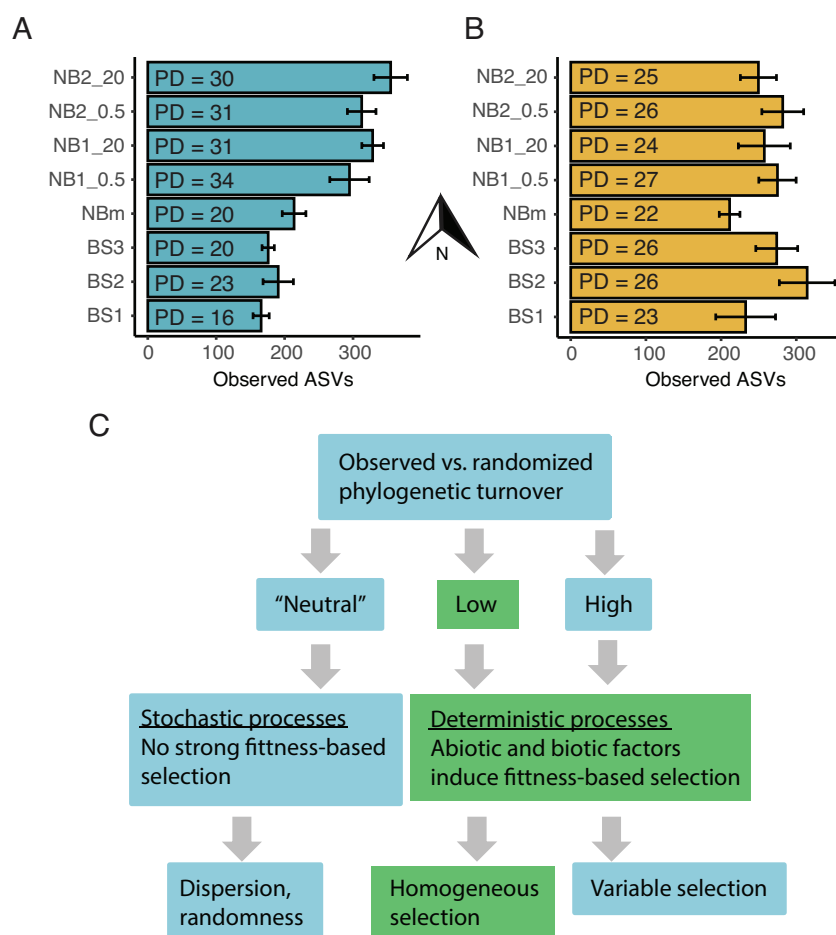


Figure 5. Patterns of alpha diversity along the studied transect and a conceptual diagram illustrating how phylogenetic turnover is used to infer ecological community selection. The prokaryotic **A**) and microeukaryotic **B**) richness measured as the observed number of ASVs with error bars indicating standard deviation of $n = 6$. The arrow denotes a northward direction of sample stations. Faith's Phylogenetic Diversity (PD) values are shown over the bars. **C**) Green color shows pathway of results through null model simulation for both 16S and 18S data set.

Key findings:

1. The microbial species richness and phylogenetic diversity (Faith's PD) were not negatively influenced by northward decreasing temperature and salinity. Prokaryotic alpha diversity increased towards north whereas microeukaryotic diversity did not reveal a latitudinal trend.
2. Regional phytoplankton blooms were identified as a major prevalent factor governing the bacterial community structure whereas the community structure of these blooms was connected to environmental differences.
3. Both prokaryotes and microeukaryotes of the surface marine microbiome were subjected to deterministic homogeneous selection, which is an indication for the presence of strong environmental selection that was consistent regardless of geographic assignments, Barents Sea vs. Nansen Basin, or influence of different water type: Atlantic Water vs. Polar Surface Water.

5 Discussion, synthesis and perspectives

This thesis work is centered around cold-water marine phytoplankton and bacterial communities with the aim to enhance understanding with respect to the carbon cycle, community dynamics and community selection within abiotic and biotic conditions in coastal nearshore and pelagic environments. Within these themes, the knowledge gaps were targeted to address both spatial and temporal dimensions of cold-water marine microbiomes to provide an important base for future studies. In Paper I we investigated atmospheric CO₂ sinks and sources in several cold-water, but not glacial or sea-ice influenced, fjords in northern Norway, a region where the topic has been inadequately surveyed. In the same region, the Paper II characterized for the first-time full diversity of phytoplankton microbial communities around *Chrysochromulina leadbeateri*-related HAB following the late phytoplankton bloom spatial and temporal succession dynamics which has received little attention. In Paper III, we used a randomized community phylogenetic relatedness analysis, which has not been used in marine cold-water environments, to provide insight into the ecological components underlying selection and patterns of microbial diversity along an environmental gradient in the Arctic Ocean from southern Barents Sea to Nansen Basin.

5.1 Temporal and spatial variation in northern Norwegian coastal area

We observed both similarities and differences between locations along the northern Norwegian fjords and coastal area (Paper I and Paper II). Strong seasonal variation in physical and biological processes and concentrations of inorganic nutrients was apparent across the region although the temporal sample coverage enabled only two-season separation: winter and spring-early summer (Paper I).

5.1.1 Phytoplankton blooms

In terms of what is known about the phytoplankton spring blooms our results are in accordance with previous studies performed in the region. The spring bloom initiated in relatively weakly stratified water columns and the phytoplankton biomass was lower in the two northernmost fjords, Altafjord and Porsangerfjord, than in the southern part of the study region (Eilertsen and Taasen, 1984; Eilertsen et al., 1995; Eilertsen and Frantzen, 2007). In those stations that were sampled in April the major diatom taxa corresponded well with previous reports (Eilertsen et al., 1981; Degerlund and Eilertsen, 2010). While the abundance of often dominating and

characteristic species for the region, prymnesiophyte *Phaeocystis* sp. (most likely *P. pouchetii*) was surprisingly low in several sample stations (Paper I and Paper II). Cell concentration of 500 000-700 000 cells L⁻¹ was noted briefly only in three stations (Paper I, data not shown). *Phaeocystis* sp. is known to undergo interannual variation and stochastic co-occurrence with diatoms, so it is possible that 2019 was a year when its presence was lower than was expected based on previous reports from the region (Eilertsen et al., 1981; Degerlund and Eilertsen, 2010). However, one could think whether it was a coincidence that in the same growth season a harmful *C. leadbeateri* associated bloom emerged. The 18S rRNA gene amplicon data revealed that, especially in those samples where *C. leadbeateri* was abundant, the presence of *Phaeocystis* sp. was a minor (Paper II). With the available data set the question remains purely speculative but perhaps it is something that could be followed up in the future studies.

Our results from the late bloom (May-June) showed highly localized and variable communities, not only at low but also high taxonomic level (Paper I and Paper II). These findings on patchy communities in a local scale are in contrast of the consensus about spring bloom that is considered to be formed rather a constant and reassemble community composition (Eilertsen et al., 1981; Degerlund and Eilertsen, 2010). It is clear, that the communities in northern Norwegian coastal area are more diverse than has been reported so far. Bringing molecular methods for ascertaining taxonomy to the region that has a long history relying on morphology-based data with a focus on the most abundant species or only certain pre-determined groups will certainly improve the current knowledge on diversity and community dynamics. The new data presented here – and in future studies that may build from this work – provide valuable information on species associations and amplify the current knowledge about ecological state as the data provides more refined results in terms of functional diversity i.e., observable richness, and inferred species importance. This also means that there may be a need to revise the current understanding of environmental processes governing the (local scale) community variability along the northern Norwegian coast.

5.1.2 CO₂ undersaturation and wind speed-controlled magnitude of CO₂ flux

The average, minimum and maximum values of $\Delta p\text{CO}_2$ per station were relatively similar among fjords and a coastal bay even though two-fold differences were obtained between some stations. Yet a station with the lowest minimum value did not correspondingly hold the lowest maximum value (Figure 1 in Paper I). This may be considered somewhat surprising because

the estimated primary production and river flow, considered often as important factors with respect to surface $p\text{CO}_2$, were rather variable between fjords. Evidence suggest that the contribution of terrestrially derived organic matter is low in northern Norwegian fjords compared to southern Norwegian and high-Arctic fjords – i.e., most of the organic carbon is produced in the system or has marine origin (Włodarska-Kowalczyk et al., 2019). Thus, it is possible that variable freshwater inputs do not create substantial difference in terms of terrestrial organic carbon content including following remineralization nor pronounced salinity and inorganic nutrient differences between fjords (Paper I). In addition, a good communication to adjacent coastal sea as has been reported for the studied fjords (Reigstad and Wassmann, 1996; Eilertsen and Skarðhamar, 2006) may flatten the major local differences within factors driving $p\text{CO}_2$ in surface water. Unfortunately, DOC analysis was not included in Paper I or Paper II to support this hypothesis. Without monthly sampling we were not able to quantify the contribution of different drivers on $\Delta p\text{CO}_2$ that would have helped to distinguish the level of importance of distinct physical and biological factors and to better understand how the between fjord variability is connected to observed variation in the strength of undersaturation.

Large-scale wind field has been recognized as an important factor controlling physical processes including regional atmospheric CO_2 uptake potential and fjord specific circulation and advection together with topography and fresh water supply (Svendsen, 1995; Chen et al., 2013). In Paper I the results revealed that even small differences in local wind speeds can have subsequent impact on the magnitude of air-sea CO_2 flux. As we used gas transfer velocity parameterization in which wind speed has a quadratic relation to CO_2 flux small changes in wind speed has a large impact, especially in spring-summer when undersaturation is strong. At most of the stations, CO_2 flux correlated with wind speed but with only 5-6 sampling campaigns it is not possible to conclude how the seasonal patterns of wind speed and CO_2 flux are related (Figure 5 in Paper I). Also, the prevailing wind direction along the coast shifts between summer and winter (Svendsen, 1995). In high-latitude coastal seas the seasonal variation of CO_2 flux is opposite to wind speed due to strong contribution of $\Delta p\text{CO}_2$ (Roobaert et al., 2019). Based on the results, it seems that the larger northernmost fjords have a higher CO_2 uptake as resulted from elevated wind speed compared to southern portion of the study region but due to limited temporal coverage it is difficult to say how extensive the difference would be in an annual scale.

A possible critique of this work may be that we missed a good opportunity to estimate the annual atmospheric CO₂ sink for the studied region. However, we did not feel confident to calculate regional or even fjord specific CO₂ uptake due to low temporal and spatial sample frequency that would likely lead to a high uncertainty. Especially because the summer and autumn months were poorly sampled, a time when surface water undergoes pronounced changes in physical and biological conditions. Annual CO₂ uptake has been calculated from monthly sampling using multiple sample points across a smaller fjord in the same region as was investigated in Paper I (Jones et al., 2020). The results of this previous study indicate that differences in surface pCO₂ and air-sea CO₂ flux between inner and outer part of the fjord were rather small and the middle station represented intermediate values. Thus, the spatial coverage does not necessarily need to be extremely high to capture within fjord variation with a sufficient level. Although for future studies that may build upon these investigations, it is good to keep in mind that specific wind fields can promote localized upwelling events in within fjord scale (Svendsen, 1995).

5.2 Phytoplankton mediated microbial communities

Phytoplankton species specific dissolved organic matter (DOM) is the major driver of co-blooming prokaryotic community structure (Teeling et al., 2012; Raina et al., 2022). Approximately half of the bacteria taxa responding to phytoplankton derived DOM are specialists, forming a specific association with phytoplankton. While the other half is more generalist responding to DOM derived from distinct species (Raina et al., 2022). Even though specific interactions and thus synchronized co-occurrence are known to be present, their characterization in species rich communities is difficult as it became apparent from the results of Paper II and Paper III. However, much of the current knowledge on co-occurrence and even associations between phytoplankton and bacteria have been obtained from studies investigating natural bloom dynamics (Teeling et al., 2012; Needham and Fuhrman, 2016; Teeling et al., 2016; Martin-Platero et al., 2018).

We examined microbial communities both in temporal (Paper II) and spatial (Paper II and Paper III) dimensions. Since spatial studies capture only a snapshot of variable community dynamics, the interpretation regarding community differences relies in large extent on environmental conditions in a way that phytoplankton community is directly linked to abiotic

conditions and bacteria community indirectly through phytoplankton bloom phenology. Phylogenetically closely related prokaryotic taxa have been assumed to have similar niche preferences due to similar functionality (role in the environment) (Losos, 2008). It has also been shown that there are highly consistent associations between specific clades of bacteria (genus or above) with different groups of microeukaryotes. Yet at the lowest taxonomic level (ASV or operational taxonomic unit) significant spatial and temporal differences occur even between algal strains (Ajani et al., 2018; Ahern et al., 2021). We followed this information to define the main differences in prokaryotic communities in relation to corresponding microeukaryotic communities (Paper II and Paper III).

One advantage of spatial studies is that they establish gradual changes of community patterns across measurable environmental gradients and geographical distances. In Arctic surface waters this is challenging because the observed changes are quickly intertwined with nearly opposite growth conditions, especially when both Atlantic- and Polar-influenced waters are targeted, due to presence of sea-ice from which it follows that microeukaryotic communities are subjected to low irradiance. Therefore, we also applied statistical inference that does not directly rely on environmental conditions to understand more about mechanisms governing the spatial patterns of microbial communities across Arctic (Paper III; discussed below).

Temporal data, with the help of statistical partitioning, allows investigations to distinguish co-varying abundance patterns. Thus, it can be considered as a promising approach, for instance, to identify biological mechanisms involved to development and course of harmful algae blooms, as was demonstrated in Paper II. The outcome, however, was somewhat more limited than desired. Certainly, the defined temporal blooming patterns were variable and most of the community members, both microeukaryotes and prokaryotes, underwent substantial fluctuation in their abundances. Yet unexpectedly high number of taxa partitioned into same k-medoid clusters hindering signs on specific interactions. It is unclear why we did not distinguish more coherent groups of co-varying taxa as has been the case in previous studies (Needham and Fuhrman, 2016; Martin-Platero et al., 2018), but it may be possible that the time series data, dictated by the *C. leadbeateri* bloom, covered too short period of time and/or was limited in its temporal frequency.

There are contradicting results whether the closely related prokaryotic taxa follow similar temporal patterns (Andersson et al., 2010; Martin-Platero et al., 2018). This question was

beyond the scope in Paper II however, our time series data indicate that most of the members from same order, except the most abundant orders such as *Flavobacteriales* and *Rhodobacterales*, were partitioned to the same k-medoid cluster – i.e., tended to follow similar temporal dynamics (Figure 5 in Paper II). Correspondingly the microeukaryotic members belonging to the same class mainly had similar abundance patterns with dinoflagellates as a major exception (Figure 4 in Paper II).

The defined temporal patterns of microeukaryotes and prokaryotes correlated poorly with environmental measurements in Paper II. Thus, this implies in the accordance with suggestions of previous studies that in order to obtain a comprehensive understanding of HABs or temporal variation in microbiome structure in general the focus should be in biological associations and not only in environmental measurements (Needham and Fuhrman, 2016; Martin-Platero et al., 2018; Telesh et al., 2021). The presented study, therefore, may act as a motivation to conduct future studies along the coast of northern Norway but also elsewhere using a holistic microbiome approach when intending to improve the understanding of HAB associated species. Also, the Paper II mapped the presence of *C. leadbeateri* across a large area in distinct coastal habitats which may help to design the future studies with the aim to resolve natural blooming cycles of this sporadically destructive species.

5.3 Cold-water driven microbiomes

The phylogenetic inferences in Paper III suggest that there are no divergent selective forces between Atlantic- and Polar-dominated surface waters which would drive high turnover between communities. As there is a strong deterministic homogeneous selection across the study transect between southern Barents Sea to high Arctic in Nansen Basin, these two seemingly highly distinct environments yet not impose unique environmental features with respect to selection, but instead the observed species pool (members of community) in each community covers similar parts of phylogeny. This of course does not necessarily mean that the community members are same. We revealed high number of exclusive ASVs per environment conditions (Figure 4 in Paper III), but the key is that these ASVs were not distinctly clustered.

Although the results presented in the Paper III do not directly confirm it, we suggest that temperature may be the main environmental filter – i.e., homogeneous selective force, on cold-water marine microbiomes. Therefore, phytoplankton microbial communities could be in common called as cold-water communities instead of using biogeographical categories of Atlantic and Arctic to define community distributions. This is in accordance with conclusions from a regional study by Degerlund and Eilertsen (2010) and global-scale study by Martin et al. (2021). The latter study based on taxonomic beta diversity and metatranscriptomics across pole-to-pole gradient found evidence for differentiation in microbial community composition but also gene expression activity between polar and non-polar oceans in relation to significant temperature related break-points. This two-regime separation where overall environmental differences are stronger than between any other oceanic regions, was suggested to be driven by strong seasonality, low temperatures, presence of sea-ice and seasonal mixing at the polar side (Martin et al., 2021). While Degerlund and Eilertsen (2010) used collected and historical data reaching from northern Norwegian fjords (60 °N) and coastal area to Arctic Barents Sea (80 °N) and found that the same diatom species that thrive in the sea-ice edge blooms in the Arctic Barents Sea are also highly abundant in northern Norwegian fjords and coastal waters. Correspondingly they suggested the usage of term cold-water species and concluded that the observed distribution pattern is enabled by species plasticity over the temperature range which is along the coast of northern Norway very similar to what we observed between southern Barents Sea and Nansen Basin.

The Paper III demonstrates how the inferences on processes of community ecology can be utilized to explain observed patterns of microbiome diversity to obtain a better understanding on the importance of environmental conditions driving these cold-water associated communities in the Arctic. It is noted that the spatial coverage was low and temporarily limited in Paper III, therefore we used presence/absence information instead of relative abundances of community members because the presence of a species is likely more long lasting than its certain state of abundance as was shown in Paper II. As the presented study uncovered the processes of community selection on the lowest level of community information, it provides “a base line” on which the future studies with higher temporal resolution may build upon to integrate abundance information within the context of community ecology to infer the real-time role of Atlantification and environmental heterogeneity to community structure and following ecosystem function.

6 Conclusion

This thesis work comprises seasonal, time series and spatial studies in the cold-water ecosystems with the aim to provide new insights on the coastal atmospheric CO₂ sinks and sources and the surface microbiomes in relation to carbon cycle, community dynamics and community selection within their physical environment. The coast of northern Norway is a unique area to study nearshore cold-water ecosystem processes such as atmospheric carbon uptake and spatiotemporal microbiome community dynamics since it is not very heavily influenced by terrestrial and freshwater inputs or sea-ice/glacial conditions. From this area the findings revealed that the studied fjords and a coastal system act as a sink for atmospheric CO₂ due to CO₂ undersaturation with respect to atmospheric CO₂. The undersaturation instead was strongly driven by primary productivity but presumably also fjord specific oceanographical properties. The first insights of holistic microbiome approach in the coastal habitats of northern Norway indicate that even though the processes and interannual variation related to the onset of spring bloom as well as primary species composition is well documented there is still much of uncovered processes and functionality with respect to spatial variation and high-resolution temporal dynamics of late spring bloom phytoplankton and associated microbial communities. We demonstrated highly localized communities and strong temporal variation in the abundance patterns of co-occurring microeukaryotes and prokaryotes. Across the Eurasian Arctic the samples were collected within a short frame (two weeks) which is uncommon among previous studies conducted in the Arctic. Thus, the study provides a temporarily synchronous overview on (dis)similarities of the surface microbiomes – community structure and phylogenetic relatedness – between southern Barents Sea and high-Arctic Nansen Basin. The result of phylogenetic turnover infers that similar phylogenetic relatedness of microbiomes across the study area is driven by strong deterministic homogeneous selection regardless of northward decreasing temperature, variable sea-ice conditions, and water type.

As a summary our findings demonstrate that both large scale and local studies are important to form the needed comprehensive understanding of these microbial ecosystems as the regional taxonomic pool is determined by fundamental ecological processes but community structure influencing ecosystem function is instead subjected to more localized variation of abiotic and biotic factors. The presented thesis work filled spatial and/or temporal knowledge gaps with respect to the topics covered in this thesis. Thus, the findings establish missing “base lines” on which the future studies can be built upon to obtain a more comprehensive understanding on

the relation between cold adapted microbial communities and their environment. This information is valuable and has an importance because the cold-water ecosystems are under transition due to Atlantification, warming and expected enhancement of land-sea connectivity.

7 References

- Aalto, N.J., Campbell, K., Eilertsen, H.C., and Bernstein, H.C. (2021). Drivers of atmosphere-ocean CO₂ flux in northern Norwegian fjords. *Frontiers in Marine Science*, 841. doi: 10.3389/fmars.2021.692093.
- Ahern, O.M., Whittaker, K.A., Williams, T.C., Hunt, D.E., and Rynearson, T.A. (2021). Host genotype structures the microbiome of a globally dispersed marine phytoplankton. *Proceedings of the National Academy of Sciences* 118(48), e2105207118.
- Ajani, P.A., Kahlke, T., Siboni, N., Carney, R., Murray, S.A., and Seymour, J.R. (2018). The Microbiome of the Cosmopolitan Diatom *Leptocylindrus* Reveals Significant Spatial and Temporal Variability. *Frontiers in Microbiology* 9. doi: 10.3389/fmicb.2018.02758.
- Amin, S.A., Hmelo, L.R., van Tol, H.M., Durham, B.P., Carlson, L.T., Heal, K.R., et al. (2015). Interaction and signalling between a cosmopolitan phytoplankton and associated bacteria. *Nature* 522(7554), 98-101. doi: 10.1038/nature14488.
- Anderson, M.J., Crist, T.O., Chase, J.M., Vellend, M., Inouye, B.D., Freestone, A.L., et al. (2011). Navigating the multiple meanings of β diversity: a roadmap for the practicing ecologist. *Ecology letters* 14(1), 19-28.
- Andersson, A.F., Riemann, L., and Bertilsson, S. (2010). Pyrosequencing reveals contrasting seasonal dynamics of taxa within Baltic Sea bacterioplankton communities. *The ISME Journal* 4(2), 171-181.
- Ardyna, M., and Arrigo, K.R. (2020). Phytoplankton dynamics in a changing Arctic Ocean. *Nature Climate Change* 10(10), 892-903.
- Arias, P., Bellouin, N., Coppola, E., Jones, R., Krinner, G., Marotzke, J., et al. (2021). Climate Change 2021: The Physical Science Basis. Contribution of Working Group I to the Sixth Assessment Report of the Intergovernmental Panel on Climate Change; Technical Summary.
- Årthun, M., Eldevik, T., Smedsrud, L., Skagseth, Ø., and Ingvaldsen, R. (2012). Quantifying the influence of Atlantic heat on Barents Sea ice variability and retreat. *Journal of Climate* 25(13), 4736-4743.
- Assmy, P., Fernandez-Mendez, M., Duarte, P., Meyer, A., Randelhoff, A., Mundy, C.J., et al. (2017). Leads in Arctic pack ice enable early phytoplankton blooms below snow-covered sea ice. *Sci Rep* 7, 40850. doi: 10.1038/srep40850.
- Azam, F., and Malfatti, F. (2007). Microbial structuring of marine ecosystems. *Nature Reviews Microbiology* 5(10), 782-791.
- Bernstein, H.C., McClure, R.S., Thiel, V., Sadler, N.C., Kim, Y.-M., Chrisler, W.B., et al. (2017). Indirect interspecies regulation: transcriptional and physiological responses of a cyanobacterium to heterotrophic partnership. *MSystems* 2(2), e00181-00116.
- Bluhm, B., Kosobokova, K., and Carmack, E. (2015). A tale of two basins: An integrated physical and biological perspective of the deep Arctic Ocean. *Progress in Oceanography* 139, 89-121.
- Blunden, J., and Arndt, D.S. (2016). State of the climate in 2015. *Bulletin of the American Meteorological Society* 97(8), Si-S275.
- Bratbak, G., and Thingstad, T. (1985). Phytoplankton-bacteria interactions: an apparent paradox? Analysis of a model system with both competition and commensalism. *Marine ecology progress series. Oldendorf* 25(1), 23-30.
- Bukin, Y.S., Galachyants, Y.P., Morozov, I., Bukin, S., Zakharenko, A., and Zemskaya, T. (2019). The effect of 16S rRNA region choice on bacterial community metabarcoding results. *Scientific Data* 6(1), 1-14.

- Burson, A., Stomp, M., Greenwell, E., Grosse, J., and Huisman, J. (2018). Competition for nutrients and light: testing advances in resource competition with a natural phytoplankton community. *Ecology* 99(5), 1108-1118.
- Caliński, T., and Harabasz, J. (1974). A dendrite method for cluster analysis. *Communications in Statistics-theory and Methods* 3(1), 1-27.
- Callahan, B.J., McMurdie, P.J., and Holmes, S.P. (2017). Exact sequence variants should replace operational taxonomic units in marker-gene data analysis. *The ISME journal* 11(12), 2639-2643.
- Callahan, B.J., McMurdie, P.J., Rosen, M.J., Han, A.W., Johnson, A.J.A., and Holmes, S.P. (2016). DADA2: high-resolution sample inference from Illumina amplicon data. *Nature methods* 13(7), 581-583.
- Cardozo-Mino, M.G., Fadeev, E., Salman-Carvalho, V., and Boetius, A. (2021). Spatial Distribution of Arctic Bacterioplankton Abundance Is Linked to Distinct Water Masses and Summertime Phytoplankton Bloom Dynamics (Fram Strait, 79°N). *Frontiers in Microbiology* 12(1067). doi: 10.3389/fmicb.2021.658803.
- Chen, C.T.A., Huang, T.H., Chen, Y.C., Bai, Y., He, X., and Kang, Y. (2013). Air–sea exchanges of CO₂ in the world's coastal seas. *Biogeosciences* 10(10), 6509-6544. doi: 10.5194/bg-10-6509-2013.
- Chierici, M., Vernet, M., Fransson, A., and Børsheim, K.Y. (2019). Net community production and carbon exchange from winter to summer in the Atlantic water inflow to the Arctic Ocean. *Frontiers in Marine Science* 6, 528.
- Cirri, E., and Pohnert, G. (2019). Algae–bacteria interactions that balance the planktonic microbiome. *New Phytologist* 223(1), 100-106.
- Coenen, A.R., Hu, S.K., Luo, E., Muratore, D., and Weitz, J.S. (2020). A primer for microbiome time-series analysis. *Frontiers in genetics* 11, 310.
- Croft, M.T., Lawrence, A.D., Raux-Deery, E., Warren, M.J., and Smith, A.G. (2005). Algae acquire vitamin B12 through a symbiotic relationship with bacteria. *Nature* 438(7064), 90-93.
- Davidson, K., Gowen, R.J., Tett, P., Bresnan, E., Harrison, P.J., McKinney, A., et al. (2012). Harmful algal blooms: How strong is the evidence that nutrient ratios and forms influence their occurrence? *Estuarine, Coastal and Shelf Science* 115, 399-413. doi: <https://doi.org/10.1016/j.ecss.2012.09.019>.
- de Sousa, A.G.G., Tomasino, M.P., Duarte, P., Fernández-Méndez, M., Assmy, P., Ribeiro, H., et al. (2019). Diversity and composition of pelagic prokaryotic and protist communities in a thin Arctic sea-ice regime. *Microbial ecology* 78(2), 388-408.
- Degerlund, M., and Eilertsen, H.C. (2010). Main species characteristics of phytoplankton spring blooms in NE Atlantic and Arctic waters (68–80 N). *Estuaries and coasts* 33(2), 242-269.
- Delpech, L.-M., Vonnahme, T.R., McGovern, M., Gradinger, R., Præbel, K., and Poste, A.E. (2021). Terrestrial inputs shape coastal bacterial and archaeal communities in a high Arctic Fjord (Isfjorden, Svalbard). *Frontiers in microbiology* 12, 614634.
- Dini-Andreote, F., Stegen, J.C., Van Elsas, J.D., and Salles, J.F. (2015). Disentangling mechanisms that mediate the balance between stochastic and deterministic processes in microbial succession. *Proceedings of the National Academy of Sciences* 112(11), E1326-E1332.
- Dinsdale, E.A., Edwards, R.A., Hall, D., Angly, F., Breitbart, M., Brulc, J.M., et al. (2008). Functional metagenomic profiling of nine biomes. *Nature* 452(7187), 629-632.
- Eilertsen, H.C., and Frantzen, S. (2007). Phytoplankton from two sub-Arctic fjords in northern Norway 2002–2004: I. Seasonal variations in chlorophyll a and bloom dynamics. *Marine Biology Research* 3(5), 319-332.

- Eilertsen, H.C., Sandberg, S., and Tøllefsen, H. (1995). Photoperiodic control of diatom spore growth: a theory to explain the onset of phytoplankton blooms. *Marine ecology progress series. Oldendorf* 116(1), 303-307.
- Eilertsen, H.C., Schei, B., and Taasen, J. (1981). Investigations on the plankton community of Balsfjorden, Northern Norway: the phytoplankton 1976–1978. Abundance, species composition, and succession. *Sarsia* 66(2), 129-141.
- Eilertsen, H.C., and Skarðhamar, J. (2006). Temperatures of north Norwegian fjords and coastal waters: Variability, significance of local processes and air–sea heat exchange. *Estuarine, coastal and shelf science* 67(3), 530-538.
- Eilertsen, H.C., and Taasen, J. (1984). Investigations on the plankton community of Balsfjorden, northern Norway. The phytoplankton 1976–1978. Environmental factors, dynamics of growth, and primary production. *Sarsia* 69(1), 1-15.
- Ericson, Y., Falck, E., Chierici, M., Fransson, A., Kristiansen, S., Platt, S.M., et al. (2018). Temporal variability in surface water pCO₂ in Adventfjorden (West Spitsbergen) with emphasis on physical and biogeochemical drivers. *Journal of Geophysical Research: Oceans* 123(7), 4888-4905.
- Fadeev, E., Rogge, A., Ramondenc, S., Nöthig, E.-M., Wekerle, C., Bienhold, C., et al. (2021). Sea ice presence is linked to higher carbon export and vertical microbial connectivity in the Eurasian Arctic Ocean. *Communications biology* 4(1), 1-13.
- Fadeev, E., Salter, I., Schourup-Kristensen, V., Nöthig, E.-M., Metfies, K., Engel, A., et al. (2018). Microbial Communities in the East and West Fram Strait During Sea Ice Melting Season. *Frontiers in Marine Science* 5(429). doi: 10.3389/fmars.2018.00429.
- Falk-Petersen, S., Hopkins, C., and Sargent, J. (1990). Trophic relationships in the pelagic, Arctic food web. *Trophic relationships in the marine environment*, 315-333.
- Falkowski, P.G., Barber, R.T., and Smetacek, V. (1998). Biogeochemical controls and feedbacks on ocean primary production. *science* 281(5374), 200-206.
- Frangópulos, M., Guisande, C., DeBlas, E., and Maneiro, I. (2004). Toxin production and competitive abilities under phosphorus limitation of *Alexandrium* species. *Harmful Algae* 3(2), 131-139.
- Frey, K., Comiso, J., Cooper, L., Grebmeier, J., and Stock, L.V. (2021). Arctic ocean primary productivity: The response of marine algae to climate warming and sea ice decline.
- Fuhrman, J.A., Cram, J.A., and Needham, D.M. (2015). Marine microbial community dynamics and their ecological interpretation. *Nature Reviews Microbiology* 13(3), 133-146.
- Gattuso, J., Pichon, M., and Frankignoulle, M. (1995). Biological control of air-sea CO₂ fluxes: effect of photosynthetic and calcifying marine organisms and ecosystems. *Marine Ecology Progress Series* 129, 307-312.
- Giesbrecht, I.J., Tank, S.E., Frazer, G.W., Hood, E., Gonzalez Arriola, S.G., Butman, D.E., et al. (2022). Watershed classification predicts streamflow regime and organic carbon dynamics in the Northeast Pacific coastal temperate rainforest. *Global Biogeochemical Cycles* 36(2), e2021GB007047.
- Glibert, P.M., Anderson, D.M., Gentien, P., Granéli, E., and Sellner, K.G. (2005). The global, complex phenomena of harmful algal blooms.
- Graham, C.H., and Fine, P.V. (2008). Phylogenetic beta diversity: linking ecological and evolutionary processes across space in time. *Ecology letters* 11(12), 1265-1277.
- Grebmeier, J.M., Bluhm, B.A., Cooper, L.W., Danielson, S.L., Arrigo, K.R., Blanchard, A.L., et al. (2015). Ecosystem characteristics and processes facilitating persistent macrobenthic biomass hotspots and associated benthivory in the Pacific Arctic. *Progress in Oceanography* 136, 92-114. doi: <https://doi.org/10.1016/j.pocean.2015.05.006>.

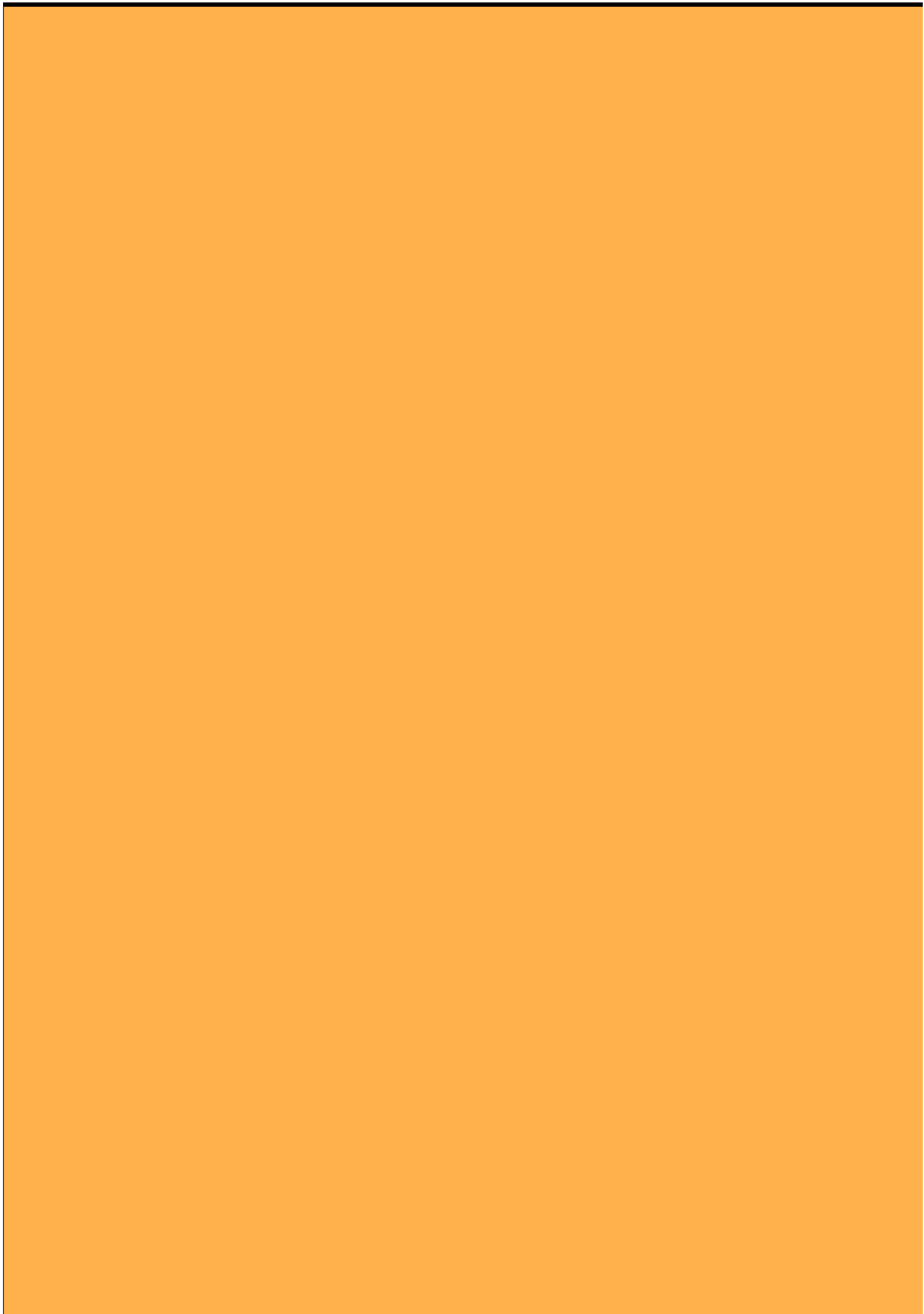
- Hadziavdic, K., Lekang, K., Lanzen, A., Jonassen, I., Thompson, E.M., and Troedsson, C. (2014). Characterization of the 18S rRNA gene for designing universal eukaryote specific primers. *PloS one* 9(2), e87624.
- Hartman, S., Hartman, M., Hydes, D., Smythe-Wright, D., Gohin, F., and Lazure, P. (2014). The role of hydrographic parameters, measured from a ship of opportunity, in bloom formation of *Karenia mikimotoi* in the English Channel. *Journal of Marine Systems* 140, 39-49.
- Holmes, R.M., McClelland, J.W., Peterson, B.J., Tank, S.E., Bulygina, E., Eglinton, T.I., et al. (2012). Seasonal and annual fluxes of nutrients and organic matter from large rivers to the Arctic Ocean and surrounding seas. *Estuaries and Coasts* 35(2), 369-382.
- Ibarbalz, F.M., Henry, N., Brandão, M.C., Martini, S., Busseni, G., Byrne, H., et al. (2019). Global trends in marine plankton diversity across kingdoms of life. *Cell* 179(5), 1084-1097. e1021.
- Jones, E.M., Renner, A.H., Chierici, M., Wiedmann, I., Lødemel, H.H., and Biuw, M. (2020). Seasonal dynamics of carbonate chemistry, nutrients and CO₂ uptake in a sub-Arctic fjord. *Elem Sci Anth* 8(1).
- Karlsen, B., Andersen, P., Arneborg, L., Cembella, A., Eikrem, W., John, U., et al. (2021). Harmful algal blooms and their effects in coastal seas of Northern Europe. *Harmful Algae* 102, 101989.
- Kaufman, L., and Rousseeuw, P.J. (Year). "Clustering by means of medoids", in: *Proceedings of the statistical data analysis based on the L1 norm conference, neuchatel, switzerland*.
- Khan, N., Maezato, Y., McClure, R.S., Brislawn, C.J., Mobberley, J.M., Isern, N., et al. (2018). Phenotypic responses to interspecies competition and commensalism in a naturally-derived microbial co-culture. *Scientific reports* 8(1), 1-9.
- Kottmeier, S.T., and Sullivan, C.W. (1988). Sea ice microbial communities (SIMCO). *Polar Biology* 8(4), 293-304.
- Kunisch, E., Graeve, M., Gradinger, R., Haug, T., Kovacs, K.M., Lydersen, C., et al. (2021). Ice-algal carbon supports harp and ringed seal diets in the European Arctic: evidence from fatty acid and stable isotope markers. *Marine Ecology Progress Series* 675, 181-197.
- Litchman, E., de Tezanos Pinto, P., Edwards, K.F., Klausmeier, C.A., Kremer, C.T., and Thomas, M.K. (2015). Global biogeochemical impacts of phytoplankton: a trait-based perspective. *Journal of ecology* 103(6), 1384-1396.
- Liu, Y., Li, Z., Xiong, H., Gao, X., and Wu, J. (Year). "Understanding of internal clustering validation measures", in: *2010 IEEE international conference on data mining: IEEE*, 911-916.
- Losos, J.B. (2008). Phylogenetic niche conservatism, phylogenetic signal and the relationship between phylogenetic relatedness and ecological similarity among species. *Ecology letters* 11(10), 995-1003.
- Martin, K., Schmidt, K., Toseland, A., Boulton, C.A., Barry, K., Beszteri, B., et al. (2021). The biogeographic differentiation of algal microbiomes in the upper ocean from pole to pole. *Nature Communications* 12(1), 1-15.
- Martin-Platero, A.M., Cleary, B., Kauffman, K., Preheim, S.P., McGillicuddy, D.J., Alm, E.J., et al. (2018). High resolution time series reveals cohesive but short-lived communities in coastal plankton. *Nature communications* 9(1), 1-11.
- Meire, L., Sogaard, D., Mortensen, J., Meysman, F., Soetaert, K., Arendt, K., et al. (2015). Glacial meltwater and primary production are drivers of strong CO₂ uptake in fjord and coastal waters adjacent to the Greenland Ice Sheet. *Biogeosciences* 12(8), 2347-2363.

- Meyer, N., Bigalke, A., Kaulfuß, A., and Pohnert, G. (2017). Strategies and ecological roles of algicidal bacteria. *FEMS Microbiology Reviews* 41(6), 880-899.
- Needham, D.M., and Fuhrman, J.A. (2016). Pronounced daily succession of phytoplankton, archaea and bacteria following a spring bloom. *Nature Microbiology* 1(4), 16005. doi: 10.1038/nmicrobiol.2016.5.
- Nielsen, T.G., Kiørboe, T., and Bjørnsen, P.K. (1990). Effects of a *Chrysochromulina polylepis* subsurface bloom on the planktonic community. *Marine Ecology Progress Series*, 21-35.
- Orkney, A., Platt, T., Narayanaswamy, B.E., Kostakis, I., and Bouman, H.A. (2020). Bio-optical evidence for increasing Phaeocystis dominance in the Barents Sea. *Philosophical Transactions of the Royal Society A* 378(2181), 20190357.
- Oziel, L., Baudena, A., Ardyna, M., Massicotte, P., Randelhoff, A., Sallée, J.-B., et al. (2020). Faster Atlantic currents drive poleward expansion of temperate phytoplankton in the Arctic Ocean. *Nature communications* 11(1), 1-8.
- Polyakov, I.V., Pnyushkov, A.V., Alkire, M.B., Ashik, I.M., Baumann, T.M., Carmack, E.C., et al. (2017). Greater role for Atlantic inflows on sea-ice loss in the Eurasian Basin of the Arctic Ocean. *Science* 356(6335), 285-291. doi: doi:10.1126/science.aai8204.
- Pruesse, E., Quast, C., Knittel, K., Fuchs, B.M., Ludwig, W., Peplies, J., et al. (2007). SILVA: a comprehensive online resource for quality checked and aligned ribosomal RNA sequence data compatible with ARB. *Nucleic acids research* 35(21), 7188-7196.
- Quere, C.L., Harrison, S.P., Colin Prentice, I., Buitenhuis, E.T., Aumont, O., Bopp, L., et al. (2005). Ecosystem dynamics based on plankton functional types for global ocean biogeochemistry models. *Global Change Biology* 11(11), 2016-2040.
- Rahmstorf, S. (2006). Thermohaline ocean circulation. *Encyclopedia of quaternary sciences* 5.
- Raina, J.-B., Lambert, B.S., Parks, D.H., Rinke, C., Siboni, N., Bramucci, A., et al. (2022). Chemotaxis shapes the microscale organization of the ocean's microbiome. *Nature* 605(7908), 132-138.
- Rapp, J.Z., Fernández-Méndez, M., Bienhold, C., and Boetius, A. (2018). Effects of Ice-Algal Aggregate Export on the Connectivity of Bacterial Communities in the Central Arctic Ocean. *Frontiers in Microbiology* 9(1035). doi: 10.3389/fmicb.2018.01035.
- Rawlins, M.A., Steele, M., Holland, M.M., Adam, J.C., Cherry, J.E., Francis, J.A., et al. (2010). Analysis of the Arctic system for freshwater cycle intensification: Observations and expectations. *Journal of Climate* 23(21), 5715-5737.
- Reigstad, M., and Wassmann, P. (1996). Importance of advection for pelagic-benthic coupling in north Norwegian fjords. *Sarsia* 80(4), 245-257.
- Reigstad, M., and Wassmann, P. (2007). "Does Phaeocystis spp. contribute significantly to vertical export of organic carbon?," in *Phaeocystis, major link in the biogeochemical cycling of climate-relevant elements*. Springer), 217-234.
- Rey, F., and Aure, J. (1991). The *Chrysochromulina leadbeateri* bloom in the Vestfjord, north Norway, May-June 1991. Environmental conditions and possible causes. *Fisk. Hav.* 3, 13-32.
- Robeson, M.S., O'Rourke, D.R., Kaehler, B.D., Ziemski, M., Dillon, M.R., Foster, J.T., et al. (2021). RESCRIPT: Reproducible sequence taxonomy reference database management. *PLoS computational biology* 17(11), e1009581.
- Roobaert, A., Laruelle, G.G., Landschützer, P., Gruber, N., Chou, L., and Regnier, P. (2019). The spatiotemporal dynamics of the sources and sinks of CO₂ in the global coastal ocean. *Global Biogeochemical Cycles* 33(12), 1693-1714.
- Rysgaard, S., Mortensen, J., Juul-Pedersen, T., Sørensen, L.L., Lennert, K., Søgaard, D., et al. (2012). High air-sea CO₂ uptake rates in nearshore and shelf areas of Southern Greenland: Temporal and spatial variability. *Marine Chemistry* 128, 26-33.

- Segata, N., Izard, J., Waldron, L., Gevers, D., Miropolsky, L., Garrett, W.S., et al. (2011). Metagenomic biomarker discovery and explanation. *Genome biology* 12(6), 1-18.
- Smayda, T.J. (1997). Harmful algal blooms: their ecophysiology and general relevance to phytoplankton blooms in the sea. *Limnology and oceanography* 42(5part2), 1137-1153.
- Smith, R.W., Bianchi, T.S., Allison, M., Savage, C., and Galy, V. (2015). High rates of organic carbon burial in fjord sediments globally. *Nature Geoscience* 8(6), 450-453.
- Smith, S., and Hollibaugh, J. (1993). Coastal metabolism and the oceanic organic carbon balance. *Reviews of Geophysics* 31(1), 75-89.
- Søreide, J.E., Leu, E.V., Berge, J., Graeve, M., and Falk-Petersen, S. (2010). Timing of blooms, algal food quality and *Calanus glacialis* reproduction and growth in a changing Arctic. *Global change biology* 16(11), 3154-3163.
- Stegen, J.C., Lin, X., Fredrickson, J.K., Chen, X., Kennedy, D.W., Murray, C.J., et al. (2013). Quantifying community assembly processes and identifying features that impose them. *The ISME journal* 7(11), 2069-2079.
- Stegen, J.C., Lin, X., Fredrickson, J.K., and Konopka, A.E. (2015). Estimating and mapping ecological processes influencing microbial community assembly. *Frontiers in Microbiology* 6. doi: 10.3389/fmicb.2015.00370.
- Stegen, J.C., Lin, X., Konopka, A.E., and Fredrickson, J.K. (2012). Stochastic and deterministic assembly processes in subsurface microbial communities. *The ISME journal* 6(9), 1653-1664.
- Straub, D., Blackwell, N., Langarica-Fuentes, A., Peltzer, A., Nahnsen, S., and Kleindienst, S. (2020). Interpretations of Environmental Microbial Community Studies Are Biased by the Selected 16S rRNA (Gene) Amplicon Sequencing Pipeline. *Frontiers in Microbiology* 11. doi: 10.3389/fmicb.2020.550420.
- Svendsen, H. (1995). Physical oceanography of coupled fjord-coast systems in northern Norway with special focus on frontal dynamics and tides. *Ecology of fjords and coastal waters*, 149-164.
- Svenning, J.B., Dalheim, L., Eilertsen, H.C., and Vasskog, T. (2019). Temperature dependent growth rate, lipid content and fatty acid composition of the marine cold-water diatom *Porosira glacialis*. *Algal Research* 37, 11-16.
- Teeling, H., Fuchs, B.M., Becher, D., Klockow, C., Gardebrecht, A., Bennke, C.M., et al. (2012). Substrate-controlled succession of marine bacterioplankton populations induced by a phytoplankton bloom. *Science* 336(6081), 608-611.
- Teeling, H., Fuchs, B.M., Bennke, C.M., Krueger, K., Chafee, M., Kappelmann, L., et al. (2016). Recurring patterns in bacterioplankton dynamics during coastal spring algae blooms. *elife* 5, e11888.
- Telesh, I., Schubert, H., and Skarlato, S. (2021). Abiotic stability promotes dinoflagellate blooms in marine coastal ecosystems. *Estuarine, Coastal and Shelf Science* 251, 107239.
- Thompson, L.R., Sanders, J.G., McDonald, D., Amir, A., Ladau, J., Locey, K.J., et al. (2017). A communal catalogue reveals Earth's multiscale microbial diversity. *Nature* 551(7681), 457-463.
- Tréguer, P., Bowler, C., Moriceau, B., Dutkiewicz, S., Gehlen, M., Aumont, O., et al. (2018). Influence of diatom diversity on the ocean biological carbon pump. *Nature Geoscience* 11(1), 27-37.
- Uribe, P., and Espejo, R.T. (2003). Effect of associated bacteria on the growth and toxicity of *Alexandrium catenella*. *Applied and environmental microbiology* 69(1), 659-662.
- Uronen, P., Lehtinen, S., Legrand, C., Kuuppo, P., and Tamminen, T. (2005). Haemolytic activity and allelopathy of the haptophyte *Prymnesium parvum* in nutrient-limited and balanced growth conditions. *Marine Ecology Progress Series* 299, 137-148.

- Vellend, M. (2010). Conceptual synthesis in community ecology. *The Quarterly review of biology* 85(2), 183-206.
- Wang, K., Yan, H., Peng, X., Hu, H., Zhang, H., Hou, D., et al. (2020). Community assembly of bacteria and archaea in coastal waters governed by contrasting mechanisms: A seasonal perspective. *Molecular Ecology* 29(19), 3762-3776.
- Wanninkhof, R. (1992). Relationship between wind speed and gas exchange over the ocean. *Journal of Geophysical Research* 97(C5). doi: 10.1029/92jc00188.
- Wanninkhof, R. (2014). Relationship between wind speed and gas exchange over the ocean revisited. *Limnology and Oceanography: Methods* 12(6), 351-362. doi: 10.4319/lom.2014.12.351.
- Wassmann, P. (2015). Overarching perspectives of contemporary and future ecosystems in the Arctic Ocean. *Progress in Oceanography* 139, 1-12.
- Wassmann, P., Kosobokova, K., Slagstad, D., Drinkwater, K., Hopcroft, R., Moore, S., et al. (2015). The contiguous domains of Arctic Ocean advection: trails of life and death. *Progress in Oceanography* 139, 42-65.
- Wassmann, P., Reigstad, M., Haug, T., Rudels, B., Carroll, M.L., Hop, H., et al. (2006). Food webs and carbon flux in the Barents Sea. *Progress in Oceanography* 71(2-4), 232-287.
- Weiss, R.F. (1974). Carbon dioxide in water and seawater: the solubility of a non-ideal gas. *Marine Chemistry* 2, 203-215.
- Wietz, M., Bienhold, C., Metfies, K., Torres-Valdés, S., von Appen, W.-J., Salter, I., et al. (2021). The polar night shift: seasonal dynamics and drivers of Arctic Ocean microbiomes revealed by autonomous sampling. *ISME Communications* 1(1), 1-12.
- Włodarska-Kowalczyk, M., Mazurkiewicz, M., Górska, B., Michel, L.N., Jankowska, E., and Zaborska, A. (2019). Organic Carbon Origin, Benthic Faunal Consumption, and Burial in Sediments of Northern Atlantic and Arctic Fjords (60–81° N). *Journal of Geophysical Research: Biogeosciences* 124(12), 3737-3751.
- Yang, B., Wang, Y., and Qian, P.-Y. (2016). Sensitivity and correlation of hypervariable regions in 16S rRNA genes in phylogenetic analysis. *BMC bioinformatics* 17(1), 1-8.
- Yasunaka, S., Murata, A., Watanabe, E., Chierici, M., Fransson, A., van Heuven, S., et al. (2016). Mapping of the air–sea CO₂ flux in the Arctic Ocean and its adjacent seas: Basin-wide distribution and seasonal to interannual variability. *Polar Science* 10(3), 323-334.
- Zingone, A., and Enevoldsen, H.O. (2000). The diversity of harmful algal blooms: a challenge for science and management. *Ocean & coastal management* 43(8-9), 725-748.

Paper I





Drivers of Atmosphere-Ocean CO₂ Flux in Northern Norwegian Fjords

Nerea J. Aalto^{1,2}, Karley Campbell^{1,3}, Hans C. Eilertsen¹ and Hans C. Bernstein^{1,2*}

¹ Faculty of Biosciences, Fisheries and Economics, UiT – The Arctic University of Norway, Tromsø, Norway, ² The Arctic Centre for Sustainable Energy, UiT – The Arctic University of Norway, Tromsø, Norway, ³ Bristol Glaciology Centre, University of Bristol, Bristol, United Kingdom

OPEN ACCESS

Edited by:

Mark James Hopwood,
Southern University of Science
and Technology, China

Reviewed by:

Mohamed M. M. Ahmed,
University of Calgary, Canada
Louise Delaigue,
Royal Netherlands Institute for Sea
Research (NIOZ), Netherlands

*Correspondence:

Hans C. Bernstein
hans.c.bernstein@uit.no

Specialty section:

This article was submitted to
Marine Biogeochemistry,
a section of the journal
Frontiers in Marine Science

Received: 07 April 2021

Accepted: 10 June 2021

Published: 07 July 2021

Citation:

Aalto NJ, Campbell K,
Eilertsen HC and Bernstein HC (2021)
Drivers of Atmosphere-Ocean CO₂
Flux in Northern Norwegian Fjords.
Front. Mar. Sci. 8:692093.
doi: 10.3389/fmars.2021.692093

High-latitude fjords and continental shelves are shown to be sinks for atmospheric CO₂, yet large spatial-temporal variability and poor regional coverage of sea-air CO₂ flux data, especially from fjord systems, makes it difficult to scale our knowledge on how they contribute to atmospheric carbon regulation. The magnitude and seasonal variability of atmosphere-sea CO₂ flux was investigated in high-latitude northern Norwegian coastal areas over 2018 and 2019, including four fjords and one coastal bay. The aim was to assess the physical and biogeochemical factors controlling CO₂ flux and partial pressure of CO₂ in surface water via correlation to physical oceanographic and biological measurements. The results show that the study region acts as an overall atmospheric CO₂ sink throughout the year, largely due to the strong undersaturation of CO₂ relative to atmospheric concentrations. Wind speed exerted the strongest influence on the instantaneous rate of sea-air CO₂ exchange, while exhibiting high variability. We concluded that the northernmost fjords (Altafjord and Porsangerfjord) showed stronger potential for instantaneous CO₂ uptake due to higher wind speeds. We also found that fixation of CO₂ was likely a significant factor controlling ΔpCO₂ from April to June, which followed phenology of spring phytoplankton blooms at each location. Decreased ΔpCO₂ and the resulting sea-air CO₂ flux was observed in autumn due to a combined reduction of the mixed layer with entrain of high CO₂ subsurface water, damped biological activity and higher surface water temperatures. This study provides the first measurements of atmospheric CO₂ flux in these fjord systems and therefore an important new baseline for gaining a better understanding on how the northern Norwegian coast and characteristic fjord systems participate in atmosphere carbon regulation.

Keywords: fjord and channel ecosystems, primary production, CO₂ sink, algae bloom, microalga

INTRODUCTION

High-latitude fjords and continental shelf regions are sinks for atmospheric carbon dioxide (CO₂) due to prominent undersaturation in surface water partial pressure (pCO₂) with respect to atmosphere, however, there exists large spatial-temporal variability as a result of heterogeneity in biogeochemical cycles and seasonal abiotic and biological processes (Takahashi et al., 2002; Bates, 2006; Chen et al., 2013; Yasunaka et al., 2016; Jones et al., 2020). The primary cause of undersaturation is complex but may be attributed to several combined processes, including:

(i) intense summer drawdown by phytoplankton primary production (PP) and subsequent vertical export of organic matter to the benthos, (ii) horizontal export of CO₂ as dissolved inorganic carbon with local ocean circulation patterns, and (iii) atmospheric cooling of surface waters in winter that increase CO₂ solubility and associated disequilibrium of the water with the atmospheric CO₂ (Tsunogai et al., 1999; Thomas et al., 2004; Bates, 2006). These entire regions or specific sections can also outgas CO₂ to the atmosphere due to river inputs and the production, export, and degradation of organic matter (Thomas et al., 2004). However, the unique oceanographic characteristics of the semi-enclosed fjord systems add to the complexity of carbon cycling and relatively little is known about their role in global atmospheric uptake or release of carbon. For example, the influence of substantial freshwater inflow and strong spatial-temporal variability in phytoplankton blooms are known to strongly influence surface water pCO₂ and corresponding CO₂ flux (Rysgaard et al., 2012; Meire et al., 2015; Ericson et al., 2018, 2019; Jones et al., 2020). Yet, there is still poor seasonal and regional coverage of how these biophysical factors interact with fjord specific hydrography to influence air-sea CO₂ exchange. In addition, similar strength of atmosphere-sea gradient of pCO₂ does not necessarily lead to equal CO₂ uptake between different fjords or regions. Wind speed has a critical role controlling instantaneous sea-air exchanges of CO₂ because it is used as a function of gas transfer velocity and can therefore cause considerable temporal and spatial variability (Sejr et al., 2011; Chen et al., 2013; Wanninkhof, 2014; Ericson et al., 2018).

A defining feature of fjord systems is the impact of current or previous glaciation. In fjords of Greenland and Svalbard, both land and ocean terminating glaciers are sources of substantial freshwater inflow. In comparison, the influence of glaciers on oceanographic conditions of fjord systems in northern Norway (> 69 N°) is largely absent (Wassmann et al., 1996; Meire et al., 2015; Ericson et al., 2018). Instead, freshwater inputs are largely attributed to riverine inflow that are seasonally focused in late spring with terrestrial snow melt (Svendsen, 1995). The result is a brief period of stratification in many fjords of northern Norway, which is often characterized by a relatively weak and shallow pycnocline. Seasonality is also present in these Norwegian fjords, to a lesser extent, in autumn during periods of heavy rain and negative heat flux throughout large parts of the year, i.e., surface water mixing induced by cooling of the surface water (Wassmann et al., 1996; Eilertsen and Skarðhamar, 2006). The topography varies in northern Norwegian fjords. Shallow sills in the mouth of the fjords are present, missing or located closer to the head. These sills are often quite deep, enabling relatively good exchange with the adjacent coastal water and frequent advection (Eilertsen and Skarðhamar, 2006). The hydrography of the northern Norwegian coastline, including its numerous fjord systems, is predominantly influenced by the North Atlantic Current that carries warm and saline Atlantic water northwards ($S > 35$; $5 < T \leq 10^\circ\text{C}$), as well as the cold and less saline Norwegian Coastal Water ($S < 35$; $4 < T \leq 12^\circ\text{C}$) that is carried north by the Norwegian Coastal Current. Together these water masses merge over the Norwegian shelf ridge (Nordby et al., 1999; Skarðhamar and Svendsen, 2005). The temperature influence of Norwegian Coastal Current is

thought to diminish northward along the North Norwegian coast and in its fjords, which are affected by more localized oceanic and climate factors like fjord-coast communication and ambient air temperature (Eilertsen and Skarðhamar, 2006).

A highly stratified water column and low surface water salinity creates high potential for CO₂ uptake (Meire et al., 2015; Ericson et al., 2019). The summertime halocline caused by glacial meltwater or river discharge into fjords can prevent CO₂ released by remineralization of organic material in subsurface layer to entrain surface water during summer that also helps to maintain the low summertime pCO₂ level (Rysgaard et al., 2012). Often, the surface water pCO₂ increases from autumn to winter maximum near atmospheric equilibrium due to erosion of stratification, i.e., entrainment of subsurface water, and increasing salinity, low biological production and sea-air CO₂ exchange in seasonal ice-free fjords (Ericson et al., 2018; Jones et al., 2020). The river runoff and glacial meltwater can have different impacts on the fjord's surface water pCO₂, as the glacial origin meltwater is usually combined with snow melt and it is low in dissolved inorganic carbon, total alkalinity (TA) and organic matter, but not necessarily undersaturated with respect to atmospheric CO₂ (Meire et al., 2015). However, it can lead to an intensive decrease in surface water pCO₂ due to thermodynamic effect of salinity on pCO₂ (Meire et al., 2015). Whereas, river runoff is a combination of river water, soil water and rainwater determined largely by characteristics in watershed and can therefore be a source of carbon as the CO₂ can be derived from the decay of organic matter and dissolution of carbonate minerals (Telmer and Veizer, 1999; Delaigue et al., 2020).

Northern Norwegian fjords, as compared to temperate fjords in southern Norway and many Arctic fjords in Svalbard, are distinct in their reception of comparatively low concentration of terrestrial originating organic matter. The total organic carbon content is similar to Arctic fjords and lower to fjords in southern Norway, thus the organic carbon material is predominantly derived from spring phytoplankton growth (Włodarska-Kowalczyk et al., 2019). The sedimentation and burial rate are low and indications of effective exportation of organic material from fjords due to advection has been reported (Reigstad and Wassmann, 1996). That results in less heterotrophic microbial activity that effectively competes with autotrophic biological drawdown of CO₂ (Włodarska-Kowalczyk et al., 2019).

Short periods for PP are defining ecological features to high-latitude fjords and responsible for significant, seasonal drops in surface water pCO₂, which usually occurs in April-May prior to major freshwater input (Meire et al., 2015; Ericson et al., 2018; Jones et al., 2020). Phytoplankton production in northern Norwegian fjords is limited between the end of March and September/October when light is available for photosynthesis (Eilertsen and Degerlund, 2010). Annual pelagic production is estimated around 100 g C m⁻² with variability predominantly being associated with available of nutrients and mixed layer depth (MLD). Limitation of nutrients like nitrate, often causes the culmination of spring microalgae blooms quickly after the onset (Eilertsen and Taasen, 1984). The weak stratification allows occasionally the introduction of nutrients to surface with mixing caused by increased wind events. The summertime riverine input

in the area contributes only to a small extent to available nutrients (Wassmann et al., 1996; Jones et al., 2020). Sometimes the mixed layer is so deep that it hinders the growth as the cells sink below euphotic zone (Eilertsen and Taasen, 1984).

The ecology of northern Norwegian fjords with respect to phytoplankton, zooplankton, benthos and fish has been extensively investigated (i.e., Eilertsen and Taasen, 1984; Bax and Eliassen, 1990; Oug and Høisøter, 2000; Michelsen et al., 2017). However, their role in sea-air CO₂ flux is still largely unknown. In this study we quantify the degree to which physical-biogeochemical environments of fjord systems in northern Norway influence sea-air CO₂ flux. Toward this purpose, we compare spatial-temporal variability in sea-air CO₂ flux along a geographical transect and assess the regional strength of the oceanic carbon sink in northern Norwegian fjords. We then relate these new insights on CO₂ flux to fjord physical-biogeochemical properties to elucidate the main drivers of sea-air CO₂ exchange. This study provides a first observation of surface water pCO₂ and CO₂ flux in these specific northern Norwegian fjords and therefore represents an important baseline for understanding potential response of CO₂ sink in this contemporary age of increasing global temperature and atmospheric CO₂ concentrations.

MATERIALS AND METHODS

Study Area

The study was performed between 2018 and 2019 in the fjords, Malangen Fjord (i), Balsfjord (ii), Altafjord (iii) and Porsangerfjord (iv), and in the bay, Finnfjord Indre (v), of coastal northern Norway (**Supplementary Table 1**). These locations were chosen to represent the range of local geographies and known oceanographic features of the studied area and are defined by the following features: (i) Malangen Fjord (MS; 240 m). A 45 km long fjord of southeast-northwest direction, consisting of two basins separated by a 160 m sill and the depth at the entrance area is 200 m (Mankettikara, 2013). Fjord waters are freely connected to the outer coastal waters of Norwegian Coastal Current and inflows of dense Atlantic water are possible (Wassmann et al., 1996). Malangen Fjord also receives significant inflow from the Malangen River (Eilertsen and Skarðhamar, 2006). Sampling was conducted in the outer part of the fjord. (ii) Balsfjord (BS; 124 m). A narrow single basin, 60 km long fjord of south/south-east direction, separated from surrounding coastal waters by 8 m and 9 m sounds and by a 35 m sill at fjord entrance (Eilertsen and Taasen, 1984). Fjord waters are exchanged and mixed to a large extent with water mass from Malangen Fjord (Svendsen, 1995). Run-off from several small rivers is moderate, and there is a typical estuarine circulation taking place during summer that is known to cause upwelling events in the head of the fjord (Svendsen, 1995). Sampling took place approximately in the middle of the fjord. (iii) Altafjord (AMØ; 405 m). A 30 km long and non-uniform width fjord, consisting of two basins: deep outer part with maximum depth of 450 m and shallow inner parts (Mankettikara, 2013). A 190 m sill at the entrance prevents free inflows of outer coastal waters

of Norwegian Coastal Current (Mankettikara, 2013). Altafjord receives inflow from Alta River (Eilertsen and Skarðhamar, 2006). Sampling was conducted approximately in the middle of the fjord. (iv) Porsangerfjord (PV; 209 m and PR; 113 m). A 100 km long and 15–20 km wide fjord of north-south oriented direction, consisting of two basins separated by a 60 m sill from 30 km of the head of the fjord. The entrance of the fjord is 200 m (no sill) and the maximum depth is 230 m. Fjord waters in outer part are freely connected to the outer coastal waters of Norwegian Coastal Current and Barents Sea (Mankettikara, 2013). Upwelling events in the middle of the fjord during summer are possible (Svendsen, 1995). Porsangerfjord receives inflow from Laks River and Børs River (Mankettikara, 2013). Sampling took place at the entrance of the fjord (PV) and in the inner basin (PR). (v) Finnfjord Indre (ST22; 62 m). A small and shallow bay adjacent to Finnsnes sound. It was chosen because of the close proximity to large CO₂ emitting industrial activity, i.e., the ferrosilicon producer Finnfjord AS. Finnfjord Indre borders to Gisund strait characterized by high current speeds (Larsen, 2015). Gisund strait opens to Malangen fjord (north) and divides into two smaller fjords (south). Finnfjord Indre receives inflow from Mevatn River. The station ST22 is approximately 1.5 km from a ferrosilicon smelter plant (Finnfjord AS) with CO₂ emission of 300 000 tons annually (Norwegian Environment Agency, 2021).

Samples from all fjords except Finnfjord Indre were collected from *R/V Johan Ruud* as a part of Sea Environmental Sampling program (Havmiljødata, HMD), coordinated through the Faculty of Biosciences, Fisheries and Economics (UiT, The Arctic University of Norway, Tromsø, Norway) (see Mankettikara, 2013). Sampling in Finnfjord Indre was performed with a 6.5 m Polarcirkel boat, equipped for oceanographic research. Wind speed values were obtained from fjord stations during cruises by automated meteorological loggers (Airmar 200WX, United States) mounted on board Johan Ruud approximately 10 m above sea level, and daily atmospheric pressure readings from the nearest meteorological station supplied by Norwegian Meteorological Institute. Whereas in Finnfjord Indre both these parameters relied on records obtained from nearest meteorological station and therefore wind speed values used in further calculations were corrected to reference height, 10 m above sea level (Hartman and Hammond, 1985).

Vertical profiles of Conductivity-Temperature-Depth (CTD) and *in vivo* fluorescence were obtained with a *Seabird Scientific* 9–11 plus CTD at the fjord stations. In Finnfjord Indre CTD casts were taken with a handheld *AML Oceanographic Base* X2 CTD, which did not support fluorescence measurements. MLD was determined from CTD-profiles using a density change threshold of 0.1 kg m³ and 10 m as a reference depth (Peralta-Ferriz and Woodgate, 2015).

Measurement of dissolved (pCO₂) and atmospheric CO₂ were obtained using an underwater and atmospheric nondispersive CO₂-infrared (NIDR) detector (Franatech Dissolved CO₂ IR, Germany), respectively, coupled to a temperature sensor (4-wire platinum temperature 1,000). The estimated error of the CO₂-sensor reported by manufacturer after product calibration is ± 5%. The NIDR detector utilizes an equilibrium system via a semi-permeable membrane in order to measure CO₂ (ppmv)

directly from gas phase. These CO₂ concentrations were then converted to mole fraction of the gas (xCO₂) according to Dalton's law. Both, atmospheric CO₂ and surface water pCO₂ were determined as a product of xCO₂ and atmospheric pressure. A water-vapor pressure correction was not used because xCO₂ was not measured in a dry air equilibrium.

Atmospheric CO₂ (ppmv) was measured in air by positioning the NIDR detector approximately 3–4 m above sea level and below exhaust of the *R/V Johan Ruud*. To minimize the influence of the vessel exhaust on measurements, the vessel was positioned with the dominant wind direction blowing away from the sensor. For these same reasons, the engine of the Polarcirkel boat was turned off for the duration of measurements while sampling in Finn fjord Indre. Measurements for surface water pCO₂ at all fjord stations were taken at 5 m depths. All measurements were performed in total for 30 min to allow time for sensor stabilization (20 min) prior to 10 min of data collection at a measurement frequency of 15 s. The data of a 10-min average with associated standard deviation (SD) is used in further calculations below. The factory calibration of the CO₂ sensor proved reliable for measuring the difference ($\Delta p\text{CO}_2$) but was not used for absolute concentrations.

Calculation of Sea-Air CO₂ Flux

CO₂ flux, F (mmol m⁻² d⁻¹), was calculated according to Eqs 1 and 2 representing the common bulk gas flux formulation (Wanninkhof, 2014);

$$F = K_0 k (p\text{CO}_2 - \text{CO}_2^{\text{air}}) \quad (1)$$

$$k = 0.251 u^2 \sqrt{\frac{660}{Sc}} \quad (2)$$

where K_0 is the solubility (moles L⁻¹ atm⁻¹) from Weiss (1974) at salinity and temperature (SST) derived from CTD measurements (above). Following these calculations, the $p\text{CO}_2 - \text{CO}_2^{\text{air}}$ is the sea-air pCO₂ difference ($\Delta p\text{CO}_2$) and k is the gas transfer velocity (cm h⁻¹). Here, negative flux values indicate the direction of CO₂ flux is from sea-air. The parameters and coefficient of gas transfer velocity (k) were calculated according to Wanninkhof (2014), where Sc is the dimensionless Schmidt number at measured temperature, u is an obtained wind speed at the moment of sampling, and 0.251 is an empirical coefficient (Wanninkhof, 2014) correcting for the gas exchange-wind speed relationship. The $\Delta p\text{CO}_2$ and CO₂ flux values are further reported with associated SD.

Water Sampling and Determination of Biogeochemical Data

Seawater was collected with a Niskin sampler from near-surface (referred as 0 m in Figure 3A), 5 (surface), 10, 20, and 50 m depths at all the stations. Water was subsampled from each depth for determination of chlorophyll *a* (chl *a*), phytoplankton taxonomy and cell volume-based biomass. Inorganic nutrient (silicate and nitrate) and pH were determined only from surface (5 m depth).

The pH was measured in sub-sample triplicates (SD of the sub-sample triplicates varied between ± 0.003 and ± 0.052), immediately after collection, except samples in Finn fjord Indre (ST22) in February where measurements were taken 2–3 h after collection. This sample was not preserved, i.e., poisoned but kept in dark and cold with minimum headspace to minimize gas exchange. Measurements of pH were completed manually using a WTW Multi 360 meter with WTW SenTix 940 IDS probe (Xylem Analytics, Germany) to an accuracy of 0.001 pH unit. A two-point calibration was performed daily using pH 4 and pH 7 WTW Technical buffers. The calibration slope was between 58.1 and 59.3 mV per unit pH.

Chlorophyll *a* was determined from depths of near-surface, 5, 10, 20, and 50 m by filtering 50–200 mL of sub-sample (triplicates) volumes (Whatman GF/C), before storage of filters at -20°C for up to 4 months and subsequent measurement of fluorescence (Turner TD-700, United States) after 24 h and 4°C extraction in 96 % ethanol (Holm-Hansen and Riemann, 1978). SD of the sub-sample triplicates varied between ± 0.001 and $\pm 0.77 \mu\text{g L}^{-1}$.

Enumeration, morphological identification and estimates of total microalgae biomass was performed on 60–100 mL of each sample that were preserved in acid Lugol's solution. Samples were stored dark at 4°C before analyses via Utermöhl settling method (Edler and Elbrächter, 2010) and inverted light microscope (AXIO Vert.A1, ZEISS). Prior to analyses, the preserved samples from each depth were mixed together, from which an average phytoplankton biomass as carbon content (mg C L⁻¹) and cell abundance (cells L⁻¹) over the 50 m water column is determined for each station representing to. Morphology-based species identification on genus and class levels was completed (mainly Tomas, 1997). The cellular biovolume (μm^3), cellular carbon content (pg C cell⁻¹) and represented trophic type (autotroph, heterotroph or mixotroph) of the species were determined using *PlanktonToolbox* open source software (version 1.3.2) developed and operated by Swedish Meteorological and Hydrological Institute (SMHI). The trophic-type classification of the phytoplankton species present in the *PlanktonToolbox* software is based on the ecological knowledge of the species in Nordic area, i.e., Baltic Sea and the Northeast Atlantic.

Water samples from 5 m depth for nutrient analyses of silicate (Si(OH)₄) and nitrate (NO₃⁻) were filtered through Whatman GF/F glass fiber into unused 50 mL polypropylene Falcon tubes. The filtration unit and the sample tube were rinsed with filtered sample water three times before the final sample was collected and stored at -20°C for 12 months before analyses. Samples were rapidly defrosted at 55°C immediately before analysis via auto analyzer (Seal Analytical) (Strickland and Parsons, 1972).

Primary Production of Phytoplankton

Estimation of net PP by photoautotrophic phytoplankton, reported as carbon synthesis per unit surface area, was determined by location specific solar irradiance, chl *a* at the time of sample collection and photo-physiological parameters. First, we estimated irradiance incident on the sea surface (Frouin et al., 1989; Iqbal, 2012). The model computes solar irradiance in Wm⁻² after input of date, time position, humidity and coefficient

for a given maritime atmosphere and solar zenith angle. In this calculation we used a visibility parameter to represent the study area 4–6 km, albedo 0.3 and 60% (maritime) humidity (Eilertsen and Holm-Hansen, 2000). Irradiance was modeled in 1 h steps for each sampling date (24 h). From this we computed mean irradiance for the illuminated depth layer of the water columns using previously described attenuation procedure (Hansen and Eilertsen, 1995; Eilertsen and Holm-Hansen, 2000). Thereafter, we assumed that the obtained mean light intensities were in the linear part of the photosynthetic slope, to estimate carbon assimilation via the following Eq. 3 from Webb et al. (1974):

$$P = \left(\frac{chl^a}{C} \right) P^B \left(1 - e^{-\alpha Q_{s(p)}/P^B} \right) \quad (3)$$

where P^B is the maximum photosynthetic rate (mg C mg chl $a^{-1} h^{-1}$), α is the photosynthetic efficiency (mg C mg chl $a^{-1} h^{-1} W m^{-2}$), and $Q_{s(p)}$ is PAR ($W m^{-2}$) at depth z . The photosynthetic coefficients (also respiration) and C:N ratios were input as means from 14°C carbon assimilation experiments (8 h incubation) performed during exponential growth of microalgae monocultures representing common and abundant members of spring blooms within our study locations: *Chaetoceros socialis*, *Skeletonema costatum* sensu lato, *Thalassiosira nordenskiöldii*, *Thalassiosira gravida*, and *Thalassiosira antactica* (Degerlund and Eilertsen, 2010), i.e., $P^B = 4.7$ mg C mg chl $a^{-1} h^{-1}$, $\alpha = 0.08$ mg C mg chl $a^{-1} h^{-1} W m^{-2}$ and a carbon to chl a ratio of 100. The carbon uptake rate was then obtained by multiplying measured chl a values, representing the mean photoautotrophic biomass in the water column (0–50 m) and computing total production in 1 h. steps. The carbon to CO₂ conversion of 3.67 was used to estimate CO₂ consumption.

Statistical Analyses

A non-parametric Spearman's rank correlation analysis was conducted to investigate the correlation between sea-air flux of CO₂, ΔpCO_2 and each environmental factor since the data of CO₂ flux and ΔpCO_2 did not show normal distribution based on the Shapiro-Wilk normality test. The non-parametric Mann-Whitney U test was used to investigate possible winter-summer contrast among flux of CO₂, ΔpCO_2 , wind, nutrients, autotrophic biomass of phytoplankton species (AU biomass) and chl a by comparing the variance of entire study period (June 2018–2019) to the variance of late spring-summer (April 2018, May 2018, June 2018, and 2019) measurements hereafter referred as summer. The Mann-Whitney U test was chosen because none of the variables, except silicate, showed normality (Supplementary Table 2).

Redundancy analysis (RDA) was applied using the R package "Vegan 2.5–7" to summarize the variation in flux of CO₂ and ΔpCO_2 by environmental conditions (Oksanen et al., 2013; R Core Team, 2013). RDA is a constrained (canonical) ordination method where variance found among species, in this case CO₂ flux and ΔpCO_2 , is explained by environmental (explanatory) variables. Prior to RDA stepwise regression (function "ordstep" in the R package "Vegan 2.5–7") was used to select the most useful environmental variables based on their statistical

significance using cut of limit of $p = 0.05$. These variables were wind speed, temperature, MLD, NO₃⁻, AU biomass and chl a . In addition, sampling month was included as quantitative environmental variable to the analysis. All data, calculations and figure generation scripts are provided and linked to R markdown files deposited on the Open Science Framework project: *Northern Norwegian Fjord CO₂ Flux*¹.

RESULTS

Seasonal Variability in ΔpCO_2 and CO₂ Flux

The driving force behind flux of CO₂ between the atmosphere and surface ocean is the difference in partial pressure of CO₂ (ΔpCO_2). All fjord systems investigated in this study were undersaturated (negative ΔpCO_2) with respect to atmospheric CO₂ throughout the year (Figure 1). The fjord stations showed similar seasonal trends with respect to ΔpCO_2 , with generally a weaker negative ΔpCO_2 gradient in autumn and winter (October-March) compared to stronger gradient in spring and summer (April-June; Figure 1). Seasonal changes in ΔpCO_2 were statistically significant (Mann-Whitney U ; $w = 378$, $p < 0.05$; Table 1). The highest ΔpCO_2 from fjord stations were observed in May (range between stations -218 ± 7 and -102 ± 7 ΔpCO_2), except at MS in Malangen Fjord in April (-160 ± 2 ΔpCO_2) and from Finn fjord Indre at ST22 in April -194 ± 7 ΔpCO_2 , whereas the smallest ΔpCO_2 at all stations occurred in December when range between stations was -49 ± 1 to -13 ± 0.4 (Figure 1).

Net transport of CO₂ was from the atmosphere to seawater, as represented by negative flux values calculated through the duration of the study (Figure 1). The CO₂ flux did not follow the seasonal variation of surface water ΔpCO_2 . That is, the rates sea-air CO₂ flux were not always positively correlated to the greatest sea-air ΔpCO_2 . For example, ΔpCO_2 at BS in Balsfjord was twice as high in May than in April, but the instantaneous rate of CO₂ uptake was greater in April. Similar occurrences were observed at all the stations. The summertime variance of CO₂ flux did not statistically differ from that of the annual variance (Mann-Whitney U ; $w = 310$, $p = 0.1$, Table 1). The two northernmost stations PV and PR in Porsangerfjord (Figure 1), showed the greatest variability and magnitude of CO₂ flux within the time series, ranging from -21.8 ± 1.49 to -1.7 ± 0.27 mmol $m^{-2} d^{-1}$ and from -47.9 ± 0.35 to -0.2 ± 0.02 mmol $m^{-2} d^{-1}$, respectively (Figure 1). This observation was in contrast with the seasonal variation observed from stations located in the other three fjords, AMØ (Altafjord), BS (Balsfjord) and MS (Malangen Fjord), which displayed a lower total magnitude and extent of variability of CO₂ flux, with range of -14.1 ± 0.17 to -0.9 ± 0.11 mmol $m^{-2} d^{-1}$ (Figure 1). Finn fjord Indre (ST22) also maintained net sea-air (i.e., negative) CO₂ flux through the study period (Figure 1). Although the CO₂ flux measured from ST22 showed considerably less variation as compared to the fjord stations, ranging only from -3.6 ± 0.72 to $-0.0 \pm < 0.00$ mmol $m^{-2} d^{-1}$ across the seasons. In fact, CO₂ flux was nearly constant

¹<https://osf.io/tbzse/>

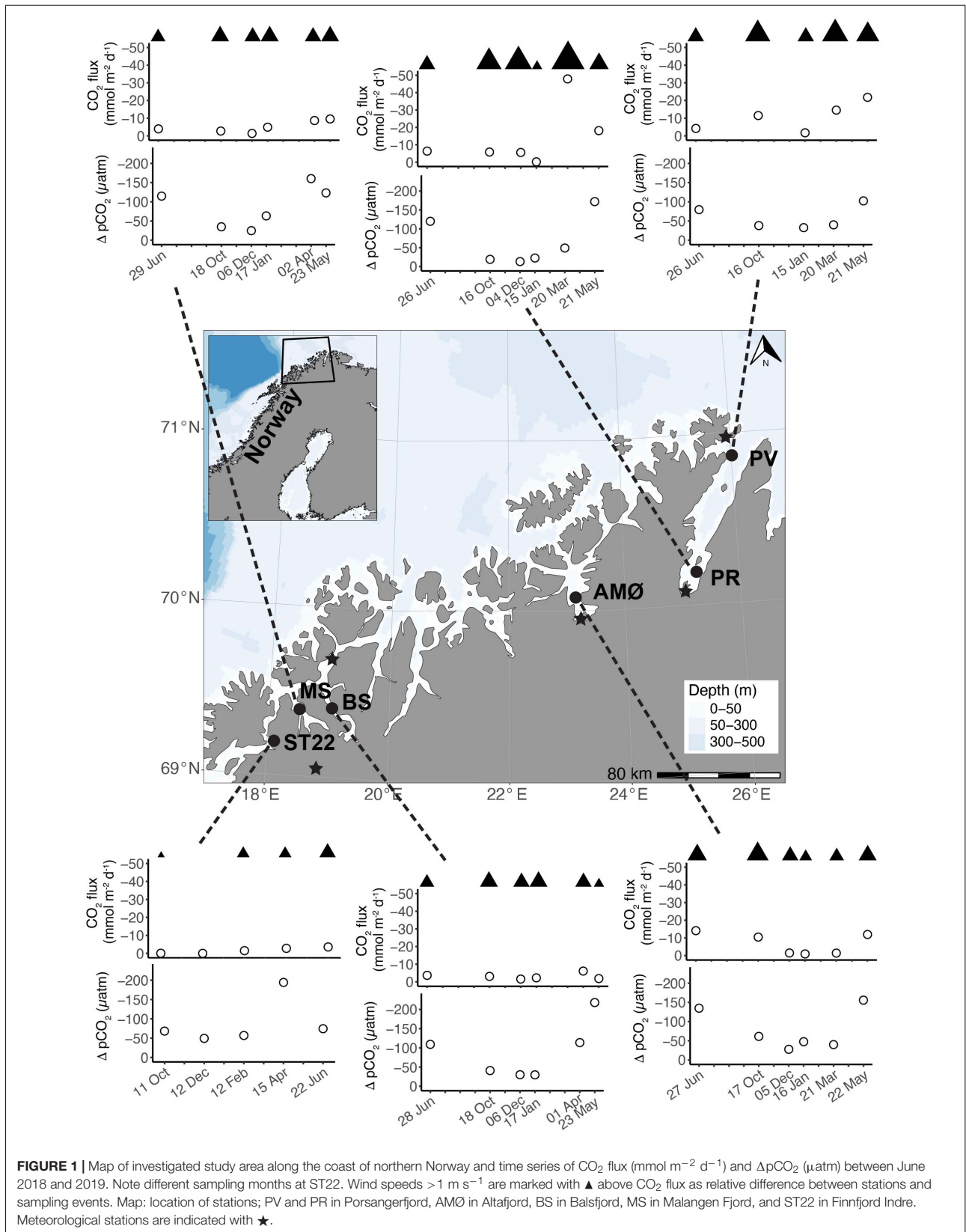


FIGURE 1 | Map of investigated study area along the coast of northern Norway and time series of CO₂ flux (mmol m⁻² d⁻¹) and ΔpCO₂ (μatm) between June 2018 and 2019. Note different sampling months at ST22. Wind speeds > 1 m s⁻¹ are marked with ▲ above CO₂ flux as relative difference between stations and sampling events. Map: location of stations; PV and PR in Porsangerfjord, AMØ in Altafjord, BS in Balsfjord, MS in Malangen Fjord, and ST22 in Finnfjord Indre. Meteorological stations are indicated with ★.

TABLE 1 | Mann-Whitney *U* test analysis of possible summer (April, May, and June) seasonality in variable of interest: CO₂ flux, ΔpCO₂, wind, chl *a*, and AU biomass.

Variable	w-statistic	p-value
CO ₂ flux	310	0.1
ΔpCO ₂	378	0.002
Wind	260.5	0.7
Chl <i>a</i>	107	0.003
AU biomass	108	0.003
NO ₃ ⁻	368	0.003
Si(OH) ₄	321	0.06

TABLE 2 | Mixed layer depth (MLD) based on density gradient.

Month	MLD (m)					
	Porsangerfjord		Altafjord	Balsfjord	Malangen Fjord	Finnfjord Indre
	PV	PR	AMØ	BS	MS	ST22
June ₂₀₁₈	30	11	11	12	11	
October	122	29	11	14	11	20
December		88	88	52	12	19
January ₂₀₁₉	145	X	18	77	17	
February						30
March	178	X	21			
April			13	80	16	16
May	98	11		14	11	
June						14

X denotes a homogeneous water column.

through the study period, though a slight increase was detected in spring and summer (Figure 1).

Geophysical Environment

The northernmost station PV in the outer part of Porsangerfjord (Figure 1), maintained a largely homogenous water column throughout sample seasons, as compared to other stations. Furthermore, the MLD varied around 100 m, except in June at 30 m (Table 2 and Supplementary Figure 1). At the other fjord stations, the MLD was shallower through summer and autumn <15 m, except 39 m at PR (inner Porsangerfjord) in October (Table 2 and Supplementary Figures 1–5). Stations BS (Balsfjord) and PR (inner Porsangerfjord) had nearly or completely mixed water columns between December and March/April. In contrast, the shallowest MLD occurred through winter measurements, in addition to summer and autumn, at MS in the southernmost fjord Malangen Fjord, and between January and March at AMØ (Altafjord). At ST22 in Finnfjord Indre, the MLD depth varied between 14 and 33 m and showed similar trend in information to BS and PR (Table 2 and Supplementary Figure 6).

The temperature-salinity plot (Figure 2A) shows that BS in Balsfjord and PR in inner Porsangerfjord were in general characterized by lower salinity (<34) than other stations. Also, the temperature range in entire water column at BS was smaller than at other stations, except PV in outer Porsangerfjord

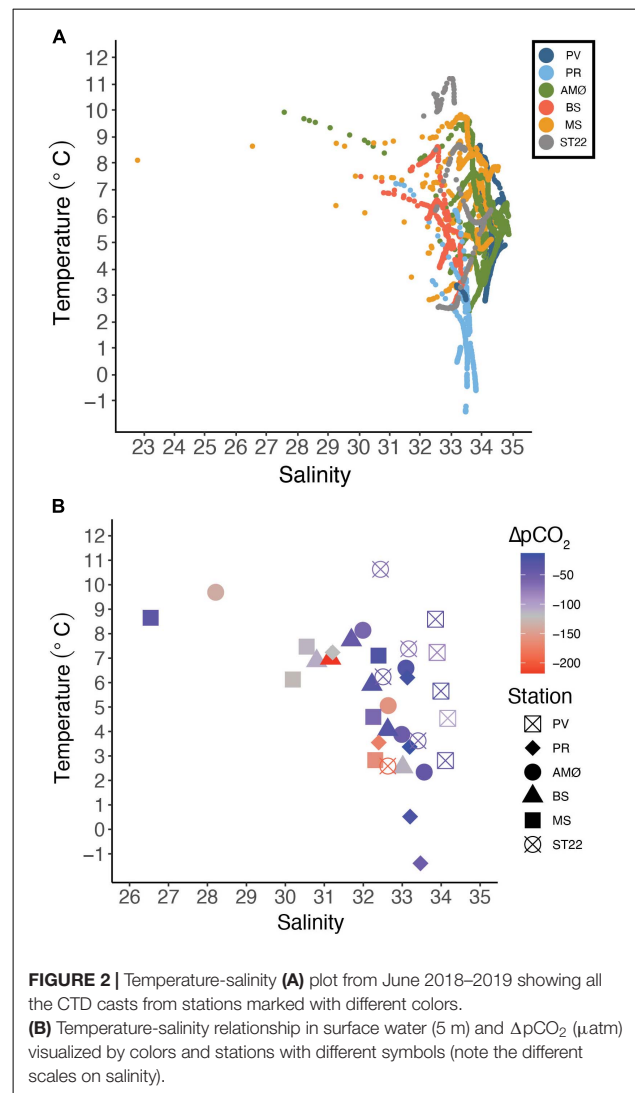


(Figure 1 and Table 3). PV in outer Porsangerfjord, AMØ in Altafjord, MS in Malangen Fjord and ST22 in Finnfjord Indre showed more similar salinity range (34–35) in subsurface water corresponding the upper salinity range of Norwegian Coastal Water (<35). The large salinity scatter is mainly from low salinity at uppermost 20–30 m at AMØ in June and at MS in May–June (Figure 2A and Supplementary Figures 3, 5). The lowest subsurface water temperature corresponds at most stations to the lower temperature range of Norwegian Coastal Water (<4°C).

The water temperature at 5 m depth, where CO₂ measurements were collected for all sites, decreased at all the stations from October to March/April, where it reached its lowest measured values in the surface waters, and thereafter increased rapidly (Supplementary Figures 1–6). The surface water temperature varied between 2.3 and 9.7°C at PV, AMØ, BS and MS stations. At PR in inner Porsangerfjord the surface water temperature was lower, –1.4 to 7.2°C, thus the entire water

TABLE 3 | Summary of all the measured parameters.

Parameter	Porsangerfjord		Altafjord	Balsfjord	Malangen Fjord	Finnfjord Indre
	PV	PR	AMØ	BS	MS	ST22
CO ₂ flux (mmol m ⁻² d ⁻¹)	-10.7 ± 2.07 (-1.7, -21.8)	-14.0 ± 1.70 (-0.2, -47.9)	-6.7 ± 0.72 (-0.9, -14.1)	-3.1 ± 0.73 (-1.6, -6.1)	-5.2 ± 0.54 (-1.3, -9.5)	-1.6 ± 0.73 (-0.0, -3.6)
ΔpCO ₂ (μatm)	-59 ± 11 (-33, -102)	-66 ± 10 (-13, -172)	-78 ± 9 (-28, -156)	-90 ± 13 (-30, -218)	-87 ± 9 (-25, -160)	-89 ± 17 (-49, -194)
Temperature (°C) (at 5 m)	5.8 ± 2.3 (2.8, 8.6)	3.2 ± 3.3 (-1.4, 7.2)	6.0 ± 2.7 (2.3, 9.7)	5.7 ± 2.0 (2.5, 7.7)	6.1 ± 2.1 (2.8, 8.6)	6.1 ± 3.2 (2.6, 10.6)
Salinity (PSU) (at 5 m)	34.0 ± 0.1 (33.9, 34.2)	32.8 ± 0.8 (31.2, 33.5)	32.1 ± 2.0 (28.2, 33.6)	31.9 ± 0.9 (30.8, 33.0)	30.7 ± 2.3 (26.5, 32.4)	32.8 ± 0.4 (32.4, 33.4)
Wind (m s ⁻¹)	9 ± 3.8 (5, 9)	10 ± 6.9 (2, 21)	6 ± 2.2 (3, 9)	5 ± 1.5 (2, 6)	5 ± 0.8 (4, 6)	2 ± 1.9 (0, 5)
pH (at 5 m)	8.11 ± 0.03 (8.06, 8.15)	8.13 ± 0.02 (8.01, 8.20)	8.14 ± 0.03 (8.09, 8.18)	8.13 ± 0.02 (8.10, 8.18)	8.15 ± 0.06 (8.11, 8.20)	8.16 ± 0.03 (8.03, 8.26)
River flow (m ³ s ⁻¹)		29 ± 30 (6, 238)	82 ± 74 (24, 467)		145 ± 91 (26, 597)	11 ± 12 (1, 90)
Chl <i>a</i> (μg L ⁻¹)(at 5 m)	0.6 ± 0.1 (0.0, 1.4)	0.4 ± 0.1 (0.1, 1.5)	0.6 ± 0.1 (0.0, 1.6)	3.0 ± 0.6 (0.0, 6.5)	3.1 ± 0.8 (0.0, 13.1)	1.2 ± 0.03 (0.0, 4.0)
PP (mg C m ² d ⁻¹)	723 ± 956 (0, 2050)	682 ± 1299 (0, 3288)	717 ± 1133 (0, 2861)	2055 ± 2349 (0, 5421)	2081 ± 2541 (0, 6352)	1229 ± 1563 (0, 3144)
NO ₃ ⁻ (μmol L ⁻¹)	4.32 ± 0.033 (1.00, 8.05)	3.46 ± 0.032 (0.08, 6.13)	2.14 ± 0.017 (0.03, 4.59)	2.76 ± 0.013 (0.77, 6.18)	2.06 ± 0.020 (0.03, 5.59)	2.08 ± 0.015 (0.01, 5.88)
Si(OH) ₄ (μmol L ⁻¹)	2.15 ± 0.056 (1.33, 3.35)	4.27 ± 0.031 (1.96, 6.26)	2.50 ± 0.015 (2.17, 2.95)	2.67 ± 0.034 (1.22, 4.56)	2.27 ± 0.033 (0.13, 4.51)	1.42 ± 0.009 (0.22, 2.37)

Values are given as mean ± SD and (min, max).

column was close to freezing during winter. In Finnfjord Indre at ST22 the lowest surface water temperature (2.6°C) was similar to PV, AMØ, BS and MS whereas the maximum measured temperature was higher, 10.6°C (Table 3).

The daily average freshwater input by rivers was highest in June 2018 (600 m³ s⁻¹) and May 2019 (500 m³ s⁻¹) in the fjords, and in the end of April and May 2019 (45–90 m³ s⁻¹) in Finnfjord Indre (Supplementary Figure 7). The strongest impact of freshwater input on salinity at 5 m depth (26.5–32.4) was at MS in Malangen Fjord (Table 3), where the Malangen River transported large quantities of meltwater from inland drainages in May and June (max. flow rate 600 m³ s⁻¹), but also freshwater peaks (flow rate >250 m³ s⁻¹) occurred in August, December and February (Supplementary Figure 7). The surface water salinity range in Porsangerfjord at PV and PR, and in Balsfjord at BS was between 30.8 and 34.2 (Figure 2B). AMØ in Altafjord also showed pronounced variability between 28.2 and 33.6 (Figure 2B). Finnfjord Indre had the smallest freshwater input (Supplementary Figure 7), and the surface water salinity range at ST22 was relatively small (32.4–33.4; Table 3).

Intermediate winds (4–15 m s⁻¹) were prevailing at fjord stations, as compared to relatively low winds (<4 m s⁻¹), except in June (5 m s⁻¹), recorded at the Finnfjord Indre station (Figure 1 and Supplementary Table 3). Wind speed did not show a seasonal trend (Mann-Whitney U; $w = 260.5$, $p = 0.7$, Table 1). Porsangerfjord was subjected to the highest wind speeds (range 2–21 m s⁻¹) as compared to the other fjords (2–9 m s⁻¹), except in June and January when difference between all fjord stations was smaller as total range between stations was 2–7 m s⁻¹

(Figure 1 and Supplementary Table 3). In Finnfjord Indre, wind speed was lower (0.3–5 m s⁻¹) than in fjords through the study period (Figure 1 and Supplementary Table 3).

Seasonal pH levels observed from ST22 in Finnfjord Indre were different as compared to the respective fjord stations. Specifically, the pH fluctuated to a greater extent and showed two maximum peaks found in October 8.23 ± 0.01 and in April 8.26 ± 0.02 . It also showed two minimum peaks observed in February 8.03 ± 0.01 and in June 8.14 ± 0.02 (Supplementary Figure 8). At PR (Porsangerfjord) pH variability was slightly greater (8.01 ± 0.01 to 8.20 ± 0.01) than in the other fjord stations (8.06 ± 0.02 to 8.20 ± 0.02 ; Table 3). The minimum pH level at stations in Porsangerfjord was measured in March whereas in other fjords it occurred mainly in December–January (Supplementary Figure 8).

The concentration of nitrate (NO₃⁻), was found to be strongly seasonal (Mann-Whitney U; $w = 368$, $p < 0.05$; Table 1), whereas silicate (Si(OH)₄) showed weaker winter–summer contrast $w = 321$, $p = 0.06$; Table 1). Most of stations showed similar seasonal trends for these nutrient concentrations measured from 5 m (Supplementary Figure 9). Concentrations of both nutrients increased from June/October to January/March and thereafter dropped in April/May. These nutrients were depleted in April at the southern stations (BS, MS and ST22) where the range between stations was <1.6 μmol L⁻¹ NO₃⁻, 0.1–1.2 μmol L⁻¹ Si(OH)₄. Thereafter, the concentration of silicate increased (range between stations 1.3–3.3 μmol L⁻¹) in May/June, while nitrate concentrations remained nearly constant through summer (Supplementary Figure 9).

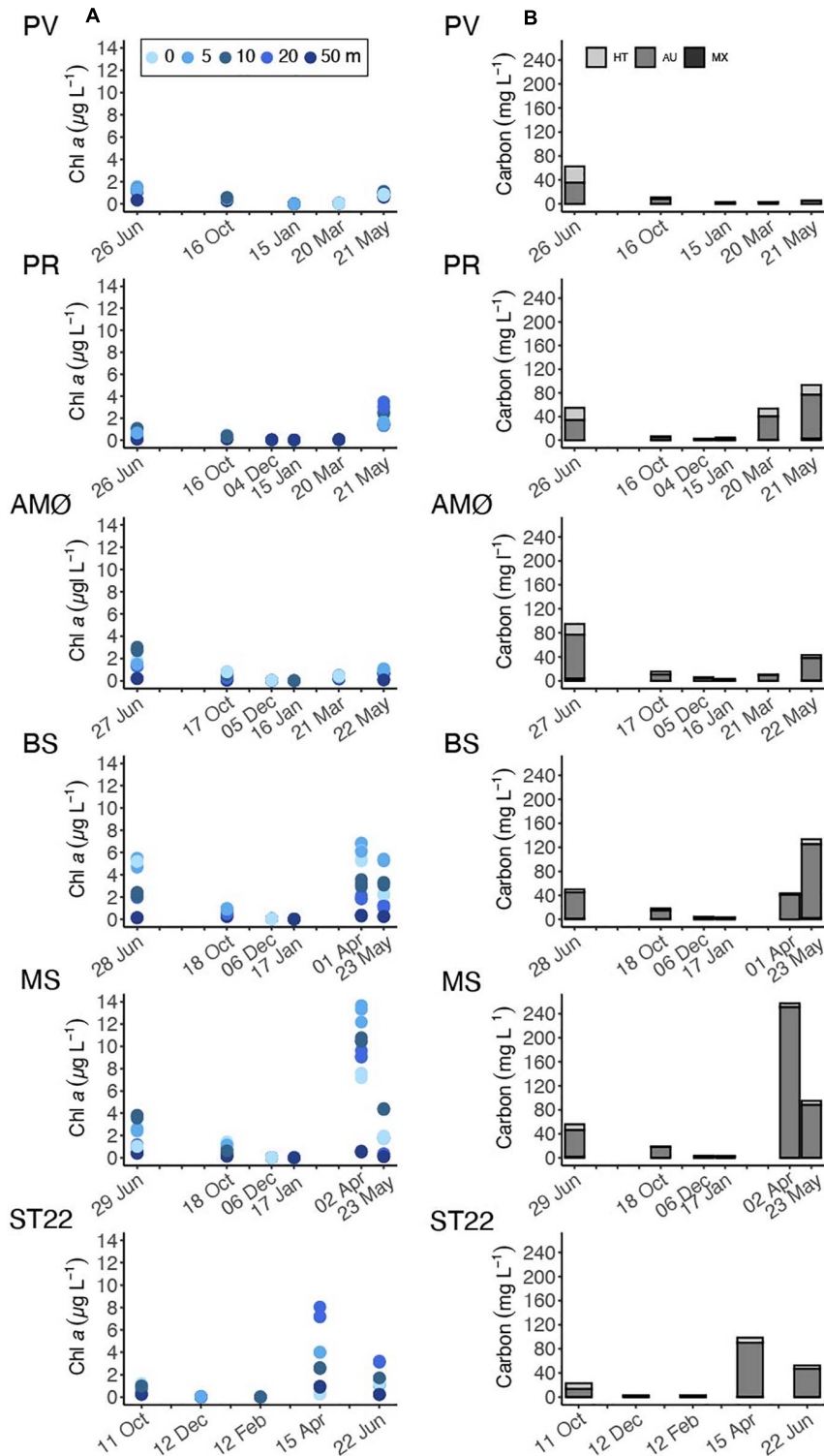
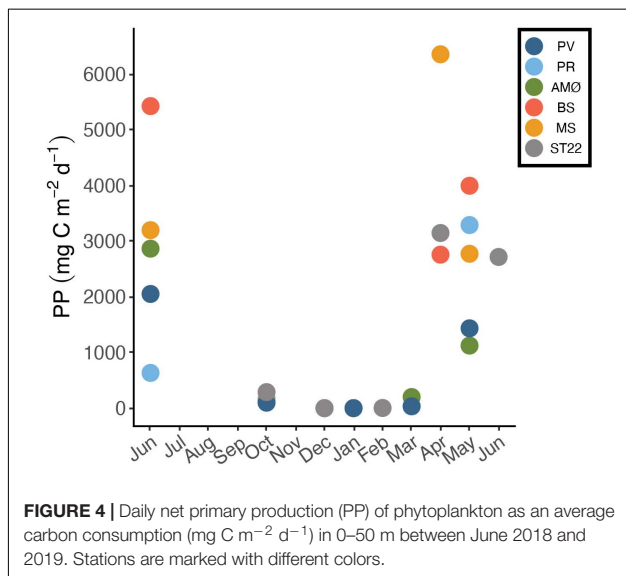


FIGURE 3 | Time series of **(A)** chl a concentration at discrete sampling depths of 0, 5, 10, 20, and 50 m. **(B)** Phytoplankton biomass estimated as carbon content from cellular biovolume and cellular carbon content and divided into trophic types: heterotrophic (HT), autotrophic (AU) and, mixotrophic (MX). Note different sampling months at ST22.



Seasonal Phytoplankton Dynamics

Phytoplankton biomass at all sample stations (**Figure 3B**) varied to a large extent with season, as also supported by the depth-discrete chl *a* measurements (**Figure 3A**) and fluorescence profiles (**Supplementary Figures 1–5**). The highest chl *a* values were observed in April, 6.6 ± 0.4 and $13.1 \pm 0.8 \mu\text{g L}^{-1}$ at 5 m within the southernmost fjord stations BS and MS, respectively (**Figure 3A**). The northernmost stations (PV, PR and AMØ) maintained relatively low chl *a* concentration across the measured time series and showed peaks in chl *a* that ranged between 1.4 ± 0.1 and $3.2 \pm 0.3 \mu\text{g L}^{-1}$ in May–June (**Figure 3A**). ST22 in Finn fjord Indre showed an increase in chl *a* concentration in April, where the maximum measured chl *a* at 20 m was $7.5 \pm 0.5 \mu\text{g L}^{-1}$ (**Figure 3A**).

During spring and summer, the total phytoplankton biomass (expressed in terms of estimated carbon content), varied between 43 and 257 mg C L^{-1} at all stations (**Figure 3B**). Strong summer seasonality was found on autotrophic phytoplankton biomass (AU biomass) (Mann-Whitney U; $w = 108$, $p < 0.05$; **Table 1**). Peaks of AU biomass blooms varied between April and June among the different fjord stations and was found in April in Finn fjord Indre at ST22 (**Figure 3B**). At most stations, the biomass of heterotrophic phytoplankton showed a slight increase in summer and autumn. The highest heterotroph/autotroph ratios ($\sim 50\%$) were observed in Porsanger fjord, where ciliates formed the majority of cells classified as heterotrophic biomass. The fraction of mixotrophic phytoplankton was very small through the study period and the main species was classified as a *Mesodinium rubrum*.

Estimated daily and maximum net PP showed variation between fjord stations. In April, PP was highest at MS in Malangen Fjord ($6352 \text{ mg C m}^{-2} \text{d}^{-1}$), whereas at PR in inner Porsanger fjord the highest PP ($3288 \text{ mg C m}^{-2} \text{d}^{-1}$) occurred in May and at BS in Balsfjord ($5421 \text{ mg C m}^{-2} \text{d}^{-1}$), AMØ ($2861 \text{ mg C m}^{-2} \text{d}^{-1}$) and PV in outer Porsanger fjord

($2050 \text{ mg C m}^{-2} \text{d}^{-1}$) in June (**Figure 4** and **Table 3**). At fjord stations the estimated PP varied most in June, when PV showed lowest $2050 \text{ mg C m}^{-2} \text{d}^{-1}$ and BS highest $5421 \text{ mg C m}^{-2} \text{d}^{-1}$ value. At ST22, in Finn fjord Indre, the PP was similar between April ($3144 \text{ mg C m}^{-2} \text{d}^{-1}$) and June ($2713 \text{ mg C m}^{-2} \text{d}^{-1}$) (**Figure 4**). In October the PP was slightly higher at ST22 ($288 \text{ mg C m}^{-2} \text{d}^{-1}$) than at fjord stations. During winter the PP was negligible, i.e., $0 \text{ mg C m}^{-2} \text{d}^{-1}$.

Relationship Between ΔpCO_2 , CO₂ Flux and Localized Environments

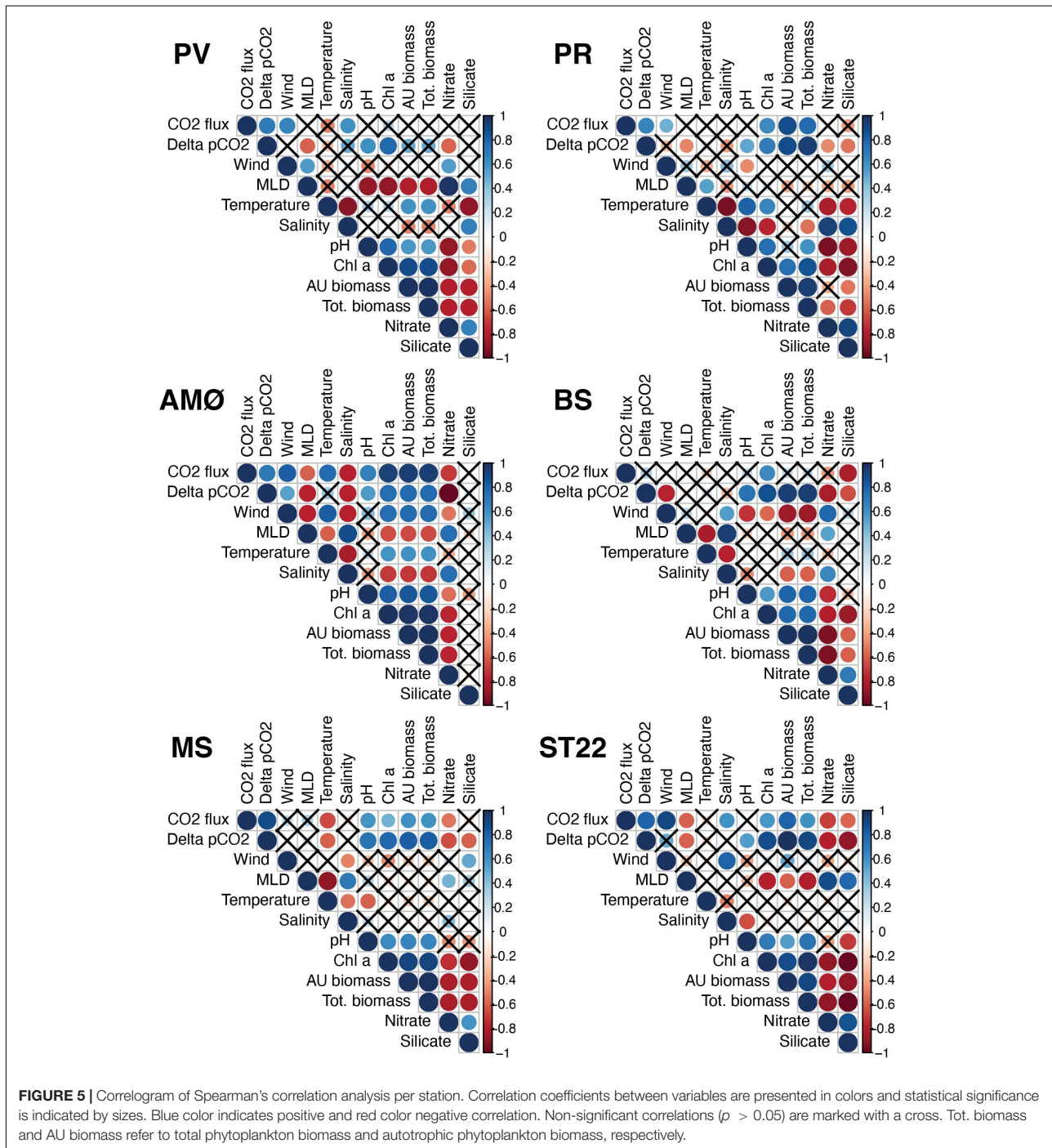
Spearman's rank correlation on fjord physical-biogeochemical conditions, CO₂ flux and ΔpCO_2 (**Figure 5**) indicate that surface water pH consistently showed the most frequent and most positive ($r = 0.5\text{--}0.7$; $p < 0.05$) correlation to ΔpCO_2 across stations and the seasonable time course. Nitrate and silicate concentrations had significant negative correlations with ΔpCO_2 at majority of sampling stations. Also, MLD showed negative correlation ($r = -0.8\text{--}-0.5$; $p < 0.05$) at PV, PR and AMØ in the two northernmost fjords (Porsanger fjord and Altafjord) and in Finn fjord Indre at ST22. Biological factors of chl *a*, total phytoplankton biomass (tot.biomass) and autotrophic phytoplankton biomass (AU biomass) correlated strongly ($r = 0.7\text{--}1$; $p < 0.05$) with ΔpCO_2 at all stations, except PV where only chl *a* showed significant positive correlation (**Figure 5**). Correlation between CO₂ flux and ΔpCO_2 was positive and significant at most of the stations and significant (positive) when evaluated with all data points ($r^2 = 0.16$; $p = 0.021$; **Supplementary Figure 10**). One or more of the biological factors and wind had positive significant relationship with flux of CO₂ at all the stations except PV, and BS and MS, respectively (**Figure 5**).

Redundancy analysis helped reveal that the flux of CO₂ and ΔpCO_2 was not strongly correlated. This is illustrated by nearly perpendicular projections in the RDA triplot (**Figure 6**). It follows that RDA supports the correlation of physical-biogeochemical properties described above, where high CO₂ flux occurred at strong wind speeds and ΔpCO_2 gradient was strong when primary productivity activity was high. In addition, MLD and temperature have clear negative relationship to ΔpCO_2 and flux of CO₂, respectively. The main difference inferred from correlations between samples at each station is that Finn fjord Indre station (ST22) differ from fjord stations, especially from PV, PR and AMØ with respect to wind speed and strength of CO₂ flux but not with environmental factors contributing to RDA1 and obtained range of variation of ΔpCO_2 within stations. The seasonal pattern of ΔpCO_2 is clearly shown in RDA analysis as it was weaker from October to March compared to months between April and June (**Figure 6**).

DISCUSSION

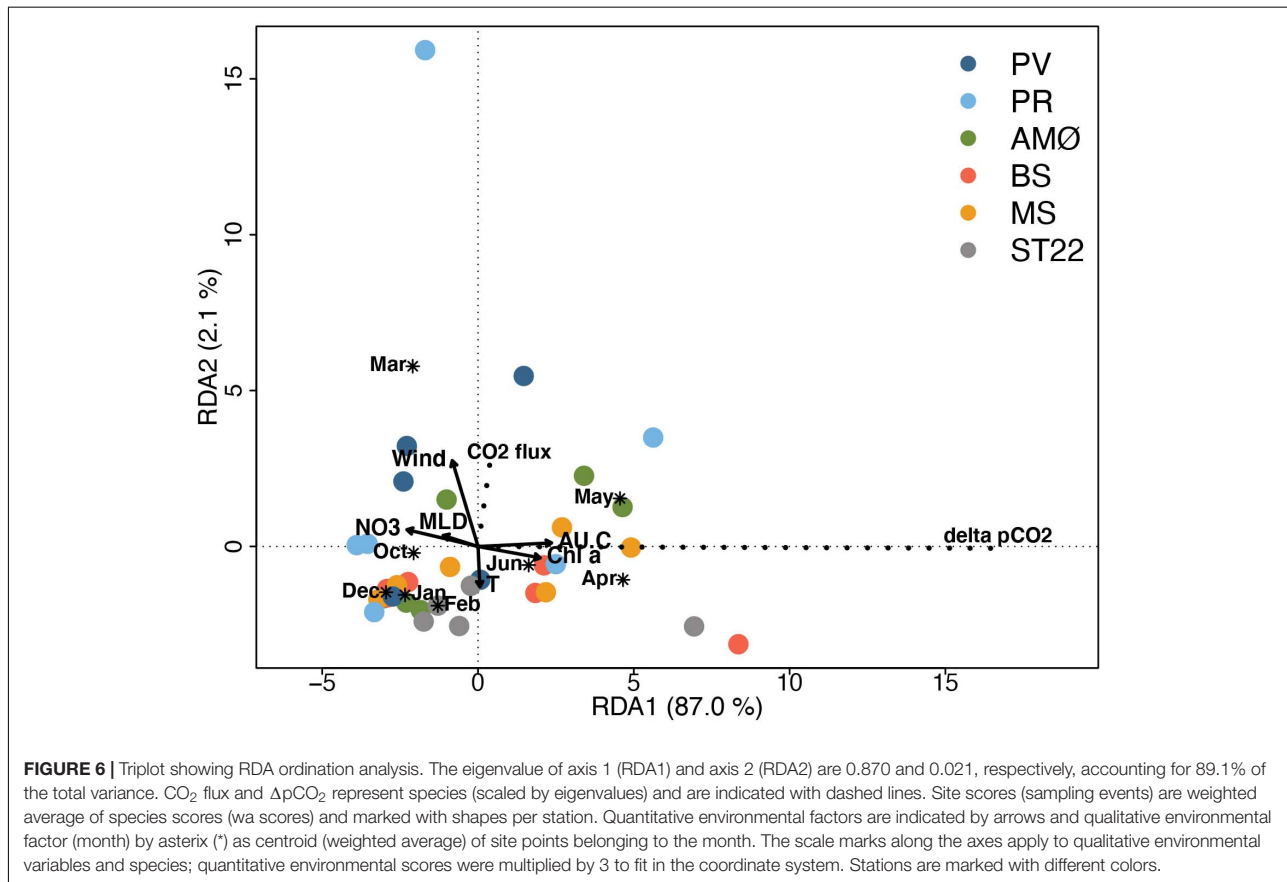
Physical Controls of Seasonality in ΔpCO_2 and CO₂ Flux

Distinct variation in sea-air CO₂ flux between stations was clearly observed despite similar seasonal trends in ΔpCO_2 among



stations. Also, the flux of CO₂ did not show the summer-winter seasonality that was prevailing in ΔpCO_2 . An expected spring/early summer increase in CO₂ flux was not as clear at all the stations as initially expected, given a low temperature and rapidly increasing CO₂ fixation by predominantly autotrophic phytoplankton. This was especially evident at BS in Balsfjord and ST22 in Finn fjord Indre where increase in CO₂ flux was almost

indistinguishable, and in addition, a difference in magnitude was observed between stations during that season (**Figure 1**). Similar observations of summer-winter contrast between ΔpCO_2 and the flux of CO₂ have been made in Barents Sea where the seasonal variation in CO₂ flux was largely determined by an interaction of wind and ΔpCO_2 (Omar et al., 2007). Turbulence of surface waters as a result of wind velocity are known to have



a significant role in controlling the instantaneous rate of sea-air exchange of CO₂ (Wanninkhof, 2014). In this study, the ΔpCO₂ was similar between stations but instantaneous wind speed varied. Therefore, the weak CO₂ uptake in Finnjord Indre was likely a result of low wind speed and correspondingly, the greatest CO₂ fluxes documented at PR and PV in Porsangerfjord may be attributed to high wind speeds. The total variation in ΔpCO₂ at ST22 in Finnjord Indre was between −194 and −49 μatm. That was well within the range of ΔpCO₂ values measured at other in-fjord stations, which were between −218 and −13 μatm. As a result, it is unlikely that ΔpCO₂ alone explains the low flux values at this location. Furthermore, modest CO₂ fluxes obtained from Kaldfjord (neighboring our study site in Balsfjord) have been attributed to low wind speed (average $3.3 \pm 2.1 \text{ m s}^{-1}$) (Jones et al., 2020). There, the low wind speed is caused by orographic steering as the fjord is surrounded by steep topography, i.e., mountains, resulting in modest annual carbon uptake compared to for example the Norwegian Sea and the non-ice covered Arctic shelf seas (Jones et al., 2020). At MS in Malangen Fjord, where wind speed was largely constant across seasons ($4\text{--}6 \text{ m s}^{-1}$), the variation in CO₂ flux is instead more related to the intensified gradient of CO₂ and changes in surface water temperature (Figures 1, 2B). It follows that the capacity for northern Norwegian fjord systems in this study to act as a CO₂ sink varied considerably with local weather

conditions, such as wind. Although, additional high frequency measurements, potentially covering greater spatial resolution are needed to confirm this relationship and to further capture sporadic variability from annual variation.

Given the central role of salinity in driving the surface pCO₂ (Weiss, 1974; Meire et al., 2015; Jones et al., 2020), the significant correlation between surface water salinity and ΔpCO₂ at AMØ in Altafjord is unsurprising. However, riverine inflow in Altafjord was considerably less than in Malangen Fjord (Supplementary Figure 7) where station MS did not show a significant relationship with surface water salinity. The watershed area around Altafjord is the largest among fjords and Finnjord Indre and therefore it might receive more freshwater runoff and precipitation than implied by the total flow rate of the main rivers. It is possible our correlation analysis did not detect the effect of low salinity on ΔpCO₂ at MS since the surface water salinity at this station was constantly lower (26.5–32.4) than any other station (28.2–34.2). Furthermore, the timing of our sampling in April that recorded the strongest ΔpCO₂ was measured before the pronounced summer and autumn salinity decreases from terrestrial inflow would have occurred (Figure 2B). In comparison, the decreases in salinity in Porsangerfjord, Balsfjord and Finnjord Indre were briefly present during summer, as seen in CTD-profiles (Supplementary Figures 1, 2, 4, 6). Despite the lack of correlation between salinity and ΔpCO₂ in this

study, it is possible that the high $\Delta p\text{CO}_2$ in June that occurred after the main spring bloom event can be associated with the surface water freshening as was observed in Kaldfjord where freshwater input in June was related for pronounced decrease in total dissolved inorganic carbon concentration (Jones et al., 2020). This is especially true at PR, AMØ and BS stations that had lower surface water salinities than at PV and ST22 (**Figure 2B** and **Supplementary Figure 7**).

The competing effects of warming temperature (warm water holds less CO₂) with PP (autotrophic uptake of CO₂) on $\Delta p\text{CO}_2$ was most pronounced at ST22 in Finn fjord Indre in June. This response was also documented at all other stations but to a lesser extent (**Figure 1**). At ST22 the seasonal increase in temperature from April to June was +4.8°C and there was a simultaneous decrease in $\Delta p\text{CO}_2$ of >100 μatm . This is approximately 50 μatm more than the effect of temperature alone, as an increase in water temperature 1°C corresponds ~10 μatm increase in $p\text{CO}_2$ (Takahashi et al., 1993). Often, the biological fixation of CO₂ compensates the effect of temperature during summer as observed at MS in Malangen Fjord and AMØ in Altafjord (Takahashi et al., 2002; Jones et al., 2020). Therefore, it indicates that at ST22, in addition to temperature and phytoplankton production, other processes affected the $\Delta p\text{CO}_2$. The temperature- $\Delta p\text{CO}_2$ relationship was only statistically significant at MS, although at all stations high surface water temperature and damped biological activity can be considered to lead to a weakened gradient of $p\text{CO}_2$ in October (Jones et al., 2020). Most likely that can be explained by few data points per station, however, the relationship was not clear in RDA analyses either when all observations were analyzed together.

A weak pycnocline, representing a prolonged period of mixing in the upper water column, has been well documented in northern Norwegian fjords (Reigstad and Wassmann, 1996; Eilertsen and Skarðhamar, 2006). These observations are further supported by this study, where all fjords and Finn fjord Indre bay experienced a weak or an absent pycnocline from late October to March/April (**Supplementary Figures 1–6**). Deep vertical mixing in winter, together with advection of Norwegian coastal waters, can entrain nutrients and increase salinity in the surface waters of fjords. The inverse relationship between MLD and $\Delta p\text{CO}_2$ was statistically significant at PV, PR and AMØ in the two northernmost fjords (Porsangerfjord and Altafjord) and at ST22 in Finn fjord Indre, potentially indicating that the MLD does not drive observed changes in $\Delta p\text{CO}_2$ at all fjords sites in this study. Small effects of mixing and advection on $p\text{CO}_2$ (0.1–10 μatm as monthly changes) is also reported in Adventfjorden in Svalbard (Ericson et al., 2018). Although, outcomes from the RDA analysis (**Figure 6**) suggest that MLD may have a greater influence on $\Delta p\text{CO}_2$ during autumn and early winter. Here, the smallest $\Delta p\text{CO}_2$ in December can be associated with the timing of water column instability indicating enrichment of CO₂ from subsurface and bottom water similar to observation made in Kaldfjord (Jones et al., 2020). The most pronounced decrease in the strength of $\Delta p\text{CO}_2$ occurred at PR in Porsangerfjord suggesting that deepening MLD merges CO₂ enriched subsurface water with higher inorganic carbon content into the surface layer than at other stations. As PR is located behind a shallow sill in the

inner part of Porsangerfjord, advection of subsurface water may be partly hindered (Mankettikara, 2013). The lower temperature and salinity (**Figure 2A**) also indicate that the waters of the inner part of Porsangerfjord (i.e., at PR) are less influenced by Norwegian Coastal Waters than outer Porsangerfjord, Altafjord and Malangen Fjord, where water exchanges with coastal waters including Atlantic Water in summer take place at frequent intervals diminishing the residence time of these fjord waters (Svendsen, 1995; Nordby et al., 1999; Eilertsen and Skarðhamar, 2006). Our measurements of high salinity and temperature below 50 m at PV, AMØ and MS stations support such processes of water mass exchange. Like Porsangerfjord, Balsfjord has low riverine runoff and limited deep water exchange with coastal waters (Svendsen, 1995; Mankettikara, 2013), as supported by generally lower salinity and lower maximum temperature than all other stations, except PV (**Figure 2A**). Despite the similarity of BS to PR, the $\Delta p\text{CO}_2$ in October and December at BS in Balsfjord was not as weak as at PR in inner Porsangerfjord (**Figure 1**). It is known that fjord circulation in Balsfjord is mainly driven by winds that alternate between down- and up-fjord wind directions (Svendsen, 1995). In spring the change from persistent down-fjord wind (to the fjord opening) to the up-fjord wind leads to the larger inflow of coastal waters into Balsfjord (Svendsen, 1995; Eilertsen and Skarðhamar, 2006). However, the surface waters (upper layer) in Balsfjord might be exchanged relatively frequently with waters from Malangen Fjord, as there is an unique multilayered (separated upper and intermediate layer) circulation (Svendsen, 1995). Shallow Finn fjord Indre with strong current likely transports effectively surface and subsurface water, thus diminishing the effect of mixing observed in autumn and winter on $\Delta p\text{CO}_2$ at ST22 compared to fjord stations.

Biological Drawdown of CO₂

Autotrophic phytoplankton consume dissolved CO₂ and thereby reduce $p\text{CO}_2$ in the photic zone. The development of a spring bloom was highly pronounced during sampling of all study locations, with latitude-dependent increases in chl *a* concentrations increasing over the spring-summer (**Figure 3A**). Bloom development was first observed in late March of the non-stratified water columns of southernmost fjord stations, BS and MS, as well as the coastal ST22 in Finn fjord Indre. The bloom was subsequently delayed by approximately 1 month in the more northern stations (AMØ, PV and PR) in Altafjord and Porsangerfjord. The strong correlation between $\Delta p\text{CO}_2$, biological variables (i.e., chl *a* and phytoplankton biomass) and nutrient at 5 m supports the strong influence of these phytoplankton blooms on CO₂ drawdown in the fjord systems of this study (**Figure 5**). The impact of phytoplankton production on $\Delta p\text{CO}_2$ was thus most notable from April to June, when average $\Delta p\text{CO}_2$ among all the stations was –134 μatm , which is nearly 3.5 times higher than the average taken across autumn and winter months (–40 μatm). The average seasonal $\Delta p\text{CO}_2$ amplitude here corresponds to those measured in Kaldfjord in northern Norway and in Godthåbsfjord in Greenland (Meire et al., 2015; Jones et al., 2020). The strong summertime $\Delta p\text{CO}_2$ was less extreme at the most open station (PV) where considerably lower chl *a* and phytoplankton biomass values

were measured compared to other stations (Figure 3A). We expect this was a result of the nearly homogenous water column at PV, which occurred as a result of enhanced seawater exchange with the coastal ocean and limited influence freshwater inflow at this location (Supplementary Figures 1, 7). This likely hindered growth of phytoplankton in the surface layer as they are constantly mixed out of the euphotic zone (Eilertsen and Frantzen, 2007).

The estimated net PP per sampling day was high in June and April, especially at BS in Balsfjord and MS in Malangen Fjord (Figure 4), but corresponds to the daily values obtained from 14°C carbon uptake measurements in Balsfjord in April (Eilertsen and Taasen, 1984). The cause of high PP at MS is uncertain. However, it may have been a result of one or a combination of i) high riverine input of nutrients, ii) prominent stratification of the water column facilitating greater light availability through positioning of cells in the upper water column, and iii) greater intensity of downwelling radiation due to the southerly location of this fjord. Between June and July daily net community production of 300–600 mg C d⁻¹ has been reported in the central Barents Sea, that corresponds to the PP estimated at PV in June (Luchetta et al., 2000). In May, the daily PP estimates at PV and AMØ are in line with, and at BS, PR, MS twice as high as, values obtained in Svalbard (Kongsfjorden) and Greenland (Godthåbsfjord) where highest PP in April/May were 1500–1850 mg C d⁻¹ (Hodal et al., 2012; Meire et al., 2015). The annual PP was not directly measured here, however, a previous estimate (Eilertsen and Taasen, 1984) of PP (100 g C m⁻² yr⁻¹) at this latitude indicates that it likely corresponds to or even exceeds at the southernmost stations. The high productivity in northern Norwegian fjords and coastal regions represents a high potential for CO₂ uptake (Smith et al., 2015). In this study, the highest PP was obtained at MS in Malangen Fjord in April corresponding to a CO₂ consumption of 23 g m⁻² d⁻¹. While an uncertain proportion of the consumed CO₂ will be released back to the atmosphere via respiration, the fate of biologically fixed CO₂ during productive season has an important role determining the saturation state of CO₂ in surface water afterward. If a large part of the produced biomass is exported from the fjords by advection as observed previously in Balsfjord and Malangen Fjord (Reigstad and Wassmann, 1996) then a higher net CO₂ uptake is possible on annual scale.

Flux Estimates in the Context of Existing Knowledge

Our CO₂ flux results correspond, in terms of magnitude, with reported findings from other high-latitude fjords and coastal shelves. The nearest observations are from Kaldfjord (near Balsfjord) with an annual average and maximum CO₂ flux of -0.86 and -2.7 mmol m⁻² d⁻¹, respectively (Jones et al., 2020). During winter the Norwegian North Atlantic current system is reported to have an average sea-air flux of CO₂ between -6 and -2 mmol m⁻² d⁻¹ (Olsen et al., 2003) while the annual flux of -11 mmol m⁻² d⁻¹ was estimated in the Norwegian Sea (Yasunaka et al., 2016). Measurements in sea-ice

free Adventfjorden in Svalbard showed sea-air flux to vary between -16 and -4 mmol m⁻² d⁻¹ across time series of 1 year (Ericson et al., 2018).

It is important to note that the above-mentioned studies applied different methods than were used here. However, with the significant overlap in flux measurements we believe use of the membrane equilibration in nondispersive IR (NDIR) spectrometry-based CO₂ instrument was an effective means of characterizing gradient of CO₂ and exchange of CO₂ gas between the atmosphere and surface water in this study. Furthermore, the parallel study of Jones et al. (2020), whom based their surface water fugacity of CO₂ (pCO₂) determination, and thereafter CO₂ flux calculations, on total inorganic carbon (DIC) and TA values in nearby Kaldfjord with comparable physical (temperature, salinity, wind) and biological conditions, especially Balsfjord and Finnfjord Indre, showed similar magnitudes of CO₂ flux and ΔpCO₂ to what is reported here. Yet, the different methods are not 100 % comparable as it has been shown that depending on choice of the dissociation constants (K₁ and K₂), computed pCO₂ values from other carbonate system parameters (TA, DIC, pH) can be up to 10 % lower than those of direct measurements (Lueker et al., 2000). Nonetheless, we assume that the estimated annual uptake of atmospheric CO₂ in Kaldfjord was -0.32 ± 0.03 mol C m⁻² can roughly be used as a reference to the Finnfjord Indre and Balsfjord measurements, based on the above-mentioned similarities.

CONCLUSION

This study was designed to characterize sea-air CO₂ flux along coastal northern Norway in the context of physical and biological factors. From our assessment we find that wind speed is the physical factor which has the greatest effect on the variability in CO₂ flux between stations, followed by the magnitude of atmospheric CO₂ flux. Despite this critical influence of wind speed on flux magnitude, ΔpCO₂ is the main driving force to pull CO₂ gas from atmosphere to sea. The spring-summer phytoplankton bloom has been documented here as a main controlling factor of ΔpCO₂ during the polar day. However, in this study we found that the strong summertime drawdown of CO₂ cannot account for the maintained state of CO₂ undersaturation, with respect to atmosphere, that was documented throughout the year at our study locations. This study provides new spatial and seasonal insights about the strength of carbon sink and CO₂ saturation state in northern Norwegian fjords and coastal regions. Also, this study supports previous estimates that high-latitude coastal areas are undersaturated with respect to atmospheric CO₂. However, better spatial, and temporal coverage within the fjords – scaling from the proximity of freshwater discharge at the head to coastal water inflow at the mouth of the fjord – is needed to further characterize the complex trends of sea-air CO₂ flux in these systems, and to quantify the annual CO₂ uptake representing the entire region. With a warmer future climate, the strong seasonality in freshwater input is expected to change

and as a result longer stratification period becomes likely prevailing in this region that can influence mixing of the water column and phytoplankton bloom dynamics and thus potential change in atmospheric carbon uptake is possible. To further understand how such changing freshwater inputs will affect the hydrography and water circulation with related CO₂ flux in these fjords, more detailed studies of water mass exchange and circulation, including the role of advection, should be included in future studies.

DATA AVAILABILITY STATEMENT

The original contributions presented in the study are included in the article/**Supplementary Material**, further inquiries can be directed to the corresponding author. All data, calculations and figure generation scripts are provided and linked to R markdown files deposited on the Open Science Framework project: Northern Norwegian Fjord CO₂ Flux (<https://osf.io/tbzse/>).

AUTHOR CONTRIBUTIONS

NJA, HCB, and HCE conceptualized the study. NJA conducted the field work, sample processing, the main analysis, and wrote the manuscript draft. HCE provided the primary production estimates. KC helped with nutrient analyses. All authors contributed to the final version.

REFERENCES

- Bates, N. R. (2006). Air-sea CO₂ fluxes and the continental shelf pump of carbon in the Chukchi Sea adjacent to the Arctic Ocean. *J. Geophys. Res.* 111:C10013. doi: 10.1029/2005jc003083
- Bax, N., and Eliassen, J.-E. (1990). Multispecies analysis in Balsfjord, northern Norway: solution and sensitivity analysis of a simple ecosystem model. *ICES J. Mar. Sci.* 47, 175–204. doi: 10.1093/icesjms/47.2.175
- Chen, C. T. A., Huang, T. H., Chen, Y. C., Bai, Y., He, X., and Kang, Y. (2013). Air-sea exchanges of CO₂ in the world's coastal seas. *Biogeosciences* 10, 6509–6544. doi: 10.5194/bg-10-6509-2013
- Degerlund, M., and Eilertsen, H. C. (2010). Main species characteristics of phytoplankton spring blooms in NE Atlantic and Arctic waters (68–80°N). *Estuaries Coasts* 33, 242–269. doi: 10.1007/s12237-009-9167-7
- Delaigue, L., Helmuth, T., and Mucci, A. (2020). Spatial variations in CO₂ fluxes in the Saguenay Fjord (Quebec, Canada) and results of a water mixing model. *Biogeosciences* 17, 547–566. doi: 10.5194/bg-17-547-2020
- Edler, L., and Elbrächter, M. (2010). “The utermöhl method for quantitative phytoplankton analysis,” in *Microscopic and Molecular Methods for Quantitative Phytoplankton Analysis*, Vol. 110, eds B. Karlson, C. Cusack, and E. Bresnan (Paris: Intergovernmental Oceanographic Commission Manual and guides), 13–20.
- Eilertsen, H. C., and Degerlund, M. (2010). Phytoplankton and light during the northern high-latitude winter. *J. Plankton Res.* 32, 899–912. doi: 10.1093/plankt/fbq017
- Eilertsen, H. C., and Frantzen, S. (2007). Phytoplankton from two sub-Arctic fjords in northern Norway 2002–2004: I. Seasonal variations in chlorophyll a and bloom dynamics. *Mar. Biol. Res.* 3, 319–332. doi: 10.1080/17451000701632877
- Eilertsen, H. C., and Holm-Hansen, O. (2000). Effects of high latitude UV radiation on phytoplankton and nekton modelled from field measurements by simple algorithms. *Polar Res.* 19, 173–182. doi: 10.3402/polar.v19i2.6543

FUNDING

This study was supported by strategic funds from UiT – The Arctic University of Norway allocated to understanding environmental impacts of the project Mass Cultivation of Diatoms at Finnfjord AS and was also supported by contributions from ARC- The Arctic Centre for Sustainable Energy. Work by KC was supported by the Diatom ARCTIC project (NE/R012849/1; 03F0810A), part of the Changing Arctic Ocean program, jointly funded by the UKRI Natural Environmental Research Council (NERC) and the German Federal Ministry of Education and Research (BMBF).

ACKNOWLEDGMENTS

We would gratefully thank the captain and crew of RV Johan Ruud for the fieldwork support. We acknowledge Ingeborg Giæver (UiT) and Reetta Sætre for the help on fieldwork in Finnfjord Indre as well as the collaborations between Finnfjord AS and UiT-The Arctic University of Norway that support field sampling facilities.

SUPPLEMENTARY MATERIAL

The Supplementary Material for this article can be found online at: <https://www.frontiersin.org/articles/10.3389/fmars.2021.692093/full#supplementary-material>

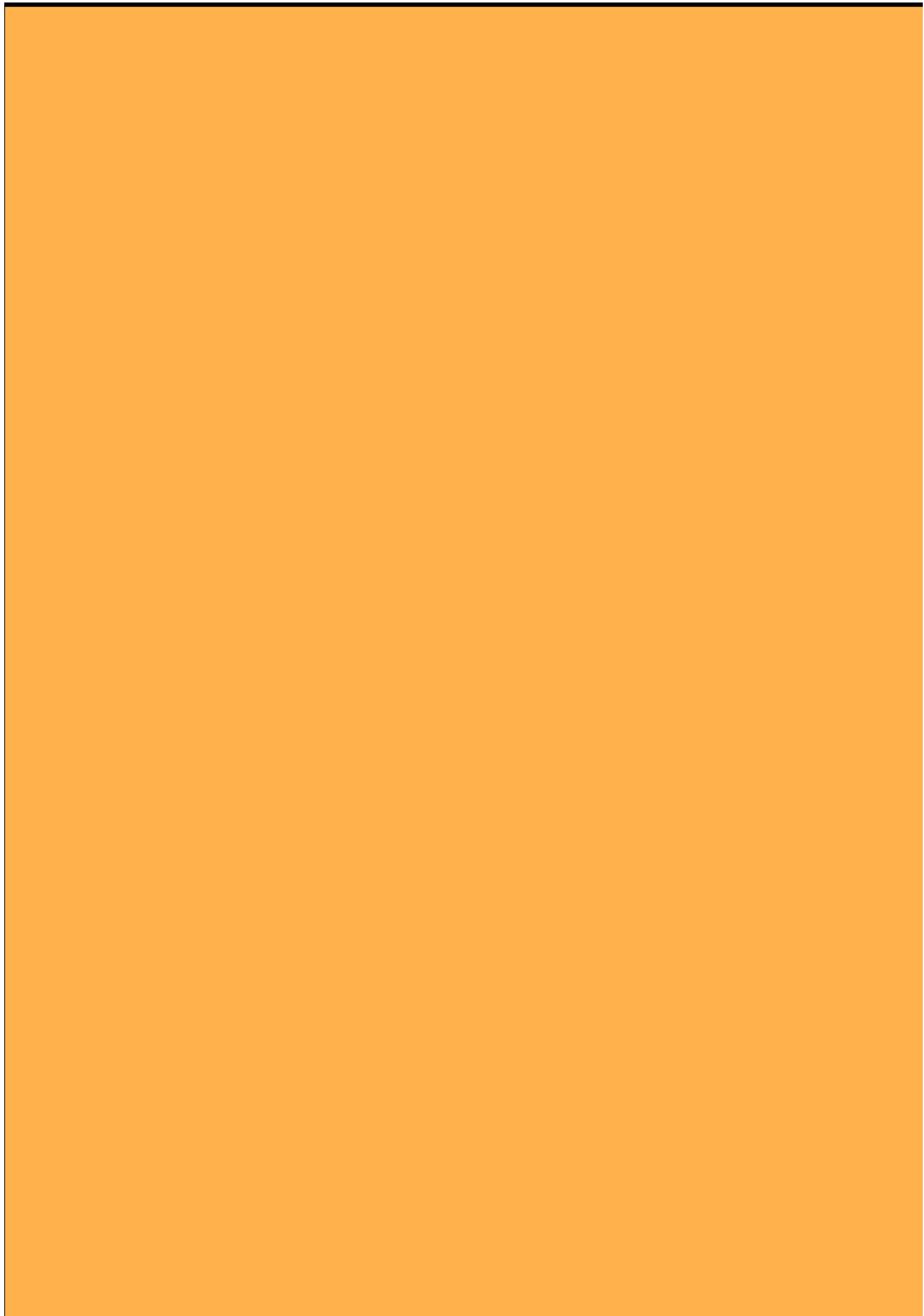
- Eilertsen, H. C., and Skarðhamar, J. (2006). Temperatures of north Norwegian fjords and coastal waters: variability, significance of local processes and air-sea heat exchange. *Estuar. Coast. Shelf Sci.* 67, 530–538. doi: 10.1016/j.ecss.2005.12.006
- Eilertsen, H. C., and Taasen, J. (1984). Investigations on the plankton community of Balsfjorden, northern Norway. The phytoplankton 1976–1978. Environmental factors, dynamics of growth, and primary production. *Sarsia* 69, 1–15. doi: 10.1080/00364827.1984.10420584
- Ericson, Y., Falck, E., Chierici, M., Fransson, A., and Kristiansen, S. (2019). Marine CO₂ system variability in a high arctic tidewater-glacier fjord system, Tempelfjorden, Svalbard. *Cont. Shelf Res.* 181, 1–13. doi: 10.1016/j.csr.2019.04.013
- Ericson, Y., Falck, E., Chierici, M., Fransson, A., Kristiansen, S., Platt, S. M., et al. (2018). Temporal variability in surface water pCO₂ in Adventfjorden (West Spitsbergen) with emphasis on physical and biogeochemical drivers. *J. Geophys. Res. Oceans* 123, 4888–4905. doi: 10.1029/2018jc014073
- Frouin, R., Lingner, D. W., Gautier, C., Baker, K. S., and Smith, R. C. (1989). A simple analytical formula to compute clear sky total and photosynthetically available solar irradiance at the ocean surface. *J. Geophys. Res. Oceans* 94, 9731–9742. doi: 10.1029/jc094ic07p09731
- Hansen, G. A., and Eilertsen, H. C. (1995). “Modelling the onset of phytoplankton blooms: a new approach,” in *Ecology of Fjords and Coastal Waters*, eds H. R. Skjoldal, C. Hopkins, K. E. Erikstad, and H. P. Leinaas (Amsterdam: Elsevier Science).
- Hartman, B., and Hammond, D. E. (1985). “Gas exchange in San Francisco Bay,” in *Temporal Dynamics of an Estuary: San Francisco Bay. Developments in Hydrobiology*, eds J. E. Cloern and F. H. Nichols (Dordrecht: Springer), 59–68. doi: 10.1007/978-94-009-5528-8_4
- Hodal, H., Falk-Petersen, S., Hop, H., Kristiansen, S., and Reigstad, M. (2012). Spring bloom dynamics in Kongsfjorden, Svalbard: nutrients, phytoplankton,

- protozoans and primary production. *Polar Biol.* 35, 191–203. doi: 10.1007/s00300-011-1053-7
- Holm-Hansen, O., and Riemann, B. (1978). Chlorophyll a determination: improvements in methodology. *Oikos* 30, 438–447. doi: 10.2307/3543338
- Iqbal, M. (2012). *An Introduction to Solar Radiation*. Amsterdam: Elsevier.
- Jones, E. M., Renner, A. H., Chierici, M., Wiedmann, I., Lødemel, H. H., and Biuw, M. (2020). Seasonal dynamics of carbonate chemistry, nutrients and CO₂ uptake in a sub-Arctic fjord. *Elem. Sci. Anth.* 8:41.
- Larsen, L.-H. (2015). *Program for Miljøundersøkelse i Vannforekomsten Finnfjorden Indre i Lenvik kommune, Troms Fylke*. Tromsø: Akvaplan-niva.
- Luchetta, A., Lipizer, M., and Socal, G. (2000). Temporal evolution of primary production in the central Barents Sea. *J. Mar. Syst.* 27, 177–193. doi: 10.1016/S0924-7963(00)00066-x
- Lueker, T. J., Dickson, A. G., and Keeling, C. D. (2000). Ocean pCO₂ calculated from dissolved inorganic carbon, alkalinity, and equations for K₁ and K₂: validation based on laboratory measurements of CO₂ in gas and seawater at equilibrium. *Mar. Chem.* 70, 105–119. doi: 10.1016/S0304-4203(00)00022-0
- Mankettikara, R. (2013). *Hydrophysical Characteristics of the Northern Norwegian Coast and Fjords*. Doctoral Thesis. Tromsø: University of Tromsø.
- Meire, L., Sogaard, D., Mortensen, J., Meysman, F., Soetaert, K., Arendt, K., et al. (2015). Glacial meltwater and primary production are drivers of strong CO₂ uptake in fjord and coastal waters adjacent to the Greenland Ice Sheet. *Biogeosciences* 12, 2347–2363. doi: 10.5194/bg-12-2347-2015
- Michelsen, H. K., Svensen, C., Reigstad, M., Nilssen, E. M., and Pedersen, T. (2017). Seasonal dynamics of meroplankton in a high-latitude fjord. *J. Mar. Syst.* 168, 17–30. doi: 10.1016/j.jmarsys.2016.12.001
- Nordby, E., Tande, K. S., Svendsen, H., Slagstad, D., and Båmstedt, U. (1999). Oceanography and fluorescence at the shelf break off the north Norwegian coast (69° N–70° 30' N) during the main productive period in 1994. *Sarsia* 84, 175–189. doi: 10.1080/00364827.1999.10420424
- Norwegian Environment Agency (2021). *Finnfjord – Releases of Carbon Dioxide fossil (CO₂ (F))*. Available online at: <https://www.norskeutslipp.no/en/Miscellaneous/Company/?CompanyID=5712&ComponentPageID=180> (accessed February 03, 2021)
- Oksanen, J., Blanchet, F. G., Kindt, R., Legendre, P., Minchin, P., O'hara, R., et al. (2013). *Community Ecology Package. R Package Version 2(0)*.
- Olsen, A., Bellerby, R. G., Johannessen, T., Omar, A. M., and Skjelvan, I. (2003). Interannual variability in the wintertime air–sea flux of carbon dioxide in the northern North Atlantic, 1981–2001. *Deep Sea Res. Part I Oceanogr. Res. Pap.* 50, 1323–1338. doi: 10.1016/S0967-0637(03)00144-4
- Omar, A. M., Johannessen, T., Olsen, A., Kaltin, S., and Rey, F. (2007). Seasonal and interannual variability of the air–sea CO₂ flux in the Atlantic sector of the Barents Sea. *Mar. Chem.* 104, 203–213. doi: 10.1016/j.marchem.2006.11.002
- Oug, E., and Høiseeter, T. (2000). Soft-bottom macrofauna in the high-latitude ecosystem of Balsfjord, northern Norway: species composition, community structure and temporal variability. *Sarsia* 85, 1–13. doi: 10.1080/00364827.2000.10414551
- Peralta-Ferriz, C., and Woodgate, R. A. (2015). Seasonal and interannual variability of pan-Arctic surface mixed layer properties from 1979 to 2012 from hydrographic data, and the dominance of stratification for multiyear mixed layer depth shoaling. *Prog. Oceanogr.* 134, 19–53. doi: 10.1016/j.pocan.2014.12.005
- R Core Team (2013). *R: A Language and Environment for Statistical Computing*. Vienna: R Foundation for Statistical Computing.
- Reigstad, M., and Wassmann, P. (1996). Importance of advection for pelagic-benthic coupling in north Norwegian fjords. *Sarsia* 80, 245–257. doi: 10.1080/00364827.1996.10413599
- Rysgaard, S., Mortensen, J., Juul-Pedersen, T., Sørensen, L. L., Lennert, K., Sogaard, D., et al. (2012). High air–sea CO₂ uptake rates in nearshore and shelf areas of Southern Greenland: temporal and spatial variability. *Mar. Chem.* 128, 26–33. doi: 10.1016/j.marchem.2011.11.002
- Sejr, M., Krause-Jensen, D., Rysgaard, S., Sørensen, L., Christensen, P., and Glud, R. N. (2011). Air–sea flux of CO₂ in arctic coastal waters influenced by glacial melt water and sea ice. *Tellus B Chem. Phys. Meteorol.* 63, 815–822. doi: 10.1111/j.1600-0889.2011.00540.x
- Skarðhamar, J., and Svendsen, H. (2005). Circulation and shelf–ocean interaction off North Norway. *Cont. Shelf Res.* 25, 1541–1560. doi: 10.1016/j.csr.2005.04.007
- Smith, R. W., Bianchi, T. S., Allison, M., Savage, C., and Galy, V. (2015). High rates of organic carbon burial in fjord sediments globally. *Nat. Geosci.* 8, 450–453. doi: 10.1038/ngeo2421
- Strickland, J. D. H., and Parsons, T. R. (1972). “Determination of carbonate, bicarbonate, and free carbon dioxide from pH and alkalinity measurements,” in *A Practical Hand Book of Seawater Analysis*, 2nd Edn, ed. J. C. Stevenson (Ottawa, ON: Fisheries Research Board of Canada), 310.
- Svendsen, H. (1995). “Physical oceanography of coupled fjord-coast systems in northern Norway with special focus on frontal dynamics and tides,” in *Ecology of Fjords and Coastal Waters*, eds H. R. Skjoldal, C. Hopkins, K. E. Erikstad, and H. P. Leinaas (Amsterdam: Elsevier), 149–164.
- Takahashi, T., Olafsson, J., Goddard, J. G., Chipman, D. W., and Sutherland, S. (1993). Seasonal variation of CO₂ and nutrients in the high-latitude surface oceans: a comparative study. *Global Biogeochem. Cycles* 7, 843–878. doi: 10.1029/93gb02263
- Takahashi, T., Sutherland, S. C., Sweeney, C., Poisson, A., Metzl, N., Tilbrook, B., et al. (2002). Global sea-air CO₂ flux based on climatological surface ocean pCO₂ and seasonal biological and temperature effects. *Deep Sea Res. Part II Top. Stud. Oceanogr.* 49, 1601–1622. doi: 10.1016/S0967-0645(02)00037-6
- Telmer, K., and Veizer, J. (1999). Carbon fluxes, pCO₂ and substrate weathering in a large northern river basin, Canada: carbon isotope perspectives. *Chem. Geol.* 159, 61–86. doi: 10.1016/S0009-2541(99)00034-0
- Thomas, H., Bozec, Y., Elkalay, K., and De Baar, H. J. (2004). Enhanced open ocean storage of CO₂ from shelf sea pumping. *Science* 304, 1005–1008. doi: 10.1126/science.1095491
- Tomás, C. R. (1997). *Identifying Marine Phytoplankton*. Amsterdam: Elsevier.
- Tsunogai, S., Watanabe, S., and Sato, T. (1999). Is there a “continental shelf pump” for the absorption of atmospheric CO₂? *Tellus B Chem. Phys. Meteorol.* 51, 701–712. doi: 10.3402/tellusb.v51i3.16468
- Wanninkhof, R. (2014). Relationship between wind speed and gas exchange over the ocean revisited. *Limnol. Oceanogr. Methods* 12, 351–362. doi: 10.4319/lom.2014.12.351
- Wassmann, P., Svendsen, H., Keck, A., and Reigstad, M. (1996). Selected aspects of the physical oceanography and particle fluxes in fjords of northern Norway. *J. Mar. Syst.* 8, 53–71. doi: 10.1016/0924-7963(95)00037-2
- Webb, W. L., Newton, M., and Starr, D. (1974). Carbon dioxide exchange of *Alnus rubra*. *Oecologia* 17, 281–291. doi: 10.1007/bf00345747
- Weiss, R. F. (1974). Carbon dioxide in water and seawater: the solubility of a non-ideal gas. *Mar. Chem.* 2, 203–215. doi: 10.1016/0304-4203(74)90015-2
- Włodarska-Kowalczyk, M., Mazurkiewicz, M., Górska, B., Michel, L. N., Jankowska, E., and Zaborska, A. (2019). Organic carbon origin, benthic faunal consumption, and burial in sediments of Northern Atlantic and Arctic Fjords (60–81° N). *J. Geophys. Res. Biogeosci.* 124, 3737–3751. doi: 10.1029/2019jg005140
- Yasunaka, S., Murata, A., Watanabe, E., Chierici, M., Fransson, A., van Heuven, S., et al. (2016). Mapping of the air–sea CO₂ flux in the Arctic Ocean and its adjacent seas: basin-wide distribution and seasonal to interannual variability. *Polar Sci.* 10, 323–334. doi: 10.1016/j.polar.2016.03.006

Conflict of Interest: The authors declare that the research was conducted in the absence of any commercial or financial relationships that could be construed as a potential conflict of interest.

Copyright © 2021 Aalto, Campbell, Eilertsen and Bernstein. This is an open-access article distributed under the terms of the Creative Commons Attribution License (CC BY). The use, distribution or reproduction in other forums is permitted, provided the original author(s) and the copyright owner(s) are credited and that the original publication in this journal is cited, in accordance with accepted academic practice. No use, distribution or reproduction is permitted which does not comply with these terms.

Paper II



1 **Microbial community dynamics during a harmful *Chrysochromulina leadbeateri* bloom**

2

3 Nerea J. Aalto^{1,2}, Hannah Schweitzer^{1,2}, Erlend Grann-Meyer¹, Stina Krsmanovic¹, Jon Brage
4 Svenning¹, Lars Dalheim¹, Sebastian Petters¹, Richard Ingebrigtsen¹, Chris J. Hulatt³, Hans C.
5 Bernstein^{1,2*}

6

7 **Affiliations:**

8 *1. Norwegian College of Fisheries Sciences, UiT - The Arctic University of Norway, Tromsø,*
9 *Norway*

10 *2. The Arctic Centre for Sustainable Energy, UiT - The Arctic University of Norway, Tromsø,*
11 *Norway*

12 *3. Faculty of Biosciences and Aquaculture, Nord University, Bodø, Norway*

13

14

15

16 ***Correspondence:** Hans C. Bernstein, UiT-The Arctic University of Norway, BFE-fak.,
17 Postboks 6050 Langnes, 9037 Tromsø, NORWAY; *Phone:* +47 776 46 114; *Email:*

18 Hans.C.Bernstein@uit.no

19

20 **Running Title:** Ecology of the Norwegian harmful algae bloom of 2019

21

22 **Keywords:** Marine Microbiome, Harmful Algae, Aquaculture, Norway, Time Series Analysis

23

24

25 **ABSTRACT**

26 In late spring 2019 a harmful algae bloom occurred across multiple, interconnected fjords and
27 bays in northern Norway. This was a major event causing severe fish mortality at several salmon
28 aquaculture facilities in the region. The reported focal taxon and suspected agent of fish
29 mortality was a *Chrysochromulina leadbeateri*-like prymnesiophyte that was morphologically
30 identical to the UiO-035 isolate collected from a similar bloom from the same region in 1991.
31 This study reports on succession dynamics of the marine microbiome via detectable changes in
32 abundance of 18S and 16S rRNA gene amplicon sequence variants and closely related taxa of
33 the focal strain *C. leadbeateri* UiO-035. This taxon co-bloomed with a diverse group of
34 microeukaryotes and prokaryotes and their temporal succession dynamics revealed high
35 variability with strong shifts in abundance during the event. These blooming patterns were
36 poorly connected to environmental conditions suggesting that other factors such as biological
37 interactions may be at least as important in shaping the dynamics of this type of harmful algae
38 bloom. A deeper understanding of microbiome succession patterns during these rare but
39 destructive bloom events will help guide future efforts to generate predictive models and
40 anticipate deviations from the natural bloom cycles of the northern Norwegian fjord systems
41 that are home to large scale aquaculture activities.

42

43

44

45

46

47

48

49

50 INTRODUCTION

51 Harmful algal blooms (HABs) are common in warm and temperate waters, but also occur in
52 northern cold water ecosystems (Hallegraeff et al., 2021; Karlson et al., 2021). These blooms
53 pose a serious risk for aquaculture activities, because farmed fish cannot escape from
54 developing adverse conditions caused by marine microalgae. Previously, the most infamous
55 northern Norwegian bloom occurred in 1991 in Ofotfjord causing high mortality in affected
56 fish farms (Rey, 1991). Smaller HAB incidents have occurred since then, although they have
57 gained little mainstream attention (Grann-Meyer, 2020). The salmon aquaculture industry has
58 expanded tremendously over the past decades to a landing value of salmon that reached 7 billion
59 USD in 2019 (Statistics Norway, 2020). While this has caused concern, it has not spurred
60 investments in long-term monitoring of algal bloom dynamics or occurrence of potentially
61 harmful algae species in areas that support salmon aquaculture. Therefore, most stakeholders
62 were taken by surprise when a deadly HAB of *Chrysochromulina leadbeateri* (prymnesiophyte)
63 reoccurred and caused massive fish mortalities in the Troms and Nordland regions of coastal
64 northern Norway from mid-May to the beginning of June 2019 (Karlsen et al., 2019). The fish
65 loss was ca. 14 500 tonnes, which is the highest amount among fish kill related HABs in
66 Scandinavia since 1988 (Karlsen et al., 2019; Karlson et al., 2021). Thus, knowledge that can
67 eventually inform causation is very limited, especially in the context of seasonal microbial
68 blooming dynamics, detailed taxonomy of co-blooming species, and the environmental
69 conditions during the 2019 incident.

70 Marine HABs are often associated with altered ratios of inorganic nitrogen-to-
71 phosphate (N:P), coupled with a long period of high irradiance, calm weather, and strong
72 surface water stratification (Nielsen et al., 1990; Anderson et al., 2002; Uronen et al., 2005).
73 However, the role of N:P ratio in determining the magnitude, frequency, and duration of HABs
74 has been questioned (Davidson et al., 2012) as more evidence is showing that abiotic conditions

75 are not the only influencing factors of microalgal bloom dynamics. The importance of intra-
76 and interspecific interactions between members of the marine microbiome has become well
77 recognized as a major factor in structuring the temporal and spatial relationships of
78 phytoplankton communities (e.g., Needham and Fuhrman, 2016; Martin-Platero et al., 2018;
79 Aalto et al., 2022). These interactions can be complex and subject to rapid change within a
80 marine microbial ecosystem. Although they are difficult to disentangle, they have the potential
81 to stimulate, enhance, and/or perpetuate the bloom of specific taxa associated with HABs.
82 Therefore, it is important (yet uncommon today) to observe and catalogue the blooming patterns
83 of whole microbiomes while studying the ecology of focal taxa involved with HAB events.

84 High-resolution (densely sampled) time series analysis combined with high-resolution
85 taxonomic screening such as 16S and 18S ribosomal RNA gene amplicon sequencing variants
86 or operational taxonomic unit-based diversity is an important method for evaluating microbial
87 succession dynamics and ecological factors that drive blooms at different time scales (Fuhrman
88 et al., 2015; Martin-Platero et al., 2018). However, knowledge about the nature of taxon-
89 specific and non-specific interactions with HAB species is poor, because identification of these
90 “hidden” patterns of interactions in dynamic and species rich communities is challenging.
91 Therefore, an increasing number of modern analytical tools has been developed to apply with
92 time series analysis. For example, WaveClust (Martin-Platero et al., 2018) and k-medoid
93 (Kaufman and Rousseeuw, 2009; Coenen et al., 2020) are applicable and promising approaches
94 to infer both temporal dynamics and networks of microbial interactions.

95 The specific mechanisms of how HABs cause fish mortality are often unknown and
96 difficult to identify, as was the case for the 1991 and 2019 *C. leadbeateri* HABs in northern
97 Norway (Meldahl et al., 1994; Edvardsen and Paasche, 1998). In fact, the toxicity of many well-
98 known toxic prymnesiophytes – such as *Chrysochromulina* spp. – are not known to be
99 dependent on cell density, which makes detection difficult (Edvardsen and Paasche, 1998). The

100 role that bacteria may play in bloom toxicity is also not clear (Uribe and Espejo, 2003). For
101 example, it has been suggested that toxin biosynthesis in dinoflagellate cells is indirectly
102 mediated by associated bacterial consortia (Green et al., 2004). Heterotrophic bacteria have
103 been shown to increase activity and biomass concentrations during a HAB due to the release of
104 dissolved organic matter from lysed microalgal competitors (Uronen et al., 2007). In order to
105 increase their supply of nutrients, many bacteria also exhibit target-specific or non-specific
106 algicidal activity that inhibit the growth or lyse microalgae; potentially even terminating HABs
107 (Doucette et al., 1999; Meyer et al., 2017). Several known marine algicide bacteria are found
108 in bloom-associated groups such as *Flavobacteria* (*Bacteroidetes*), *Alphaproteobacteria* and
109 *Gammaproteobacteria* (Mayali and Azam, 2004). However, not all bacteria-algae interactions
110 are negative. Several mutualistic and growth enhancing relationships have also been identified,
111 which include metabolite exchange of vitamins and growth hormones from bacteria that trade
112 with microalgae for amino acids and dissolved organic carbon (Cirri and Pohnert, 2019).

113 The spring-summer phytoplankton seasonal succession along the coast of northern
114 Norway has been extensively studied in the past 40 years with specific focus on spring bloom
115 dynamics. The majority of data collected to-date has used only morphology-based identification
116 of microalgal taxa, which has limited the extent to which the full diversity of these communities
117 has been described (Eilertsen et al., 1981; Reigstad and Wassmann, 1996; Degerlund and
118 Eilertsen, 2010; Aalto et al., 2021). From previous studies, we know that the onset of the “spring
119 bloom” occurs in late March/early April, and it is driven by increased irradiance as the region
120 undergoes a shift from polar night to spring, which results in elevated winter nutrient
121 concentrations and a well-mixed water column (Eilertsen and Taasen, 1984; Eilertsen and
122 Frantzen, 2007; Aalto et al., 2021). This leads to a rapid and intense increase of many chain
123 forming centric diatoms that co-bloom with *Phaeocystis pouchetii* (haptophyte), who often
124 outlasts the diatoms and persists throughout the summer (Degerlund and Eilertsen, 2010). The

125 spatial and interannual variation of the late bloom (May-June) phytoplankton community can
126 comprise a diverse mix of low-nutrient-tolerant, heterotrophic, and mixotrophic species
127 belonging to dinoflagellates, cryptophytes, ciliates, and other small flagellates (Eilertsen et al.,
128 1981; Aalto et al., 2021). HAB incidents in northern Norway tend to occur after the primary
129 spring diatom bloom, although historical sampling of these events is sparse and the onset and
130 development of HAB conditions is essentially unknown for the region.

131 Our aim was to contribute to the knowledge of the ecology and microbial succession
132 dynamics associated with the *C. leadbeateri* HAB, which has now proven to be a reoccurring
133 and devastating event in northern Norway. This was accomplished by asking three targeted
134 research questions: i) how did the marine microbiome composition change during the 2019
135 HAB event in relative relation to the focal taxon?; (ii) what were the major blooming (temporal)
136 patterns among prokaryotes and microeukaryotes and which taxa co-bloomed with the focal
137 taxon?; and iii) which environmental factors were associated with the observable differences in
138 the marine microbiome composition? This study represents the first molecular ecology-based
139 investigation of a *C. leadbeateri* HAB and presents new insights into a seasonal marine
140 microbial ecosystem that can have a major impact on the social-economic welfare of Norway
141 through its relation to the aquaculture industry.

142

143 **MATERIALS AND METHODS**

144 **Study areas and sample collection.** Time series sampling was performed between May 27th
145 (sample day 0) and June 21st (sample day 25) in 2019, at two primary stations (Supplementary
146 Table S1). The first station was named Grøtsund sampling station (**GSSS**, 69.80 N, 19.36 E).
147 The second station, named as Finnfjord sampling station (**FSS**, 69.19 N, 18.03 E), is located 60
148 km south of GSSS, within the same interconnected fjord-sound system (Figure 1a). Samples
149 were collected from each station twice a week, except station FSS was sampled once in the

150 second sampling week (starting the week of May 27th, 2019), from fixed sampling depth of 10
151 m using a 1.7 L Niskin bottle to get approximately 8.5 L of seawater. The collected seawater
152 was prefiltered for large biomass with a 150 µm plankton mesh, and transported to shore in a
153 15 L Nalgene plastic carboy. All sampling equipment was rinsed with 2% bleach prior and
154 between each sampling effort followed by a rinsing with MilliQ water and a minimum of two
155 volumes of station sampling water prior to collection. Temperature and salinity profiles down
156 to 15–50 m were recorded with a hand-held AML oceanographic X2 electron conductivity-
157 temperature-depth (CTD) instrument (AML Oceanographic, Canada). Seawater particles – i.e.
158 microbial biomass – was collected by vacuum filtration onto 0.22 µm polycarbonate filters (GE
159 Healthcare Whatman 47 mm Nucleopore Polycarbonate Track Etched Membranes; GE
160 Healthcare 111106). All filtering was done inside a sterile laminar flow hood, and the total
161 filtered volume per sample varied from 500 – 750 mL depending on turbidity. Filters were
162 immediately flash frozen and stored at -80 °C. All filtering equipment was disinfected with 2%
163 bleach prior and between sampling efforts and thereafter rinsed with MilliQ water. Water
164 samples for macronutrients: silicate (Si(OH)₄), phosphate (PO₄³⁻), and nitrate + nitrite (NO₃⁻ +
165 NO₂⁻), were filtered through 47 mm GF/F glass microfiber filters (Whatman) into Falcon tubes
166 using disposable syringes and thereafter stored at -20 °C.

167 In addition to the time series samples from FSS and GSSS, filtered microbial biomass
168 was collected from eight separate locations as single time points between May 27th and June
169 21st (Figure 1a and Supplementary Table S1). The data of these samples is not included within
170 time series analyses but used to compare the 2019 HAB affected area via spatial variation in
171 the relative abundance of the focal taxon and associated microbial communities. The DNA
172 extraction and downstream analysis of all samples were performed at the UiT – The Arctic
173 University of Norway as described below.

174

175 **Environmental factors.** The vertical surface water properties from the time series sampling
176 stations (FSS and GSSS) were inspected using CTD-profile data (Supplementary Figure S1 and
177 S2). The difference in surface water stratification between sampling stations was determined
178 by calculating the mixed layer depth (MLD) from each CTD-profile data using potential
179 density. The depth of 1 m was used as a reference depth as the deployed handheld CTD-sensor
180 enables measurements near surface. A density threshold of 0.1 kg m^{-3} was used to define MLD
181 – i.e. the depth below 1 m where density first exceed the defined threshold (Peralta-Ferriz and
182 Woodgate, 2015). Temperature and salinity values from the depth of 10 m (corresponding the
183 depth of collected biomass) as well as MLD values were further used in statistical analyses. As
184 the CTD-casts between sampling days 11 and 17 were unsuccessful, temperature, salinity, and
185 MLD values for these days were interpolated using the R function ‘na.approx’ from the R
186 package ‘zoo’ to fill the missing values. Nutrient concentrations were analyzed 20 months later
187 at the UiT – The Arctic University of Norway with a Quattro39 autoanalyser (Seal Analytical,
188 UK). PO_4^{3-} concentrations below the detection limit of $0.04 \mu\text{mol L}^{-1}$ were replaced with a small
189 value (0.001) to enable the estimation of this variable in statistical analysis.

190

191 **Unialgal control cultures.** Controls were performed with the *Chrysochromulina leadbeateri*
192 UiO-035 (Edvardsen et al., 2011) culture obtained from the Norwegian Culture Collection of
193 Algae (NORCCA) repository and cultivated at $6 \text{ }^\circ\text{C}$ on *f/2* medium (Guillard, 1975), fortified
194 with 20 nM of selenium. The cultured *C. leadbeateri* was isolated from a toxic bloom of 1991
195 in Vestfjorden, northern Norway (Eikrem and Throndsen, 1998). Taxonomic identification of
196 the cultured isolate has been mainly based on scale morphology in comparison to holotype
197 (Estep, 1984) and other previous reports on *C. leadbeateri*-like cells both from northern and
198 southern hemisphere (Eikrem and Throndsen, 1998). Several *Chrysochromulina* species are
199 characterized by species-specific bilayer scales which have been considered a morphotype-

200 specific character (Eikrem and Throndsen, 1998). Cells were collected and processed
201 identically to the environmental samples described below. The 18S amplicon analysis assigned
202 four abundant ASVs comprising these control cultures (>1000 ASV counts in all replicates)
203 (Supplementary Figure S3). All four of these ASVs had identical taxonomic assignments within
204 the SILVA v138.1 database: Family = Prymnesiales, Genus = OLI16029, Species = Unknown.
205 Of these four ASVs, ASV *24a92740c5af4cd5a5ac0db70830fbc0* (hereafter referred to as the
206 “focal ASV”) comprised 88 % of the OLI16029 unialgal control (Supplementary Figure S4).

207

208 **Amplicon sequencing.** Genomic DNA was extracted and downstream amplicon sequences
209 were obtained using the same protocol as described in Aalto et al. (2022). All the samples were
210 processed together in accordance with the Earth Microbiome Project protocols (Gilbert et al.,
211 2010) with modifications according to Amaral-Zettler et al. (2009). This included
212 recommended primers and barcodes for the V4 hypervariable region of the 16S SSU rRNA
213 gene using the V4 forward (515F) and V4 reverse (806R) primers, and the V9 hypervariable
214 region of the 18S SSU rRNA was targeted with the V9 forward (1391F) and V9 reverse (EukBr)
215 primers. Biological replicates, four or five, were sequenced on an Illumina MiSeq instrument
216 (Illumina, San Diego, CA) according to (Caporaso et al., 2010) at Argonne National Laboratory
217 (Lemont, IL, USA). The realized length of forward and reverse reads was 151 bp.

218

219 **Amplicon analysis.** The amplicon analyses were performed through the QIIME2 environment
220 and using QIIME2 plugins as previously described (Aalto et al. 2022). Briefly, Illumina reads
221 and the corresponding barcode files were imported and demultiplexed using the Earth
222 Microbiome Project paired end flag. All reads were filtered, de-replicated, and chimera checked
223 using all default parameters in the DADA2 v2021.2.0 (Callahan et al., 2016). Reads were
224 merged and amplicon sequence variants (ASVs) were determined using DADA2 v2021.2.0.

225 The DADA2 statistic on sequence reads is provided in Supplementary Data S1 (osf.io). A 16S
226 and 18S rRNA gene classifier from the SILVA v138.1 database was trained using RESCRIPt
227 (Quast et al., 2012; Robeson et al., 2020). The ASVs were classified with the self-trained
228 classifier database. (Yilmaz et al., 2014). It is noted that the major challenge in 16S and 18S
229 based taxonomy is its dependency on taxonomic resolution limitations of the database. We
230 chose to use all classifications given from the SILVA v138 database because it is a standardized
231 approach. Manual curation of taxonomic classification was beyond the scope of this study.

232

233 **Statistics, clustering and correlation.** All ASVs not assigned to the expected kingdom
234 (*Archaea*, *Bacteria* and *Chloroplast*) were removed along with all mitochondria assignments
235 from 16S data set. ASVs assigned to *Archaea*, *Bacteria*, *Vertebrata* and *Arthropoda* and phyla
236 *Cnidaria*, *Echinodermata*, *Annelida*, *Nematozoa*, *Nemertea*, *Porifera*, *Mollusca*, *Ctenophore*
237 and *Tunicata* or phyla belonging to macroalgae and land plants or land fungi such as *Bangiales*,
238 *Florideophycidae*, *Ochrophyta*, *Phragmoplastophyta*, *Ascomycota*, *Basidiomycota* and
239 *Myxogastria* were removed from the 18S data set. Additional information on number of ASVs
240 and sequencing depths before and after removal of unwanted taxa is provided in Supplementary
241 Table S2. The total number of classified ASVs in FSS for 18S and 16S data set was 900 and
242 1309, respectively, and in GSSS 2196 and 1865, respectively. As an exception regarding
243 correction of taxonomic annotations, classified 16S order *Enterobacteriales* was manually
244 changed to closely related order *Alteromonadales* as the main genera of this order were
245 *Pseudoalteromonas*, *Colwellia* and *Glaciacola* that are known to be members of
246 *Alteromonadales* (Parte et al., 2020).

247 Downstream analysis was completed in R (R Core Team, 2021), using the ‘microeco’
248 (Liu et al., 2021) and ‘vegan’ packages (Oksanen et al., 2013). This study also made use of the
249 K-medoids clustering method adapted from a previously described approach applied to time

250 series microbiome data to examine distinct temporal trends in blooming patterns within
251 communities (Coenen et al., 2020). Briefly, ASV counts from each sample type – i.e., sampling
252 station (FSS or GSSS) and PCR amplification primer type (16S or 18S) – were preprocessed
253 via z-score and variance stabilizing transformations using the ‘DESeq2’ package in R (Love et
254 al., 2014). Pairwise distance matrices were calculated by the Euclidean distance prior to
255 partitioning each sample-specific ASV into K clusters according to similarity criterion over the
256 time series. The quality of each cluster per each sample type was assessed via the Calinski-
257 Harabasz index (Supplementary Figure S5) (Lord et al., 2017). Pearson’s correlation was used
258 to examine the relationship between each temporal dynamic, represented by medoid taxon
259 (cluster centroids), and environmental measurements but also, to obtain the positively and
260 negatively co-blooming microalgae and bacterial taxa with focal ASV.

261 The difference in microbial communities, i.e. beta-diversity, between sampling stations
262 was measured using unweighted UniFrac distance metric which accounts occurrence -
263 presence/absence of ASV - and phylogenetic diversity (Lozupone et al., 2011). The beta-
264 diversity and relationship between community compositions and environmental factors
265 (temperature, salinity, MLD, Si(OH)_4 , PO_4^{3-} , $\text{NO}_3^- + \text{NO}_2^-$, and relative abundance of focal
266 taxon (OLI16029)) was visualized and conducted via distance based redundancy analysis
267 (dbRDA). The permutational multivariate analysis of variance (PERMANOVA) was
268 performed to test the (dis)similarity in prokaryotic and microeukaryotic community
269 compositions between stations (pairwise) and within stations (Anderson, 2001). The Tukey test
270 was performed on inorganic nutrients to determine if the mean concentration values were
271 statistically different between stations (Abdi and Williams, 2010).

272

273 **Data repository and reproducible analyses.** All sequencing and environmental data is
274 available on the Open Science Framework (osf.io), along with all R Markdown scripts used for

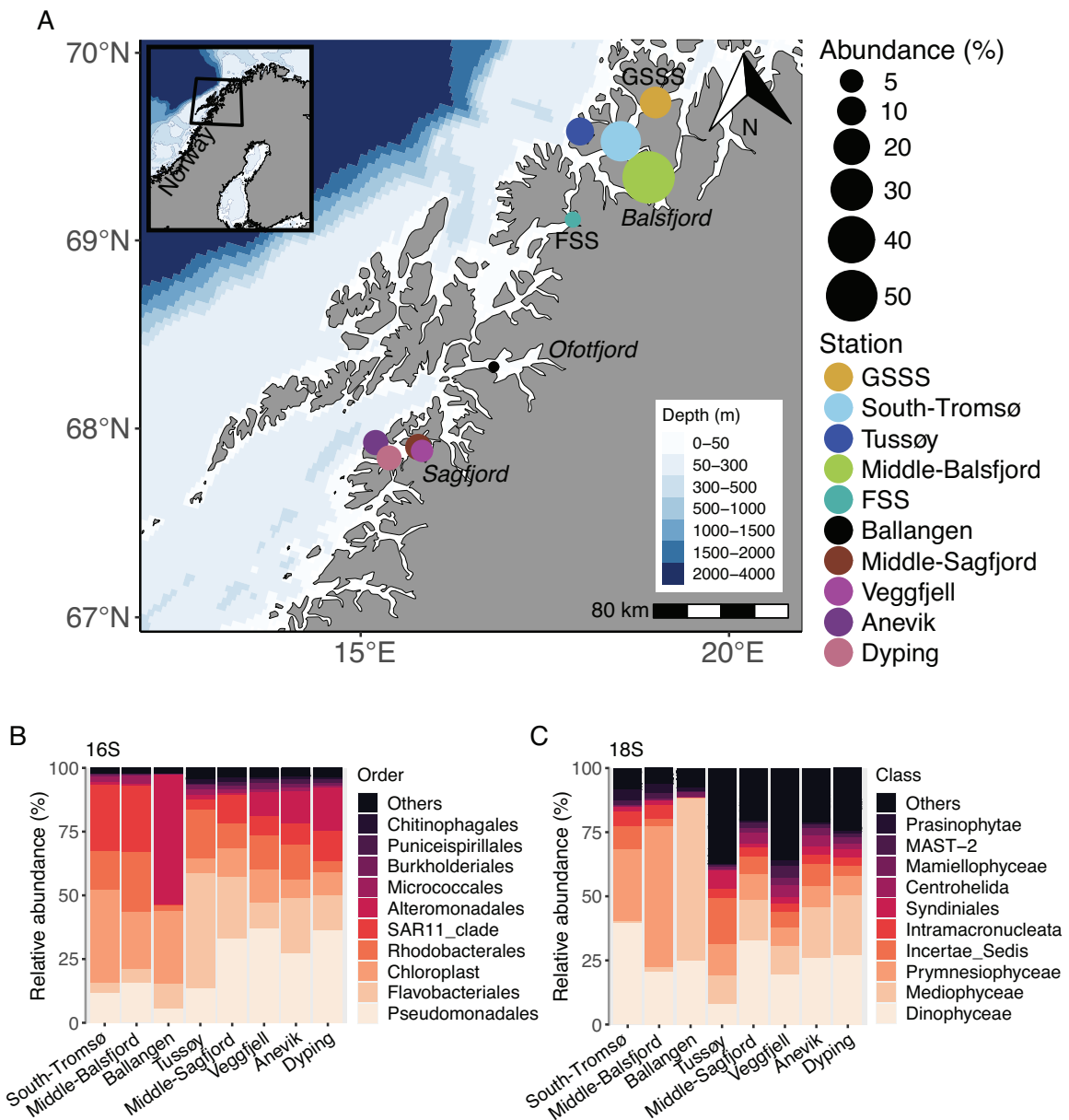
275 analyses and graphing (osf.io/4wjhp/). All Supplementary Data S1–S11, referred to in this
276 study, is available and found on osf.io/4wjhp/.

277

278 **RESULTS**

279 **Geographical distribution of focal taxon in relation to fish mortality.** The focal taxon was
280 assessed as those ASVs assigned to OLI16029, representing the *Chrysochromulina leadbeateri*
281 UiO-035 unialgal strain within the class *Prymnesiophyceae*. This taxon was detected during the
282 2019 harmful *C. leadbeateri* bloom in varying relative abundance across the northern
283 Norwegian coast and fjords (Figure 1). It's abundance varied between 0.4 % and 51.8 % of the
284 microeukaryotic community assessed via 18S amplicon sequencing through the HAB affected
285 region. The highest relative abundances of the focal taxon – recorded in our molecular sampling
286 campaign – were obtained in the northern portion of the HAB affected region that included
287 Middle-Balsfjord, South-Tromsø, GSSS, and Tussøy stations (Figure 1a). The microbial
288 community composition was relatively similar between Middle-Balsfjord, South-Tromsø, and
289 GSSS stations with increased relative abundance of 18S ASVs and 16S ASVs indicative of
290 dinoflagellates (class *Dinophyceae*) and order *Flavobacteriales*, respectively, towards station
291 GSSS (Figure 1b-c). The relative abundance of ASVs belonging to the focal taxon were low in
292 Ballangen (Ofotfjord) where the HAB was first reported to originate with high fish mortality in
293 mid-May (Karlsen et al., 2019). The community structure from Ballangen was also distinct,
294 compared to other samples, as it was dominated by 18S ASVs indicative of centric diatoms
295 notably from the genus *Skeletonema* (class *Mediophyceae*) and 16S ASVs classified within the
296 genera *Pseudoalteromonas* and *Colwellia* (order *Alteromonadales*) (Figure 1b-c and
297 Supplementary Data S2 and S3 (osf.io)). The relative abundance of the focal taxon was higher
298 in samples collected from Sagfjord stations (Anevik, Dyping, Veggfjell, and Middle-Sagfjord),
299 south from Ofotfjord, than in the Ballangen and FSS stations (Figure 1a). The microeukaryotic

300 community in the Sagfjord location was especially diverse, comprising multiple distinct groups
 301 of dinoflagellates and centric diatoms being the most abundant. In contrast to the other sampling
 302 locations, the 16S prokaryotic ASVs among the Sagfjord stations were predominantly
 303 comprised by the order *Pseudomonadales* (Figure 1b-c).
 304



305

306 **Figure 1.** A map showing the geographical area in northern Norway where *Chrysochromulina*
 307 *leadbeateri*-related harmful algal bloom occurred in summer 2019. The main sample locations
 308 are named on the map. A) Microbial DNA for 18S rRNA and 16S rRNA amplicon sequence

309 analysis was collected once from the marked stations, except from FSS (Finnfjord sampling
310 station) and GSSS (Grøtsund sampling station) which are the primary stations of this time series
311 study and were sampled 7 and 8 times, respectively, between May 27th and June 21st. The size
312 of the circles represents the relative abundance of focal taxon (average relative abundance for
313 FSS and GSSS stations across all samples). Not all of the stations represent localities where
314 HAB- related fish mortality was experienced. Taxonomic composition of the most abundant **B**)
315 prokaryotes (16S) and **C**) microeukaryotes (18S) retrieved from Amplicon Sequence Variants
316 (ASVs) tables specified at the order and class taxonomic rank level, respectively. Note that FSS
317 and GSSS stations are excluded from **B** and **C** as the taxonomic composition across time series
318 is shown in Figure 2.

319

320 **Microbiome dynamics across the bloom.** The microeukaryotic and prokaryotic community
321 composition changed across the time series sampling campaign at FSS (PERMANOVA: 16S,
322 $R^2 = 0.11$ and $p = 0.001$; 18S, $R^2 = 0.19$ and $p = 0.001$) and GSSS (PERMANOVA: 16S, $R^2 =$
323 0.13 and $p = 0.001$; 18S, $R^2 = 0.13$ and $p = 0.001$). These dynamic communities were also
324 significantly dissimilar between the two time series stations (PERMANOVA: 16S, $R^2 = 0.30$
325 and $p = 0.001$; 18S, $R^2 = 0.46$ and $p = 0.001$) (Supplementary Table S3). GSSS showed higher
326 species richness as compared to FSS as measured by the number of observed ASVs per sample
327 day; 235–288 and 244–358 ASVs for 16S and accordingly 161–265 and 306–415 ASVs for
328 18S in FSS and GSSS, respectively (Supplementary Figure S6).

329 Among the most abundant microeukaryotes assigned to the taxonomic level class, only
330 18S ASVs indicative of *Cryptophyceae*, *Mediophyceae*, *Dinophyceae* and *Prymnsiophyceae*
331 (including the focal taxon) were shared between both stations (Figure 2a-b). The observed
332 community in FSS was dominated by taxa classified as *Cryptophyceae* (9 – 49 % of the relative
333 abundance), comprising mainly ASVs assigned to the genus *Teleaulax*, that showed strong
334 temporal variability in the second half of the time series (Figure 2a and Supplementary Data S4
335 (osf.io)). The predominant taxon observed from GSSS was classified as *Dinophyceae*, which
336 accounted for 34–54 % of the relative abundance during the time series (Figure 2b). Most of
337 the ASVs belonging to the class *Dinophyceae* were not assigned to a lower taxonomic level.

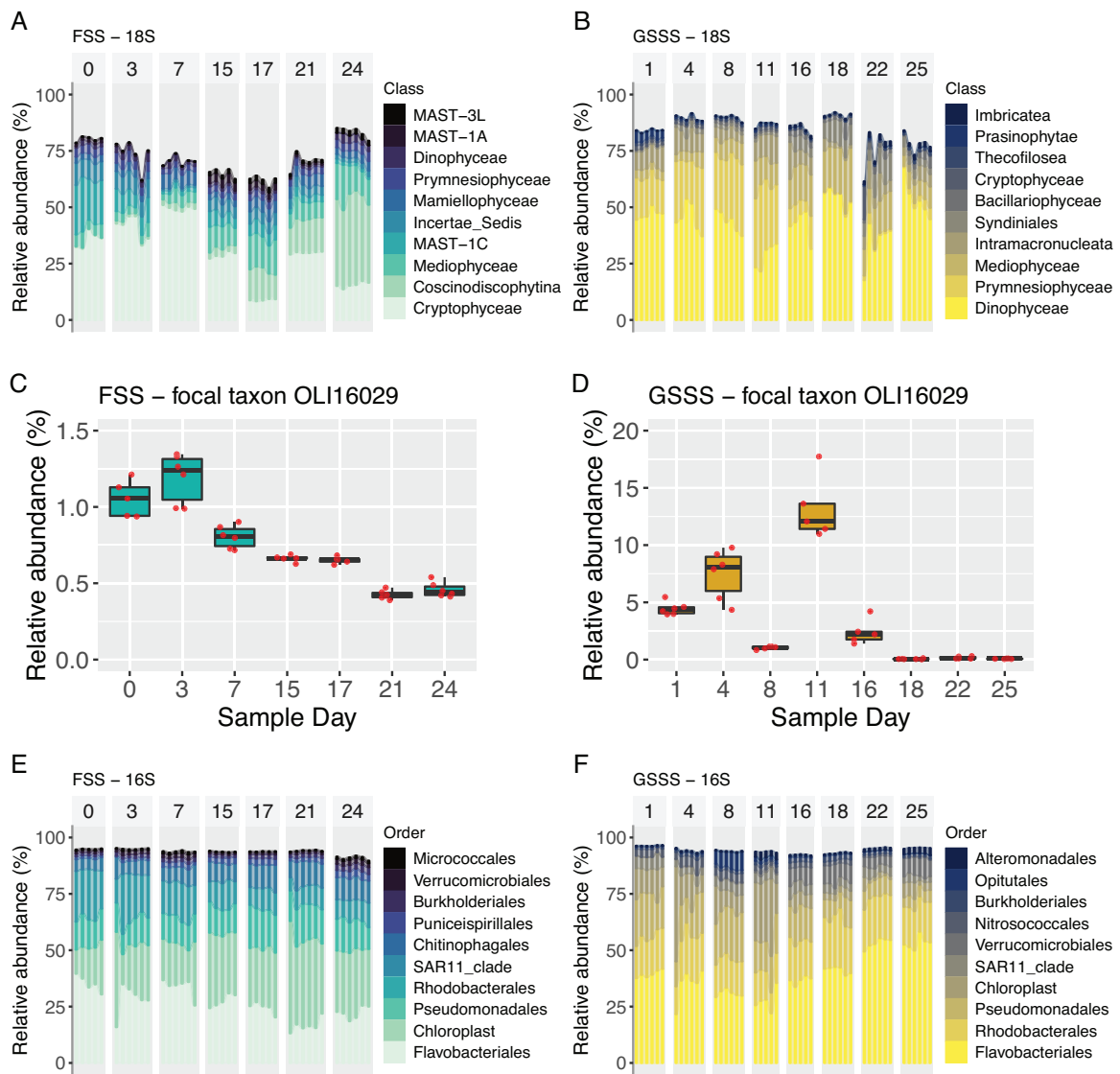
338 A change in community structure was observed at both stations during the middle of the
339 observed bloom; between days 7 and 15 in FSS and between days 11 and 16 at the GSSS station
340 (Figure 2a-b). This shift was observed with an increased relative abundance of ASVs indicative
341 of centric diatoms (class *Mediophyceae*) in both stations and the class *Coscinodiscophytina* in
342 FSS which were almost exclusively represented by ASVs indicative within genus
343 *Leptocylindrus* (Figure 2a-b and Supplementary Data S4). The class *Mediophyceae* comprised
344 ASVs that were classified within different genera between stations, such as *Acrocellulus* at FSS
345 and *Thalassiosira* at GSSS (Supplementary Data S4-S5 (osf.io)). In FSS, the contribution of
346 class *Prymnesiophyceae* to the community composition was minor in comparison to GSSS
347 (Figure 2a-b) and was composed mainly by ASVs classified to the genus *Chrysochromulina* (2
348 – 3 % of relative abundance) but also ASVs assigned to the focal taxon, OLI16029 (0.5 – 1 %
349 of relative abundance) (Figure 2c and Supplementary Data S4-S5 (osf.io)). In GSSS, class
350 *Prymnesiophyceae* prevailed until day 11 (42 % of the relative abundance) and thereafter
351 drastically decreased while ASVs assigned to *Syndiniales* concurrently increased (Figure 2b).
352 The majority of those ASVs belonging to the class *Prymnesiophyceae* were assigned to the
353 genera *Phaeocystis* and the focal taxon (OLI16029) (Supplementary Data S5 (osf.io)). The
354 pronounced decrease in abundance of the focal taxon at day 8 coincided with highest relative
355 abundance of *Phaeocystis* (Figure 2d and Supplementary Data S5 (osf.io)). We note here for
356 clarity that ASVs assigned to the genus *Chrysochromulina* are not indicative of the focal taxon
357 (OLI16029), even though the unialgal control has been deposited and frequently referred to as
358 *Chrysochromulina leadbeateri* UiO-035.

359 The 16S ASVs – classified at the level of order – showed less temporal variability than
360 the 18S ASVs (at the class level) across the time series in FSS and GSSS. The taxa with the
361 highest relative abundances were the same in FSS and GSSS sample stations (Figure 2e-f).
362 Taxa classified to the order *Flavobacteriales* showed the highest relative abundance with ASVs

363 belonging *Rhodobacterales* and *Pseudomonadales* being common as well in both time series
364 stations (Figure 2e-f). The FSS and GSSS locations harbored distinctly different relative
365 abundances of genera assigned to *Flavobacteriales*. At station GSSS, the dominant genera were
366 *Polaribacter*, *Ulvibacter*, *Formosa* and the NS5 marine group, as compared to FSS where the
367 NS5 and NS9 marine groups were dominant (Supplementary Data S6 and S7 (osf.io)). At
368 GSSS, members of the order *Verrucomicrobiales* increased in relative abundance (from 1 % to 8
369 %) within the same time frame as major changes in the microeukaryotes were observed (Figure
370 2f). Also, the abundance of the *Pseudomonadales* order decreased towards the end of the time
371 series while the contribution of *Flavobacteriales* simultaneously increased (Figure 2f). The
372 influence of Archaea to the 16S ASV composition was minor at both stations and accounted
373 for only 0.1 % and 0.4 % of the relative abundance in FSS and GSSS, respectively
374 (Supplementary Data S6 and S7 (osf.io)).

375 Since this study did not include measurements of chlorophyll *a* to indicate changes in
376 phytoplankton abundance, the 16S ASVs identified as Chloroplast were used as an inference.
377 The average relative abundance of ASVs assigned to Chloroplast was nearly three times higher
378 in FSS than in GSSS and the temporal pattern was different: the abundance increased towards
379 the end of the time series in FSS whereas in GSSS this was opposite (Figure 2e-f).

380



381

382 **Figure 2.** Comparative composition of the most common microeukaryotic and prokaryotic taxa
 383 collected from the time series sample stations and determined via 16S and 18S rRNA amplicon
 384 analysis. Microeukaryotes classified at the class taxonomic rank level **A**) in FSS and **B**) in
 385 GSSS. The temporal change in relative abundance of the focal taxon assigned as genus
 386 *OLI16029* (class *Prymnesiophyceae*) **C**) in FSS and **D**) in GSSS. Prokaryotes classified at the
 387 order taxonomic rank level **E**) in FSS and **F**) in GSSS.

388

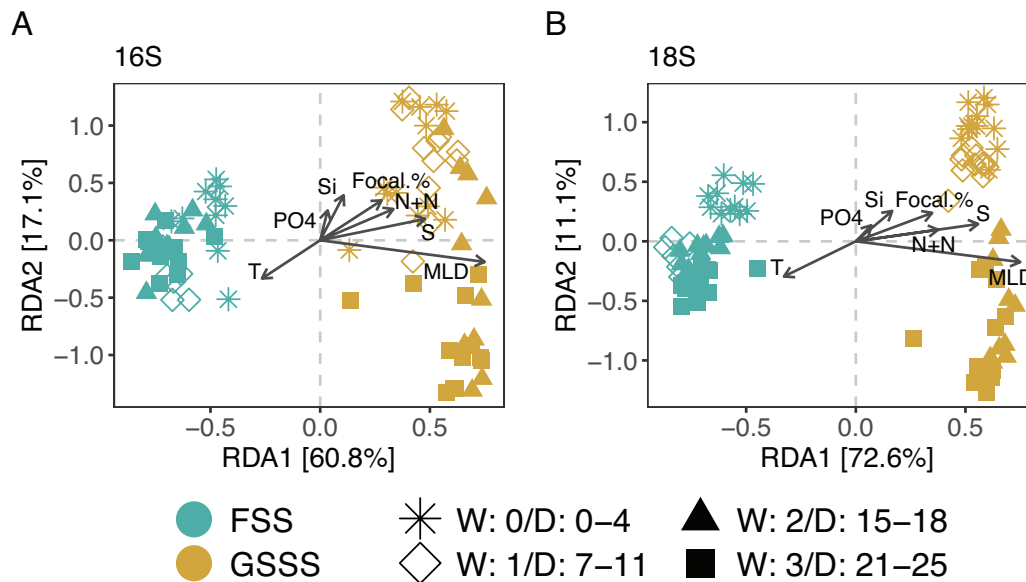
389 **Environmental variability during the HAB.** The surface water properties – temperature and
 390 salinity – were relatively similar during the HAB, as observed from both time series stations
 391 (FSS and GSSS) at 10 m depth from where microbial biomass was collected (Supplementary
 392 Table S4). The overlaying surface water was more stratified in FSS than GSSS. This was due

393 to a low salinity layer (< 30) which persisted near the surface during the entire time series
394 simultaneously with a strong increase in observed temperature (Supplementary Figure S1 and
395 S2). The mixed layer depth was observed near the surface (3 m) throughout the study period in
396 FSS and in the beginning in GSSS time series, where it then sank down to 7 m by the end of
397 the GSSS time series while the surface water became more homogeneous after day 8
398 (Supplementary Figure S1 and S2). The mean $\text{NO}_3^- + \text{NO}_2^-$ concentration was significantly
399 higher in GSSS than in FSS (0.43 and $0.18 \mu\text{mol L}^{-1}$, respectively; Tukey, $p < 0.02$) whereas
400 the $\text{Si}(\text{OH})_4$ and PO_4^{3-} concentrations did not show statistically significant differences between
401 stations (Supplementary Table S4).

402

403 **Beta diversity in context with the environment.** Both the microeukaryotic and prokaryotic
404 components of the HAB-associated microbiome were dissimilar between GSSS and FSS
405 stations and throughout the observed time series. This was measured via unweighted UniFrac
406 distances that were ordinated by dbRDA analysis to infer the correlation between selected
407 environmental measurements to differences in community composition (Figure 3). Results of
408 beta diversity also corroborated the observed change in community structure during the middle
409 of the time series that was seen and noted above by inspecting changes in relative taxonomic
410 abundance (Figure 2). The dbRDA analysis (i.e., sum of RDA1 and RDA2) showed that 77.9
411 % and 83.7 % of the total variation in the prokaryotic and microeukaryotic community
412 composition was correlated to environmental measurements during the time series (Figure 3).
413 Most of this variation was explained by the first RDA component (RDA1: 16S = 60.8 % and
414 18S = 72.6 %) inferring that the variation of both prokaryotic and microeukaryotic communities
415 between FSS and GSSS may be driven by response to environmental factors such as MLD,
416 salinity, and $\text{NO}_3^- + \text{NO}_2^-$ (Figure 3). Whereas the temporal variability within stations was

417 mainly explained by the second RDA component (RDA2) which accounted for 17.1 % and 11.1
 418 % of the variance in prokaryotic and microeukaryotic communities, respectively.
 419



421 **Figure 3.** Dissimilarity in prokaryotic and microeukaryotic community composition between
 422 sample stations was inferred via beta-diversity as measured with unweighted UniFrac distances
 423 and related to environmental measurements. Distance-based redundancy analysis (dbRDA)
 424 biplot of **A**) prokaryotes and **B**) microeukaryotes. Color represents station and shape comprises
 425 samples (sample scores) within each sample week according to legend information. Arrows
 426 indicate environmental factors and point to the direction of maximum variation of the respective
 427 factor. T, temperature; S, salinity; MLD, mixed layer depth, Si, Si(OH)₄; PO₄, PO₄³⁻; N+N,
 428 NO₂⁻ + NO₃⁻; Focal %, relative abundance of focal taxon in 18S data set.

429

430 **Temporal trends and co-blooming taxa.** The HAB-associated marine microbiome was
 431 complex and consisted of a minimum of 235 and 161 16S and 18S ASVs, respectively, each
 432 maintaining its own dynamic trajectory during the observed time series. Examination and
 433 subsequent clustering of the most predominant blooming patterns was performed via the k-
 434 medoids clustering method. The resulted number of clusters per data set and time series station,
 435 as assessed via the Calinski-Harabasz index (normalized ratio for inter-intra-cluster variance)
 436 (Supplementary Figure S5), was 3, except for 18S at FSS where 4 clusters were selected. The

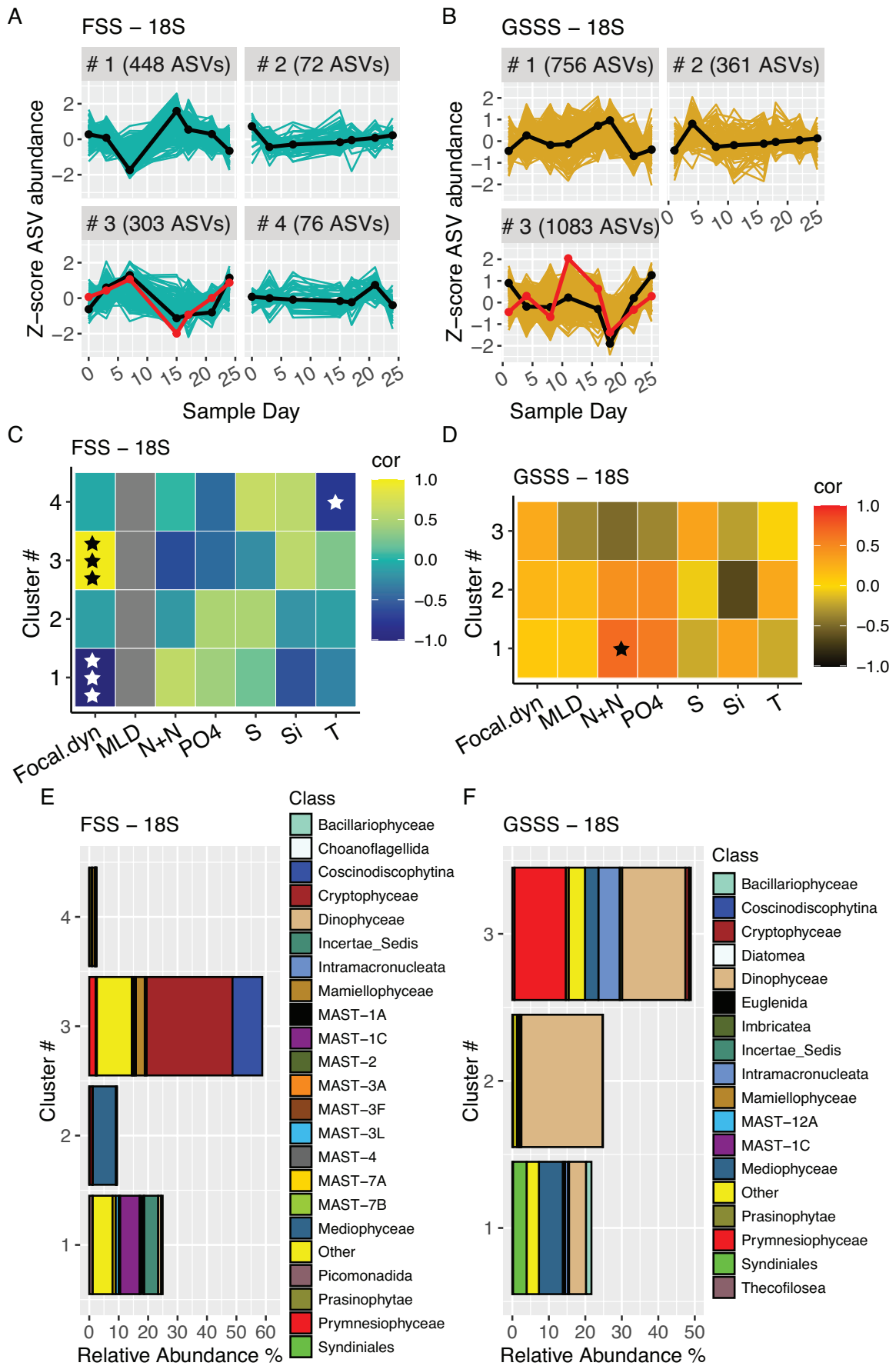
437 temporal pattern of each cluster was specified by its medoid taxon as a representative shape for
438 cluster's blooming dynamics of microeukaryotes (Figure 4a-b) and co-blooming taxa assigned
439 to 16S ASVs (Figure 5a-b).

440 The medoid 18S taxon of cluster 1 and 3, from both stations, exhibited approximately
441 inverse blooming patterns. These clusters also showed strong fluctuation in relative abundances
442 across the time series, including a strong positive and negative shift, respectively, around the
443 middle time points and negative correlations to environmental measurements (Figure 4a-d).
444 The medoid taxon of cluster 2 and 4 in FSS and cluster 2 in GSSS exhibited a short increase in
445 abundance in the beginning or end of time series (Figure 4a-b).

446 The focal ASV was included within cluster 3, at both stations (Figure 4a-b). There were
447 several microalgae that co-bloomed with the focal ASV, but these were distinct between the
448 FSS and GSSS stations (Figure 4). In FSS the focal ASV co-bloomed with genera *Teleaulax*
449 (class *Cryptophyceae*) and *Leptocylindrus* (class *Coscinodiscophytina*) which comprised 16 –
450 53 % and 1 – 53 % of the relative abundance within their respective cluster 3 (Figure 4e and
451 Supplementary Data S8 (osf.io)). A diverse composition of ASVs indicative of MAST clades
452 (marine stramenopiles) were also detected, although their relative abundances were minor (< 1
453 % of relative abundance within the cluster 3). This group was represented with other nano- and
454 picoplankton such as genera *Telonema* (class *Insertea Sedis*) and *Picomonas* (class
455 *Picomonadida*) the taxa in cluster 1 with inverse blooming pattern to cluster 3 (Figure 4c,e and
456 Supplementary Data S9 (osf.io)). ASVs from the genus *Phaeocystis* predominantly co-bloomed
457 at GSSS with the focal ASV (within cluster 3) together with a less abundant group of ciliates
458 (class *Intramacronucleata*) and members belonging to genus *Thalassiosira* (class
459 *Mediophyceae*) (Figure 4d,f and Supplementary Data S10 (osf.io)). ASVs belonging to the class
460 *Dinophyceae* also included in cluster 3 from GSSS (along with the focal ASV), and these were
461 composed mainly of members classified within the genus indicative of *Gymnodinium*.

462 The blooming patterns of 16S ASVs were also clustered. Among these, two clusters (1 and
463 2 from FSS and GSSS, respectively) showed significant positive correlation (FSS: $r = 0.79$, p
464 $= 0.036$ and GSSS: $r = 0.71$, $p = 0.047$) with the focal ASV. Only cluster 2 from station FSS
465 showed a significant negative correlation with the focal ASV ($r = -0.96$, $p < 0.001$) (Figure 5c-
466 d). The temporal trend represented by the medoid taxon was nearly identical in cluster 3 at both
467 stations corresponding to the blooming pattern of cluster 2 and inverse blooming pattern of
468 cluster 4 for microeukaryotes in GSSS and FSS, respectively.

469

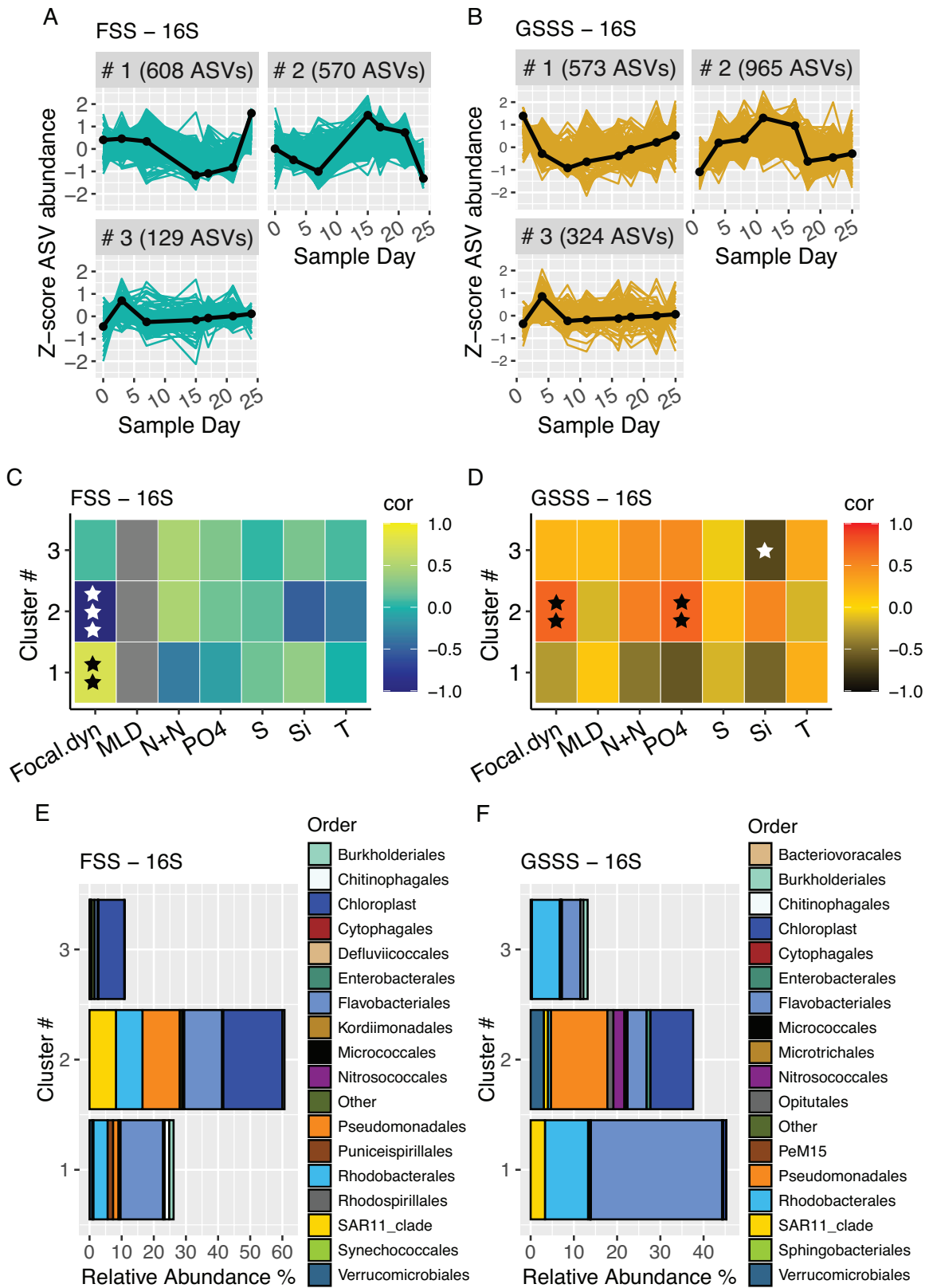


471 **Figure 4.** Characterization of major blooming patterns in microeukaryotic communities
472 assessed by K-medoid clustering analysis with z-transformation and detrending of 18S ASVs.
473 Temporal dynamics of microeukaryotic taxa and number of ASVs per defined cluster **A)** in FSS
474 and **B)** in GSSS station. The blooming pattern of each cluster is specified by medoid taxon and
475 drawn with black line. The red line specifies the blooming pattern of focal ASV. Y-axis is a z-
476 score and a value 0 denotes the mean abundance. Heatmap of Pearson's correlation between
477 temporal dynamics of medoid taxon (z-scores) of each cluster and focal ASV (z-scores) and
478 environmental factors **C)** in FSS and **D)** in GSSS. Color indicates Pearson's correlation
479 coefficient according to the color legend and level of significance is marked with ★ (★, $p \leq$
480 0.1; ★★, $p \leq 0.05$; ★★★, $p \leq 0.001$). The grey color for MLD in FSS denotes undefined
481 correlation as MLD values remained the same through the study period. Focal.dyn, temporal
482 dynamic of focal ASV; MLD, mixed layer depth; N+N, $\text{NO}_2^- + \text{NO}_3^-$; PO4, PO_4^{3-} ; S, salinity;
483 Si, Si(OH)_4 ; T, temperature. Taxonomic profile of the most common microeukaryotes of each
484 cluster as relative abundance in a whole community classified at the class taxonomic rank level
485 **E)** in FSS **F)** in GSSS.

486

487 We infer that the bacterial taxa from the GSSS station belonging to cluster 2 co-bloomed
488 with phototrophic protists in general, because the ASVs assigned to Chloroplasts occupied the
489 same cluster (Figure 5f and Figure 4f). This cluster was also the only one to show a statistically
490 significant correlation with phosphate concentrations. The same pattern was not observed in
491 FSS where approximately two thirds of Chloroplast ASVs were identified within cluster 2 and
492 rest in cluster 3 (Figure 5e).

493 Pearson correlation enabled us to infer that different bacterial taxa co-bloomed with the
494 focal ASV at each time series sampling stations, FSS and GSSS (Figure 5c-d) corresponding to
495 the observations within 18S microeukaryotes. Cluster 1 at station FSS was dominated by the
496 order *Flavobacteriales* (35 – 63 % relative abundance within cluster 1) (Figure 5e) and was
497 predominated by sequences identified within the NS5 marine group but also *Ulvibacter*
498 (Supplementary Data S11 (osf.io)). ASVs assigned to *Rhodobacterales*, notably evenly
499 dominating genera *Amylibacter* and *Planktomarina*, also shared the similar temporal dynamics
500 with the focal ASV (Figure 5e and Supplementary Data S11 (osf.io)). The positive co-blooming
501 trend between *Flavobacteriales* and *Rhodobacterales* classes and the focal ASV was not
502 observed at station GSSS.



505 **Figure 5.** Characterization of major blooming patterns in prokaryotic communities assessed by
506 K-medoid clustering analysis with z-transformation and detrending of 16S ASVs. Temporal
507 dynamics of microeukaryotic taxa and number of ASVs per defined cluster **A)** in FSS and **B)**
508 in GSSS station. The blooming pattern of each cluster is specified by medoid taxon and drawn
509 with black line. Y-axis is a z-score and a value 0 denotes the mean abundance. Heatmap of
510 Pearson's correlation between temporal dynamics of medoid taxon (z-scores) of each cluster
511 and focal ASV (z-scores; Figure 4) and environmental factors **C)** in FSS and **D)** in GSSS. Color
512 indicates Pearson's correlation coefficient according to the color legend and level of
513 significance is marked with ★ (★, $p \leq 0.1$; ★★, $p \leq 0.05$; ★★★, $p \leq 0.001$). The grey color
514 for MLD in FSS denotes undefined correlation as MLD values remained the same through the
515 study period. Focal.dyn, temporal dynamic of focal ASV; MLD, mixed layer depth; N+N, NO_2^-
516 + NO_3^- ; PO_4 , PO_4^{3-} ; S, salinity; Si, Si(OH)_4 ; T, temperature. Taxonomic profile of the most
517 common prokaryotes of each cluster as relative abundance in a whole community classified at
518 the class taxonomic rank level **E)** in FSS **F)** in GSSS.

519

520 **DISCUSSION**

521 The results from this study show distinct spatial variation and differences in the dynamic
522 community composition across the portion of the northern Norwegian coast that was strongly
523 affected during the 2019 *Chrysochromulina leadbeateri* HAB. This was a major and disruptive
524 event due to severe fish mortality and hence there were several sampling campaigns launched
525 simultaneously by public and private stakeholders. To our knowledge, this study represents the
526 only molecular-based investigation of the holistic marine microbiome during this HAB event.

527

528 **Indication for separate focal blooms.**

529 The 2019 HAB was reported on and monitored daily with focus on afflicted fish farm localities
530 by the Norwegian Directorate of Fisheries (Karlsen et al., 2019). The results obtained from our
531 amplicon-based sequencing approach are expected to be more complex and distinct from the
532 concurrent morphology-based taxonomy and cell counting surveys. However, our results share
533 some reassuring similarities to other reports, such as the observation that high focal taxon
534 (OLI16029 as representative ASVs for *C. leadbeateri* UiO-035 unialgal strain) abundance was
535 found in Balsfjord, which corresponds with microscopy enumerations conducted by Institute of
536 Marine Research and Akvaplan-Niva (Karlsen et al., 2019; Grann-Meyer, 2020). The current

537 study did not capture the onset of the HAB due to a reactive sampling effort to an event that is
538 (at least today) impossible to predict.

539 According to the prevailing consensus based on reported fish mortality, the toxic bloom
540 of the focal taxon initiated in Ofotfjord. The last report on fish mortality in Ofotfjord was dated
541 four days before the sample in Ballangen was taken (Karlsen et al., 2019), thus there was,
542 presumably, a mismatch between the bloom peak and time of sampling. We do not have data
543 that represents the community composition during the first reports of fish mortality. This may
544 explain why we found a surprising high disparity between expected and observed microbial
545 community composition at Ballangen, which did not correspond with any other sampled
546 microbial community composition (Figure 1). The microeukaryotic community was dominated
547 by diatoms, nearly exclusively composed by *Skeletonema*. A similar shift from *C. leadbeateri*
548 presence to absence with concurrent predominance of diatoms was observed during the 1991
549 HAB around Ofotfjord and surrounding areas (Hegseth and Eilertsen, 1991; Rey and Aure,
550 1991). Correspondingly, the sampled prokaryotic community composition in Ballangen does
551 not presumably represent either the situation with *C. leadbeateri* as a disruptive causative agent
552 as several genera belonging to the observed predominant bacterial order *Alteromonadales* have
553 been found to associate with *Skeletonema* sp. (Deng et al., 2021).

554 *C. leadbeateri* and presumably the cells assigned to the focal taxon in our sequencing
555 analysis are common and natural members of phytoplankton community along the entire
556 northern Norwegian coast, although its spatial and interannual variation has not been well
557 described since the 1991 HAB, as only two following years of monitoring was conducted in
558 area south and north from Ofotfjord (Hegseth and Eilertsen, 1991; Heidal and Mohus, 1995).
559 The present study, however, provides evidence for high spatial variation and non-cell-density-
560 dependent toxicity. As mentioned, the high abundance of our designated focal taxon in the
561 Balsfjord area was corroborated by manual cell counts and revealed by 18S rRNA amplicon

562 sequencing samples in this study (Figure 1). This was two weeks after the first reported fish
563 mortalities from Ofotfjord (Karlsen et al., 2019). Thus, this raises the question whether a bloom
564 of focal taxon commenced locally in Balsfjord. Due to limited connectivity, it is likely that *C.*
565 *leadbeateri* blooms developed independently in both fjords since its relative abundance was
566 low in FSS station (Figure 2c) and no afflicted fish farms were reported near the FSS station,
567 despite of the affect on fish farms in the area north of Ofotfjord (Karlsen et al., 2019).
568 Interestingly, despite high abundance of the focal taxon and effective advection-driven
569 dispersal of cells from the inner part of Balsfjord towards GSSS and Tussøya stations, only one
570 fish farm near Tussøya was afflicted. However, this farm experienced limited impacts, and its
571 relation to the HAB remained somewhat questionable (Karlsen et al., 2019). This observation
572 also lends some indications to the idea that there may have been at least two distinct
573 physiological states between these two *C. leadbeateri* blooms, and that only one of them was
574 “harmful”.

575

576 **Localized microbial communities.**

577 One of the major questions that drove this study was to ask how the marine microbiome
578 composition compared across locations during the HAB time series. The results revealed
579 distinct communities between sample locations, each possessing different predominating
580 bacterial and eukaryotic microbial groups (Figure 1 and Figure 2). This observation on spatial
581 heterogeneity provides new information on the development of the late bloom phase within an
582 interconnected coastal area (Wassmann et al., 1996). GSSS was the only station where
583 *Phaeocystis* abundance exceeded that of the focal taxon. In fact, the relative abundance of
584 *Phaeocystis* was less than 1 % at all other stations, which was an unexpected result given
585 previously reported ubiquity and prolonged prevalence (March-August) in this region (Eilertsen
586 et al., 1981; Degerlund and Eilertsen, 2010).

587 Although the predominant microalgae groups found in the two time series stations were
588 different (FSS: cryptophytes, *Leptocylindrus*, heterotrophic nanoflagellates; GSSS;
589 dinoflagellates, prymnesiophyte, *Thalassiosira*), the most abundant bacterial taxa – i.e. orders
590 *Flavobacteriales*, *Rhodobacterales* and *Pseudomonadales* – were essentially consistent.
591 Previously reported studies have also shown that members belonging to these orders commonly
592 accompany microalgae in marine environments, except in the case of *Teleaulax* sp. and *C.*
593 *leadbeateri*, which may be due to lack of previous records from events such as the 1991 HAB
594 of northern Norway (Teeling et al., 2016; Ajani et al., 2018; Zhou et al., 2018; Aalto et al.,
595 2022). The bacterial community compositions obtained from Middle-Balsfjord and South-
596 Tromsø stations were distinct and corresponded to the highest observed relative abundance of
597 the focal taxon. Specifically, they harboured high relative abundances of SAR11 (mainly clade
598 Ia) and low contributions of *Flavobacteriales*, which is interesting given that SAR11 tend to be
599 negatively correlated with copiotrophic bacterial groups before and after the primary
600 phytoplankton bloom (Needham and Fuhrman, 2016; Teeling et al., 2016). However, the single
601 time point stations present a major limitation for interpreting the HAB microbiome, given that
602 the time series stations (FSS and GSSS) showed pronounced temporal variability during the
603 event.

604

605 **Temporal community dynamics.**

606 Another major aim of this study was to identify the temporal patterns of the HAB associated
607 microbiome and attempt to determine which taxa co-bloomed with the focal ASV. We found
608 that most of the microeukaryotic and bacterial taxa either co-bloomed or inversely co-bloomed
609 with the focal ASV – i.e. the clusters that showed significant positive or negative correlation
610 with the focal ASV also had the highest taxonomic richness (Figure 4 and Figure 5). There has
611 been evidence that the most abundant taxa undergo stronger shifts in their abundance than rare

612 taxa, which corresponds with our results where the most abundant bacterial orders and
613 microeukaryotic classes were mainly found within the clusters of highest temporal variability
614 (Lindh et al., 2015). However, the high number of taxa in these clusters is somewhat surprising
615 with regard of previous findings of highly coherent communities with well-defined groups of
616 interacting organisms (Martin-Platero et al., 2018). It is likely that the prescribed temporal
617 (sampling) resolution of this study was too coarse to capture the true frequency of taxonomic
618 turnover, which can be very fast (Needham and Fuhrman, 2016; Martin-Platero et al., 2018).
619 However, when an unpredicted and regionally large (250 km wide) HAB occurs, it poses major
620 logistical challenges to react quickly and access the sample locations with frequency that would
621 be the most optimal with biological perspective. The choice of optimal sampling locations is
622 also limited by immediate accessibility to sampling resources, such as suitable water craft.

623

624 **The environment.**

625 The third major question of this study was related to the abiotic environment and how it may
626 have influenced the microbiome composition and presence of the focal taxon. The HAB – as
627 inferred from relative abundance of the focal taxon – was stronger at GSSS than at FSS, yet it
628 occurred concurrently at both stations. The strong decrease in focal taxon abundance in the
629 middle of time series coincided, especially at GSSS, with a change in community composition.
630 However, this was evidenced poorly by environmental factors at both stations. Intriguingly,
631 these results are in accordance with previous findings suggesting lower importance of
632 continuous environmental factors such as temperature, inorganic nutrients and chlorophyll *a* on
633 a change in community composition after seasonal bloom initiation than biotic interactions
634 (Lindh et al., 2015; Needham and Fuhrman, 2016). Whereas, a strong periodical physical
635 forcing (wind, turbulence) can cause a change of entire community (Martin-Platero et al., 2018).
636 The measured water column properties did not indicate strong vertical mixing. However, the

637 surface water became somewhat more homogenous after the first week in the time series at
638 GSSS as revealed from CTD-profiles (Supplementary Figure S2).

639 The difference in microeukaryotic composition between the two time series stations
640 may be related to environmental factors as revealed by dbRDA analysis (Figure 3). The
641 phosphate concentration was low at both stations and in addition the $\text{NO}_3^- + \text{NO}_2^-$ level was low
642 in FSS, which potentially promoted the development of communities of heterotrophic and
643 mixotrophic protists. Several MAST-clades (e.g., MAST-1C as dominant in FSS) are known to
644 be bacterivores and *Teleaulax* has been determined to be mixotrophic, feeding heterotrophically
645 on bacteria, thus relaxing the need for inorganic nutrients (Massana et al., 2006; Du Yoo et al.,
646 2017). It is difficult to draw a link between nutrients and the focal taxon with the current data
647 due to lack of nutrient measurements from stations with high focal taxon abundance such as
648 Middle-Balsfjord and South-Tromsø. Despite the nutrient information, a plausible connection
649 would be unlikely as even a 14-year survey in southern Norway on *Chrysochromulina* spp. cell
650 and nutrients concentration did not provide a clear connection (Dahl et al., 2005). However,
651 there are indications that *Chrysochromulina* spp. thrive in high N:P ratios during low phosphate
652 concentration which potentially promotes toxicity if the condition becomes phosphate limited
653 (Dahl et al., 2005; Edvardsen and Imai, 2006).

654

655 **CONCLUSION**

656 A summary of investigations of the 1991 *Chrysochromulina leadbeateri* related harmful algal
657 bloom in northern Norway writes that it would not have been possible to predict such an
658 incident but it would be necessary to launch a coastal monitoring program (Rey, 1991). Three
659 decades later, we fully agree with the latter statement. We certainly have a long way to go in
660 order to predict how ecological principles underpin this sporadic event in a highly variable
661 coastal area and it is difficult to get there by performing investigations that simply react to only

662 those blooms that have acute economic impacts. It is also difficult to plan to observe such a
663 bloom that happens so infrequently. It has become highly evident that this type of reoccurring
664 bloom is extremely destructive because it causes substantial losses for the fish farmers. In 1991
665 the fish kill damage linked to *C. leadbeateri* was 742 tonnes with a corresponding direct short
666 term economic cost of 3.5 million USD, while in 2019 these values were increased to 14 500
667 tonnes and more than 100 million USD (Karlson et al., 2021). Thus, it is expected these numbers
668 will become even higher in the future with increasing aquaculture industry, and there is no
669 reason to believe that this type of HAB will not reoccur. It is challenging to draw any
670 conclusions about exact causation behind the 2019 HAB, especially since the natural bloom
671 cycles of *C. leadbeateri* are not well understood. Therefore, this study relying on molecular-
672 based methods provides a first insight on the spatial and temporal variability of the *C.*
673 *leadbeateri*-like focal taxon together with its associated marine microbiome. It also supports
674 future molecular-based studies by providing a genetic link with currently available taxonomic
675 annotation between current and year 1991 *C. leadbeateri*. Otherwise the focal taxon may be
676 overlooked due to database limitations – an issue also present in this study. We found that most
677 of the taxa – including the most abundant members of prokaryotes and microeukaryotes and
678 the focal taxon – underwent strong and rapid variability in their succession dynamics. These
679 temporal dynamics were poorly connected to the environmental conditions measured,
680 suggesting that other factors such as biological interactions might drive the late bloom
681 dynamics.

682

683 **AUTHOR CONTRIBUTIONS**

684 NJA and HCB conceptualized the study. NJA, EG-M, JBS, LD, CJH and RI carried out the
685 sampling. NJA, HS, SK and SP performed lab work and processed amplicon sequence analyses.

686 NJA and HCB conducted data analysis and NJA wrote the manuscript draft. All authors
687 contributed to the final version.

688

689 **ACKNOWLEDGMENTS**

690 We greatly appreciate the logistical support by staff at Lerøy Aurora’s aquaculture facility at
691 Solheim. We also acknowledge the collaboration between Finnfjord AS and UiT-The Arctic
692 University of Norway for lending sampling infrastructure and support. We would like thank
693 Åge Mohus and Vigdis Tverberg at Nord University for their help with sample coordination in
694 southern portion of the HAB affected area.

695

696 **FUNDING**

697 This study was funded directly by the Faculty of Biosciences, Fisheries and Economics at UiT
698 – The Arctic University of Norway as the “2019 Harmful Algae Rapid Response Plan”. The
699 authors would like to specifically thank Terje Aspen, Terje Martinussen and Kathrine Tveiterås
700 for providing rapid support and guidance.

701

702 **CONFLICT OF INTEREST**

703 The authors have no conflicts of interest to declare.

704

705 **REFERENCES CITED**

- 706 Aalto, N.J., Campbell, K., Eilertsen, H.C., and Bernstein, H.C. (2021). Drivers of atmosphere
707 ocean CO₂ flux in northern Norwegian fjords. *Frontiers in Marine Science*, 841. doi:
708 10.3389/fmars.2021.692093.
- 709 Aalto, N.J., Schweitzer, H., Krsmanovic, S., Campbell, K., and Bernstein, H.C. (2022). Diversity
710 and selection of surface marine microbiomes in the Atlantic-influenced Arctic.
711 *Frontiers in Microbiology*. doi: 10.3389/fmicb.2022.892634/abstract.
- 712 Abdi, H., and Williams, L.J. (2010). Tukey’s honestly significant difference (HSD) test.
713 *Encyclopedia of research design* 3(1), 1-5.
- 714 Ajani, P.A., Kahlke, T., Siboni, N., Carney, R., Murray, S.A., and Seymour, J.R. (2018). The
715 Microbiome of the Cosmopolitan Diatom *Leptocylindrus* Reveals Significant Spatial

716 and Temporal Variability. *Frontiers in Microbiology* 9. doi:
717 10.3389/fmicb.2018.02758.

718 Amaral-Zettler, L.A., McCliment, E.A., Ducklow, H.W., and Huse, S.M. (2009). A method for
719 studying protistan diversity using massively parallel sequencing of V9 hypervariable
720 regions of small-subunit ribosomal RNA genes. *PloS one* 4(7), e6372.

721 Anderson, D.M., Glibert, P.M., and Burkholder, J.M. (2002). Harmful algal blooms and
722 eutrophication: nutrient sources, composition, and consequences. *Estuaries* 25(4),
723 704-726.

724 Anderson, M.J. (2001). A new method for non-parametric multivariate analysis of variance.
725 *Austral ecology* 26(1), 32-46.

726 Caporaso, J.G., Kuczynski, J., Stombaugh, J., Bittinger, K., Bushman, F.D., Costello, E.K., et al.
727 (2010). QIIME allows analysis of high-throughput community sequencing data. *Nat*
728 *Methods* 7(5), 335-336.

729 Cirri, E., and Pohnert, G. (2019). Algae– bacteria interactions that balance the planktonic
730 microbiome. *New Phytologist* 223(1), 100-106.

731 Coenen, A.R., Hu, S.K., Luo, E., Muratore, D., and Weitz, J.S. (2020). A primer for microbiome
732 time-series analysis. *Frontiers in genetics* 11, 310.

733 Dahl, E., Bagøien, E., Edvardsen, B., and Stenseth, N.C. (2005). The dynamics of
734 Chrysochromulina species in the Skagerrak in relation to environmental conditions.
735 *Journal of Sea Research* 54(1), 15-24.

736 Davidson, K., Gowen, R.J., Tett, P., Bresnan, E., Harrison, P.J., McKinney, A., et al. (2012).
737 Harmful algal blooms: How strong is the evidence that nutrient ratios and forms
738 influence their occurrence? *Estuarine, Coastal and Shelf Science* 115, 399-413. doi:
739 <https://doi.org/10.1016/j.ecss.2012.09.019>.

740 Degerlund, M., and Eilertsen, H.C. (2010). Main species characteristics of phytoplankton
741 spring blooms in NE Atlantic and Arctic waters (68–80 N). *Estuaries and coasts* 33(2),
742 242-269.

743 Deng, Z., Chen, S., Zhang, P., Zhang, X., Adams, J.M., Luo, Q., et al. (2021). Dynamics of Free-
744 Living and Attached Bacterial Assemblages in Skeletonema sp. Diatom Cultures at
745 Elevated Temperatures. *Frontiers in Marine Science* 8. doi:
746 10.3389/fmars.2021.626207.

747 Doucette, G.J., McGovern, E.R., and Babinchak, J.A. (1999). ALGICIDAL BACTERIA ACTIVE
748 AGAINST GYMNODINIUM BREVE (DINOPHYCEAE). I. BACTERIAL ISOLATION AND
749 CHARACTERIZATION OF KILLING ACTIVITY1, 3. *Journal of Phycology* 35(6), 1447-1454.

750 Du Yoo, Y., Seong, K.A., Jeong, H.J., Yih, W., Rho, J.-R., Nam, S.W., et al. (2017). Mixotrophy in
751 the marine red-tide cryptophyte Teleaulax amphioxeia and ingestion and grazing
752 impact of cryptophytes on natural populations of bacteria in Korean coastal waters.
753 *Harmful Algae* 68, 105-117.

754 Edvardsen, B., Eikrem, W., Throndsen, J., Saez, A.G., Probert, I., and Medlin, L.K. (2011).
755 Ribosomal DNA phylogenies and a morphological revision provide the basis for a
756 revised taxonomy of the Prymnesiales (Haptophyta). *European journal of phycology*
757 46(3), 202-228.

758 Edvardsen, B., and Imai, I. (2006). "The ecology of harmful flagellates within
759 Prymnesiophyceae and Raphidophyceae," in *Ecology of harmful algae*. Springer), 67-
760 79.

761 Edvardsen, B., and Paasche, E. (1998). Bloom dynamics and physiology of Prymnesium and
762 Chrysochromulina. *NATO ASI SERIES G ECOLOGICAL SCIENCES* 41, 193-208.

763 Eikrem, W., and Throndsen, J. (1998). Morphology of *Chrysochromulina leadbeateri*
764 (Prymnesiophyceae) from northern Norway. *Phycologia* 37(4), 292-299.

765 Eilertsen, H.C., Falk-Petersen, S., Hopkins, C., and Tande, K. (1981). Ecological investigations
766 on the plankton community of Balsfjorden, northern Norway: program for the
767 project, study area, topography, and physical environment. *Sarsia* 66(1), 25-34.

768 Eilertsen, H.C., and Frantzen, S. (2007). Phytoplankton from two sub-Arctic fjords in northern
769 Norway 2002–2004: I. Seasonal variations in chlorophyll a and bloom dynamics.
770 *Marine Biology Research* 3(5), 319-332.

771 Eilertsen, H.C., and Taasen, J. (1984). Investigations on the plankton community of
772 Balsfjorden, northern Norway. The phytoplankton 1976–1978. Environmental
773 factors, dynamics of growth, and primary production. *Sarsia* 69(1), 1-15.

774 Estep, K. (1984). Chloroplast containing microflagellates in natural populations of north
775 Atlantic nanoplankton, their identification and distribution; including a description of
776 5 new species of *Chrysochromulina* (Prymnesiophyceae). *Protistologica* 20, 613-634.

777 Fuhrman, J.A., Cram, J.A., and Needham, D.M. (2015). Marine microbial community
778 dynamics and their ecological interpretation. *Nature Reviews Microbiology* 13(3),
779 133-146.

780 Gilbert, J.A., Meyer, F., Antonopoulos, D., Balaji, P., Brown, C.T., Brown, C.T., et al. (2010).
781 Meeting report: the terabase metagenomics workshop and the vision of an Earth
782 microbiome project. *Stand Genomic Sci* 3(3), 243.

783 Grann-Meyer, E. (2020). *Chrysochromulina leadbeateri* - Understanding the presumed causal
784 agent behind the harmful algal bloom of 2019. Master's thesis, UiT - Arctic University
785 of Norway.

786 Green, D.H., Llewellyn, L.E., Negri, A.P., Blackburn, S.I., and Bolch, C.J. (2004). Phylogenetic
787 and functional diversity of the cultivable bacterial community associated with the
788 paralytic shellfish poisoning dinoflagellate *Gymnodinium catenatum*. *FEMS*
789 *Microbiology Ecology* 47(3), 345-357.

790 Guillard, R.R. (1975). "Culture of phytoplankton for feeding marine invertebrates," in *Culture*
791 *of marine invertebrate animals*. Springer), 29-60.

792 Hallegraeff, G.M., Anderson, D.M., Belin, C., Bottein, M.-Y.D., Bresnan, E., Chinain, M., et al.
793 (2021). Perceived global increase in algal blooms is attributable to intensified
794 monitoring and emerging bloom impacts. *Communications Earth & Environment* 2(1),
795 1-10.

796 Hegseth, E.N., and Eilertsen, H.C. (1991). The *Chrysochromulina leadbeateri* bloom in Troms
797 May/June 1991. Development and causes. . *Fisk. Hav.* 3, 45-61.

798 Heidal, K., and Mohus, A. (1995). The toxic *Chrysochromulina*-- salmon disaster of 1991 in
799 northern Norway with some follow-up monitoring records of 1992 and-93.
800 *LAVOISIER, PARIS(FRANCE)*. 163-168.

801 Karlsen, K.M., Robertsen, R., and Hersoug, B. (2019). Mapping the course of events and
802 preparedness for algal blooms in spring 2019 - Astafjorden, Ofotfjorden, Vestfjorden
803 og Tysfjorden. *Nofima AS* 29, 1-44.

804 Karlson, B., Andersen, P., Arneborg, L., Cembella, A., Eikrem, W., John, U., et al. (2021).
805 Harmful algal blooms and their effects in coastal seas of Northern Europe. *Harmful*
806 *Algae* 102, 101989.

807 Kaufman, L., and Rousseeuw, P.J. (2009). *Finding groups in data: an introduction to cluster*
808 *analysis*. New York: John Wiley & Sons.

809 Lindh, M.V., Sjöstedt, J., Andersson, A.F., Baltar, F., Hugerth, L.W., Lundin, D., et al. (2015).
810 Disentangling seasonal bacterioplankton population dynamics by high-frequency
811 sampling. *Environmental microbiology* 17(7), 2459-2476.

812 Liu, C., Cui, Y., Li, X., and Yao, M. (2021). microeco: an R package for data mining in microbial
813 community ecology. *FEMS Microbiology Ecology* 97(2), fiae255.

814 Lord, E., Willems, M., Lapointe, F.-J., and Makarenkov, V. (2017). Using the stability of
815 objects to determine the number of clusters in datasets. *Information Sciences* 393,
816 29-46.

817 Love, M.I., Huber, W., and Anders, S. (2014). Moderated estimation of fold change and
818 dispersion for RNA-seq data with DESeq2. *Genome biology* 15(12), 1-21.

819 Lozupone, C., Lladser, M.E., Knights, D., Stombaugh, J., and Knight, R. (2011). UniFrac: an
820 effective distance metric for microbial community comparison. *The ISME journal* 5(2),
821 169-172.

822 Martin-Platero, A.M., Cleary, B., Kauffman, K., Preheim, S.P., McGillicuddy, D.J., Alm, E.J., et
823 al. (2018). High resolution time series reveals cohesive but short-lived communities in
824 coastal plankton. *Nature communications* 9(1), 1-11.

825 Massana, R., Terrado, R., Forn, I., Lovejoy, C., and Pedrós-Alió, C. (2006). Distribution and
826 abundance of uncultured heterotrophic flagellates in the world oceans.
827 *Environmental microbiology* 8(9), 1515-1522.

828 Mayali, X., and Azam, F. (2004). Algicidal bacteria in the sea and their impact on algal blooms
829 1. *Journal of Eukaryotic Microbiology* 51(2), 139-144.

830 Meldahl, A.S., Edvardsen, B., and Fonnum, F. (1994). Toxicity of four potentially ichthyotoxic
831 marine phytoflagellates determined by four different test methods. *Journal of*
832 *Toxicology and Environmental Health, Part A Current Issues* 42(3), 289-301.

833 Meyer, N., Bigalke, A., Kaulfuß, A., and Pohnert, G. (2017). Strategies and ecological roles of
834 algicidal bacteria. *FEMS Microbiology Reviews* 41(6), 880-899.

835 Needham, D.M., and Fuhrman, J.A. (2016). Pronounced daily succession of phytoplankton,
836 archaea and bacteria following a spring bloom. *Nature Microbiology* 1(4), 16005. doi:
837 10.1038/nmicrobiol.2016.5.

838 Nielsen, T.G., Kiørboe, T., and Bjørnsen, P.K. (1990). Effects of a *Chrysochromulina polylepis*
839 subsurface bloom on the planktonic community. *Marine Ecology Progress Series*, 21-
840 35.

841 Oksanen, J., Blanchet, F.G., Kindt, R., Legendre, P., Minchin, P.R., O'hara, R., et al. (2013).
842 Package 'vegan'. *Community ecology package, version* 2(9).

843 Parte, A.C., Carbasse, J.S., Meier-Kolthoff, J.P., Reimer, L.C., and Göker, M. (2020). List of
844 Prokaryotic names with Standing in Nomenclature (LPSN) moves to the DSMZ.
845 *International Journal of Systematic and Evolutionary Microbiology* 70(11), 5607.

846 Peralta-Ferriz, C., and Woodgate, R.A. (2015). Seasonal and interannual variability of pan-
847 Arctic surface mixed layer properties from 1979 to 2012 from hydrographic data, and
848 the dominance of stratification for multiyear mixed layer depth shoaling. *Progress in*
849 *Oceanography* 134, 19-53.

850 R Core Team (2021). R: A language and environment for statistical computing, R Foundation
851 for Statistical Computing.

852 Reigstad, M., and Wassmann, P. (1996). Importance of advection for pelagic-benthic
853 coupling in north Norwegian fjords. *Sarsia* 80(4), 245-257.

854 Rey, F. (1991). The *Chrysochromulina leadbeateri* bloom in Vestfjorden, north Norway, May-
855 June 1991: Proceedings from a scientific working meeting. *Fisk. Hav.* 3, 1-122.

856 Rey, F., and Aure, J. (1991). The *Chrysochromulina leadbeateri* bloom in the Vestfjord, north
857 Norway, May-June 1991. Environmental conditions and possible causes. *Fisk. Hav.* 3,
858 13-32.

859 Statistics Norway (2020). *Aquaculture 2019* [Online]. Statistics Norway. Available:
860 <https://www.ssb.no/jord-skog-jakt-og-fiskeri/statistikker/fiskeoppdrett> [Accessed
861 23.04 2022].

862 Teeling, H., Fuchs, B.M., Bennke, C.M., Krueger, K., Chafee, M., Kappelmann, L., et al. (2016).
863 Recurring patterns in bacterioplankton dynamics during coastal spring algae blooms.
864 *elife* 5, e11888.

865 Uribe, P., and Espejo, R.T. (2003). Effect of associated bacteria on the growth and toxicity of
866 *Alexandrium catenella*. *Applied and environmental microbiology* 69(1), 659-662.

867 Uronen, P., Kuuppo, P., Legrand, C., and Tamminen, T. (2007). Allelopathic Effects of Toxic
868 Haptophyte *Prymnesium parvum* Lead to Release of Dissolved Organic Carbon and
869 Increase in Bacterial Biomass. *Microbial Ecology* 54(1), 183-193. doi:
870 10.1007/s00248-006-9188-8.

871 Uronen, P., Lehtinen, S., Legrand, C., Kuuppo, P., and Tamminen, T. (2005). Haemolytic
872 activity and allelopathy of the haptophyte *Prymnesium parvum* in nutrient-limited
873 and balanced growth conditions. *Marine Ecology Progress Series* 299, 137-148.

874 Wassmann, P., Svendsen, H., Keck, A., and Reigstad, M. (1996). Selected aspects of the
875 physical oceanography and particle fluxes in fjords of northern Norway. *Journal of*
876 *Marine Systems* 8(1-2), 53-71.

877 Zhou, J., Richlen, M.L., Sehein, T.R., Kulis, D.M., Anderson, D.M., and Cai, Z. (2018). Microbial
878 Community Structure and Associations During a Marine Dinoflagellate Bloom.
879 *Frontiers in Microbiology* 9. doi: 10.3389/fmicb.2018.01201.

880
881
882
883
884
885
886
887
888
889
890
891
892

893
894
895
896
897
898
899
900
901
902
903
904
905
906
907
908
909
910
911
912
913
914
915
916
917

SUPPLEMENTARY MATERIAL

Microbial community dynamics during a harmful *Chrysochromulina leadbeateri* bloom

Nerea J. Aalto^{1,2}, Hannah Schweitzer^{1,2}, Erlend Grann-Meyer¹, Stina Krsmanovic¹, Jon Brage
Svenning¹, Lars Dalheim¹, Sebastian Petters¹, Richard Ingebrigtsen¹, Chris J. Hulatt³, Hans C.
Bernstein^{1,2*}

Affiliations:

1. Norwegian College of Fisheries Sciences, UiT - The Arctic University of Norway, Tromsø,
Norway
2. The Arctic Centre for Sustainable Energy, UiT - The Arctic University of Norway, Tromsø,
Norway
3. Faculty of Biosciences and Aquaculture, Nord University, Bodø, Norway

***Correspondence:** Hans C. Bernstein, UiT-The Arctic University of Norway, BFE-fak.,
Postboks 6050 Langnes, 9037 Tromsø, NORWAY; *Phone:* +47 776 46 114; *Email:*
Hans.C.Bernstein@uit.no

918 **Supplementary Table S1.** Station positions, sample dates, and corresponding sample day and
 919 week during time series sample campaign (May 27th = Sample day 0 and June 21st = Sample
 920 day 25).
 921

Station	Position	Sample date	Sample day/Sample week
FSS	69.19 N, 18.03 E	27.05.2019	0/0
		30.05.2019	3/0
		03.06.2019	7/1
		11.06.2019	15/2
		13.06.2019	17/2
		17.06.2019	21/3
		20.06.2019	24/3
GSSS	69.80 N, 19.36 E	28.05.2019	1/0
		31.05.2019	4/0
		04.06.2019	8/1
		07.06.2019	11/1
		12.06.2019	16/2
		14.06.2019	18/2
		18.06.2019	22/2
		21.06.2019	25/3
South-Tromsø	69.60 N, 18.80 E	27.05.2019	0/0
Middle-Balsfjord	69.40 N, 19.20 E	29.05.2019	2/0
Tussøy	69.66 N, 18.18 E	06.06.2019	10/1
Ballangen	68.41 N, 16.83 E	05.06.2019	9/1
Middle-Sagfjord	67.98 N, 15.75 E	14.06.2019	18/2
Veggfjell	67.96 N, 15.80 E	14.06.2019	18/2
Anevik	68.00 N, 15.14 E	14.06.2019	18/2
Dyping	67.92 N, 15.34 E	14.06.2019	18/2

922

923

924

925

926

927

928

929

930

931 **Supplementary Table S2.** The number of classified ASVs and sequencing depth per sample
 932 and data set before and after removal of unwanted taxa. Time series sample set includes
 933 stations FSS and GSSS; Single-time-point sample set includes stations Tussøya, South-
 934 Tromsø, Middle-Balsfjord, Ballangen, Middle-Sagfjord, Veggfjell, Anevik and Dyping;
 935 Unialgal control sample set includes *Chrysochromulina leadbeateri* UiO-035 strain culture.
 936

Condition	Sample set	Data set	# ASVs	Sample depth
All taxa	Time series	16S	2761	54160–217118
	Time series	18S	7500	72831–34835
	Single-time-point	16S	1414	83315–168168
	Single-time-point	18S	3687	143296–469129
	Unialgal control (UiO-035)	18S	123	134563–273163
Removed unwanted taxa	Time series	16S	2644	53962–214722
	Time series	18S	2674	56789–331887
	Single-time-point	16S	1368	83253–167400
	Single-time-point	18S	1682	118101–451910
	Unialgal control (UiO-035)	18S	15	125686–265853

937

938

939

940

941

942

943

944

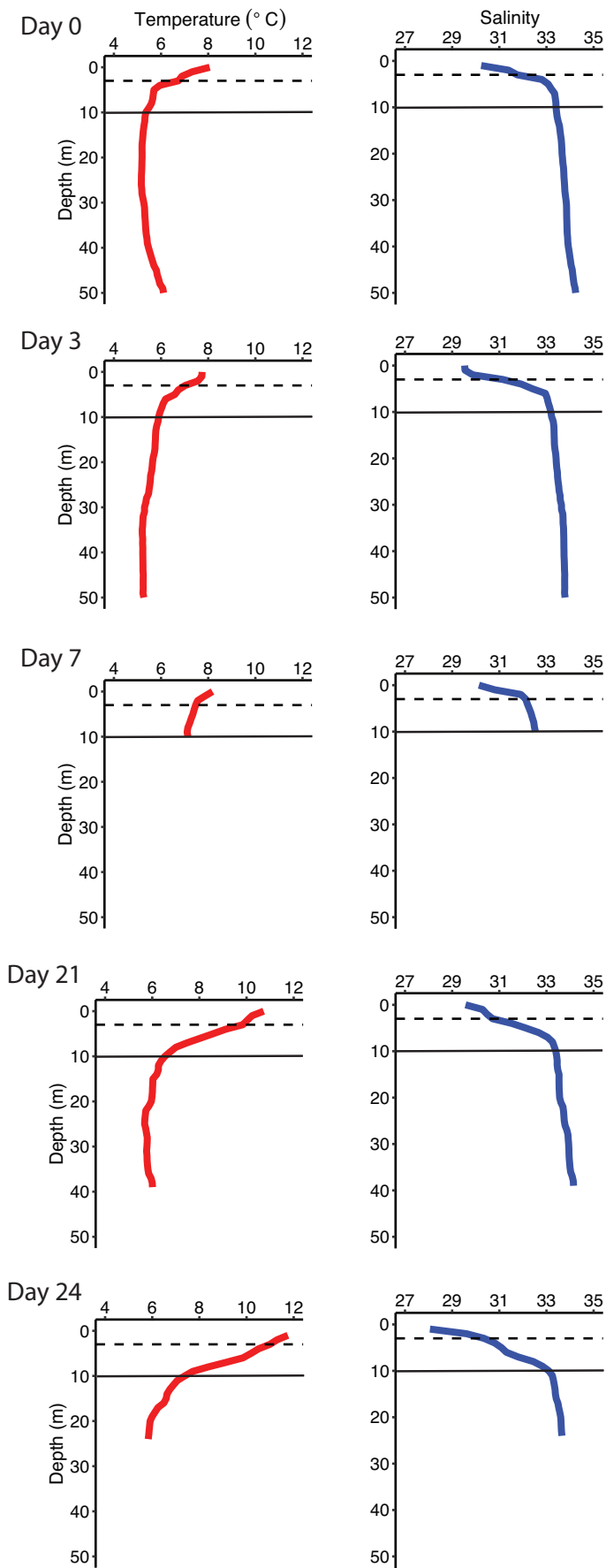
945

946

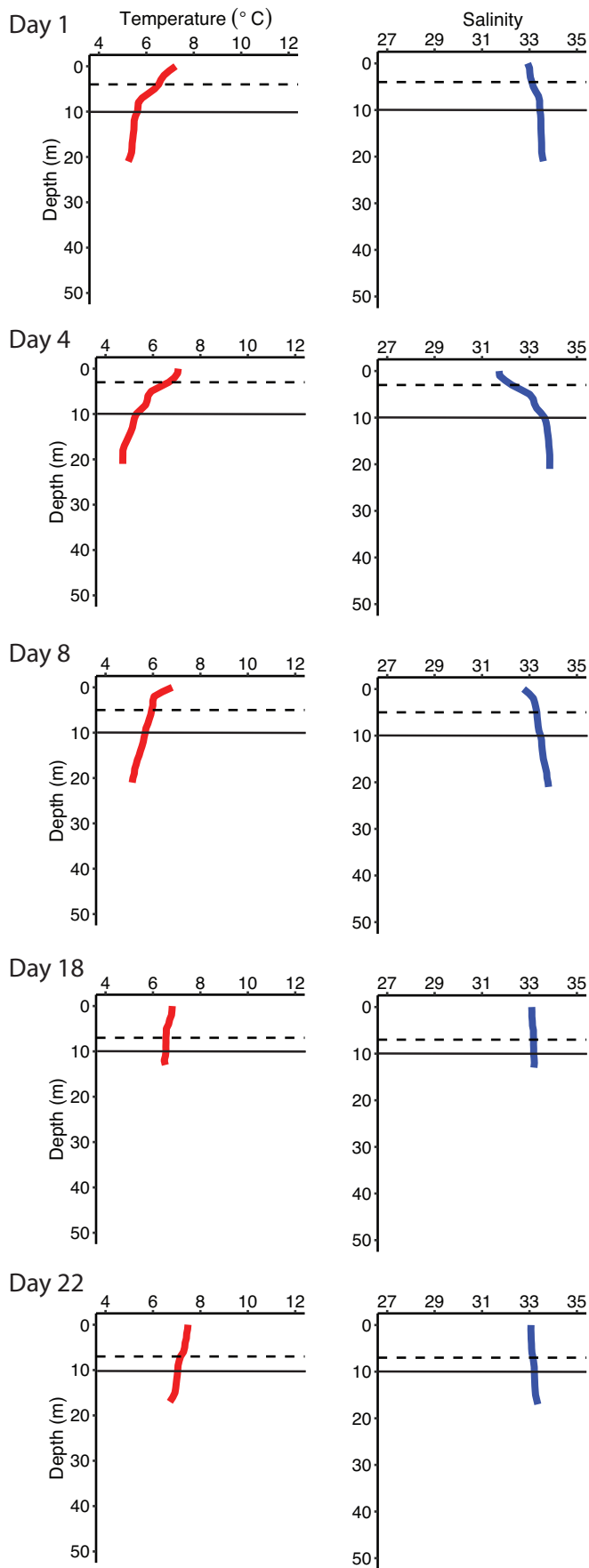
947

948

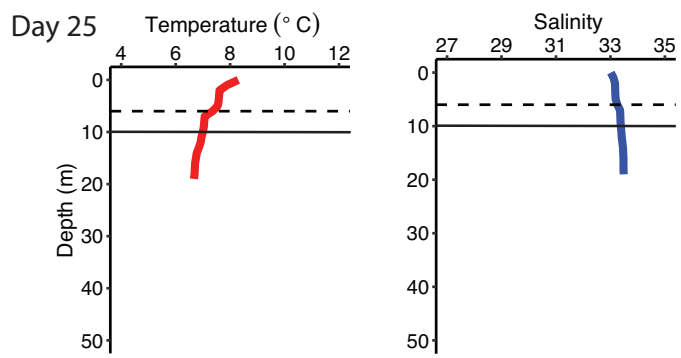
949



Supplementary Figure S1. Surface water profiles of temperature and salinity obtained from CTD-casts in FSS time series station. The dashed line denotes calculated mixed layer depth (MLD) based on density gradient and solid line marks the depth of sampled microbial communities (10 m). Note missing CTD-casts in sample days of 15 and 17



Supplementary Figure S2. Surface water profiles of temperature and salinity obtained from CTD-casts in GSSS time series station. The dashed line denotes calculated mixed layer depth (MLD) based on density gradient and solid line marks the depth of sampled microbial communities (10 m). Note missing CTD-casts in sample days of 11 and 16.



952

953

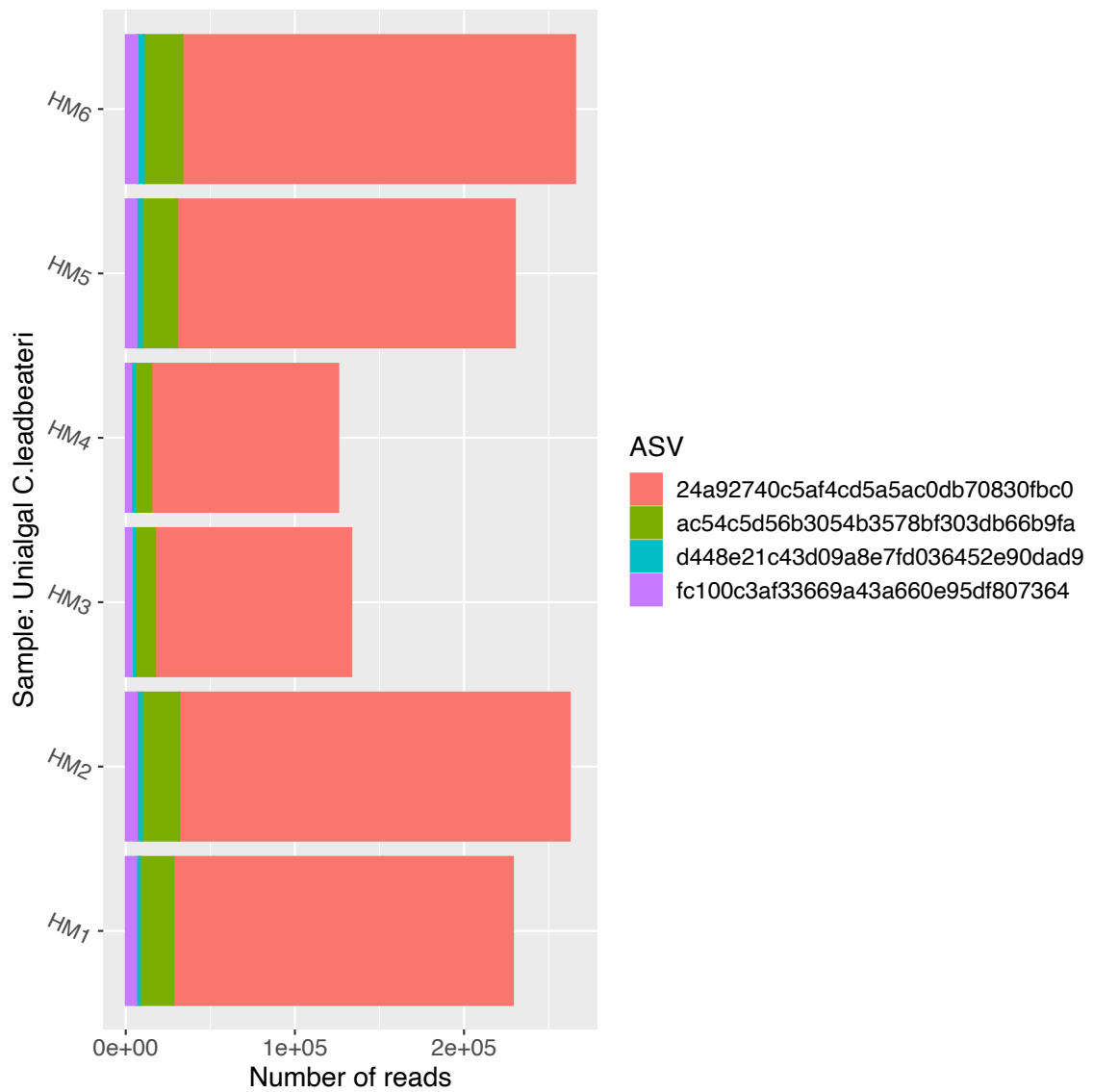
954 **Supplementary Figure S2 continues.**

955

956

957

958

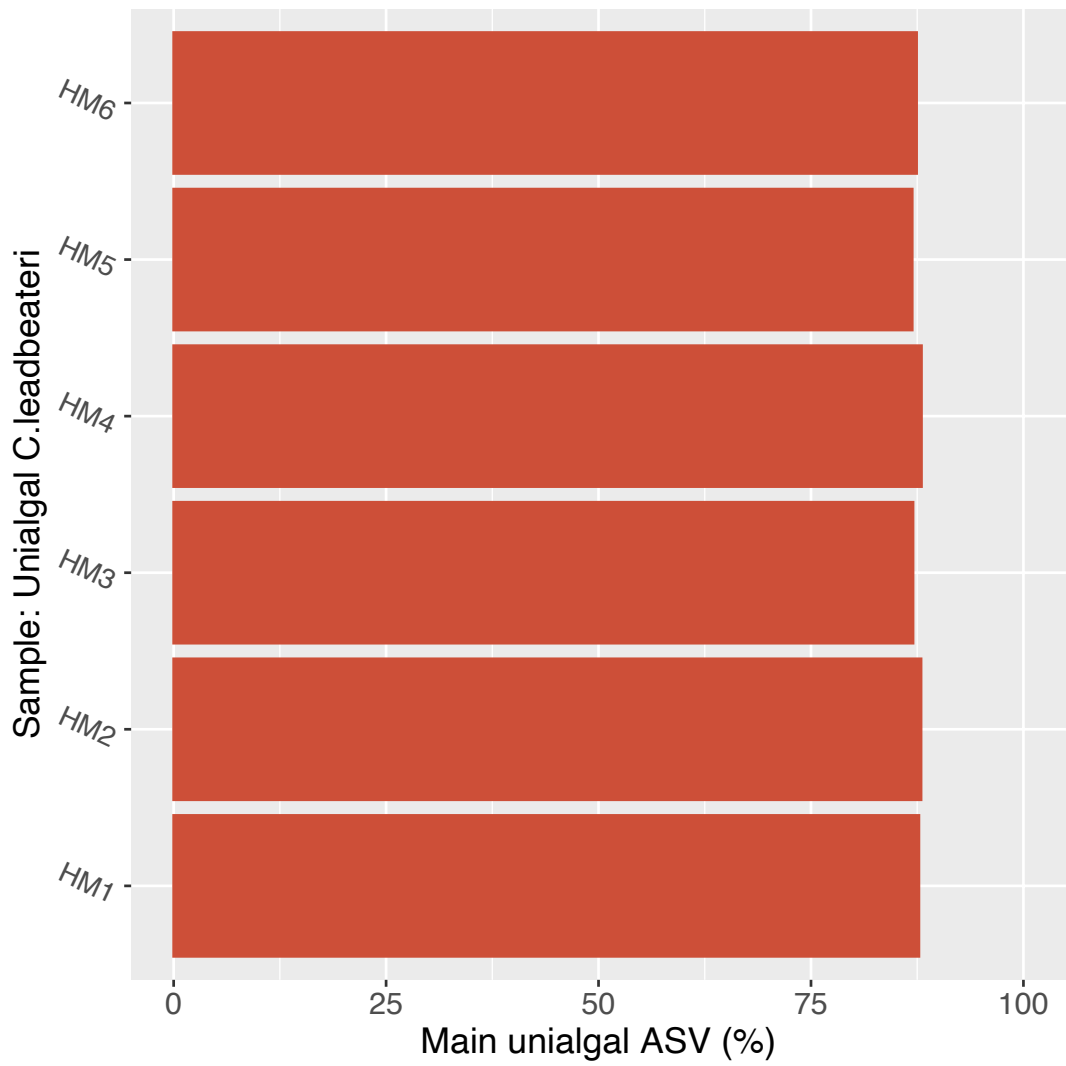


959

960 **Supplementary Figure S3.** Number of amplicon sequence reads of each ASV assigned to

961 OLI16029, in unialgal *Chrysochromulina leadbeateri* UiO-035 control culture.

962



963

964 **Supplementary Figure S4.** Relative abundance of the most abundant ASV

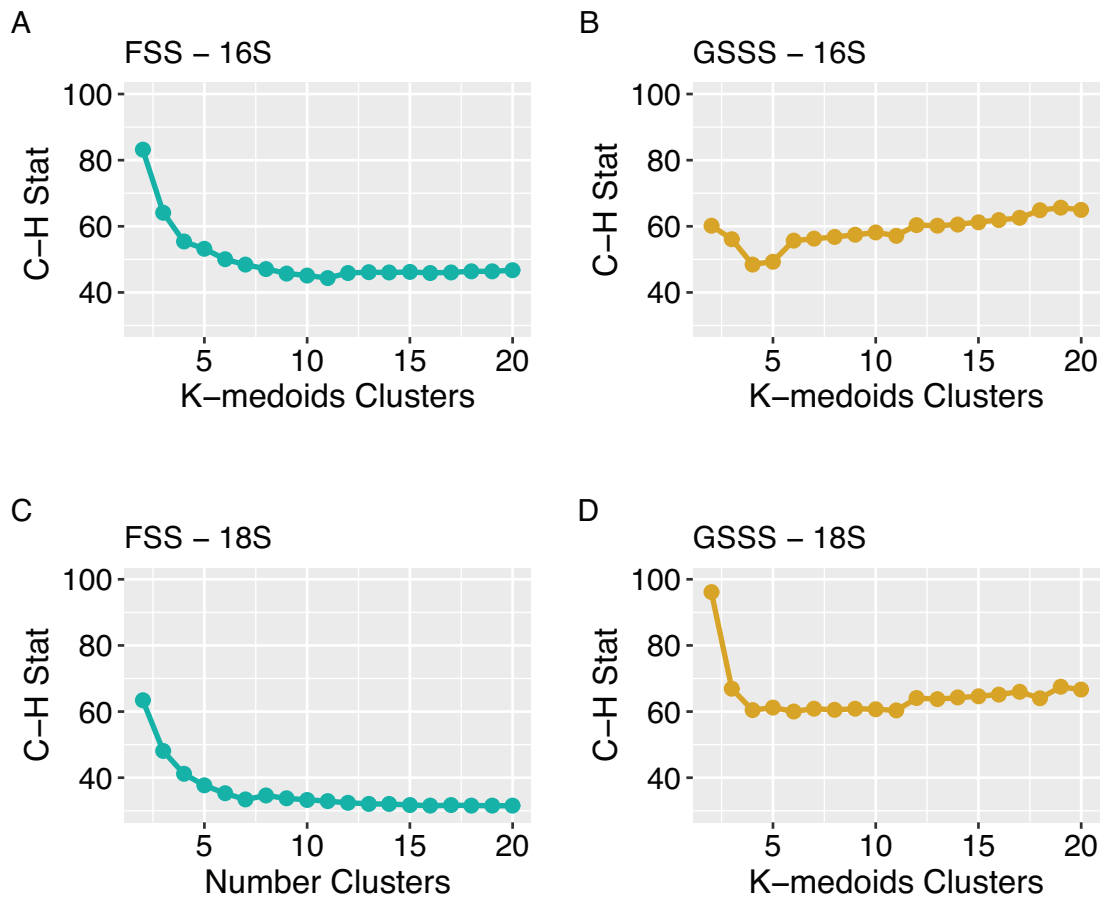
965 (*24a92740c5af4cd5a5ac0db70830fbc0*, referred as a focal ASV) in unialgal

966 *Chrysochromulina leadbeateri* Uio-035 control culture among all the ASVs assigned to

967 OLI16029.

968

969



970

971 **Supplementary Figure S5.** The Calinski-Harabasz index (y-axis, C-H Stat) was used to
 972 determine the number of K-medoids clusters. C-H Stat is a normalized ratio of the inter and
 973 intra cluster variance calculated for each sample-specific K-medoids cluster. High C-H Stat
 974 value indicates more uniquely portioned clusters. A) Three clusters were chosen to represent
 975 16S ASVs from FSS time series. B) Three clusters were chosen to represent 16S ASVs from
 976 the from GSSS time series. C) Four clusters were chosen to represent 18S ASVs from FSS
 977 time series. D) Three clusters were chosen to represent 18S ASVs from the from GSSS time
 978 series.

979

980

981

982

983

984

985

986

987 **Supplementary Table 3.** Results of perMANOVA pairwise comparison between 1) time
 988 series sample stations, 2) sample weeks and 3) sample days within each sample station for
 989 prokaryotic and microeukaryotic communities, respectively. Unweighted UniFrac was used as
 990 a distance metric, and number of permutations was 999.
 991

Groups	R2	r	p.value	Data type	Station
FSS vs GSSS	0.3	0.54	0.001	16S	
FSS vs GSSS	0.46	0.68	0.001	18S	
Week_0 vs Week_1	0.22	0.47	0.001	16S	FSS
Week_0 vs Week_2	0.16	0.39	0.002	16S	FSS
Week_0 vs Week_3	0.21	0.45	0.001	16S	FSS
Week_1 vs Week_2	0.25	0.5	0.001	16S	FSS
Week_1 vs Week_3	0.17	0.41	0.001	16S	FSS
Week_2 vs Week_3	0.13	0.36	0.001	16S	FSS
Week_0 vs Week_1	0.08	0.28	0.013	16S	GSSS
Week_0 vs Week_2	0.16	0.4	0.001	16S	GSSS
Week_0 vs Week_3	0.21	0.46	0.001	16S	GSSS
Week_1 vs Week_2	0.14	0.38	0.001	16S	GSSS
Week_1 vs Week_3	0.23	0.48	0.001	16S	GSSS
Week_2 vs Week_3	0.11	0.32	0.003	16S	GSSS
Week_0 vs Week_1	0.38	0.61	0.002	18S	FSS
Week_0 vs Week_2	0.33	0.58	0.001	18S	FSS
Week_0 vs Week_3	0.34	0.58	0.001	18S	FSS
Week_1 vs Week_2	0.42	0.65	0.002	18S	FSS
Week_1 vs Week_3	0.27	0.51	0.001	18S	FSS
Week_2 vs Week_3	0.24	0.49	0.001	18S	FSS
Week_0 vs Week_1	0.08	0.28	0.024	18S	GSSS
Week_0 vs Week_2	0.16	0.4	0.001	18S	GSSS
Week_0 vs Week_3	0.21	0.46	0.001	18S	GSSS
Week_1 vs Week_2	0.14	0.38	0.003	18S	GSSS
Week_1 vs Week_3	0.23	0.48	0.001	18S	GSSS
Week_2 vs Week_3	0.11	0.32	0.003	18S	GSSS
0 vs 3	0.11	0.33	0.356	16S	FSS
0 vs 7	0.32	0.57	0.003	16S	FSS
0 vs 15	0.24	0.49	0.01	16S	FSS
0 vs 17	0.27	0.52	0.006	16S	FSS
0 vs 21	0.29	0.54	0.001	16S	FSS
0 vs 24	0.36	0.6	0.007	16S	FSS
3 vs 7	0.25	0.5	0.009	16S	FSS
3 vs 15	0.21	0.46	0.006	16S	FSS
3 vs 17	0.24	0.49	0.007	16S	FSS
3 vs 21	0.25	0.5	0.005	16S	FSS
3 vs 24	0.29	0.54	0.005	16S	FSS
7 vs 15	0.36	0.6	0.004	16S	FSS

7 vs 17	0.29	0.54	0.003	16S	FSS
7 vs 21	0.29	0.54	0.006	16S	FSS
7 vs 24	0.23	0.48	0.004	16S	FSS
15 vs 17	0.22	0.47	0.009	16S	FSS
15 vs 21	0.22	0.46	0.004	16S	FSS
15 vs 24	0.36	0.6	0.001	16S	FSS
17 vs 21	0.16	0.4	0.01	16S	FSS
17 vs 24	0.27	0.52	0.003	16S	FSS
21 vs 24	0.25	0.5	0.004	16S	FSS
1 vs 4	0.28	0.53	0.002	16S	GSSS
1 vs 8	0.23	0.48	0.004	16S	GSSS
1 vs 11	0.31	0.56	0.006	16S	GSSS
1 vs 16	0.34	0.59	0.004	16S	GSSS
1 vs 18	0.4	0.63	0.005	16S	GSSS
1 vs 22	0.29	0.54	0.002	16S	GSSS
1 vs 25	0.36	0.6	0.002	16S	GSSS
4 vs 8	0.18	0.43	0.002	16S	GSSS
4 vs 11	0.14	0.38	0.009	16S	GSSS
4 vs 16	0.17	0.42	0.002	16S	GSSS
4 vs 18	0.37	0.61	0.003	16S	GSSS
4 vs 22	0.31	0.56	0.004	16S	GSSS
4 vs 25	0.37	0.61	0.004	16S	GSSS
8 vs 11	0.21	0.46	0.001	16S	GSSS
8 vs 16	0.2	0.44	0.002	16S	GSSS
8 vs 18	0.33	0.58	0.002	16S	GSSS
8 vs 22	0.27	0.52	0.004	16S	GSSS
8 vs 25	0.32	0.56	0.004	16S	GSSS
11 vs 16	0.19	0.43	0.007	16S	GSSS
11 vs 18	0.41	0.64	0.002	16S	GSSS
11 vs 22	0.34	0.58	0.002	16S	GSSS
11 vs 25	0.38	0.62	0.002	16S	GSSS
16 vs 18	0.32	0.56	0.004	16S	GSSS
16 vs 22	0.27	0.52	0.001	16S	GSSS
16 vs 25	0.32	0.56	0.003	16S	GSSS
18 vs 22	0.15	0.38	0.005	16S	GSSS
18 vs 25	0.24	0.49	0.003	16S	GSSS
22 vs 25	0.18	0.42	0.004	16S	GSSS
0 vs 3	0.19	0.43	0.017	18S	FSS
0 vs 7	0.48	0.69	0.002	18S	FSS
0 vs 15	0.5	0.71	0.008	18S	FSS
0 vs 17	0.47	0.69	0.009	18S	FSS
0 vs 21	0.44	0.67	0.004	18S	FSS
0 vs 24	0.56	0.75	0.001	18S	FSS

3 vs 7	0.42	0.65	0.002	18S	FSS
3 vs 15	0.44	0.66	0.003	18S	FSS
3 vs 17	0.4	0.63	0.002	18S	FSS
3 vs 21	0.37	0.61	0.001	18S	FSS
3 vs 24	0.49	0.7	0.004	18S	FSS
7 vs 15	0.54	0.74	0.006	18S	FSS
7 vs 17	0.44	0.66	0.002	18S	FSS
7 vs 21	0.41	0.64	0.005	18S	FSS
7 vs 24	0.37	0.61	0.002	18S	FSS
15 vs 17	0.31	0.56	0.007	18S	FSS
15 vs 21	0.35	0.59	0.002	18S	FSS
15 vs 24	0.54	0.74	0.002	18S	FSS
17 vs 21	0.23	0.48	0.001	18S	FSS
17 vs 24	0.44	0.66	0.004	18S	FSS
21 vs 24	0.31	0.55	0.004	18S	FSS
1 vs 4	0.28	0.53	0.002	18S	GSSS
1 vs 8	0.23	0.48	0.001	18S	GSSS
1 vs 11	0.31	0.56	0.004	18S	GSSS
1 vs 16	0.34	0.59	0.003	18S	GSSS
1 vs 18	0.4	0.63	0.002	18S	GSSS
1 vs 22	0.29	0.54	0.003	18S	GSSS
1 vs 25	0.36	0.6	0.007	18S	GSSS
4 vs 8	0.18	0.43	0.002	18S	GSSS
4 vs 11	0.14	0.38	0.008	18S	GSSS
4 vs 16	0.17	0.42	0.009	18S	GSSS
4 vs 18	0.37	0.61	0.001	18S	GSSS
4 vs 22	0.31	0.56	0.003	18S	GSSS
4 vs 25	0.37	0.61	0.005	18S	GSSS
8 vs 11	0.21	0.46	0.002	18S	GSSS
8 vs 16	0.2	0.44	0.005	18S	GSSS
8 vs 18	0.33	0.58	0.003	18S	GSSS
8 vs 22	0.27	0.52	0.005	18S	GSSS
8 vs 25	0.32	0.56	0.004	18S	GSSS
11 vs 16	0.19	0.43	0.012	18S	GSSS
11 vs 18	0.41	0.64	0.001	18S	GSSS
11 vs 22	0.34	0.58	0.004	18S	GSSS
11 vs 25	0.38	0.62	0.002	18S	GSSS
16 vs 18	0.32	0.56	0.003	18S	GSSS
16 vs 22	0.27	0.52	0.006	18S	GSSS
16 vs 25	0.32	0.56	0.002	18S	GSSS
18 vs 22	0.15	0.38	0.004	18S	GSSS
18 vs 25	0.24	0.49	0.006	18S	GSSS
22 vs 25	0.18	0.42	0.004	18S	GSSS

992 **Supplementary Table S4.** Summary of physical environmental measurements and analyzed
 993 inorganic nutrients as well as the relative abundance of Focal taxon, OLI16029. Mean values
 994 and (min, max) are shown.
 995

	Station	
	FSS	GSSS
Temperature (°C) ^a	6.6 (5.4, 7.4)	6.2 (5.3, 7.0)
Salinity ^a	33.1 (32.5, 33.4)	33.4 (33.2, 33.6)
MLD (m)	3 (3.3)	5 (3, 7)
Si(OH) ₄ (μmol L ⁻¹)	1.24 (0.69, 1.87)	1.56 (0.09, 3.00)
NO ₂ ⁻ + NO ₃ ⁻ (μmol L ⁻¹)	0.18 (0.07, 0.41)	0.43 (0.09, 1.20)
PO ₄ ³⁻ (μmol L ⁻¹)	0.06 (< 0.04, 0.12)	0.07 (< 0.04, 0.39)
Focal taxon (%) ^b	0.7 (0.4, 1.3)	3.4 (0.02, 17.7)

996 ^a Values at the depth of 10 m

997 ^b Relative abundance of ASVs assigned to OLI16029

998

999

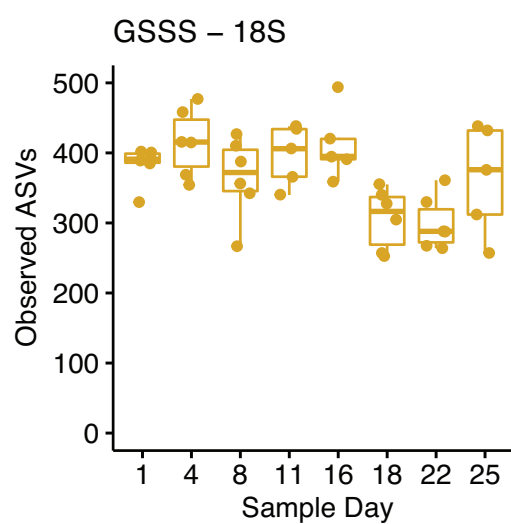
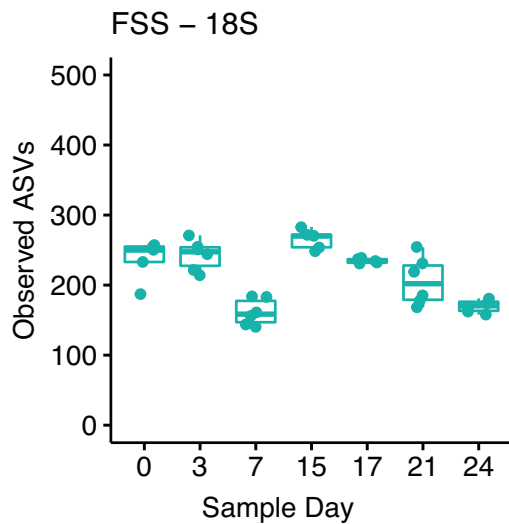
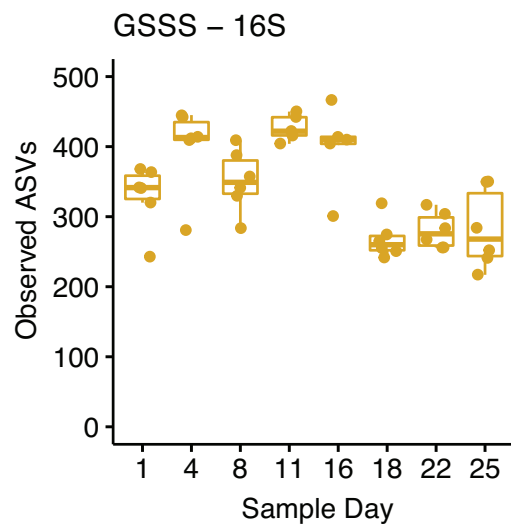
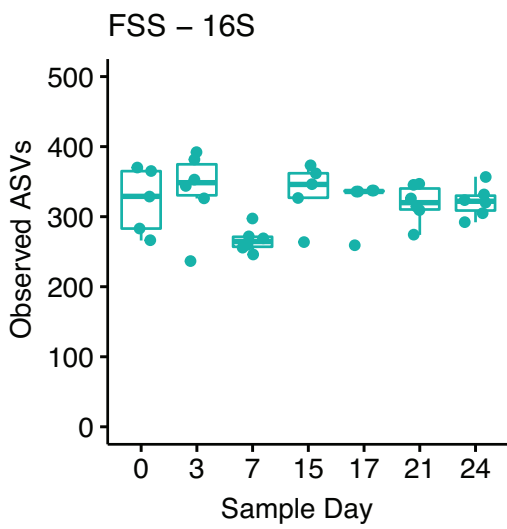
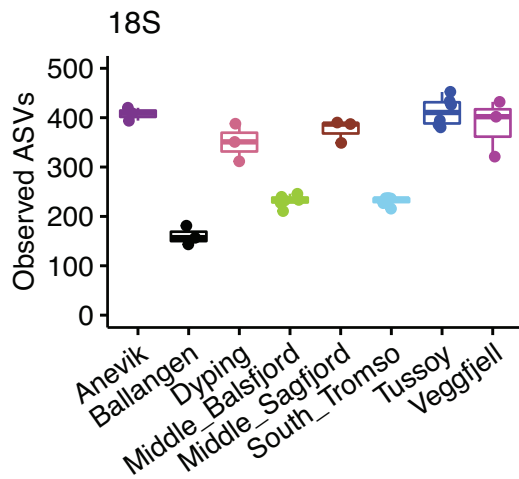
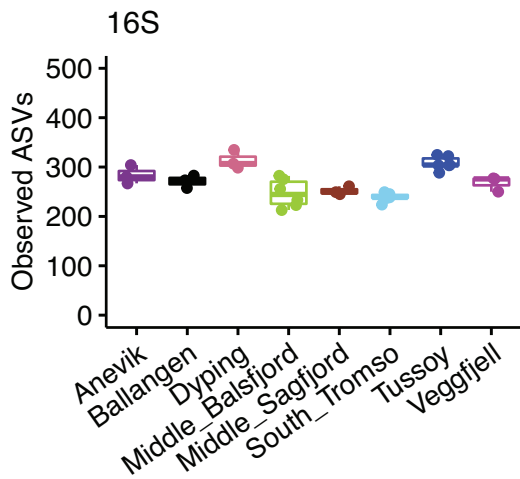
1000

1001

1002

1003

1004



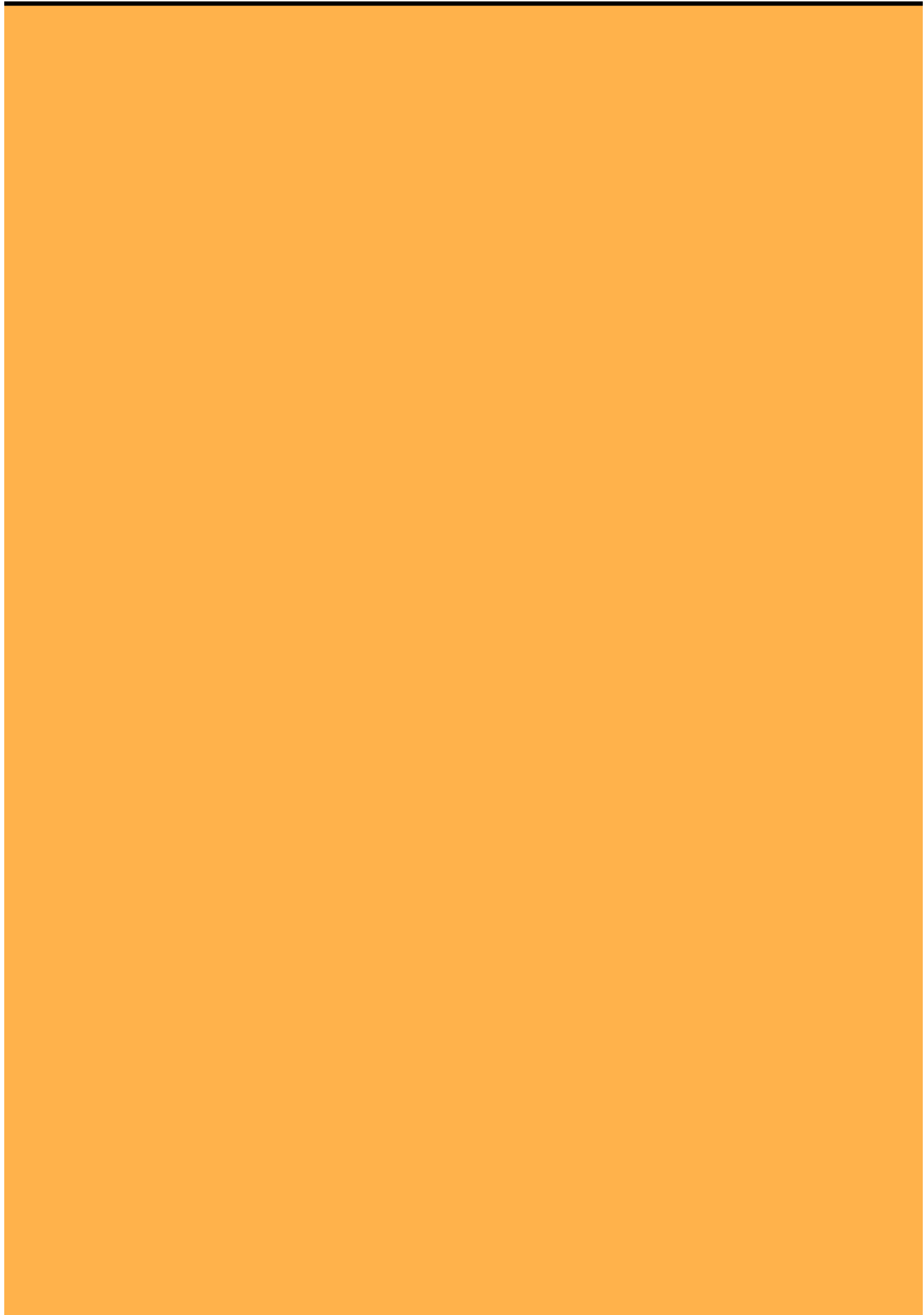
1005

1006 **Supplementary Figure S6.** Alpha diversity as observed number of ASVs per sample set:
 1007 single-time-point stations and time series stations.

1008

1009

Paper III





Diversity and Selection of Surface Marine Microbiomes in the Atlantic-Influenced Arctic

Nerea J. Aalto^{1,2}, Hannah D. Schweitzer^{1,2}, Stina Krsmanovic¹, Karley Campbell¹ and Hans C. Bernstein^{1,2*}

¹ Faculty of Biosciences, Fisheries, and Economics, UiT—The Arctic University of Norway, Tromsø, Norway, ² The Arctic Centre for Sustainable Energy, UiT—The Arctic University of Norway, Tromsø, Norway

OPEN ACCESS

Edited by:

Catarina Magalhães,
University of Porto, Portugal

Reviewed by:

Mafalda S. Baptista,
University of Porto, Portugal
Richard Allen White III,
University of North Carolina at
Charlotte, United States

*Correspondence:

Hans C. Bernstein
hans.c.bernstein@uit.no

Specialty section:

This article was submitted to
Aquatic Microbiology,
a section of the journal
Frontiers in Microbiology

Received: 09 March 2022

Accepted: 14 June 2022

Published: 14 July 2022

Citation:

Aalto NJ, Schweitzer HD,
Krsmanovic S, Campbell K and
Bernstein HC (2022) Diversity and
Selection of Surface Marine
Microbiomes in the Atlantic-Influenced
Arctic. *Front. Microbiol.* 13:892634.
doi: 10.3389/fmicb.2022.892634

Arctic marine environments are experiencing rapid changes due to the polar amplification of global warming. These changes impact the habitat of the cold-adapted microbial communities, which underpin biogeochemical cycles and marine food webs. We comparatively investigated the differences in prokaryotic and microeukaryotic taxa between summer surface water microbiomes sampled along a latitudinal transect from the ice-free southern Barents Sea and into the sea-ice-covered Nansen Basin to disentangle the dominating community (ecological) selection processes driving phylogenetic diversity. The community structure and richness of each site-specific microbiome were assessed in relation to the physical and biogeochemical conditions of the environment. A strong homogeneous deterministic selection process was inferred across the entire sampling transect *via* a phylogenetic null modeling approach. The microbial species richness and diversity were not negatively influenced by northward decreasing temperature and salinity. The results also suggest that regional phytoplankton blooms are a major prevalent factor in governing the bacterial community structure. This study supports the consideration that strong homogeneous selection is imposed across these cold-water marine environments uniformly, regardless of geographic assignments within either the Nansen Basin or the Barents Sea.

Keywords: diatoms, Arctic Ocean, sea-ice, null model, temperature, Atlantification, Nansen Basin

INTRODUCTION

Surface waters of the Arctic marine system are inhabited by cold-adapted microbial taxa that persist under high availability of organic carbon sources and seasonal extremes in light (Bussmann and Kattner, 2000; Riedel et al., 2006). These unique microbiomes, encompassing both prokaryotic and microeukaryotic taxa, are in transition as Arctic habitats change from global warming and Atlantification. Environmental alterations to the Arctic Ocean include decreases in sea-ice extent and volume (Kwok, 2018) and increases in surface water temperature in regions influenced by Atlantic inflow (Polyakov et al., 2017). To understand the ecological implications of these changes, it is important to investigate the diversity and structure of microbial communities because these cold-adapted microbiomes have an important role in underpinning biogeochemical cycles (Falkowski et al., 2008) and marine food webs.

Pelagic prokaryotes (Bacteria and Archaea) and microeukaryotes (microalgae and heterotrophic protists) comprise a wide range of functional types within cold-water marine ecosystems and have distinct environments or nutrient requirements (Quere et al., 2005; Cao et al., 2020). A growing body of evidence shows that environmental disturbances alter the diversity and structure of these microbial communities (Barton et al., 2016; Assmy et al., 2017; Orkney et al., 2020; Oziel et al., 2020), which can impact ecosystem functioning and marine carbon sequestration *via* deep-sea carbon export (Assmy et al., 2017; Schweitzer et al., 2021).

Due to the importance of marine microbiomes and the rapid development of molecular tools in the past decade, there have been increasing numbers of studies investigating environmental and ecophysiological factors selecting for a regional to global scale microbial diversity and richness. For example, several studies have revealed a decrease in both prokaryote and microeukaryote taxonomic diversity and richness with increasing latitude at the global scale (Fuhrman et al., 2008; Ibarbalz et al., 2019; Salazar et al., 2019; Martin et al., 2021). This observed pattern has been linked to the latitudinal relationship with temperature, suggesting that temperature is one of the most important environmental factors driving the species richness and taxonomic composition of upper ocean microbial communities. Multiple studies have also illustrated biogeographical differentiation in the taxonomic and transcriptomic diversity of microbial communities between comparatively cold (polar) and warm (non-polar) waters, as well as unique algal microbiome co-occurrence networks and rates of net primary production (Behrenfeld et al., 2006; Ibarbalz et al., 2019; Salazar et al., 2019; Martin et al., 2021). Many of these differences are suggested to occur in the northern hemisphere around an annual-mean isotherm of 14–15°C as an ecological boundary or “breakpoint,” potentially selecting for thermal tolerance limits and affecting the kinetics of metabolism (Thomas et al., 2012).

The availability of nutrients and photosynthetically active radiation (PAR), which are both linked to the mixed layer depth (MLD), have been implicated to control regional differences in the phytoplankton community structure, more so than temperature (Barton et al., 2016; Oziel et al., 2017; Aalto et al., 2021). Phytoplankton blooms are also known to exert major influences on localized marine microbiomes (Cirri and Pohnert, 2019). Microalgae form complex interactions with prokaryotes that utilize and remineralize dissolved organic matter released by phytoplankton and in some cases exchange metabolites back to their photoautotrophic hosts (Buchan et al., 2014). Temperate and cold-water bacterial community structure have been shown to vary with the species composition of phytoplankton blooms, as well as within the dynamic time course of a bloom (Teeling et al., 2012; Fadeev et al., 2018; Rapp et al., 2018). Thus, the surface water bacterioplankton community structure is hypothesized to largely be determined by environmental factors associated with phytoplankton bloom phenology (Fadeev et al., 2018).

The Barents Sea, a relatively shallow and large shelf sea, is well described with respect to hydrography, seasonal phytoplankton community, and primary production (e.g., Loeng,

1991; Wassmann et al., 2006a; Degerlund and Eilertsen, 2010). However, the spatial heterogeneity of prokaryote taxonomic diversity and community structure is poorly documented. Typically, the annual primary production is highest in the ice-free and marginal ice zones of the Barents Sea (Wassmann et al., 2006a). Diatoms are highly abundant in these locations and contribute to high dissolved organic carbon (DOC) production and vertical carbon flux (Wassmann et al., 2006b; Matrai et al., 2007). The influence of this seasonally high diatom abundance and associated DOC on co-occurring microbial communities remains poorly understood within the Barents Sea (Wassmann et al., 2006a). In studies from other areas, a small number of genera from bacteria phyla Proteobacteria and Bacteroidetes have been observed to respond to a diatom bloom, but it has been also found that the associated microbiome can vary between and within diatom species (Amin et al., 2012; Teeling et al., 2012; Ajani et al., 2018). Overall, the spring phytoplankton blooms in the Barents Sea follow a transition from diatoms such as centric *Chaetoceros* spp. and *Thalassiosira* spp. and haptophyte algae *Phaeocystis* sp. domination to a more diverse group of flagellates and dinoflagellates (Wassmann et al., 2006a; Degerlund and Eilertsen, 2010).

In contrast to the Barents Sea, the Nansen Basin in the high Arctic Ocean is characterized by deep topography and surface water temperature near the freezing point (~-1.5°C). Phytoplankton production in the ice-covered Arctic is comparatively low to the open ocean due to restricted light availability. Despite the low production in the Nansen Basin region, the surface water comprises a diverse group of autotrophic and heterotrophic flagellates and dinoflagellates (Rapp et al., 2018; de Sousa et al., 2019). However, diatom and *Phaeocystis* sp. dominated blooms have been reported beneath sea ice during times of enhanced light transmission to the upper ocean due to the formation of leads and melt ponds (Arrigo et al., 2012; Assmy et al., 2017).

Heat transfer to the Barents Sea and the Eurasian Basin of the Arctic Ocean occurs by the northward inflow of North Atlantic water. The Barents Sea and the Nansen Basin are influenced by Atlantic water as the Norwegian Atlantic current enters the Barents Sea and the Fram Strait (Rudels et al., 1994). However, surface waters in the Nansen Basin are characterized by less saline and colder Polar Surface water in comparison to Atlantic water (Anderson et al., 1989). The influence of Atlantic water has increased substantially during the last decades, by a phenomenon known as Atlantification (Oziel et al., 2017).

Exclusive focus between microbial taxa and regional variation of environmental factors, as is most often the case in previous studies, can impede the comprehensive understanding of underlying fundamental community (ecological) selection processes governing the phylogenetic diversity (Stegen et al., 2012, 2013). Only a small number of studies, none of them in the Arctic (as we are aware), have applied this concept and related statistical tools such as null modeling-based randomization to infer the spatial and/or temporal influence of stochastic and deterministic selection processes on surface water microbiomes (e.g., Allen et al., 2020). Stochasticity refers to weak (neutral) selection so that the community composition is not determined

according to the environmental fitness of the members but rather dispersion rate and randomness (Vellend, 2010; Dini-Andreote et al., 2015; Evans et al., 2017). Whereas abiotic and biotic factors in deterministic selection processes act as a strong selection force for species with different fitness (Vellend, 2010).

As the Barents Sea, and to a lesser extent the Nansen Basin, are influenced by Atlantic water, it is important to investigate how ongoing Atlantification and associated warming of surface waters affects the marine microbiomes. In this study, we surveyed surface water (0.5 and/or 20 m) microbial community structure during the summer using rRNA gene amplicon sequencing across a latitudinal transect spanning from the southern Barents Sea to the sea-ice-covered Nansen Basin. Four main research questions were addressed: (1) How does the surface water microbial community structure change along the transect and what are the differentially represented taxa designating these areas? (2) What are the main environmental factors linked to the differences in microbial community composition and how does the relative abundance of diatoms impact the prokaryotic structure? (3) How does the change in salinity from sea-ice melt in summer influence the microbial community beneath the sea-ice bottom in the Nansen Basin? and (4) Do stochastic or deterministic processes play greater roles in the ecological selection that influence the prokaryote and microeukaryote members of these microbiomes?

METHODS

Study Area

This study was conducted across a transect from 71.7 to 84.7° north on the *Bioprospecting 2019* expedition with RV Kronprins Haakon (July 04–18 2019). Sampling took place from the ice-free southern Barents Sea (Nord Cape Bank) into the ice-covered Arctic Ocean (Nansen Basin), with a total of six sampling stations: BS1, BS2, and BS3 along the open-water Barents Sea; NBm near the ice-edge over the slope between deep Nansen Basin and shallower Barents Sea in the region referred to as the Nansen Basin margin, and NB1 and NB2 in the sea-ice covered Nansen Basin (Figure 1; Supplementary Table 1; Supplementary Figure 1).

Water Sampling and Data Collection

At the Barents Sea stations (BS1, BS2, and BS3), measurements of temperature, salinity, and *in vivo* fluorescence through the water column were taken with a SeaBird 9–11 plus (Seabird Scientific, US) conductivity-temperature-depth (CTD) sensor. In the Nansen Basin (NB1 and NB2) and the Nansen Basin margin (NBm) stations, CTD casts were taken down to 50–60 m with a hand-held AML oceanographic X2 electronic CTD sensor (AML Oceanographic, Canada). Water samples were collected from fixed sampling depths of 20 m at all stations and at 0.5 m (directly under sea-ice) at NB1 and NB2 stations (hereafter these samples are referred to as NB1_0.5, NB1_20, NB2_0.5, and NB2_20). The samples from 20 m were collected using a rosette sampler, and the sample water was drawn from several (between 3 and 5) parallelly mounted Niskin samplers (10 L) at open water Barents Sea stations (BS1, BS2, and BS3), while a Niskin sampler (2 L) was manually deployed multiple times (between 10 and 20 casts)

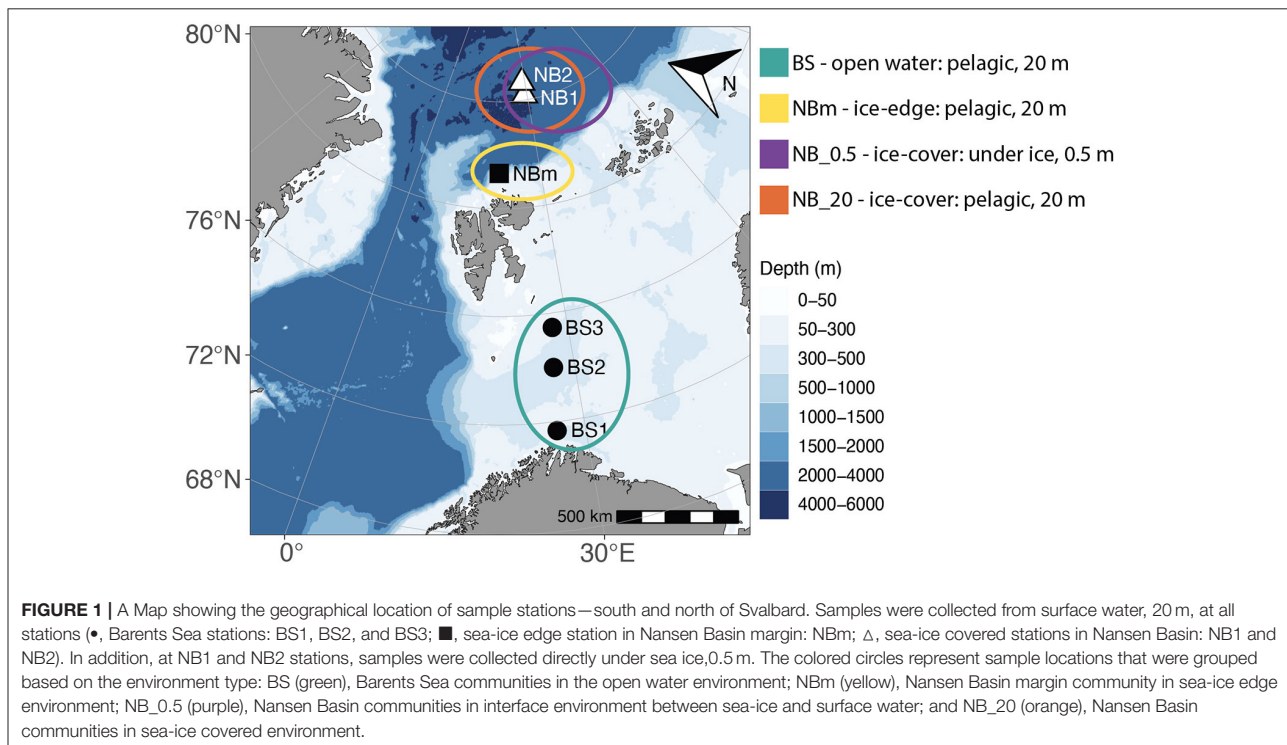
through the sea ice at Nansen Basin stations (NB1 and NB2) and over the vessel deck in the vicinity of the ice-edge at NBm station (Nansen Basin margin). Subsamples were collected for analysis of total dissolved inorganic carbon (DIC), dissolved organic carbon (DOC), *in vitro* chlorophyll *a* (chl *a*), and inorganic macronutrients of nitrate (NO_3^-), phosphate (PO_4^{3-}), and silicic acid ($\text{Si}(\text{OH})_4$). Seawater for microbial biomass both for prokaryotic and eukaryotic community investigation was first passed through a 150 μm zooplankton mesh into three clean (aseptically prepared) 20 L carboys and thereafter biological replicates of six were filtered onto 0.22 μm polycarbonate filters (Whatman) *via* vacuum filtration. The filtered volume per filter was 600 ml. Filters were immediately flash-frozen in liquid N_2 and stored onboard at -80°C . All filtering equipment and ship laboratory spaces were disinfected with 2% bleach prior to and between samples to prevent cross-contamination.

Sample Analyses

DIC samples were drawn into borosilicate glass bottles *via* silicon tubing and preserved immediately after sampling with saturated mercuric chloride (0.02% of the total volume corresponding to the final concentration of 0.0015%). Samples were stored in dark at $+6^\circ\text{C}$ until they were sent to the accredited laboratory of the Norwegian Institute for Water Research (NIVA) 10 months after. DIC was analyzed with VINDTA 3C (Marianda, Germany), and coulometric titration was deployed using a UIC CM5015 coulometer. Samples were warmed up to $\sim 25^\circ\text{C}$ prior to measurement. Certified reference material for seawater DIC from batch 169 (A. Dickson, Scripps Institution of Oceanography) was measured two times daily. The procedure follows the recommended SOP: “SOP 2: Determination of total dissolved inorganic carbon in seawater” (Dickson et al., 2007).

Samples for $\text{Si}(\text{OH})_4$ and PO_4^{3-} were filtered immediately after sampling through pre-combusted (450°C) GF/C glass microfiber filters (Whatman) into 50 ml polypropylene Falcon tubes. These nutrients were analyzed in subsample triplicates spectrophotometrically onboard, using Spectroquant (Merck Millipore, US) kits, specifically for each nutrient, whereas NO_3^- samples were frozen and stored at -20°C and analyzed 2 months later at the University of Tromsø, Norway. As low NO_3^- concentration in seawater is difficult to measure due to its reduction potential, it was analyzed by applying a cadmium reduction column where NO_3^- is reduced to nitrite (NO_2^-) (Strickland and Parsons, 1972), and thereafter, the NO_2^- kit was used and NO_3^- concentration (NO_2^- is not included to NO_3^- values) was recalculated from the predetermined standard curve. Quartz cuvettes (5 mL) were used to determine the nutrient concentrations using a spectrometer (UV/Visible spectrometer, UV-6300PC, VWR, US). The absorbance of NO_2^- was measured at 541 nm, $\text{Si}(\text{OH})_4$ at 822 nm, and PO_4^{3-} at 840 nm.

Disposable polyethersulfone 0.2 μm membrane filter (VWR Sterile Syringe Filter) together with disposable syringes (60 ml) were used to filter DOC samples into acid-washed and pre-combusted (450°C) glass vials of 60 ml (Assistant, Germany) and thereafter stored at -20°C . DOC samples were analyzed 15 months later at the University of Tromsø, Norway with a TOC-VCPH analyzer (Shimadzu, Japan).



A Turner TD-700 fluorometer (Turner Designs, USA) was used to measure *in vitro* chl *a* and pheophytin concentration 24 h after extraction in 96% ethanol at 4°C (Holm-Hansen and Riemann, 1978). For the chl *a*, the extraction sample volume of 5–200 ml was filtrated in subsample triplicate onto the Whatman GF/C filter.

Water Type Analysis and Mixed Layer Depth

Different water masses were determined from sampling station temperature and salinity. Specifically, the identification of water masses was based on practical salinity, potential temperature, and potential density values outlined for the Barents Sea (Loeng, 1991) and the north region of Svalbard in the Nansen Basin (Pérez-Hernández et al., 2017). The mixed layer depth (MLD) was determined from each CTD-profile data using potential density. The reference depth of 20 m and density threshold of 0.1 kg m^{-3} were used to define MLD, i.e., depth below 20 m where density first exceeds the criteria threshold. The chosen density criteria are typical for the Arctic region (Peralta-Ferriz and Woodgate, 2015) although smaller criteria of 0.003 kg m^{-3} are also used in spring to avoid possible overestimation (Meyer et al., 2017); however, the criteria were not applied here since the shallowest measured CTD-profile depth at Barents Sea stations was 8–15 m and the method is not very criteria sensitive (Peralta-Ferriz and Woodgate, 2015).

Amplicon Sequencing

Genomic DNA was extracted from 0.22 μm polycarbonate filters using the DNeasy PowerWater Kit (Qiagen, Carlsbad, CA) and

all downstream amplicon sequencing analyses were performed in accordance with the Earth Microbiome Project protocols (Gilbert et al., 2010) with minor modifications in quality checks. Quality checks were run on the PCR products using the DNA 12,000 assay with the Agilent Bioanalyzer (Agilent Technologies, Germany). PCR template-free negative controls were also amplified and sequenced in order to identify background sequences. Sequencing was performed on an Illumina MiSeq instrument (Illumina, San Diego, CA) at Argonne National Laboratory (Lemont, IL, USA). From each station and depth template from biological replicates of six were processed *via* 16S and 18S rRNA gene amplification reactions. The Illumina sequencing primer binding site was used with V4 forward primer (515F) and V4 reverse primer (806R) targeting the hypervariable region of 16S rRNA (Caporaso et al., 2010) and correspondingly V9 forward primer (1391F) and V9 reverse primer (EukBr) were used for 18S rRNA as outlined by the Earth Microbiome Project and modified from Amaral-Zettler et al. (2009).

Amplicon Sequence Analysis

Trimmed Illumina reads were imported and demultiplexed using a corresponding Barcode file into QIIME2 using the Earth Microbiome Project paired-end flag. All reads were denoised and merged using the DADA2 v2021.2.0 algorithm from within QIIME2 (Callahan et al., 2016). The denoising steps of the DADA2 package pooled, filtered, de-replicated, and chimera-checked all reads. After discarding chimeras and singletons, reads were merged, and amplicon sequence variants (ASVs) were inferred using DADA2. Taxonomy was assigned to each ASV using a 16S and 18S rRNA gene self-trained classifier from the

SILVA database v138.1 (Quast et al., 2012; Yilmaz et al., 2014). Classifiers were trained using RESCRIPt (Robeson et al., 2020). The phylogenetic rooted tree was generated using the MAFFT algorithm from within QIIME2 and was used for downstream diversity analysis.

Diversity Analysis

Downstream analysis was completed in R (R Core Team, 2021), using primarily the “microeco” (Liu et al., 2021) and “vegan” packages (Oksanen et al., 2020). From 16S data, reads not assigned to their expected kingdom (Archaea and Bacteria) were removed along with all mitochondria and chloroplast assignments. ASVs belonging to the kingdom of Archaea and Bacteria and phyla of *Vertebrata*, *Arthropoda*, *Cnidaria*, *Echinodermata*, and *Mollusca* were removed from 18S data. After removing unwanted taxa, the number of ASVs decreased from 2,179 to 1,731 in the 16S dataset and from 3,052 to 1,812 in the 18S dataset. Samples were rarified to an even depth of 29,746 and 74,750 reads per 16S and 18S sample, respectively, based on minimum sample depths as all the analyzed samples reached asymptote (**Supplementary Figure 2**). This reduced the total number of ASVs from 1731 to 1505 in the 16S data set and from 1812 to 1752 in the 18S data set. Alpha diversity was quantified by using counts of observed unique ASVs (species richness) and calculating Faith’s phylogenetic diversity (PD) to assess the biodiversity of features inherent in genetic sequences (Faith, 1992; Faith and Baker, 2006). A Tukey test was performed to determine the differences in species richness and Faith’s PD between samples. The sampled microbial communities were further grouped according to environment conditions, i.e., sea-ice coverage and sample depth. These groups were as follows: BS as a pelagic ice-free environment including all samples collected from the Barents Sea (3 stations, $n = 6$ per station); NBm as a pelagic ice-edge environment containing a sample from the Nansen Basin margin (1 station, $n = 6$); NB_0.5 as the interface environment between the sea-ice bottom and surface water including samples from 0.5 m in the Nansen Basin (2 stations, $n = 6$ per station); and NB_20 as the pelagic sea-ice environment including samples from 20 m in the Nansen Basin (2 stations, $n = 6$ per station; **Figure 1**). A Venn diagram was generated to provide any additional information on the distribution of shared and exclusive ASVs between grouped communities (BS, NBm, NB_0.5, and NB_20). Beta diversity was measured by calculating unweighted UniFrac distances which consider the presence/absence of ASVs (Lozupone et al., 2011) across all samples (stations and depths) and visualized through distance-based redundancy analysis (dbRDA) with contextual environmental variables (salinity, temperature, DOC, DIC, Si(OH)₄, chl *a* and relative abundance of diatoms) followed by permutational multivariate analysis of variance (PERMANOVA) (Anderson, 2001).

Differential Abundance

Linear discriminant analysis effect size (LEfSe) was used to identify specific taxa (i.e., indicator taxa) which were differentially represented between environmentally grouped communities (Segata et al., 2011). The LEfSe analysis consists of

three statistical parts (Segata et al., 2011). First, the significant ($p < 0.01$) differential abundance of taxa between grouped communities was obtained by the non-parametric factorial Kruskal-Wallis sum-rank test. Secondly, significantly different taxa were investigated using the pairwise Wilcoxon rank-sum test to encode biological consistency within the grouped communities. The last step was to assign linear discriminant analysis (LDA) for effect size estimation to determine the order of magnitude difference in abundances and induce the ranking of taxa. The specific LDA score of each taxon is obtained by ranking and scaling the taxa based on relative differences among groups along with the $1-10^6$ interval and by computing the logarithm (base 10) of those taxa (Segata et al., 2011). The threshold of LDA score was set to 4.0 to obtain taxa with higher relevance as many taxa were differentially abundant with a commonly used LDA score of 2. As the indicator taxa are obtained *via* sets of pairwise comparisons, there is no need for multiple testing corrections when more than two groups are used (Segata et al., 2011). The indicator taxa determined by LEfSe analysis were used further to investigate relationships between taxa and environmental factors *via* Pearson’s correlation.

Null Models

Null model analysis was implemented by calculating the beta Mean Nearest Taxon Distance (β MNTD), and the beta Nearest Taxon Index (β NTI) was obtained to infer contributions of stochastic versus deterministic selection forces between grouped communities using the R package “picante” (Kembel et al., 2010). The method is based on phylogenetic distances (mean minimum) to assess if the spatial or temporal phylogenetic turnover in the community composition is significantly higher or lower than that expected by chance (Stegen et al., 2012). First, β MNTD (for observed data) quantifies the phylogenetic distance between communities, which is compared to the mean of the null distribution of β MNTD. The null distribution of β MNTD was generated by randomization (here 1000 times) of the phylogenetic position of ASVs in grouped communities (Stegen et al., 2012). β NTI, that is the difference between observed β MNTD and the mean of the null distribution of β MNTD, was quantified by normalizing the null distribution of β MNTD by its standard deviation (Stegen et al., 2012). Thus, β NTI values are given on the z-score scale and the common interpretation is that values greater than +2 and below -2 indicate the dominance of the deterministic selection processes where variable selection and homogeneous selection are prevailing, respectively. Variable selection infers that phylogenetic turnover between communities is higher than expected by chance and homogeneous selection infers the opposite. The dominance of stochastic processes (i.e., no significant selection occurs when the β NTI values are between -2 and +2) is near-zero (Stegen et al., 2012; Dini-Andreote et al., 2015).

Data Repository and Reproducible Analyses

All data along with R scripts used for analysis and graphing are available on the Open Science Framework as part of this project: <https://osf.io/g8wxc/>.

TABLE 1 | Summary of the measured and analyzed physical and biogeochemical environmental factors (mean \pm standard deviation) at the depth of sampled microbial communities.

Station	BS1	BS2	BS3	NBm	NB1		NB2	
Sample ID/measurement	BS1	BS2	BS3	NBm	NB1_0.5	NB1_20	NB2_0.5	NB2_20
	20 m	20 m	20 m	20 m	0.5 m	20 m	0.5 m	20 m
Sea-ice cover (%)	0	0	0	~50	~85	~85	~90	~90
Temperature ^a	6.9	6.9	6.1	-1.1	-0.5	-1.8	-0.03	-1.2
Salinity ^b	34.4	35.0	35.0	33.9	10.9	34.3	8.6	34.3
DIC ($\mu\text{mol kg}^{-1}$)	2,073.5	2,097.1	2,089.7	2,075.8	688.8	2,113.2	233.3	2124.7
DOC (mg L^{-1})	28.3	31.8	41.9	34.0	24.6	28.3	27.6	34.1
NO_3^- ($\mu\text{mol L}^{-1}$)	b.d	0.28 ± 0.145	0.65 ± 0.083	3.29 ± 1.088	n.d	n.d	0.78 ± 0.063	2.03 ± 0.205
PO_4^{3-} ($\mu\text{mol L}^{-1}$)	0.10 ± 0.005	0.18 ± 0.005	0.12 ± 0.001	0.63 ± 0.005	0.01 ± 0.008	0.03 ± 0.026	0.02 ± 0.008	0.36 ± 0.032
$\text{Si}(\text{OH})_4$ ($\mu\text{mol L}^{-1}$)	0.70 ± 0.006	0.95 ± 0.016	0.40 ± 0.047	1.44 ± 0.040	0.16 ± 0.005	0.17 ± 0.002	0.18 ± 0.026	2.24 ± 0.102
chl <i>a</i> ($\mu\text{g L}^{-1}$)	2.8 ± 0.5	0.7 ± 0.2	2.8 ± 0.1	11.2 ± 0.4	0.2 ± 0.01	0.2 ± 0.01	0.2 ± 0.02	0.2 ± 0.04
Rel.abund. of diatoms (%) ^c	14	3	13	61	9	4	11	4

n.d, not determined; b.d, below detection level.

^aPotential temperature.

^bPractical salinity.

^cRelative abundance of diatoms revealed from the 18S rRNA gene amplification dataset.

RESULTS

Comparing the Physical and Biogeochemical Marine Environments

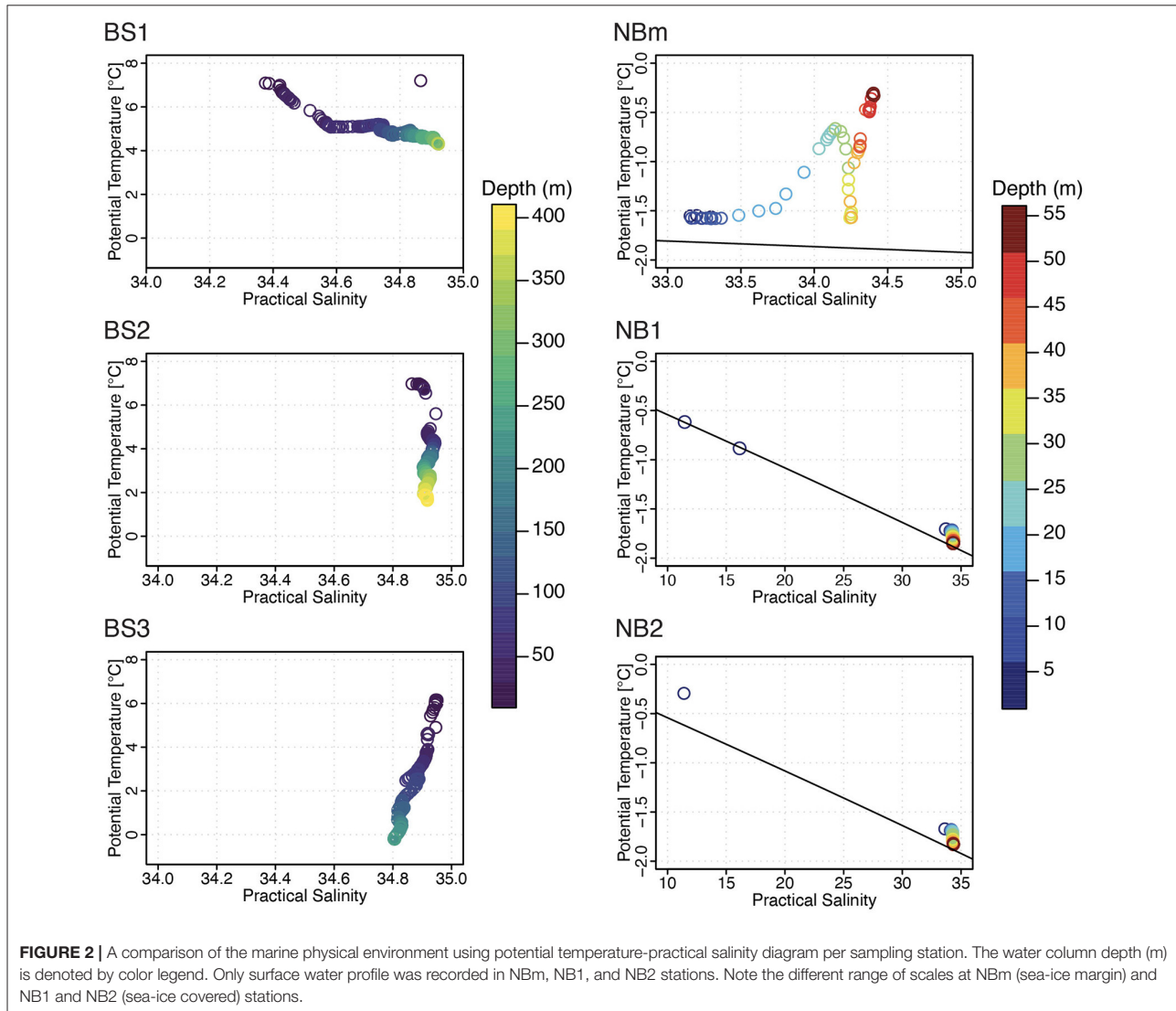
Each environment sampled in this study (Figure 1) was unique with respect to one or more factors such as temperature, salinity, nutrients, and/or phytoplankton content (Table 1). According to water type definitions for the Barents Sea and the Arctic Ocean (Loeng, 1991; Pérez-Hernández et al., 2017), the surface layer in the BS1 station was identified to consist of Norwegian coastal current ($T > 2^\circ\text{C}$; $S < 34.7$), and Atlantic water ($T > 3^\circ\text{C}$; $S > 34.9$) was the main water type in BS2 station (Figure 2). Whereas, in the BS3 station, the water column properties corresponded to locally formed Polar Front water ($T -0.5 - +2^\circ\text{C}$; $S 34.8-35$) (Loeng, 1991). The surface water at the representing ice-edge station, NBm, consisted of sea-ice melt and Polar Surface water ($T < 0^\circ\text{C}$). This was similar to the water type for NB1 and NB2 stations in the Nansen Basin where, in addition, a sharp and clearly distinct freshwater lens ($S < 16.2$) was found at the surface above 2 m induced by sea-ice melt (Figure 2) (Pérez-Hernández et al., 2017). The MLD became shallower from the southern Barents Sea to the Nansen Basin margin, and in the Nansen Basin, the surface water below the low-salinity layer was homogeneous with respect to temperature and salinity (Supplementary Figures 3, 4).

In the Nansen Basin, the DIC concentration was lowest in the samples collected directly under sea-ice (233.3 and 688.8 $\mu\text{mol kg}^{-1}$), likely due to the dilution effect caused by sea-ice melt (Meire et al., 2015). In contrast, the highest DIC concentrations were obtained in the counterpart depth (20 m) at the same stations where the temperature was low and salinity was high. DOC concentration varied between stations (24.6–41.9 mg C L^{-1}) and did not show a clear trend across the transect (Table 1). The overall inorganic nutrient concentration

was higher in samples from NBm and NB2_20 than in other samples (Table 1). The *in vitro* chl *a* concentration was clearly highest ($11.2 \pm 0.4 \mu\text{g L}^{-1}$) at the vicinity of the ice edge (NBm). In contrast, the lowest chl *a* concentrations were measured in the ice-covered Nansen Basin (Table 1).

Taxonomic Components of Marine Microbiomes Sampled

The most common prokaryotic and microeukaryotic taxa (at the order and class level, respectively) were shared by all environments sampled, although relative abundances differed between locations (Figures 3A,B). The most common bacterial taxa were classified within the *Flavobacteriales* order (class *Bacteroidia*), which accounted for an average of 35% of the relative abundance of all 16S samples. However, an overwhelming predominance of ASVs classified as *Flavobacteriales* (relative abundance 78%) were observed at the NBm station, which represents both the boundary of Nansen Basin waters and the transition zone between ice-covered and open water environments (Figure 3A). The genus indicative of *Polaribacter* comprised the majority of ASVs belonging to the order *Flavobacteriales* at all stations with exception of the surface (20 m) Nansen Basin samples, where the genus NS5 marine group was predominant (Supplementary Data 1). The sampling stations located in the Barents Sea (BS1, BS2, and BS3) were also heavily comprised of sequences classified within the *Flavobacteriales* order (relative abundance 31–50%) but also composed of members within the orders of *Rhodobacterales* (relative abundance 30–43%; class *Alphaproteobacteria*) and *Pseudomonadales* (relative abundance 5–29%; class *Gammaproteobacteria*) (Figure 3A). The Nansen Basin stations (NB1 and NB2) also revealed the prevalence of ASVs indicative of the order *Pseudomonadales* (class *Gammaproteobacteria*),



representing on average 20% of the relative abundances at these stations. The dominating members within *Pseudomonadales* were classified within the *Nitrocolacaea* family and genus SAR92 clade (**Supplementary Data 1**). In contrast, to open water and ice-edge communities, the heavily sea-ice-covered environment in the Nansen Basin was predominated by sequences identified within the order SAR11 (relative abundance 21–37%; class *Alphaproteobacteria*), including a majority of ASVs comprising the members of SAR11 clade Ia (**Supplementary Data 1**).

The most common microeukaryotic taxa, at the level of class, were indicative of *Dinophyceae*, which comprised an average of 35% of the relative abundance of all 18S samples (**Figure 3B**). However, there were two stations where the microeukaryotic portion of the microbiome was not predominated by ASVs belonging to the class *Dinophyceae*: BS3 in the Barents Sea

and NBm at the vicinity of the ice-edge. The prevalent microeukaryotic ASVs at the NBm station were classified as class *Mediophyceae* (centric diatoms), which represented 54% of the relative abundance (**Figure 3B**) and consisted of sequences indicative of genus *Thalassiosira* (**Supplementary Data 2**). The NBm station is in the transition environment where the prokaryotic community was characterized by prokaryotic ASVs within the order *Flavobacteriales*. The relative abundance of *Dinophyceae* decreased along the Barents Sea toward the north (**Figure 3B**). The northernmost Barents Sea station, BS3, revealed a high relative abundance of sequences classified within the class *Prymnesiophyceae* (relative abundance of 30%), which were dominated by ASVs indicative of genera *Chrysochromulina* and *Phaeocystis* (**Supplementary Data 2**). In comparison to other stations, the Nansen Basin stations (NB1 and NB2) revealed

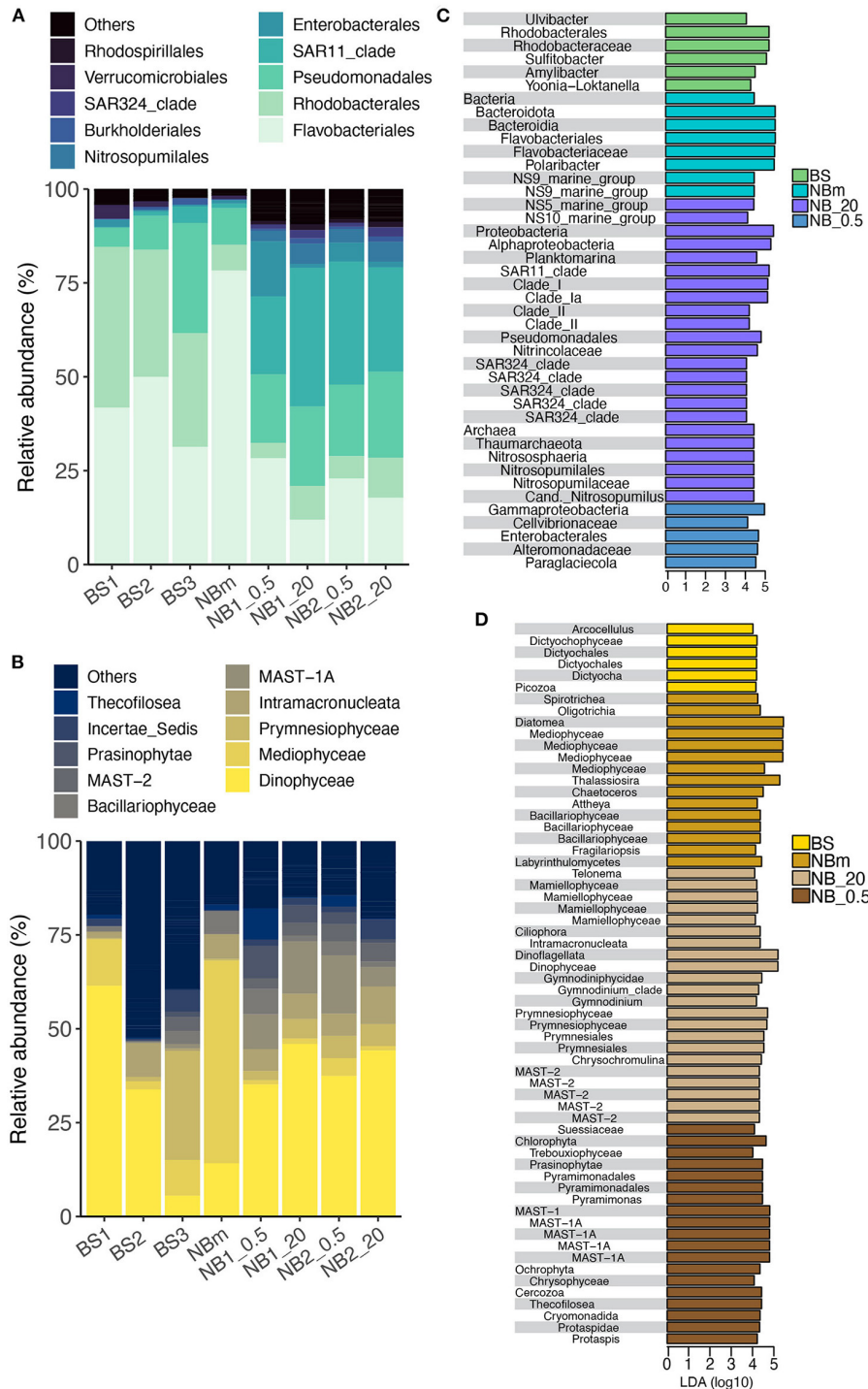


FIGURE 3 | Comparison of prokaryotic and microeukaryotic members of the surface marine microbiomes sampled across the study's transect. The taxonomic profile of the most abundant prokaryotes (A) and microeukaryotes (B) retrieved from Amplicon Sequence Variants (ASVs) tables specified at the order and class taxonomic rank level, respectively. Prokaryotes (C) and microeukaryotes (D) identified from the LEfSe analysis at all taxonomic levels that describe the differences between each community grouped by environment type: BS, Barents Sea communities in open water environment; NBm, Nansen Basin margin community in sea-ice edge environment; NB_5, Nansen Basin communities at the interface environment between sea-ice and surface water; NB_20, Nansen Basin communities in sea-ice covered environment. The x-axis is the LDA score (log 10) that indicates the scale of difference between groups.

higher relative abundances of ASVs indicative of organisms from within two MAST clades (marine stramenopiles): MAST-1A and MAST2 (Figure 3B).

The LEfSe method was used to infer indicator taxa that were differentially abundant among each grouped environment type (Segata et al., 2011). Relative abundances can show the predominant organisms in each environment, whereas LEfSe allows the detection of rare taxa that are significantly important per environment. LEfSe determines the significance of each taxonomic level and therefore also helps to infer whether only a certain genus is important or if the importance may be linked to higher taxonomic level similarities. It should be noted that results based on relative abundance metrics—such as LEfSe—can be highly time-dependent as the microbiome community structure tends to exhibit short-term temporal fluctuations in abundance (Needham and Fuhrman, 2016; Martin-Platero et al., 2018). The results show that multiple prokaryotic and microeukaryotic genera belonging to the same taxonomic order or class were differentially represented in different environments. LEfSe identified members of the order *Flavobacteriales* and more specifically the dominant member, *Polaribacter*, are indicator taxa of the ice-edge environment in the Nansen Basin margin (NBm), while the genus *Ulvibacter* is more prevalent in the open water Barents Sea (BS) at the time of this sampling campaign (Figure 3C). The sequences classified as genus *Planktomarina* belonging to the order *Rhodobacterales* represented indicator species of surface water in the sea-ice-covered Nansen Basin (NB_20). In comparison, three other genera from the same order (*Rhodobacterales*) were differentially represented as indicator taxa within the Barents Sea community (BS). The Nansen Basin (NB_20) was distinguished from other environments by the prevalence of organisms within the kingdom *Archaea*, which was represented by members indicative of the family *Nitrospumilaceae*. The microeukaryote communities in the Nansen Basin (NB_0.5 and NB_20) were nearly solely described by nanophytoplanktons and picophytoplanktons, such as classes *Prasinophytae* and *Mamiellophyceae* from the phylum *Chlorophyta*, and MAST-1A and MAST-2 clades and small dinoflagellates (families *Gymnodinium* clade and *Successiae*) (Figure 3D).

Diversity and Overlapping Distribution of Taxa Across Environments

The observed number of prokaryotic ASVs increased from the south (ASVs: 166 ± 12) toward the north (ASVs: 355 ± 24) and this increase was statistically significant (Tukey, $p < 0.05$) (Figure 4A; Supplementary Table 2), while the microeukaryotic richness had no significant differences between the north and south stations (Figure 4B; Supplementary Table 2). The prokaryotic diversity (Faith's PD) was statistically significant (Tukey, $p < 0.05$) (Supplementary Table 3) and increased from the south (PD: 16 ± 1.2) toward the north (PD: 30 ± 1.2) (Figure 4C), while this was not observed for the microeukaryotes (Figure 4D; Supplementary Table 3).

The total number of classified prokaryotic and microeukaryote ASVs after rarefaction were 1505 and 1752,

respectively, from which a considerably low number of ASVs were shared by all grouped communities (Figures 4E,F). However, the ASVs that were shared between all environment groups were highly abundant in their relative abundances as these ASVs comprised 81% and 61.9% of the total prokaryotic and microeukaryote sequences, respectively. In contrast, the high number of observed ASVs that were exclusive to each environment type accounted for the low proportion of the total sequences (Figures 4E,F).

Biological and Physical Factors Are Associated With Different Microbiome Structures

The observable differences in community composition between samples were also represented by different environmental measurements. Beta diversity was visualized *via* the dbRDA analysis showing significant dissimilarities in prokaryotic (PERMANOVA, $r^2 = 0.71$, $p = 0.001$) and microeukaryotic (PERMANOVA, $r^2 = 0.78$, $p = 0.001$) community composition across all samples (Figures 5A,B). The prokaryotic and eukaryotic components of each environmentally grouped microbiome showed similar dissimilarity patterns. The dbRDA analysis revealed that the environmental factors explained in total (sum of RDA1 and RDA2) 60.5 and 64.8% of the variance among prokaryotes and microeukaryotes, respectively (Figures 5A,B). The first RDA component indicates the variation of communities between the Barents Sea, the Nansen Basin margin, and the Nansen Basin for both prokaryotic and microeukaryotic ASVs. The environmental factors salinity, DIC, and temperature correlated with the first RDA component and may drive the differences in community compositions between these regions (Figures 5A,B). As salinity and DIC showed a strong correlation with each other (DIC concentration is dependent on salinity), it is difficult to separate the influence of these two factors on community composition. This correlation is presumably highly influenced by very low salinity under sea-ice bottom as the DIC concentration was higher in Nansen Basin at 20 m (NB1_20 and NB2_20) than in Barents Sea samples (BS1, BS2, and BS3) with higher salinity (Table 1). Also, chl *a* and relative abundance of diatoms are interrelated, but due to the compositional nature of diatoms, these measurements explain the environment differently, e.g., the relative abundance of diatoms can be similar between samples but chl *a* concentration can be highly different as shown in Table 1. The variation between Barents Sea stations, as well as among them (BS1, BS2, and BS3), and NBm station was explained mainly by the second RDA component, which accounted for 15.7 and 21.5% of the variance in prokaryotic and microeukaryotic community composition, respectively (Figures 5A,B). The concentration of silicate and relative abundance of diatoms and to a lesser extent chl *a* and DOC were the environmental factors that correlated more with the second RDA component and may explain the observed differences in microbial community compositions between the stations in the Barents Sea (BS1, BS2, and BS3) and the Nansen Basin margin (NBm) (Figures 5A,B).

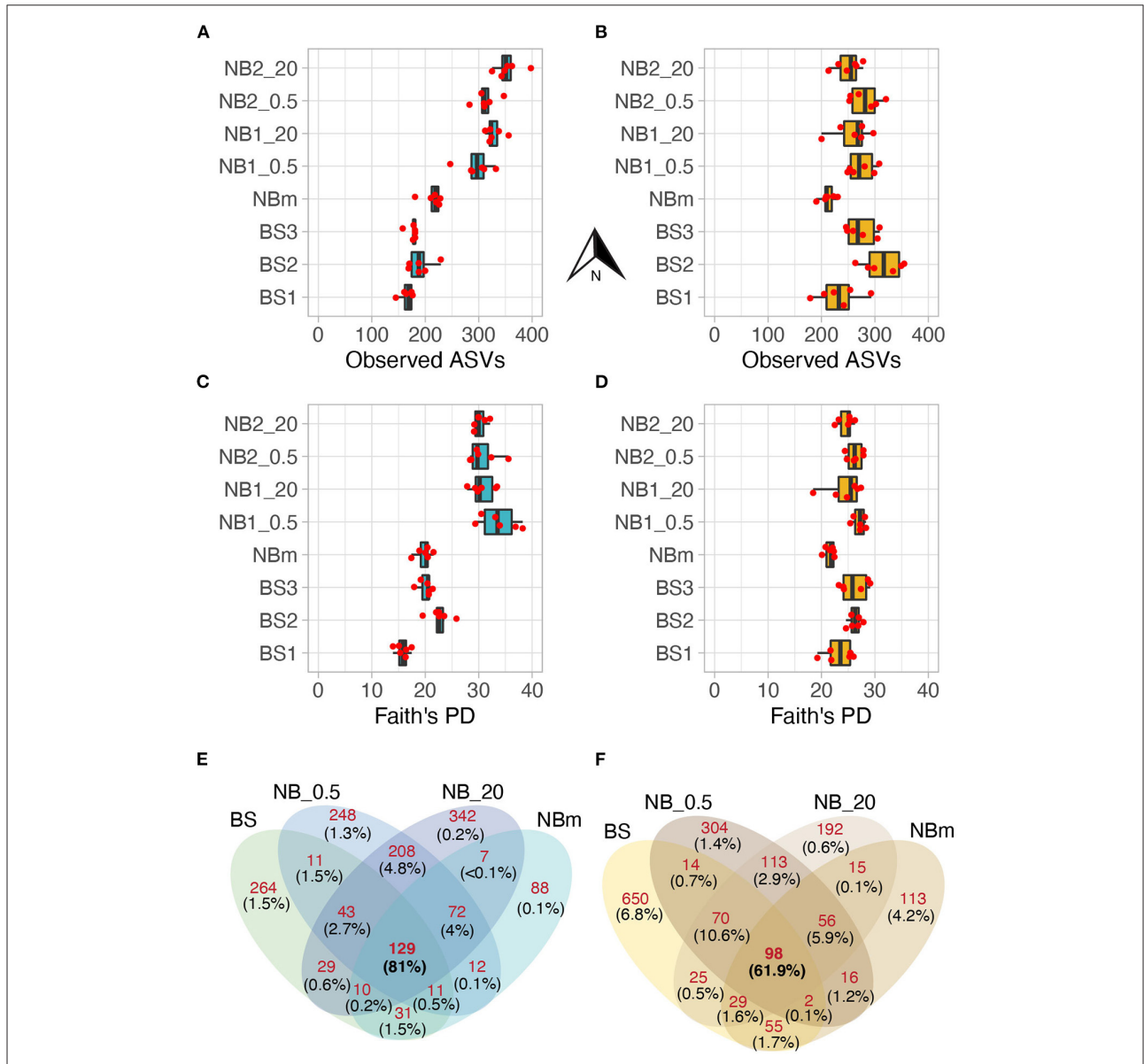
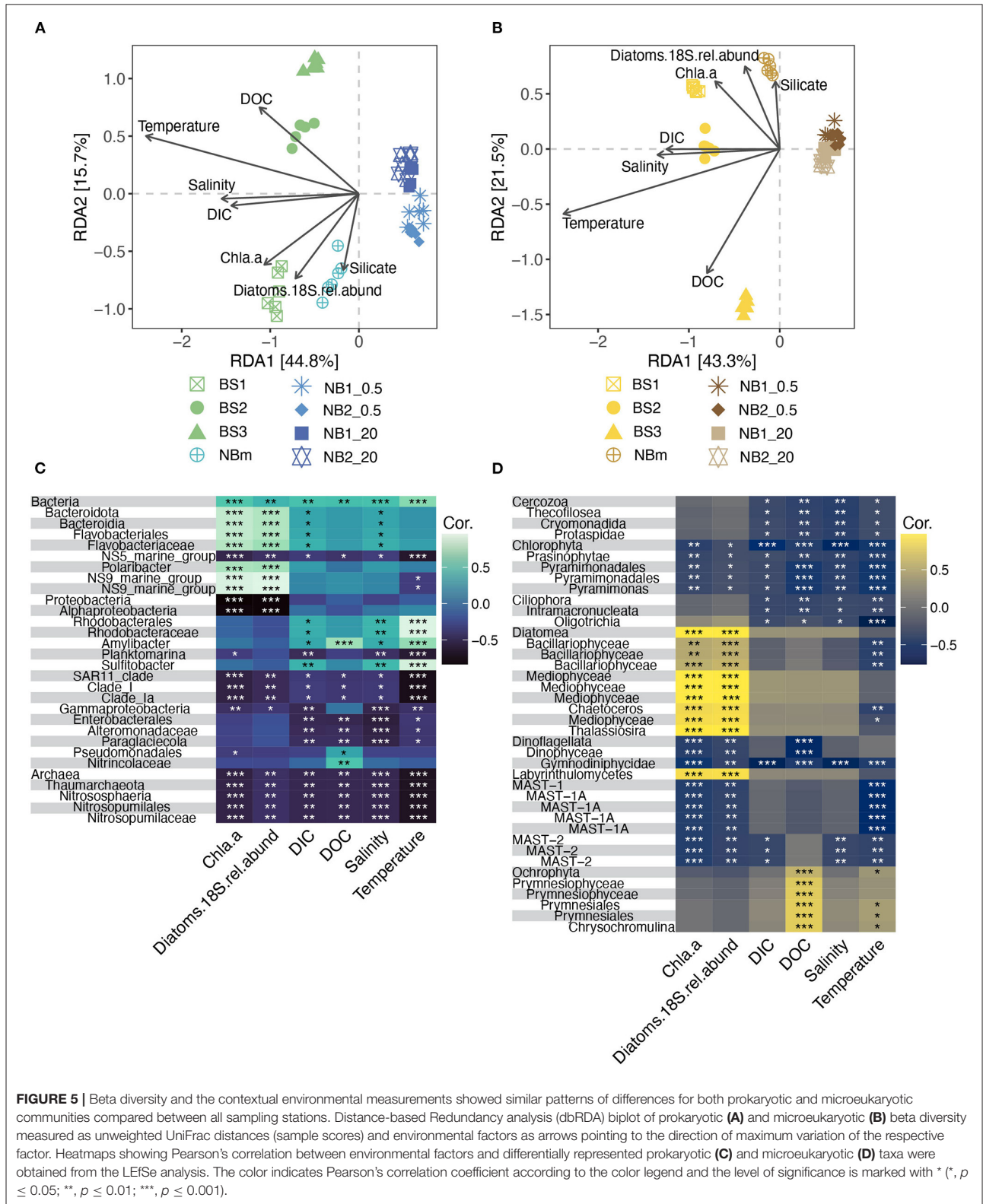


FIGURE 4 | The prokaryotic (A) and microeukaryotic (B) richness were measured as the observed number of ASVs. Corresponding Faith's Phylogenetic Diversity (PD) values for prokaryotes (C) and microeukaryotes (D). The values of biological replicates ($n = 6$) are shown over boxplots, and the arrow denotes a northward direction of sample stations. Alpha diversity showed a distinct increasing trend along the study transect for the prokaryotic but not the eukaryotic members of the sampled microbiomes. The diversity increases with increasing Faith's PD. Venn diagrams reporting a number of exclusive prokaryotic (E) and microeukaryotic (F) ASVs between grouped communities. Integers (shown in red color) represent the shared/exclusive number of ASVs. The relative abundance as a proportion of sequences of these ASVs from a total number of sequences is shown in parenthesis (black color). The ASVs shared by all grouped communities comprised the majority of total sequences per 16S and 18S data set. For example, (F) 129 ASVs shared by all grouped communities have high relative abundance as these ASVs comprised 81% of all sequences in the 16S dataset, whereas 264 ASVs exclusive to BS stations accounted for only 1.5% of a total number of sequences in the same dataset.

The role that specific environmental factors play in structuring each unique microbiome was also inferred from Pearson's correlations between the environmental measurements and prokaryotic and eukaryotic taxa obtained from the LEfSe analysis (Figures 5C,D). Most of the differentially abundant indicator taxa (Figures 3C,D) for the Barents Sea (BS) and the

Nansen Basin margin (NBm) showed positive correlations to the environment factors (Figures 5C,D). This trend was opposite for differentially represented taxa (indicator taxa) identified for the heavily sea-ice-covered Nansen Basin (Figures 3C,D, 5C,D). The weaker negative correlation between prokaryotic and microeukaryotic indicator taxa for NB_20 (Nansen Basin



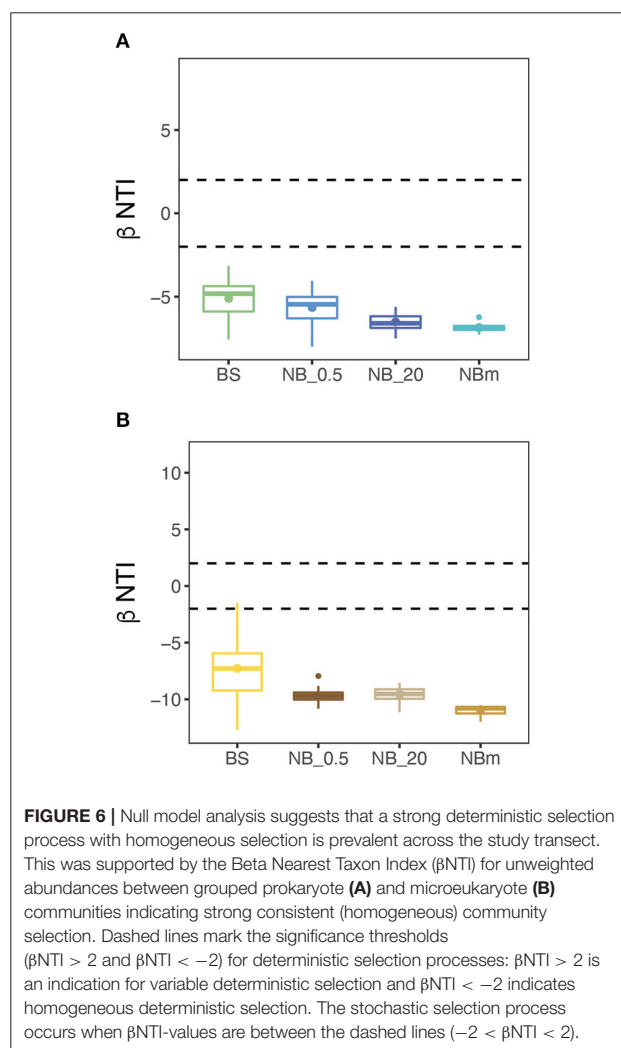
20 m samples) and relative abundance of diatoms than chl *a* is explained by higher diatom abundance compared to under sea-ice bottom samples (NB_0.5) (Table 1, Figures 3C,D, 5C,D). The sequences classified as *Sulfitobacter* and *Amylibacter* within the order *Rhodobacterales* were indicator taxa for the Barents Sea (Figure 3C) and showed significant (positive) relationships to temperature, salinity, and DIC (Table 1; Figure 5C). Instead, ASVs indicative of members from the order *Flavobacteriales*, except the NS5 marine group, were the predominant taxa at the NBm station (Figure 3C) and showed strong positive (significant) relationships to chl *a* and the relative abundance of diatoms, but not temperature (Figures 5A,B). This is likely because the order *Flavobacteriales* was also found to be relatively abundant within the colder Nansen Basin environments (Figure 3A). The microeukaryotic taxa that were prevalent in both the Barents Sea and the Nansen Basin were indicative of members from within the class *Prymnesiophyceae* (Supplementary Data 3) but showed no significant correlations to most of the environment factors (Figure 5D). Weak correlations were also observed within some of the differentially abundant indicator taxa from the Nansen Basin margin (i.e., class *Mediophyceae*) (Figures 3D, 5D). Many of the indicator taxa from the low-salinity lens at the sea-to-ice interface environment in the Nansen Basin (NB_0.5), such as ASVs indicative of phyla *Chlorophyta* and *Cercozoa*, showed strong negative correlations to salinity (Figures 3D, 5D).

Phylogenetic Diversity and Inference of Selection Processes Between Environments

The investigation of ecological processes governing microbial community composition revealed that the community composition between grouped communities was more similar than expected by randomization (Stegen et al., 2012). This was determined from null model analysis by calculating β NTI values both for prokaryote and eukaryote communities. The β NTI values were clearly below the significance threshold (-2), thus indicating strong homogeneous deterministic selection with consistent selection pressure across the entire sampling transect (Figure 6). This means that environmental factors are likely select for the observed phylogenetic composition. This result also suggests that the community members are phylogenetically spread, i.e., more distantly related than expected by chance. The calculated Faith's phylogenetic diversity (PD) values also support this inference, where the relative level of phylogenetic clustering or paucity of clustering was observed to be similar between communities as the values increased with richness (Figures 4C,D).

DISCUSSION

This study characterized and compared the structure and selection of surface marine microbiomes across specific environments spanning the Atlantic-influenced Barents Sea to the heavily sea-ice-covered Nansen Basin waters. We found that the most common microeukaryotic and prokaryotic taxa were



shared across the sampling locations and that these taxa were similar to what has been observed previously in the Nansen Basin, as well as more broadly in the Arctic Ocean (Hatam et al., 2014; Rapp et al., 2018; Signori et al., 2018; de Sousa et al., 2019). Here, the prokaryotic members of each community showed a clear increase in richness and diversity (i.e., Faith's PD) across the transect from south to north (Figure 4C). This increase occurred alongside a decrease in surface temperature and the transition from the open water to the sea-ice dominating environment.

Our findings on diversity trends over the northward transect are in contrast with the current understanding of latitudinal decrease in upper water microbial richness and diversity due to changes in temperature, which has been reported previously (Fuhrman et al., 2008; Ibarbalz et al., 2019; Martin et al., 2021). Our findings can be partly explained by the recent empirical-based demonstration of temperature breakpoints, 9.49°C for prokaryotes and 13.96°C for eukaryotes, which separate cold microbial communities (determined from beta-diversity) and

their associated metabolism from warm ones (Martin et al., 2021). This means that further temperature decreases below these recently suggested ecological breakpoints do not necessarily negatively impact microbial diversity (Supplementary Figure 5), as we have observed here. The cold temperature may be a major selection force for community composition but the separation to “cold” microbiomes likely occurs further south of this studied area (Martin et al., 2021). The temperature range of this relatively large study area across the Arctic Ocean ($-1.8 - +6.9^{\circ}\text{C}$) can therefore be considered as a relatively homogeneous and consistent habitat for the microorganisms representing certain parts of the phylogeny that have been selected by cold temperature as a strong environmental filter (Vellend, 2010; Dini-Andreote et al., 2015). This is supported by our results from βNTI null models (Figure 6) that inferred strong deterministic homogeneous selection governing more similar microbial taxa pools than expected by chance (Stegen et al., 2012; Brislawn et al., 2019). Consequently, the observed difference in relative abundances of the members of this pool is instead determined mainly by other factors than temperature. The results obtained from this study are limited to single snapshots at certain times taken across a large geographical area of the Arctic Ocean and certainly cannot account for all ecological niches resident in the region throughout the year. Therefore, we do not attempt to project these results to infer phylogenetic selection processes that may be occurring during fall, winter, or spring conditions.

In addition to temperature as a prevailing selective force, the constant northward traveling Atlantic currents in the area of the Arctic Ocean studied here may also contribute to continuous habitat formation. This may enable some level of horizontal species dispersion, which is necessary; otherwise, stochasticity is more likely to become the prevalent ecological process governing community composition between geographical locations (Evans et al., 2017). Although the surface waters in the Nansen Basin margin and the Nansen Basin were characterized by Polar Surface water (Figure 2), the presence of modified Atlantic water has been observed in the Nansen Basin above 100 m (Meyer et al., 2017). Thus, there are no physical limitations for the surface water microbial taxa pool that have passed the temperature filter to take advantage of the entire region.

Multiple studies have addressed the present and future impact of Atlantification on microbiomes in the North Atlantic, the Barents Sea, and to the west and north of Svalbard. Many of these recent observations and future predictions have focused on shifts in phytoplankton biogeography (poleward expansion), the blooming dynamics, and/or the relative abundances of phytoplankton rather than the distinction of specific taxa or notably the invasion of new taxa (Barton et al., 2016; Carter-Gates et al., 2020; Orkney et al., 2020; Oziel et al., 2020; Cardozo-Mino et al., 2021). These changes were mainly connected to changing bottom-up controls and intensified surface current velocities instead rather than being directly linked to increasing temperature. It is less clear how shifts in prokaryote components of these microbiomes might be restructured by Atlantification. It has been proposed that Atlantification may cause the extinction of rare microbial taxa that are more localized and niche specialized and thus have a lower tolerance to environmental

changes compared to the abundant taxa (Carter-Gates et al., 2020). We did not emphasize the rare taxa in this study although a high number of rare ASVs were observed between different environment types (Figures 4E,F). According to the model-predicted future temperature regimes in the North Sea, the temperature is expected to rise, although not above the recently identified temperature-dependent diversity breakpoints (Martin et al., 2021). Therefore, it is unlikely that the surface water-associated microbial taxa, especially the most abundant members, will change dramatically across the investigated area in the near future. In turn, the stronger presence of Atlantic water may even act as a stronger homogeneous selection between the Barents Sea and the Nansen Basin.

One of the goals of this study was to determine if and how microbiomes inhabiting waters directly under the sea ice are different from those sampled from the surface waters at 20 m. We found a high degree of similarity in microbial communities between the two sampled depths (0.5 m and 20 m) in the Nansen Basin (Figures 5A,B), which highlights that vertical mixing likely plays a larger role in prokaryotic and microeukaryotic community composition than environmental selection with respect to differences in temperature and salinity. This insight is supported by previous findings that revealed high vertical similarity in microbial community structure between two surface depths occurring above the MLD both in sea-ice-covered and open water areas (de Sousa et al., 2019; Allen et al., 2020). However, in this study, we detected a strong difference in salinity between the depths whereas the abiotic environment was relatively constant in the previous studies that showed similar findings. It is possible that the microbial community in the low-salinity layer under the sea ice can become partly isolated (trapped) during the progressive sea-ice melting, which can potentially lead to a variation in the selective environment (Dini-Andreote et al., 2015). However, without measurements that directly assess the vertical flux of cells between 20 m and the sea-ice interface, it is difficult to estimate how strongly the organisms in the low-salinity layer were isolated from the community below or the temporal scale to evaluate the development of this layer. Since the pycnocline was very sharp, it suggests that the physical mixing and thus community blending across the halocline was at least temporally limited.

We observed differentially represented taxa in the Nansen Basin between the different surface water depths (0.5 m and 20 m) (Figures 3C,D), yet the results did not reveal clear evidence of whether the change in salinity would favor certain taxa over the others among the “trapped” taxa pool. Among the indicator microeukaryote taxa for the Nansen Basin (NB_0.5 and NB_20), a majority were classified as taxa known to be heterotrophic or mixotrophic. These microeukaryotes are widely distributed across high-latitudes and/or global waters comprising organisms indicative of members within the class *Intramacronucleata* (Ciliates), phylum *Cercozoa*, orders MAST-1A and MAST-2, and *Gymnodinium*-like dinoflagellates from the order *Gymnodiniophycidae*. These taxa are often found in low-irradiance and low-nutrient environments that are prevalent under heavy sea ice (such as the Nansen Basin) (Levinsen et al., 2000; Rapp et al., 2018). Hence, they do not necessarily represent specificity

for Polar Surface water or brackish systems. Contrastingly, these taxa, with the exception of MAST-1A, revealed a strong negative relationship to salinity. In the Nansen Basin, the differentially represented ASVs indicative of class *Mamiellophyceae* for 20 m and classes *Prasinophyceae* and *Trebouxiophyceae* for 0.5 m, all members of the phylum *Chlorophyta*, are highly common photoautotrophs in global coastal waters and they have a wide distribution with respect to temperature and salinity (Tragin and Vaulot, 2018). *Pyramimonas*, a genus within the *Prasinophyceae* class, can dominate the high Arctic near-surface picophytoplankton community under and between sea-ice floes in summer (Zhang et al., 2015), which is compatible with the presented results of the sea-to-ice interface community of the Nansen Basin (Figure 3D). Also, the predominance of class *Dinophyceae* in Nansen Basin, as well as, within some of the Barents Sea stations (BS1 and BS2) is not uncommon as its strong presence is well documented in both areas (Wassmann et al., 2006a; Rapp et al., 2018; de Sousa et al., 2019).

The phylum *Thaumarchaeota* (kingdom *Archaea*) contains mainly members of ammonium oxidizers like *Candidatus Nitrosopumilus*, which was the only thaumarchaeal genus observed here, (Kirchman et al., 2007; Connelly et al., 2014), was nearly exclusively present at the Nansen Basin stations (NB1 and NB2) and differentially abundant in 20 m (NB_20) (Figures 3C,D), although in lower abundance than what was observed in winter surface waters in the Nansen Basin (de Sousa et al., 2019). The explanation for this is likely not related to salinity but to the impact of sea-ice on light availability in the ocean water below, as most of the ammonia-oxidizing archaea are known to be light-sensitive and inhibited by harmful reactive oxygen species produced by increased irradiance (Tolar et al., 2016). This may explain the near absence of *Thaumarchaeota* in Barents Sea surface waters as the members of this phylum are often found abundant in the mesopelagic layer (Karner et al., 2001).

Diatoms are prevalent in surface waters and sea-ice-associated marine microbiomes with an important role in the Arctic marine ecosystem functioning by influencing biogeochemical cycles, transporting organic matter to higher trophic levels, and contributing to biological carbon sequestration (Wassmann et al., 2006a; Litchman et al., 2015; Tréguer et al., 2018). As these processes are also aided by interacting microbes, we sought to better understand how diatoms might structure localized communities across the Barents Sea and the Nansen Basin by evaluating the bacterial response on phytoplankton blooms observed between sampling locations. Large diatom blooms are often associated with higher DOC concentrations (Norrman et al., 1995; Smith et al., 1995), yet DOC was relatively similar across the study area (Table 1), which further supports an inference of more homogeneous selection across larger geographical areas than initially suspected. Although the DOC compound composition was likely variable due to different sources, variable substrate availability might promote the paucity of phylogenetic clustering as several taxa are known to have the ability to not only utilize a wide spectrum of organic matter but also have different preferences between taxa within the same group (Teeling et al., 2016; Underwood et al., 2019). Our study

lacks the temporal scale required to detect diatom “bloom” events, yet we detected spatial variation in chl *a* and relative abundance of diatoms as well as in the relative abundances of the most common microeukaryote taxa. Thus, more comprehensive, diatom bloom targeted studies are needed to fully describe the microbiome succession in detail. We concluded that the Barents Sea stations (BS1, BS2, and BS3) exhibited phytoplankton post-bloom conditions at the time that it was sampled for this study and presumably at some different stages between stations based on the measured chl *a* concentration, the eukaryotic community composition, and the previously documented timing of phytoplankton bloom from that area (Wassmann et al., 2006a; Oziel et al., 2017). However, the high chl *a* concentration ($11.2 \mu\text{g L}^{-1}$) and proportional abundance of centric diatoms (i.e., genus *Thalassiosira*) observed at NBm station revealed a strong indication of prevailing ice-edge bloom and intense primary production (Wassmann et al., 2006a). Very low chl concentrations were measured at the Nansen Basin stations (NB1 and NB2), and thus, these stations were considered to have low autotrophic phytoplankton biomass. Also, the higher DIC concentration at 20 m than at the other stations indicated lower inorganic carbon uptake (Norrman et al., 1995; Meire et al., 2015).

The Barents Sea and the Nansen Basin margins were dominated by ASVs indicative of copiotrophic bacteria like the predominant genus *Polaribacter* (order *Flavobacteriales*) and order *Rhodobacterales*, which are attributed to phytoplankton blooms as they are known to utilize phytoplankton-derived exudates (Teeling et al., 2012; Buchan et al., 2014). The significantly high contribution of *Polaribacter* to the community in the ice-edge at the NBm station can therefore be connected to the exemplary centric diatom thriven surface water ice-edge bloom. The differentially abundant order *Rhodobacterales* and the predominant genera (*Sulfitobacter* and *Amylibacter*) in the Barents Sea were the only prokaryotic taxa that showed a significant positive correlation with temperature (Figure 5C), corresponding to the previous finding of *Sulfitobacter* in relatively warm, saline, and productive Arctic surface water (Lee et al., 2019). However, *Sulfitobacter* has also been found in association with diatom-dominated ice-algal aggregates in the high Arctic Ocean (Rapp et al., 2018), suggesting that its very low presence in the Nansen Basin was not temperature-limited but instead due to low algal biomass. Many *Rhodobacteria* affiliates are rapid algal colonizers (Buchan et al., 2014), and therefore, their low relative abundance in the Nansen Basin margin was not expected. It is possible that the initial abundance of *Polaribacter* was already relatively high prior to the ice-edge bloom as it can be also abundant in sea-ice-associated communities (Rapp et al., 2018) and therefore responded faster to the inferred bloom than *Sulfitobacter*. The high relative abundance of *Rhodobacterales* at the Barents Sea stations (BS1, BS2, and BS3) may be related to the decline of *Polaribacter* in post-bloom conditions with the decrease of diatom abundance (Teeling et al., 2012).

The Nansen Basin was characterized by low phytoplankton biomass (as a proxy from chl *a*) and the prokaryotic community was dominated by taxa that have been classified as small molecule degraders such as SAR11 clade (class *Alphaproteobacteria*) and

Pseudomonadales (class *Gammaproteobacteria*) (Giovannoni, 2017; Francis et al., 2021). Although sequences classified within the order *Flavobacteriales*, notably genera *Polaribacter* and NS5 marine group, were also abundant in the Nansen Basin, these two genera have been observed in the Arctic under sea-ice before (Rapp et al., 2018) and *Polaribacter* is known to utilize organic matter from variable sources (Teeling et al., 2012; Underwood et al., 2019). The high relative abundance of SAR11 clade Ia (class *Alphaproteobacteria*) observed at NB1 and NB2 stations corresponded to the findings in epipelagic waters between the Yermak Plateau and the southern Nansen Basin (de Sousa et al., 2019). The SAR11 clade is ubiquitous, and it is suggested to be one of the most abundant bacterioplankton in surface oceans prospering oligotrophic systems both in dark and light conditions (Morris et al., 2002) using mainly small organic molecules (Gomez-Pereira et al., 2013). Also, SAR11 can utilize exogenous sources of sulfur-like dimethylsulfoniopropionate (DMSP) (Tripp et al., 2008). The high relative abundance of both SAR11 clade and dinoflagellates in the sea-ice-covered Nansen Basin in this study (Figure 3) corresponds with a previous finding from the same area, where it was suggested that the growth of SAR11 under sea-ice may be sustained by DMSP produced by dinoflagellates (de Sousa et al., 2019). SAR11 clade was also present at other stations although in low relative abundance, likely due to being outcompeted by faster-growing copiotrophs (Teeling et al., 2012).

CONCLUSION

This study investigated the phylogenetic diversity and structure of the cold marine ecosystems across different environments and specifically drew comparisons between the Atlantic-influenced Barents Sea and Nansen Basin environments. A sampling of open water in the Barents Sea and alongside a sea-ice edge in the Nansen Basin margin revealed the dominance of copiotrophic prokaryote taxa such as genera *Polaribacter* and *Sulfitobacter*, which are thought to be associated with phytoplankton bloom/post-bloom phenology and the resultant high abundance of diatoms. Whereas, highly sea-ice-covered environments in the high Arctic Nansen Basin were more characterized by widely common nanophytoplankton and picophytoplankton and oligotrophic prokaryotes, like SAR11 clade. In accordance with previous findings, we surmise that phytoplankton blooms are an important factor in determining the bacterial community structure in Arctic surface waters. Our results suggest that both prokaryotic and microeukaryotic components of the surface marine microbiome were subjected to deterministic homogeneous selection, which is an indication of the presence of strong environmental selection that was consistent across the large area of the Arctic Ocean surveyed here. Furthermore, we found that the decreasing temperature along the sampling transect did not negatively impact microbial species richness. This is likely due to temperature-driven selection for cold- and warm-water microbiomes that takes effect at warmer temperatures than are present in the contemporary

Barent Sea environment. Hence, despite the major influence of Atlantic waters, this selection occurs further south (in the North Sea) where the temperature-dependent microbial diversity breakpoints have been observed (Martin et al., 2021). We also suggest that the influence of Atlantic water between the Barents Sea (strongly influenced) and the Nansen Basin (less influenced) has implications for homogeneous habitat formation by allowing a necessary level of horizontal species dispersion. Although this study covered a large geographical area, the spatial sampling resolution is small in comparison to larger studies such as the Tara Oceans project. However, this study presents research questions focused on the Barents Sea and the Nansen Basin, which are difficult to access and therefore underrepresented in marine microbiology. We believe long-term time-series studies across this transect are needed to infer the real-time role of Atlantification on microbial community selection. The null modeling approach can be considered a valuable tool for that, as it helps to identify the role of ecological selection resulting from the Atlantification of marine microbiomes.

DATA AVAILABILITY STATEMENT

The datasets presented in this study can be found in online repositories: <https://osf.io/g8wxc/>.

AUTHOR CONTRIBUTIONS

NJA and HCB conceptualized the study and conducted data analyses. NJA, HDS, and HCB conducted the fieldwork. NJA and KC processed the environmental samples. HDS and SK processed molecular samples and amplicon sequence analyses. NJA wrote the manuscript draft. All authors contributed to the final version.

FUNDING

This work was supported by strategic funding allocation, from UiT—The Arctic University of Norway to the project ABSORB—Arctic Carbon Storage from Biomes.

ACKNOWLEDGMENTS

The authors would like to thank the captain and crew of the RV Kronprins Haakon for their support during the cruise. We also thank Ingeborg Giæver, Linn Israelsen, Therese Smelror Løkken, and Jon Brage Svenning for their help with sample preparation on the cruise. We kindly acknowledge assistance from the Environmental Sample Preparation and Sequencing Facility in the Biosciences Division of the Argonne National Laboratory.

SUPPLEMENTARY MATERIAL

The Supplementary Material for this article can be found online at: <https://www.frontiersin.org/articles/10.3389/fmicb.2022.892634/full#supplementary-material>

REFERENCES

- Aalto, N. J., Campbell, K., Eilertsen, H. C., and Bernstein, H. C. (2021). Drivers of atmosphere-ocean CO₂ flux in northern Norwegian fjords. *Front. Marine Sci.* 21, 841. doi: 10.3389/fmars.2021.692093
- Ajani, P. A., Kahlke, T., Siboni, N., Carney, R., Murray, S. A., and Seymour, J. R. (2018). The microbiome of the cosmopolitan diatom *leptocylindrus* reveals significant spatial and temporal variability. *Front. Microbiol.* 9, 2758. doi: 10.3389/fmicb.2018.02758
- Allen, R., Hoffmann, L. J., Lacombe, M. J., Louissou, Z., and Summerfield, T. C. (2020). Homogeneous environmental selection dominates microbial community assembly in the oligotrophic South Pacific Gyre. *Mol. Ecol.* 29, 4680–4691. doi: 10.1111/mec.15651
- Amaral-Zettler, L. A., McCliment, E. A., Ducklow, H. W., and Huse, S. M. (2009). A method for studying protistan diversity using massively parallel sequencing of V9 hypervariable regions of small-subunit ribosomal RNA genes. *PLoS One* 4, e6372. doi: 10.1371/annotation/50c43133-0df5-4b8b-8975-8cc37d4f2f26
- Amin, S. A., Parker, M. S., and Armbrust, E. V. (2012). Interactions between diatoms and bacteria. *Microbiol. Mol. Biol. Rev.* 76, 667–684. doi: 10.1128/MMBR.00007-12
- Anderson, L., Jones, E., Koltermann, K., Schlosser, P., Swift, J., and Wallace, D. (1989). The first oceanographic section across the Nansen Basin in the Arctic Ocean. *Deep Sea Res. Part A. Oceanograph. Res. Pap.* 36, 475–482. doi: 10.1016/0198-0149(89)90048-4
- Anderson, M. J. (2001). A new method for non-parametric multivariate analysis of variance. *Austr. Ecol.* 26, 32–46. doi: 10.1111/j.1442-9993.2001.01070.pp.x
- Arrigo, K. R., Perovich, D. K., Pickart, R. S., Brown, Z. W., Van Dijken, G. L., Lowry, K. E., et al. (2012). Massive phytoplankton blooms under Arctic sea ice. *Science* 336, 1408–1408. doi: 10.1126/science.1215065
- Assmy, P., Fernandez-Mendez, M., Duarte, P., Meyer, A., Randelhoff, A., Mundy, C. J., et al. (2017). Leads in Arctic pack ice enable early phytoplankton blooms below snow-covered sea ice. *Sci. Rep.* 7, 40850. doi: 10.1038/srep40850
- Barton, A. D., Irwin, A. J., Finkel, Z. V., and Stock, C. A. (2016). Anthropogenic climate change drives shift and shuffle in North Atlantic phytoplankton communities. *Proceed. Nat. Acad. Sci.* 113, 2964–2969. doi: 10.1073/pnas.1519080113
- Behrenfeld, M. J., O'Malley, R. T., Siegel, D. A., McClain, C. R., Sarmiento, J. L., Feldman, G. C., et al. (2006). Climate-driven trends in contemporary ocean productivity. *Nature* 444, 752–755. doi: 10.1038/nature05317
- Brislawn, C. J., Graham, E. B., Dana, K., Ihardt, P., Fansler, S. J., Chrisler, W. B., et al. (2019). Forfeiting the priority effect: turnover defines biofilm community succession. *The ISME Journal* 13, 1865–1877. doi: 10.1038/s41396-019-0396-x
- Buchan, A., LeCleir, G. R., Gulvik, C. A., and González, J. M. (2014). Master recyclers: features and functions of bacteria associated with phytoplankton blooms. *Nat. Rev. Microbiol.* 12, 686–698. doi: 10.1038/nrmicro3326
- Bussmann, I., and Kattner, G. (2000). Distribution of dissolved organic carbon in the central Arctic Ocean: the influence of physical and biological properties. *J. Marine Syst.* 27, 209–219. doi: 10.1016/S0924-7963(00)00068-3
- Callahan, B. J., McMurdie, P. J., Rosen, M. J., Han, A. W., Johnson, A. J. A., and Holmes, S. P. (2016). DADA2: high-resolution sample inference from Illumina amplicon data. *Nat. Methods* 13, 581–583. doi: 10.1038/nmeth.3869
- Cao, S., Zhang, W., Ding, W., Wang, M., Fan, S., Yang, B., et al. (2020). Structure and function of the Arctic and Antarctic marine microbiota as revealed by metagenomics. *Microbiome* 8, 1–12. doi: 10.1186/s40168-020-00826-9
- Caporaso, J. G., Kuczynski, J., Stombaugh, J., Bittinger, K., Bushman, F. D., Costello, E. K., et al. (2010). QIIME allows analysis of high-throughput community sequencing data. *Nat. Methods* 7, 335–336. doi: 10.1038/nmeth.f.303
- Cardozo-Mino, M. G., Fadeev, E., Salman-Carvalho, V., and Boetius, A. (2021). Spatial Distribution of arctic bacterioplankton abundance is linked to distinct water masses and summertime phytoplankton bloom dynamics (Fram Strait, 79°N). *Front. Microbiol.* 12, 1067. doi: 10.3389/fmicb.2021.658803
- Carter-Gates, M., Balestreri, C., Thorpe, S. E., Cottier, F., Baylay, A., Bibby, T. S., et al. (2020). Implications of increasing Atlantic influence for Arctic microbial community structure. *Scientific Rep.* 10, 1–13. doi: 10.1038/s41598-020-76293-x
- Cirri, E., and Pohnert, G. (2019). Algae–bacteria interactions that balance the planktonic microbiome. *New Phytol.* 223, 100–106. doi: 10.1111/nph.15765
- Connelly, T. L., Baer, S. E., Cooper, J. T., Bronk, D. A., and Wawrik, B. (2014). Urea uptake and carbon fixation by marine pelagic bacteria and archaea during the Arctic summer and winter seasons. *Appl. Environ. Microbiol.* 80, 6013–6022. doi: 10.1128/AEM.01431-14
- de Sousa, A. G. G., Tomasino, M. P., Duarte, P., Fernández-Méndez, M., Assmy, P., Ribeiro, H., et al. (2019). Diversity and composition of pelagic prokaryotic and protist communities in a thin Arctic sea-ice regime. *Microbial Ecol.* 78, 388–408. doi: 10.1007/s00248-018-01314-2
- Degerlund, M., and Eilertsen, H. C. (2010). Main species characteristics of phytoplankton spring blooms in NE Atlantic and Arctic waters (68–80°N). *Estuaries Coasts* 33, 242–269. doi: 10.1007/s12237-009-9167-7
- Dickson, A. G., Sabine, C. L., and Christian, J. R. (2007). *Guide to Best Practices for Ocean CO₂ Measurements*. British Columbia: North Pacific Marine Science Organization.
- Dini-Andreote, F., Stegen, J. C., Van Elsas, J. D., and Salles, J. F. (2015). Disentangling mechanisms that mediate the balance between stochastic and deterministic processes in microbial succession. *Proceed. Nat. Acad. Sci.* 112, E1326–E1332. doi: 10.1073/pnas.1414261112
- Evans, S., Martiny, J. B., and Allison, S. D. (2017). Effects of dispersal and selection on stochastic assembly in microbial communities. *ISME J.* 11, 176–185. doi: 10.1038/ismej.2016.96
- Fadeev, E., Salter, I., Schourup-Kristensen, V., Nöthig, E.-M., Metfies, K., Engel, A., et al. (2018). Microbial communities in the east and west from strait during sea ice melting season. *Front. Marine Sci.* 5, 429. doi: 10.3389/fmars.2018.00429
- Faith, D. P. (1992). Conservation evaluation and phylogenetic diversity. *Biologic. Conserv.* 61, 1–10. doi: 10.1016/0006-3207(92)91201-3
- Faith, D. P., and Baker, A. M. (2006). Phylogenetic diversity (PD) and biodiversity conservation: some bioinformatics challenges. *Evol. Bioinform.* 2, 117693430600200007. doi: 10.1177/117693430600200007
- Falkowski, P. G., Fenchel, T., and DeLong, E. F. (2008). The microbial engines that drive Earth's biogeochemical cycles. *Science* 320, 1034–1039. doi: 10.1126/science.1153213
- Francis, B., Urich, T., Mikolasch, A., Teeling, H., and Amann, R. (2021). North Sea spring bloom-associated Gammaproteobacteria fill diverse heterotrophic niches. *Environ. Microbiom.* 16, 1–16. doi: 10.1186/s40793-021-00385-y
- Fuhrman, J. A., Steele, J. A., Hewson, I., Schwalbach, M. S., Brown, M. V., Green, J. L., et al. (2008). A latitudinal diversity gradient in planktonic marine bacteria. *Proceed. Nat. Acad. Sci.* 105, 7774–7778. doi: 10.1073/pnas.0803070105
- Gilbert, J. A., Meyer, F., Antonopoulos, D., Balaji, P., Brown, C. T., Brown, C. T., et al. (2010). Meeting report: the terabase metagenomics workshop and the vision of an Earth microbiome project. *Stand. Genomic. Sci.* 3, 243. doi: 10.4056/signs.1433550
- Giovannoni, S. J. (2017). SAR11 bacteria: the most abundant plankton in the oceans. *Ann. Rev. Marine Sci.* 9, 231–255. doi: 10.1146/annurev-marine-010814-015934
- Gomez-Pereira, P. R., Hartmann, M., Grob, C., Tarran, G. A., Martin, A. P., Fuchs, B. M., et al. (2013). Comparable light stimulation of organic nutrient uptake by SAR11 and *Prochlorococcus* in the North Atlantic subtropical gyre. *ISME J.* 7, 603–614. doi: 10.1038/ismej.2012.126
- Hatam, I., Charchuk, R., Lange, B., Beckers, J., Haas, C., and Lanoil, B. (2014). Distinct bacterial assemblages reside at different depths in Arctic multiyear sea ice. *FEMS Microbiol. Ecol.* 90, 115–125. doi: 10.1111/1574-6941.12377
- Holm-Hansen, O., and Riemann, B. (1978). Chlorophyll a determination: improvements in methodology. *Oikos* 11, 438–447. doi: 10.2307/3543338
- Ibarbalz, F. M., Henry, N., Brandão, M. C., Martini, S., Busseni, G., Byrne, H., et al. (2019). Global trends in marine plankton diversity across kingdoms of life. *Cell* 179, 1084–1097. doi: 10.1016/j.cell.2019.10.008
- Karner, M. B., DeLong, E. F., and Karl, D. M. (2001). Archaeal dominance in the mesopelagic zone of the Pacific Ocean. *Nature* 409, 507–510. doi: 10.1038/35054051
- Kemmel, S. W., Cowan, P. D., Helmus, M. R., Cornwell, W. K., Morlon, H., Ackerly, D. D., et al. (2010). Picante: R tools for integrating phylogenies and ecology. *Bioinformatics* 26, 1463–1464. doi: 10.1093/bioinformatics/btq1166
- Kirchman, D. L., Elifantz, H., Dittel, A. I., Malmstrom, R. R., and Cottrell, M. T. (2007). Standing stocks and activity of Archaea and Bacteria in the western Arctic Ocean. *Limnol. Oceanograph.* 52, 495–507. doi: 10.4319/lo.2007.52.2.0495

- Kwok, R. (2018). Arctic sea ice thickness, volume, and multiyear ice coverage: losses and coupled variability (1958–2018). *Environ. Res. Lett.* 13, 105005. doi: 10.1088/1748-9326/aae3ec
- Lee, J., Kang, S.-H., Yang, E. J., Macdonald, A. M., Joo, H. M., Park, J., et al. (2019). Latitudinal distributions and controls of bacterial community composition during the summer of 2017 in Western Arctic Surface Waters (from the Bering Strait to the Chukchi Borderland). *Scientific Rep.* 9, 1–10. doi: 10.1038/s41598-019-53427-4
- Levinson, H., Nielsen, T. G., and Hansen, B. W. (2000). Annual succession of marine pelagic protozoans in Disko Bay, West Greenland, with emphasis on winter dynamics. *Marine Ecol. Progr. Series* 206, 119–134. doi: 10.3354/meps206119
- Litchman, E., de Tezanos Pinto, P., Edwards, K. F., Klausmeier, C. A., Kremer, C. T., and Thomas, M. K. (2015). Global biogeochemical impacts of phytoplankton: a trait-based perspective. *J. Ecol.* 103, 1384–1396. doi: 10.1111/1365-2745.12438
- Liu, C., Cui, Y., Li, X., and Yao, M. (2021). microeco: an R package for data mining in microbial community ecology. *FEMS Microbiol. Ecol.* 97, fiaa255. doi: 10.1093/femsec/fiaa255
- Loeng, H. (1991). Features of the physical oceanographic conditions of the Barents Sea. *Polar Res.* 10, 5–18. doi: 10.3402/polar.v10i1.6723
- Lopezone, C., Lladser, M. E., Knights, D., Stombaugh, J., and Knight, R. (2011). UniFrac: an effective distance metric for microbial community comparison. *ISME J.* 5, 169–172. doi: 10.1038/ismej.2010.133
- Martin, K., Schmidt, K., Toseland, A., Boulton, C. A., Barry, K., Beszteri, B., et al. (2021). The biogeographic differentiation of algal microbiomes in the upper ocean from pole to pole. *Nat. Commun.* 12, 1–15. doi: 10.1038/s41467-021-25646-9
- Martin-Platero, A. M., Cleary, B., Kauffman, K., Preheim, S. P., McGillicuddy, D. J., Alm, E. J., et al. (2018). High resolution time series reveals cohesive but short-lived communities in coastal plankton. *Nat. Commun.* 9, 1–11. doi: 10.1038/s41467-017-02571-4
- Matrai, P., Vernet, M., and Wassmann, P. (2007). Relating temporal and spatial patterns of DMSP in the Barents Sea to phytoplankton biomass and productivity. *J. Marine Syst.* 67, 83–101. doi: 10.1016/j.jmarsys.2006.10.001
- Meire, L., Sogaard, D., Mortensen, J., Meysman, F., Soetaert, K., Arendt, K., et al. (2015). Glacial meltwater and primary production are drivers of strong CO₂ uptake in fjord and coastal waters adjacent to the Greenland Ice Sheet. *Biogeosciences* 12, 2347–2363. doi: 10.5194/bg-12-2347-2015
- Meyer, A., Fer, I., Sundfjord, A., and Peterson, A. K. (2017). Mixing rates and vertical heat fluxes north of Svalbard from Arctic winter to spring. *J. Geophys. Res. Oceans* 122, 4569–4586. doi: 10.1002/2016JC012441
- Morris, R. M., Rappé, M. S., Connon, S. A., Vergin, K. L., Siebold, W. A., Carlson, C. A., et al. (2002). SAR11 clade dominates ocean surface bacterioplankton communities. *Nature* 420, 806–810. doi: 10.1038/nature01240
- Needham, D. M., and Fuhrman, J. A. (2016). Pronounced daily succession of phytoplankton, archaea and bacteria following a spring bloom. *Nat. Microbiol.* 1, 16005. doi: 10.1038/nmicrobiol.2016.5
- Norrman, B., Zwiefel, U. L., Hopkinson Jr, C. S., and Brian, F. (1995). Production and utilization of dissolved organic carbon during an experimental diatom bloom. *Limnol. Oceanograph.* 40, 898–907. doi: 10.4319/lo.1995.40.5.0898
- Oksanen, J., Simpson, G. L., Guillaume Blanchet, F., Kindt, R., Legendre, P., Minchin, P. R., et al. (2020). *Vegan: Community Ecology Package*. Rpackage version 2.5-7. Available online at: <https://CRAN.R-project.org/package=vegan>
- Orkney, A., Platt, T., Narayanaswamy, B. E., Kostakis, I., and Bouman, H. A. (2020). Bio-optical evidence for increasing Phaeocystis dominance in the Barents Sea. *Philosophic. Transact. Royal Soc. A* 378, 20190357. doi: 10.1098/rsta.2019.0357
- Oziel, L., Baudena, A., Ardyna, M., Massicotte, P., Randelhoff, A., Sallée, J.-B., et al. (2020). Faster Atlantic currents drive poleward expansion of temperate phytoplankton in the Arctic Ocean. *Nat. Commun.* 11, 1–8. doi: 10.1038/s41467-020-15485-5
- Oziel, L., Neukermans, G., Ardyna, M., Lancelot, C., Tison, J. L., Wassmann, P., et al. (2017). Role for Atlantic inflows and sea ice loss on shifting phytoplankton blooms in the Barents Sea. *J. Geophys. Res. Oceans* 122, 5121–5139. doi: 10.1002/2016JC012582
- Peralta-Ferriz, C., and Woodgate, R. A. (2015). Seasonal and interannual variability of pan-Arctic surface mixed layer properties from 1979 to 2012 from hydrographic data, and the dominance of stratification for multiyear mixed layer depth shoaling. *Progr. Oceanograph.* 134, 19–53. doi: 10.1016/j.pocean.2014.12.005
- Pérez-Hernández, M. D., Pickart, R. S., Pavlov, V., Våge, K., Ingvaldsen, R., Sundfjord, A., et al. (2017). The Atlantic Water boundary current north of Svalbard in late summer. *J. Geophys. Res. Oceans* 122, 2269–2290. doi: 10.1002/2016JC012486
- Polyakov, I. V., Pnyushkov, A. V., Alkire, M. B., Ashik, I. M., Baumann, T. M., Carmack, E. C., et al. (2017). Greater role for Atlantic inflows on sea-ice loss in the Eurasian Basin of the Arctic Ocean. *Science* 356, 285–291. doi: 10.1126/science.aai8204
- Quast, C., Pruesse, E., Yilmaz, P., Gerken, J., Schweer, T., Yarza, P., et al. (2012). The SILVA ribosomal RNA gene database project: improved data processing and web-based tools. *Nucleic Acids Res.* 41, D590–D596. doi: 10.1093/nar/gks1219
- Quere, C. L., Harrison, S. P., Colin Prentice, I., Buitenhuis, E. T., Aumont, O., Bopp, L., et al. (2005). Ecosystem dynamics based on plankton functional types for global ocean biogeochemistry models. *Global Change Biol.* 11, 2016–2040. doi: 10.1111/j.1365-2486.2005.1004.x
- R Core Team (2021). *R: A Language and Environment for Statistical Computing*. New York, NY: R Foundation for Statistical Computing.
- Rapp, J. Z., Fernández-Méndez, M., Bienhold, C., and Boetius, A. (2018). Effects of ice-algal aggregate export on the connectivity of bacterial communities in the Central Arctic Ocean. *Front. Microbiol.* 9, 1035. doi: 10.3389/fmicb.2018.01035
- Riedel, A., Michel, C., and Gosselin, M. (2006). Seasonal study of sea-ice exopolymeric substances on the Mackenzie shelf: implications for transport of sea-ice bacteria and algae. *Aquatic Microb. Ecol.* 45, 195–206. doi: 10.3354/ame045195
- Robeson, M. S., O'Rourke, D. R., Kaehler, B. D., Ziemski, M., Dillon, M. R., Foster, J. T., et al. (2020). RESCRIPT: Reproducible sequence taxonomy reference database management for the masses. *bioRxiv.* 20, 504. doi: 10.1101/2020.10.05.326504
- Rudels, B., Jones, E., Anderson, L., and Kattner, G. (1994). On the intermediate depth waters of the Arctic Ocean. *Polar Oceans Role Shaping Global Environ.* 85, 33–46. doi: 10.1029/GM085p0033
- Salazar, G., Paoli, L., Alberti, A., Huerta-Cepas, J., Ruscheweyh, H.-J., Cuenca, M., et al. (2019). Gene expression changes and community turnover differentially shape the global ocean metatranscriptome. *Cell* 179, 1068–1083. doi: 10.1016/j.cell.2019.10.014
- Schweitzer, H., Aalto, N. J., Busch, W., Chan, D. T. C., Chiesa, M., Elvevoll, E. O., et al. (2021). Innovating carbon-capture biotechnologies through ecosystem-inspired solutions. *One Earth* 4, 49–59. doi: 10.1016/j.oneear.2020.12.006
- Segata, N., Izard, J., Waldron, L., Gevers, D., Miropolsky, L., Garrett, W. S., et al. (2011). Metagenomic biomarker discovery and explanation. *Genome biology* 12, 1–18. doi: 10.1186/gb-2011-12-6-r60
- Signori, C. N., Pellizari, V. H., Enrich-Prast, A., and Sievert, S. M. (2018). Spatiotemporal dynamics of marine bacterial and archaeal communities in surface waters off the northern Antarctic Peninsula. *Deep Sea Research Part II: Topic. Stud. Oceanograph.* 149, 150–160. doi: 10.1016/j.dsr2.2017.12.017
- Smith, D. C., Steward, G. F., Long, R. A., and Azam, F. (1995). Bacterial mediation of carbon fluxes during a diatom bloom in a mesocosm. *Deep Sea Res. Part II: Topic. Stud. Oceanograph.* 42, 75–97. doi: 10.1016/0967-0645(95)00005-B
- Stegen, J. C., Lin, X., Fredrickson, J. K., Chen, X., Kennedy, D. W., Murray, C. J., et al. (2013). Quantifying community assembly processes and identifying features that impose them. *ISME J.* 7, 2069–2079. doi: 10.1038/ismej.2013.93
- Stegen, J. C., Lin, X., Konopka, A. E., and Fredrickson, J. K. (2012). Stochastic and deterministic assembly processes in subsurface microbial communities. *ISME J.* 6, 1653–1664. doi: 10.1038/ismej.2012.22
- Strickland, J. D. H., and Parsons, T. R. (1972). "Inorganic micronutrients in sea water," in *A practical Hand Book of Seawater Analysis*, ed J. C. Stevenson (Ottawa, ON: Fisheries Research Board of Canada).
- Teeling, H., Fuchs, B. M., Becher, D., Klockow, C., Gardebrecht, A., Bennke, C. M., et al. (2012). Substrate-controlled succession of marine bacterioplankton populations induced by a phytoplankton bloom. *Science* 336, 608–611. doi: 10.1126/science.1218344
- Teeling, H., Fuchs, B. M., Bennke, C. M., Krueger, K., Chafee, M., Kappelmann, L., et al. (2016). Recurring patterns in bacterioplankton dynamics during coastal spring algae blooms. *elife* 5, e11888. doi: 10.7554/eLife.11888

- Thomas, M. K., Kremer, C. T., Klausmeier, C. A., and Litchman, E. (2012). A global pattern of thermal adaptation in marine phytoplankton. *Science* 338, 1085–1088. doi: 10.1126/science.1224836
- Tolar, B. B., Powers, L. C., Miller, W. L., Wallsgrove, N. J., Popp, B. N., and Hollibaugh, J. T. (2016). Ammonia oxidation in the ocean can be inhibited by nanomolar concentrations of hydrogen peroxide. *Front. Marine Sci.* 3, 237. doi: 10.3389/fmars.2016.00237
- Tragin, M., and Vault, D. (2018). Green microalgae in marine coastal waters: the Ocean Sampling Day (OSD) dataset. *Scien. Rep.* 8, 1–12. doi: 10.1038/s41598-018-32338-w
- Tréguer, P., Bowler, C., Moriceau, B., Dutkiewicz, S., Gehlen, M., Aumont, O., et al. (2018). Influence of diatom diversity on the ocean biological carbon pump. *Nature Geosci.* 11, 27–37. doi: 10.1038/s41561-017-0028-x
- Tripp, H. J., Kitner, J. B., Schwalbach, M. S., Dacey, J. W., Wilhelm, L. J., and Giovannoni, S. J. (2008). SAR11 marine bacteria require exogenous reduced sulphur for growth. *Nature* 452, 741–744. doi: 10.1038/nature06776
- Underwood, G. J., Michel, C., Meisterhans, G., Niemi, A., Belzile, C., Witt, M., et al. (2019). Organic matter from Arctic sea-ice loss alters bacterial community structure and function. *Nat. Clim. Change* 9, 170–176. doi: 10.1038/s41558-018-0391-7
- Vellend, M. (2010). Conceptual synthesis in community ecology. *Q. Rev. Biol.* 85, 183–206. doi: 10.1086/652373
- Wassmann, P., Reigstad, M., Haug, T., Rudels, B., Carroll, M. L., Hop, H., et al. (2006a). Food webs and carbon flux in the Barents Sea. *Progr. Oceanograph* 0.000 71, 232–287. doi: 10.1016/j.pocean.2006.10.003
- Wassmann, P., Slagstad, D., Riser, C. W., and Reigstad, M. (2006b). Modelling the ecosystem dynamics of the Barents Sea including the marginal ice zone: II. carbon flux and interannual variability. *J. Marine Syst.* 59, 1–24. doi: 10.1016/j.jmarsys.2005.05.006
- Yilmaz, P., Parfrey, L. W., Yarza, P., Gerken, J., Pruesse, E., Quast, C., et al. (2014). The SILVA and “all-species living tree project (LTP)” taxonomic frameworks. *Nucleic Acids Res.* 42, D643–D648. doi: 10.1093/nar/gkt1209
- Zhang, F., He, J., Lin, L., and Jin, H. (2015). Dominance of picophytoplankton in the newly open surface water of the central Arctic Ocean. *Polar Biol.* 38, 1081–1089. doi: 10.1007/s00300-015-1662-7

Conflict of Interest: The authors declare that the research was conducted in the absence of any commercial or financial relationships that could be construed as a potential conflict of interest.

Publisher's Note: All claims expressed in this article are solely those of the authors and do not necessarily represent those of their affiliated organizations, or those of the publisher, the editors and the reviewers. Any product that may be evaluated in this article, or claim that may be made by its manufacturer, is not guaranteed or endorsed by the publisher.

Copyright © 2022 Aalto, Schweitzer, Krsmanovic, Campbell and Bernstein. This is an open-access article distributed under the terms of the Creative Commons Attribution License (CC BY). The use, distribution or reproduction in other forums is permitted, provided the original author(s) and the copyright owner(s) are credited and that the original publication in this journal is cited, in accordance with accepted academic practice. No use, distribution or reproduction is permitted which does not comply with these terms.

